Investigating the role of DNA (cytosine-5)-methyltransferase 1 in mitochondrial DNA methylation

Nicolini, Francesco

Awarding institution:
King's College London

Investigating the role of DNA (cytosine-5)-methyltransferase 1 in mitochondrial DNA methylation

Francesco Nicolini

Ph.D. Thesis

Cardiovascular Division
BHF Centre of Research Excellence
School of Medicine
King's College London

Submitted for the Degree of Doctor of Philosophy from
King's College London

Supervised by
Professor Kinya Otsu
Professor Elisabeth Zeisberg

Abstract

Mitochondrial DNA (mtDNA) that escapes from autophagy-mediated degradation after hemodynamic stress can cause inflammation in the heart by activating TLR9 signalling pathway, in which unmethylated CpG motifs bind to TLR9. DNA methyltransferases (DNMTs) such as DNMT1 and DNMT3A are involved in nuclear DNA methylation. It has also been reported that two additional potential transcription initiation codons exist at 5' region to the original DNMT1 and that this 1st-to-3rd ATG sequence fused to GFP cDNA can localise in mitochondria, suggesting that DNMT1 might affect mtDNA methylation patterns. The aim of this study is to elucidate the role of DNMT1 in mtDNA methylation. To achieve this aim, three different isoforms of mouse DNMT1 sequences ("nuclear DNMT1", "whole DNMT1" and "mtDNMT1") as well as a mouse DNMT3A isoform were generated through molecular cloning. Mitoprot II software analysis predicted a high chance of mitochondrial localization (>90%) for both whole DNMT1 and mtDNMT1 isoforms. Western blotting analysis confirmed overexpression of all DNMT1 constructs, and immunocytochemistry experiments confirmed the predicted localisation of DNMT1 isoforms. DNMT3A localisation was detected at nuclear level, but not at mitochondrial level. Adenoviral vectors for nuclear DNMT1 and mtDNMT1 were generated and the methylated-DNA immunoprecipitation/qPCR methylation analysis of the D-Loop showed a 3-to-5 fold increase in total methylation levels in mtDNMT1 overexpressed mouse cardiac endothelial cells. However, global percentage of methylation is low. CoIP-MS analysis after mtDNMT1 overexpression failed to highlight any candidates for mtDNMT1 co-interaction. These data suggest that the 1st-to-3rd ATG sequence contains the mitochondrial localisation signal for DNMT1, and that DNMT1 can localise to mitochondria through it and methylate mtDNA.

Acknowledgements

I would like to thank all the people who have helped me through my PhD. Firstly, my supervisors Professor Kinya Otsu and Professor Elisabeth Zeisberg, for giving me the opportunity to work in their groups. Prof Kinya Otsu dedicated a lot of his time and energies to guide me through my PhD, and Prof Elisabeth Zeisberg provided much needed direction on the epigenetics-side of my PhD, as well as making sure I had correct guidance in the lab during my time in Goettingen. I would also like to thank the British Heart Foundation (BHF) for their financial support throughout my PhD.

The most important person for me to thank is Dr Kazuhiko Nishida, he spent copious amounts of time dealing with all of my questions and problems, I could not have completed my PhD without him, and will be forever grateful.

Another big thank you goes to my colleagues who have helped me working in the lab and discussing ideas – Minoru Takaoka, Manabu Taneike, Shigemiki Omiya, Tomofumi Misaka, Elham Zarrinpashneh, Trusha Mistry, Yosuke Omori and Rika Taneike. I would also like to thank Aleksandar Ivetic and Xingbo Xu for their invaluable help, definitely the most "out of the ordinary" scientists I have ever met. Numerous wonderful people have also made this experience even more enjoyable; Moritz, Craig, Andrew, Matteo, Stephen, Giulia, Izajur, Giancarlo, Vito, Jasper, Fed, the medwinians (you know who you are) and my family, whom I thank for their support and encouragement.

Finally I would like to thank my lovely other half Beatrice to whom this thesis is dedicated, for her unending support, levelheadedness and love.

Declaration

I declare that I am the sole author of this Ph.D. thesis and it contains my own work, except where indicated.

Francesco Nicolini

Table of Contents

Table of Figures

Table of Tables

Abbreviations

Abbreviation	Meaning
2-ME	2-mercaptoethanol
5hmC	5-hydroximethylcytosine
5mC	5-methylcytosine
Ab	Antibody
Ad	Adenovirus
ANF	Atrial natriuretic factor
BAH1	Bromo-adjacent homology domain 1
BAH2	Bromo-adjacent homology domain 2
BCA	Bicinchoninic acid
BHF	British heart foundation
BNP	Brain natriuretic peptide
BSA	Bovine serum albumin
$CaCl_2$	Calcium chloride
CAD	Coronary artery disease
CCCP	Carbonyl cyanide m-chlorophenyl hydrazone
cDNA	Complementary deoxyribonucleic acid
CMV	Cytomegalovirus
CO_2	Carbon dioxide
CVD	Cardiovascular disease
DAMP	Danger-associated molecular pattern
DAPI	4',6-diamidino-2-phenylindole
DCM	Dilated cardiomyopathy
dH2O	Distilled water
DMEM	Dulbecco's modified eagle medium
DNA	Deoxyribonucleic acid
Dnase	Deoxyribonuclease
DNMT1	DNA (cytosine-5)-methyltransferase 1
DNMT3A	DNA (cytosine-5)-methyltransferase 3A
E1	Adenovirus early region 1
E3	Adenovirus early region 3
E3UL	E3 ubiquitin ligase
EDTA	Ethylenediaminetetraacetic acid
EGTA	Ethylene glycol tetra acetic acid
ENCODE	Encyclopedia of DNA elements
EtOH	Ethanol
FBS	Foetal bovine serum
H9C2	Rattus norvegicus cardiomyoblasts
HAT	Histone acetyltransferase
HBP	High blood pressure
HDAC	Histone deacetylases

HEK293A	Human embryonic kidney cells
HEPES	4-(2-hydroxyethyl)-1-piperazineethanesulfonic acid
HF	Heart failure
HFpEF	Heart failure with preserved ejection fraction
HFrEF	Heart failure with reduced ejection fraction
HSP	Heavy-strand promoter
IkBα	Inhibitor of nuclear factor kappa-B
IKK	IκB kinase
IKKα	Inhibitor of nuclear factor kappa-B kinase subunit alpha
IKKβ	Inhibitor of nuclear factor kappa-B kinase subunit beta
IL	Interleukin
IL-1R	Interleukin 1 receptor
IN	Integrase
IRAK	IL-1R-associated kinase
IRF	Interferon regulatory factor
KCl	Potassium chloride
LLR	Leucine-rich repeat
LPS	Lipopolysaccharide
LSP	Light-strand promoter
LVEF	Left ventricular ejection fraction
MCEC	Mouse cardiac endothelial cells
MCS	Multiple cloning site
$MgCl_2$	Magnesium chloride
$MgSO_4$	Magnesium sulphate
MI	Myocardial infarction
MIA	Mitochondrial import and assembly machinery protein
MIM	Mitochondrial import complex
MLS	Mitochondrial localisation signal
mRNA	Messenger ribonucleic acid
MyD88	Myeloid differentiation primary response protein 88
NaAc	Sodium acetate
NaCl	Sodium chloride
ncRNA	Non-coding ribonucleic acid
ND1	NADH dehydrogenase subunit 1
ND6	NADH-ubiquinone oxidoreductase chain 6
NF-κB	Nuclear factor kappa-light-chain-enhancer of activated B cells
NLS	Nuclear localisation signal
NUMT	Nuclear insertions of mitochondrial origin
OXA	Oxidase assembly machinery
PAMP	Pathogen-associated molecular pattern
PBS	Phosphate buffered saline
PBS-G	PBS with 100mM Glycine

PCR	Polymerase chain reaction
PI	Protease inhibitors
PMSF	Phenylmethylsulfonyl fluoride
PRR	Pattern recognition receptor
PSG	L-Glutamine-Penicillin-Streptomycin solution
qRT-PCR	Quantitative real time PCR
RFD	Replication foci-targeting domain
RNA	Ribonucleic acid
RNase	Ribonuclease
rRNA	Ribosomal ribonucleic acid
RT	Reverse transcription
SAM	S-adenosyl methionine
SAM protein	Sorting and assembly machinery protein
SDS	Sodium dodecyl sulphate
SDS-PAGE	Sodium dodecyl sulphate-polyacrylamide gel electrophoresis
TAB2	TGF-beta-activated kinase 1 and MAP3K7 binding protein 2
TAB3	TGF-beta-activated kinase 1 and MAP3K7 binding protein 3
TAK1	Transforming growth factor beta-activated kinase 1
TAP	Tandem affinity purification
TBE	Tris/borate/EDTA
TBS	Tris-buffered saline
TBS-T	TBS with 0.1% Tween20
TET	Ten-eleven translocation methylcytosine dioxygenase
TFAM	Transcription factor of activated mitochondria
TIM22	Carrier translocase of the inner membrane
TIM23	Translocase of the inner membrane
TIR	Toll/IL-1R homology domain
TLR	Toll-like receptor
TOM	Translocase of the outer membrane
TRAF3	TNFR-associated factor 3
TRAF6	TNFR-associated factor 6
TRD	Target recognition domain
tRNA	Transfer ribonucleic acid
VSV-G	Vesicular stomatitis virus protein G
WT	Wild-type
βMHC	β-myosin heavy chain
Δψ	Membrane potential

Chapter 1 : General introduction

1.1 Heart failure

Heart failure (HF) is a leading cause of morbidity and mortality[1], with 2.3 million people in the UK diagnosed with this complex clinical syndrome; the lifetime risk of developing heart failure is roughly one in five for a person aged 40 years, and with the number of new cases detected each year increasing rapidly. Thus, understanding the pathogenesis of heart failure is highly important to develop new therapies against this condition. The heart is a pump that drives blood carrying oxygen and nutrients to the organs around the body and heart failure happens when the heart is not capable of pumping enough blood to meet the systemic metabolic demands. This can have complications and leads to symptoms such as excessive tiredness, shortness of breath, dizziness and oedema. Heart failure is associated with a number of molecular signs such as elevated levels of catecholamines[2] and proinflammatory cytokines (tumour necrosis factor alpha, interleukin 6, interleukin 8, interleukin 1 beta)[3,4], and is caused by structural and/or functional cardiac abnormalities, leading to myocyte death and/or ventricular remodelling[5]. The classification can be based on the time from ventricular dysfunction to clinical manifestations[6], the ejection fraction (the fraction of blood in the left and right ventricles pumped out with each heartbeat), or the main site of congestion. Heart failure is a chronic illness which develops gradually over time, and long-term therapies are used to treat patients with the symptoms. It is generally triggered as a secondary effect of other conditions, such as diabetes and high blood pressure (HBP), which indirectly damage the heart. Acute heart failure is due to cardiac-related events, such as myocardial infarction (MI). An MI occurs when blood stops flowing properly to a part of the heart (myocardial ischemia), and the heart muscle is injured because it is not receiving enough oxygen. Conventionally, HF was seen to result from the failure of the

heart to pump enough blood into the circulation due to ventricular systolic dysfunction (heart failure with a reduced ejection fraction, HFrEF), but patients with non-decreased left ventricular ejection fraction (LVEF) can develop HF when higher filling pressures are needed to achieve a normal end-diastolic ventricular volume[6] (**Figure 1.1**). Half of patients with heart failure have a preserved left ventricular ejection fraction (HFpEF), and while morbidity and mortality in HFpEF are similar to values observed in patients with HFrEF, no effective treatment has been identified[7]. While early research focused on the importance of diastolic dysfunction in the pathophysiology of HFpEF, recent studies have revealed that multiple non-diastolic abnormalities in cardiovascular function also contribute[8].

Heart failure may also be defined based on which side of the heart is not functioning effectively[6,9]. When the left ventricle is not pumping adequately, a build-up of blood in the left atrium and the lungs affects the supply of oxygenated blood to the rest of the body, and this is known as left-sided heart failure. The main symptoms include shortness of breath, fatigue and lung congestion. On the other hand, when the right ventricle is not pumping adequately, systemic congestion develops, leading to liver congestion, appetite loss, fluid retention and swelling in the legs and ankles. Right-sided heart failure usually occurs as a direct result of left-sided heart failure but can also be caused by severe cardiac hypertrophy, lung diseases or valvular diseases[10]. Although many conditions may lead to HF, the predominant aetiologies are myocardial ischemia and HBP with coronary artery disease (CAD) being the initiating cause in almost 70% of cases of heart failure[11] and HBP being responsible for boosting heart failure risk by two- to three-fold[9].

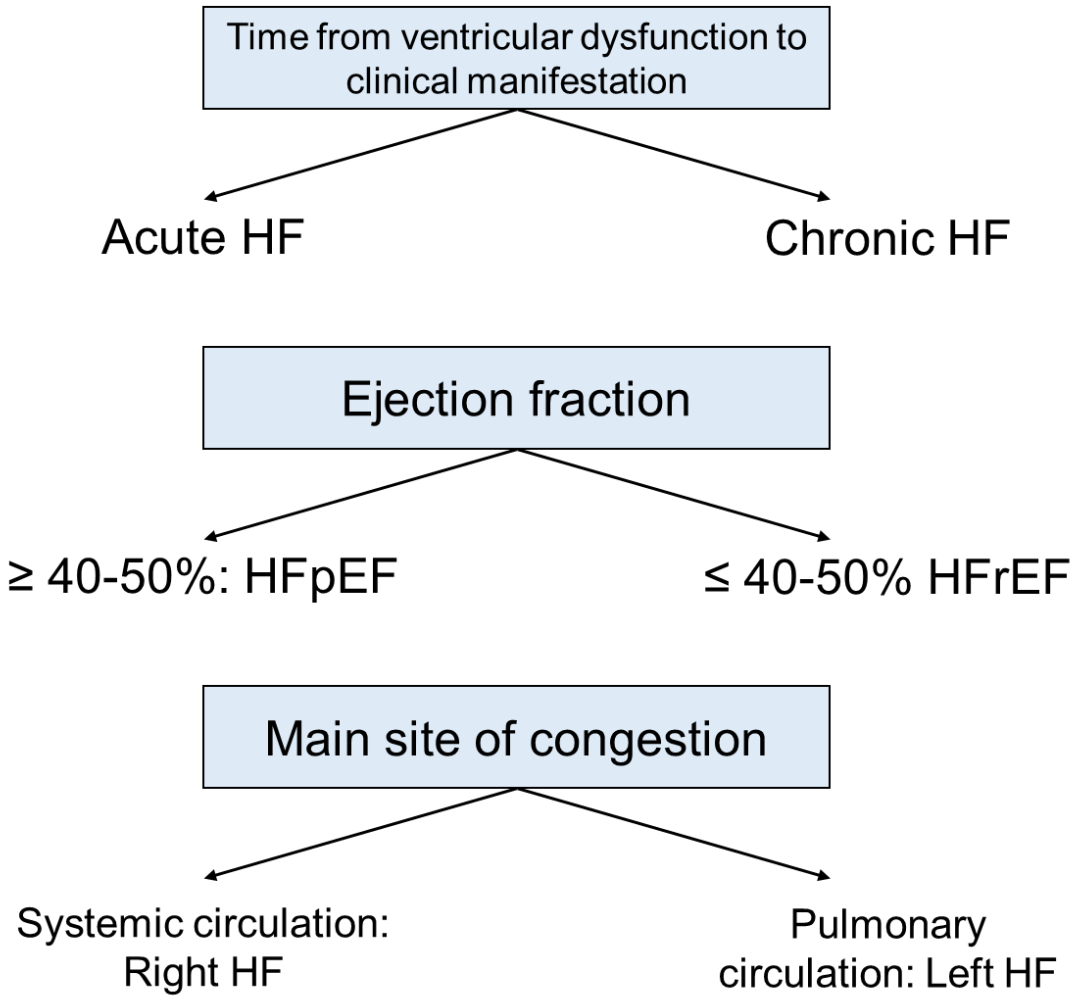

Figure 1.1: Types of heart failure. Abbreviations: HF, heart failure; HFrEF, heart failure with reduced ejection fraction; HFpEF heart failure with preserved ejection fraction. Adapted from Pazos-Lopez P. et al, *The causes, consequences, and treatment of left or right heart failure*. Vascular health and risk management, 2011[6].

1.2 Cardiac remodelling and hypertrophic responses

Under conditions such as HBP or during exercise, the heart must adapt itself to conduct extra work and normalize the load. The hypertrophic response is initiated, enlarging the size of cardiomyocytes and leading to increased wall thickness. This improves the pumping function of the cardiac muscle and decreases ventricular wall tension[12]. Three different types of cardiac remodelling (defined as the changes in size, shape, structure and physiology of the heart after injury to the myocardium) exist: physiological hypertrophy, pathological hypertrophy and cardiac dilation[13] (**Figure 1.2**).

Physiological hypertrophy, also known as eccentric hypertrophy, happens in response to stimuli such as exercise or pregnancy. The heart undergoes a uniform cardiac hypertrophic response in which the sarcomeres are added in series elongating the cardiomyocytes, and there is a matched increase in ventricular wall thickness and chamber dimensions. This type of adaptive response is accompanied with normal or enhanced cardiac function[12].

Pathological hypertrophy occurs due to sustained hypertension (high blood pressure), MI, diabetes and several types of cardiomyopathies. It is associated with increased protein synthesis, reactivation of the foetal gene program (that involves increased size of cardiomyocytes) and increased expression of atrial natriuretic factor (ANF), brain natriuretic peptide (BNP) and β-myosin heavy chain (βMHC)[14,15]. During pathological hypertrophy, the cardiomyocytes undergo concentric hypertrophy that corresponds to thicker ventricular and septal walls, but with a decrease in chamber dimensions. These changes altogether can improve the pumping function of the heart at first[16], however over time this type of cardiac remodelling alters the extracellular matrix leading to impaired cardiac

function due to fibrosis and cell death of myocytes. This results in an increased risk of adverse cardiac events[16,17] (**Figure 1.3**).

Finally, cardiac dilation has a similar yet harsher phenotype than pathological hypertrophy, in which cardiac fibrosis and myocardial cell death are detected and there is eccentric growth of the cardiomyocytes. Sarcomeres are added in series making the cells longer, inducing dilatory growth of the cardiac muscle and leading to heart failure[13].

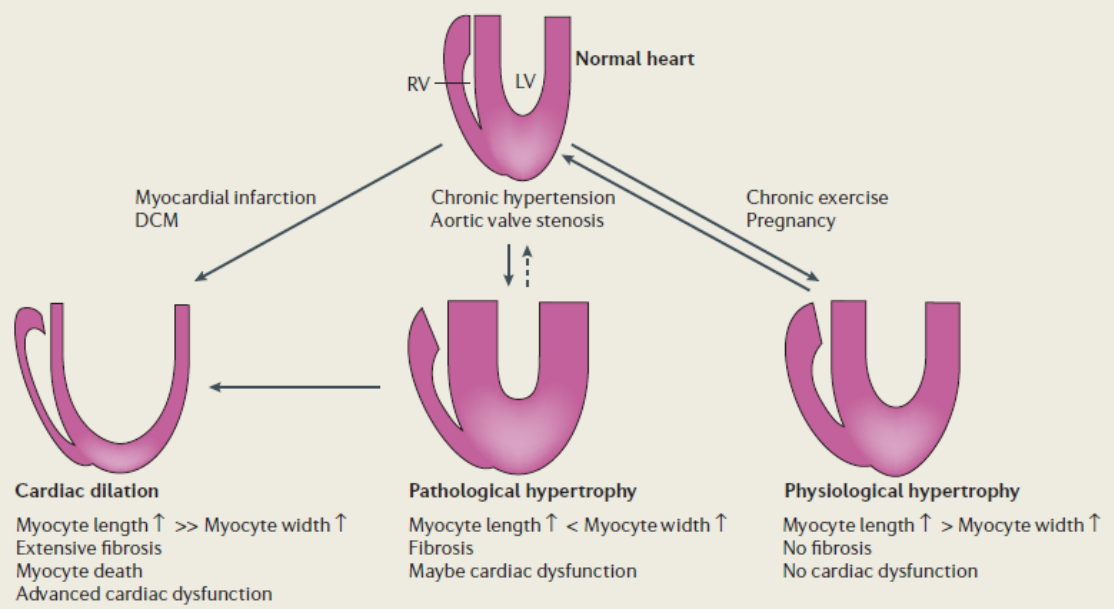

Figure 1.2: Cardiac hypertrophic responses. The adaptive and reversible physiological hypertrophic response to exercise and pregnancy leads to eccentric cell growth. Pathological hypertrophy induces concentric hypertrophy, leading to a greater increase in cardiomyocyte width, rather than length. These changes can aid cardiac function, however over time this type of cardiac remodelling is detrimental as fibrosis and cell death impair the cardiac function. Cardiac dilation may occur from normal hearts under conditions such as myocardial infarction (MI) or dilated cardiomyopathy (DCM), or from severe pathological hypertrophy. Abbreviations: RV, right ventricle; LV, left ventricle; DCM, dilated cardiomyopathy. Taken from Heineke J. et al, *Regulation of cardiac hypertrophy by intracellular pathways*, Nature Reviews Molecular Cell Biology, 2006.

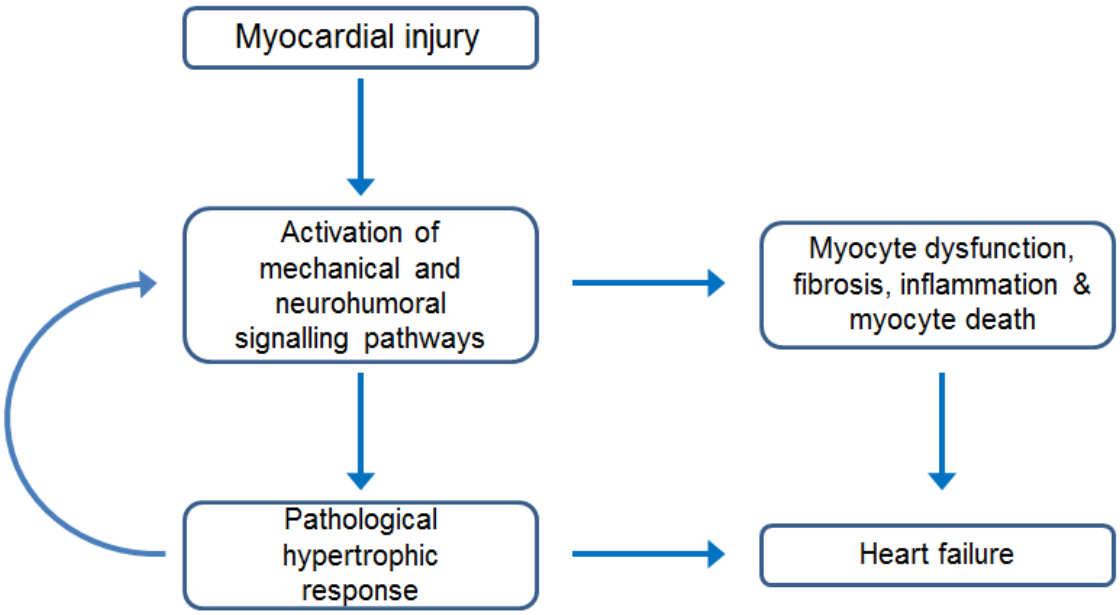

Figure 1.3: Pathological hypertrophic response. Myocardial injury leads to the activation of mechanical and neurohumoral signalling pathways to aid the cardiac workload. Stimulating these signalling pathways leads to pathological hypertrophy with an increase in myocyte size, increased protein synthesis, altered gene expression and changes in sarcomeric organization. The initial adaptive response is beneficial to the heart, but over time it becomes pathological and eventually leads to heart failure.

1.3 Inflammation

The mammalian immune system possesses a variety of strategies to defend the body against external pathogens and tumors[18], which are divided in two branches: innate and acquired immunity. The innate immune system is the first line of host defence against pathogens and is mediated by phagocytes including macrophages and dendritic cells (DCs). Inflammation is part of the innate immunity and is an initial and fast-acting immune defence mechanism that removes injurious stimuli and initiates the healing process[19]. The tissue-residing macrophages and the complement system detect the presence of foreign substances and antigens, stimulating the release of chemotactic cytokines (chemokines) such as interleukin (IL)-8 and proinflammatory cytokines such as IL-1, IL-6 and Tumour necrotic factor α (TNFα). Complement activation stimulates mast cells to degranulate releasing histamine and prostaglandins into the extracellular space, which in turn instigates dilation of local blood vessels and permeabilisation of the capillaries, leading to the recruitment and extravasation of leukocytes to the area[2]. The increased blood flow and warmth to the injured area are unfavourable for micro-organisms and result in swelling of the affected area, isolating the foreign substance from further contact with bodily tissues. Inflammation will persist until the microorganism has been eradicated. However, if the inflammation is too much or lasts for a long time, it can result in damage to the host tissues and lead to neurodegenerative and autoimmune disorders[2], thereby requiring for inflammation to be tightly regulated to maintain homeostasis. Increased levels of circulating proinflammatory cytokines, such as TNFα, IL-6 and IL-1β [3,4] are associated with the progression and adverse outcomes of heart failure in chronic heart failure patients. Moreover, inflammation has been implicated with the pathogenesis of this condition, even though infection by micro-

organisms is most likely not involved[20], and the mechanisms responsible for initiating and integrating inflammatory responses within the heart remain poorly defined.

1.3.1 Toll-like receptors (TLRs)

Macrophages and dendritic cells are important sentinels for detecting infectious material. Infectious material is sensed by pattern recognition receptors (PRRs) found at the plasma membrane or intracellularly. PRRs recognize non-self, exogenous pathogen-associated molecular patterns (PAMPs) or endogenous danger-associated molecular patterns (DAMPs) such as heat shock proteins[21]. A subset of PRRs includes the toll-like receptors (TLRs). Toll, the founding member of the TLR family, was initially identified as a gene product essential for the development of embryonic dorsoventral polarity in Drosophila, and was later shown to play a critical role in the antifungal response of flies[22]. TLRs are evolutionarily conserved, from the worm Caenorhabditis elegans to mammals[23], and 12 members of the TLR family have currently been identified in mammals. TLRs are type I integral membrane glycoproteins characterized by the extracellular domain containing varying numbers of leucine-rich repeat (LRR) motifs and a cytoplasmic signalling domain homologous to that of the interleukin 1 receptor (IL-1R), termed the Toll/IL-1R homology (TIR) domain[24]. Based on their primary sequences, TLRs can be further divided into several subfamilies, each of which is capable of recognizing different types of PAMPs: the subfamily of TLR1, TLR2 and TLR6 recognizes lipids, whereas the highly related TLR7, TLR8 and TLR9 recognize nucleic acids. However, some TLRs (i.e. TLR4) are unusual in a way that they can recognize several structurally unrelated PAMPs

such as lipopolysaccharide (LPS), fibronectin, heat shock proteins and many others.

TLRs are expressed on various immune cells such as macrophages, dendritic cells, B cells, specific types of T cells, and sometimes even on nonimmune cells such as fibroblasts and epithelial cells. Activation of TLRs instigates an intracellular signalling pathway which is typical for each TLR, but all end up by activating the inflammatory cascade[25].

1.3.2 Autophagy

Autophagy is a general term for the non-selective degradation of cytoplasmic components within lysosomes[26]. The principal role of autophagy is to supply nutrients for survival[27], and a level of constitutive autophagy is required in order to maintain cell function through controlling the quality of proteins and organelles[28]. The process is distinct from endocytosis-mediated lysosomal degradation of extracellular and plasma membrane proteins, and there are three types of autophagy – macroautophagy, microautophagy, and chaperone-mediated autophagy[29]. The non-selective nature of this process is in contrast to the ubiquitin-proteasome system, which specifically recognizes only ubiquitinated proteins for proteasomal degradation, and has numerous specific functions as it can selectively target a wide range of substrates. Autophagy has also been involved in the regulation of a variety of physiological and pathophysiological roles such as starvation adaptation, development, anti-aging, cell death, tumour suppression[30], and it consists of several sequential steps (**Figure 1.4**). A portion of cytoplasm, including organelles, is enclosed by an isolation membrane to compose an autophagosome. The outer membrane of the autophagosome

subsequently fuses with the endosome and then the lysosome, and the internal material is degraded.

As previously mentioned, growing evidence suggests that cardiac inflammation contributes to progression of heart failure, and altered autophagy has been observed in various heart diseases[31,32]. Moreover, it has been reported that autophagy plays a different role in cardiomyocytes in the basal state and in response to hemodynamic stress through pressure overload experiments[33]. Constitutive autophagy in the heart, under baseline conditions, is a homeostatic mechanism for maintaining cardiomyocyte size and cardiac structure and function, whereas under conditions of hemodynamic stress it becomes an adaptive response to protect cardiac tissues from damage[33]. Despite accumulating evidence that inflammation is involved in pathogenesis, an infection with microorganisms is not involved in the development of the majority of heart failure cases[34], though elevated levels of circulating pro-inflammatory cytokines are present. This state is called "sterile inflammation"[3], and the underlining mechanism and involvement of sterile inflammation in the development of heart failure is currently subject of intense studies.

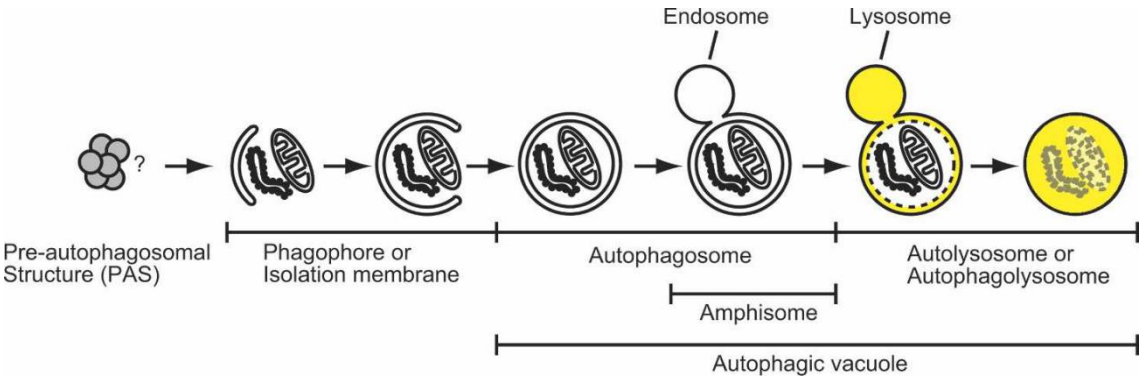

Figure 1.4: The process of macroautophagy in mammalian cells. Following formation of the autophagolysosome, the material internalised by the autophagosome formation is degraded. Abbreviations: PAS, Pre-autophagosomal Structure. Figure taken from Mizushima N., *Autophagy: process and function*, Genes and development, 2007[29].

1.3.2.1 Involvement of mitochondrial DNA in cardiac inflammation and heart failure

The TLR9 receptor usually recognizes unmethylated CpG motifs found within bacterial and viral DNA[35], but it has also been reported that mtDNA that escapes from autophagy is capable of triggering a TLR9-mediated inflammatory response[36] (**Figure 1.5**).

Endosomally located TLR9 recognizes unmethylated CpG motifs on DNA. Activation of TLR9 leads to the recruitment of the adaptor protein MyD88, which forms a complex with IL-1R-associated kinase 4 (IRAK4), E3 ubiquitin ligase (E3UL) and TNFR-associated factor 6 (TRAF6). E3UL ubiquitinates TRAF 6 enabling regulatory proteins Transforming growth factor beta-activated kinase 1 (TAK1), TGF-beta-activated kinase 1 and MAP3K7 binding protein 2 (TAB2) and TGF-beta-activated kinase 1 and MAP3K7 binding protein 3 (TAB3) to bind to the ubiquitinated sites of TRAF6. Activated TAK1 phosphorylates inhibitor of nuclear factor kappa-B kinase (IkB) subunit beta (IKKβ) within the IKK complex, which in turn phosphorylates the inhibitor of nuclear factor kappa B (IκBα). This phosphorylation leads to degradation of IκBα via the ubiquitin-proteasome system and the release of nuclear factor kappa-light-chain-enhancer of activated B cells (NF-κB). NF-κB translocates into the nucleus and activates the transcription of proinflammatory cytokine genes and type 1 interferons (such as IFNα). TRAF6 activates interferon regulatory factor (IRF)-5 to enter into the nucleus and activate the transcription of proinflammatory cytokine genes. In addition, MyD88 also forms a signalling complex with TNFR-associated factor 3 (TRAF3), IL-1R-associated kinase 1 (IRAK1) and inhibitor of nuclear factor kappa-B kinase subunit alpha (IKKα), and phosphorylation of interferon

regulatory factor 7 (IRF7) by IRAK1 or IKKα enables IRF7 to enter into the nucleus, which in turn initiates the transcription of type 1 interferons[25].

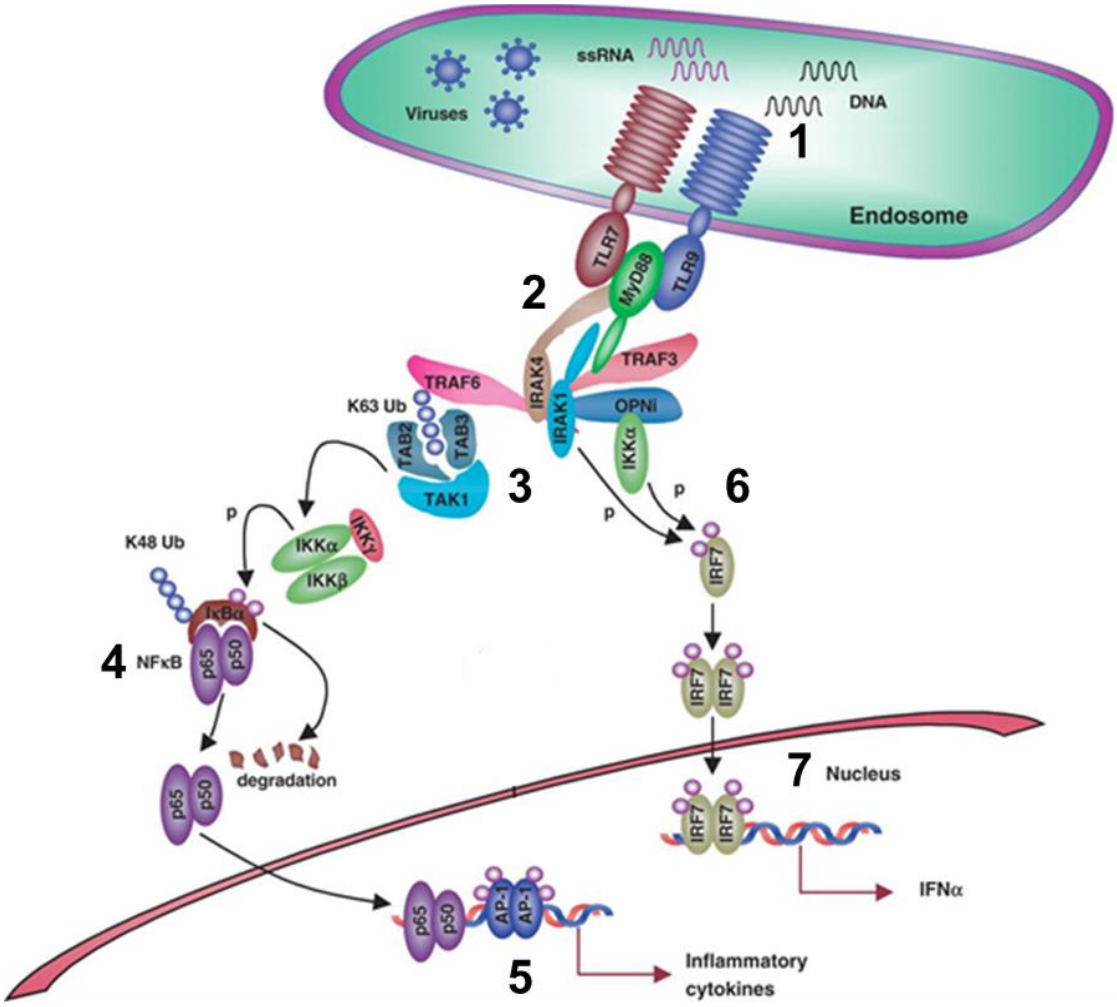

Figure 1.5: Downstream signalling of the TLR9 receptor. After recognition of unmethylated CpG motifs by TLR9 (1), MyD88 adaptor protein is recruited and forms a complex with the IRAK-4-TRAF6 complex (2). Ubiquitination of TRAF6 allows for TAK1, TAB2 and TAB3 binding (3). Phosphorylation of IKKβ by TAK1 triggers IκBα phosphorylation, which leads to the release of NF-κB (4). This allows for NF-κB nuclear translocation and the subsequent production of proinflammatory cytokines (5). MyD88 also allows for nuclear localisation of IRF7 through a signalling complex with TRAF3, IRAK1 and IKKα (6), which leads to the production of IFNα (7).

1.4 Mitochondria

1.4.1 Structure and role

The mitochondrion is a cellular organelle that derives from an ancient α-proteobacterium that, according to the endosymbiotic theory, was taken up by a primordial eukaryotic cell ~1.5-2 billion years ago[37]. Mitochondria have a central role in energy conversion and are thus termed the powerhouses of eukaryotic cells. The complexes of the respiratory chain in the mitochondrial inner membrane use energy, which is gained from the oxidation of food molecules, to pump protons across the membrane and generate a membrane potential (Δψ). The proton gradient is then used to drive the mitochondrial ATP synthase that produces the bulk of ATP for the cell, although eukaryotic cells also integrated mitochondria into multiple metabolic and signalling pathways[38,39].

Like Gram-negative bacteria, mitochondria contain two membranes (an outer membrane and an inner membrane) and two aqueous spaces (the intermembrane space and the matrix) (**Figure 1.6**).

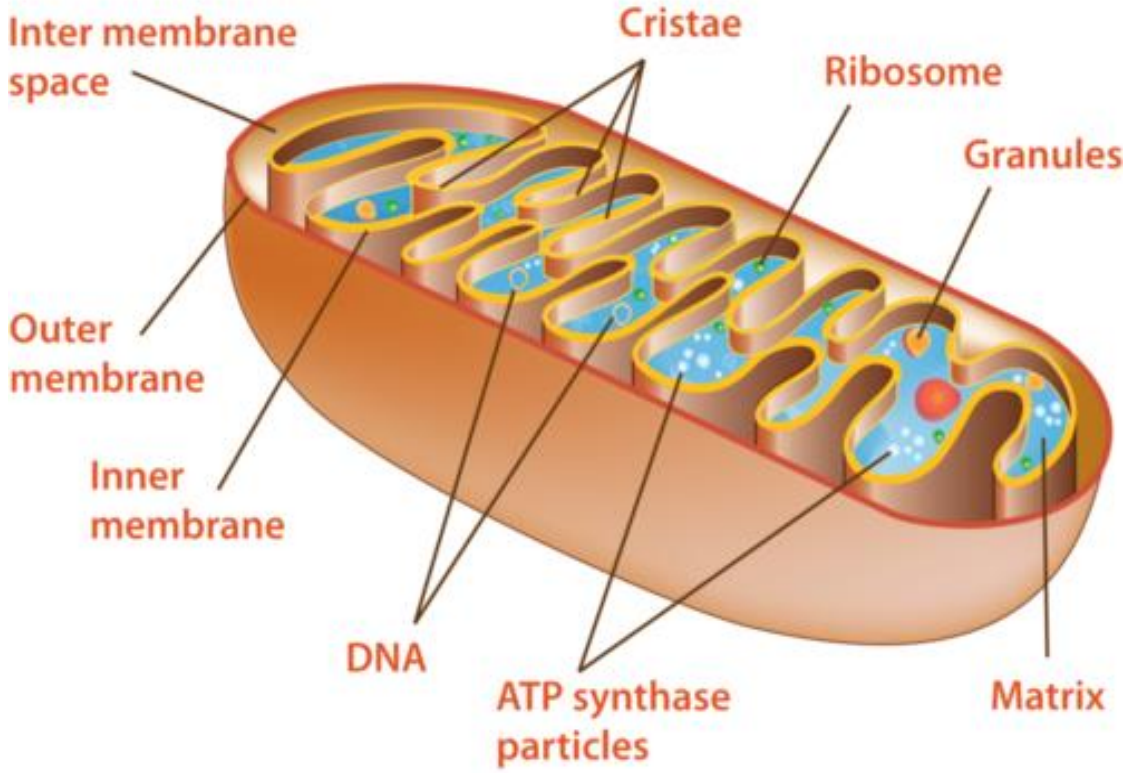

Figure 1.6: Mitochondrion inner structure. The mitochondrion contains 2 membranes (outer and inner) with an inter membrane space in between. The mtDNA is trapped within the matrix, along with ATP synthase particles.

1.4.2 Similarities between mitochondria and bacteria

Mitochondria are the only organelles of bacterial origin within eukaryotic cells[40,41], and due to their origin, they share several similarities with bacteria (**Table 1.1**). The most striking similarity is the presence of a closed circle DNA molecule, which encodes for 37 genes[42].

Table 1.1: Similarities between mitochondria and bacteria.

Characteristic	Mitochondria	Bacteria
Size (Width)	0.2-1 µ	0.2-2.0 µ
Size (Length)	1.0-4.0 µ	0.3 – 10.0 µ
Lipoprotein membrane	60-70 Å	70-80 Å
DNA shape	Closed circle	Closed circle
Inhibitor of protein synthesis	Chloramphenicol	Chloramphenicol
Ribosomes	60S-78S	70S

1.4.3 The mitochondrial genome

Mitochondria carry a DNA sequence known as mitochondrial DNA (mtDNA). The mtDNA is a circular double-stranded genome which is about 16,600 bp long in humans (**Figure 1.7**) and 16,300 bp in mouse cells, and carries a total of 37 genes, encoding 13 of the ~90 different proteins present in the respiratory chain of mammalian mitochondria (Cytb, ND1-2-3-4-4L-5-6, CO1-2-3, ATP6-8) and that are all essential for cellular ATP production by oxidative phosphorylation, 2 ribosomal RNAs (rRNAs) and 22 transfer RNAs[43] (tRNAs) which are needed for mitochondrial translation, whereas the nuclear genome encodes for thousands other proteins necessary for mitochondrial structure, function and for mtDNA replication and transcription[44]. The existence of mtDNA is explained by the widely accepted endosymbiotic theory according to which, during the course of time, ancestral bacterial genes have been transferred from the mitochondrial to the nuclear genome, as presence of orthologous genes in the mitochondrial or nuclear genomes of some species has been reported[45]. This gene transfer also explains why all proteins necessary for mtDNA replication, as well as transcription and translation of mtDNA-encoded proteins, are encoded in the nucleus.

Currently, there are a few theories regarding why mitochondria have retained their genetic material, and why elaborate enzymatic machineries are necessary to replicate and express a separate genome containing only a few genes. For example, it has been suggested that due to the fact that some hydrophobic proteins are difficult to import across the mitochondrial membranes, they must be produced within the mitochondrion[46].

In mammalians, mtDNA is maternally inherited and mitochondria in mammalian sperm are destroyed by ubiquitination inside the oocyte cytoplasm and later on subjected to proteolysis during preimplantation development[47]. This usually blocks the transmission of paternal mtDNA, although it has been reported that interspecific crosses of mice can lead to transmission of low levels of paternal mtDNA[48]. A somatic mammalian cell contains ~1000-10,000 copies of mtDNA, which are continuously turned over and replicated during the entire cell cycle, displaying no strict phase specificity as is the case with nuclear DNA synthesis[49]. In mammals, oxidative stress results in stabilization of peroxisome proliferator-activated receptor γ-coactivator 1α (PGC1α), which activates the transcription of several nuclear encoded transcription factors, including nuclear respiratory factor 1 (NRF1). PGC1α and NRF1 form a complex that in turn up-regulates transcription of transcription factor of activated mitochondria (TFAM) and multiple members of mitochondrial respiratory chain complexes[50].

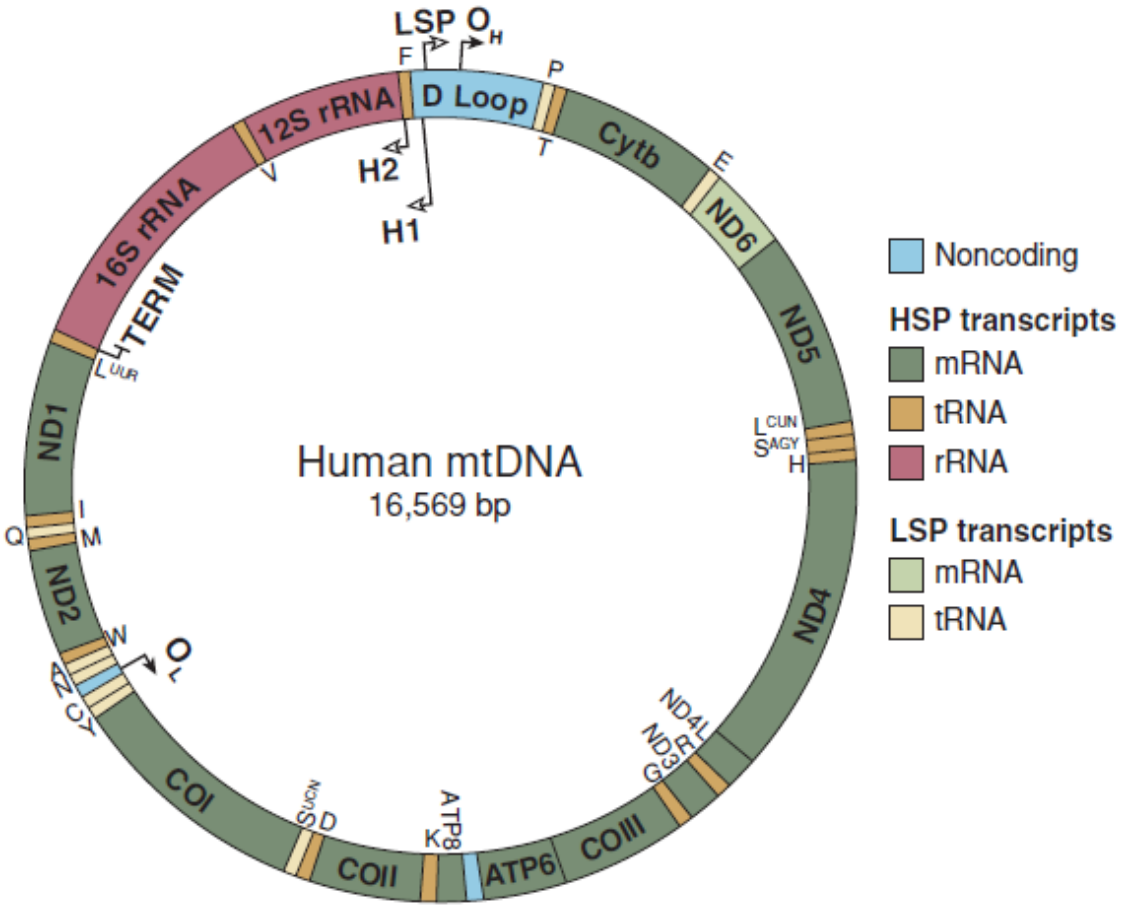

Figure 1.7: Map of human mtDNA. Transcription starting at the Light strand promoter (LSP) produces the NADH-ubiquinone oxidoreductase chain 6 (ND6) mRNA molecule and primers for initiations of DNA synthesis at O_H, whereas heavy strand transcription is initiated from two sites, H1 and H2. Each of the protein and rRNA genes is immediately flanked by at least one tRNA gene, and excision of tRNA molecules is required to produce mature mRNA and rRNA molecules. Key abbreviations: HSP, heavy strand promoter; LSP, light strand promoter, O_H, origin of replication of the heavy strand; O_L, origin of replication of the light strand; H1, heavy strand promoter 1; H2, heavy strand promoter 2. Figure taken from Falkenberg M et al, *DNA Replication and Transcription in Mammalian Mitochondria*, Annu Rev Biochem, 2007[43].

1.4.4 Mitochondria in inflammation

As previously mentioned, mtDNA has many similarities with bacterial DNA because of their shared common ancestry. Increasing evidence demonstrates mtDNA to be a potent danger signal that is recognised by the innate immune system and can directly modulate the inflammatory response through inflammatogenic unmethylated CpG motifs[51-53]. Freely circulating mtDNA can be detected, and studies have associated mtDNA in plasma and serum with several diseases including HIV[54], rheumatoid arthritis[55], septic shock[56], liver failure[57], stroke[58-60], several types of cancer[61-63] and heart disease[64-67].

In the heart, damaged mitochondria are usually degraded by autophagy, which acts as an adaptive mechanism to protect the tissues from haemodynamic stress[33], and involves the sequestration of cytoplasmic contents in a double-membraned vacuole, the autophagosome and the fusion of the autophagosome with the lysosome[68]. A recent study showed that when mitochondrial DNA escapes from the autophagy process, it can be recognized by TLR9 receptors, thereby triggering the cascade of signals that lead to inflammation and contribute to heart failure[36]. Thus, mtDNA methylation may also play a role in its ability to activate the TLR9 receptor, but the mechanisms have been infrequently studied.

1.5 Epigenetics

1.5.1 Definition and epigenetic marks

An epigenetic mechanism is defined as any mitotically heritable change which does not alter the genomic sequence but results in different gene expression potential[69]. In mammalians, all cells in the body carry the same DNA complement, and highly orchestrated epigenetic mechanisms facilitate the complex patterning required to ensure normal development and support stable regulation of appropriate patterns of gene expression in diverse cell types. All these mechanisms are highly regulated by a large number of proteins that establish, read, and erase specific epigenetic modifications, thereby defining where and when transcriptional machinery can access the primary DNA sequences to drive normal growth and differentiation.

In the nucleus, there are several types of epigenetic marks that work in concert in order to drive appropriate gene expression: DNA methylation[70] and modifications of histone proteins[71] (**Figure 1.8**) are the main marks, but non-coding RNAs (ncRNAs)[72] and other complementary and unique mechanisms also exist[73,74]. Though these mechanisms are often described separately, it is worth mentioning that there is cross-talk between the different marks to regulate the epigenome[75,76]. Epigenetic mutations that arise can lead to a variety of disorders, and environmental factors such as maternal starvation during foetal development can result in epigenetic alterations that persist through adulthood and can contribute to late-onset disorders such as cardiovascular disorders and type 2 diabetes[77-79].

Recently, the ENCODE (ENCyclopedia Of DNA Elements) Project was born as a large collaborative effort to define all of the functional elements in the human genome, and over the past few years several data sets of transcription, histone

modifications, and additional protein binding data were published[80,81]. Since this project's main focus is the methylation of mtDNA sequences, the phenomenon of DNA methylation will be described in detail in the upcoming chapter.

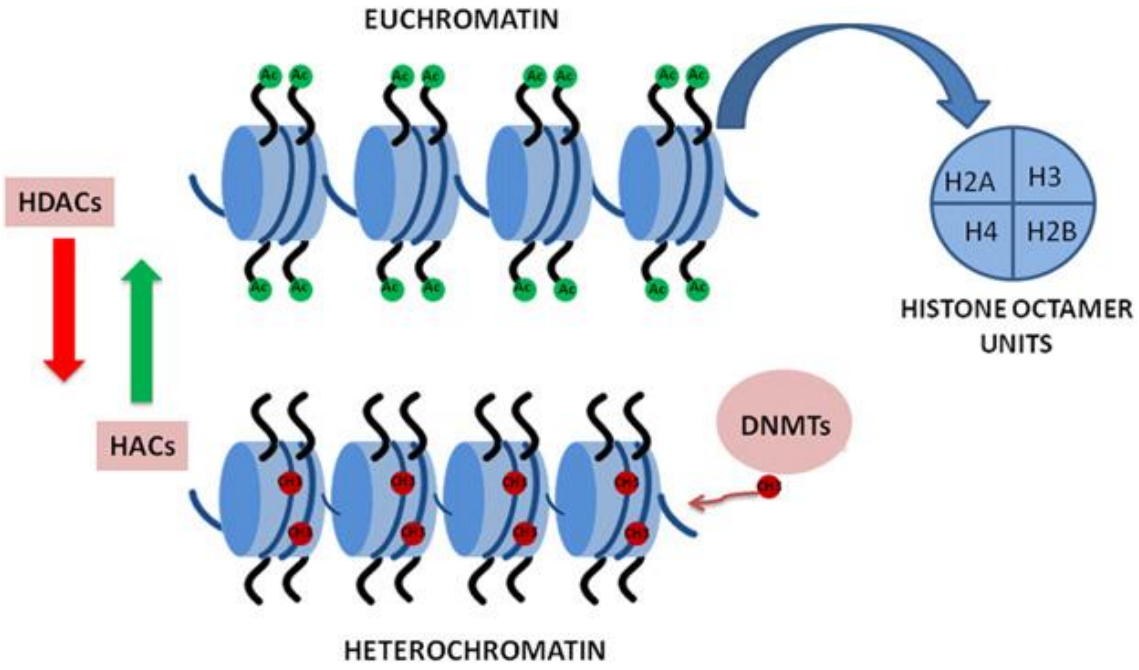

Figure 1.8: Covalent modifications of histone proteins and DNA methylation. Histone modifications are regulated by several enzymes including hystone acetyltransferases (HACs) and deacetylases (HDACs). Acetylation of histone proteins results in a relaxed state of chromatin (euchromatin) and is associated with active transcription, whilst deacetylation of histone proteins and methylation of DNA is a hallmark of a condensed state of chromatin (heterochromatin), which is associated with transcriptional repression. Abbreviations: HACs, histone acetyltransferases; HDACs, hystone deacetylases; DNMTs, DNA methyltransferases. Figure taken from Inbarg-Feigenberg M. et al, *Basic concepts of epigenetics*, Fertility and Sterility, 2013[82].

1.5.2 DNA methylation principles

Among the epigenetic processes, DNA methylation is the best understood epigenetic adaption and the most common DNA modification[83]. DNA methylation at the 5 position of cytosine has the specific effect of reducing gene expression and has been found in every vertebrate examined. In adult somatic cells, DNA methylation typically occurs in a CpG dinucleotide context, as non-CpG methylation is prevalent in embryonic stem cells[84].

This reversible process is a result of the enzymatic activity of the DNMT family, which catalyses the transfer of a methyl group from S-adenosyl methionine (SAM) to cytosines in CpG dinucleotides. First, methionine receives an adenosine group from ATP, a reaction catalysed by S-adenosyl-methionine synthetase, to give SAM. SAM then transfers the methyl group to an acceptor molecule, (i.e., DNMT as an intermediate acceptor in the process of DNA methylation). Two methylated cytosine-derived bases, 5-methylcytosine (5mC) and 5-hydroximethylcytosine (5hmC), have been detected in the DNA. 5mC is derived from incorporation of a methyl group at position 5 of cytosine (mediated by DNMTs), whereas 5 hmC is produced from 5mC through a hydroxymethylation reaction catalysed by the Ten-Eleven translocation (TETs) family of proteins[85] (**Figure 1.9**).

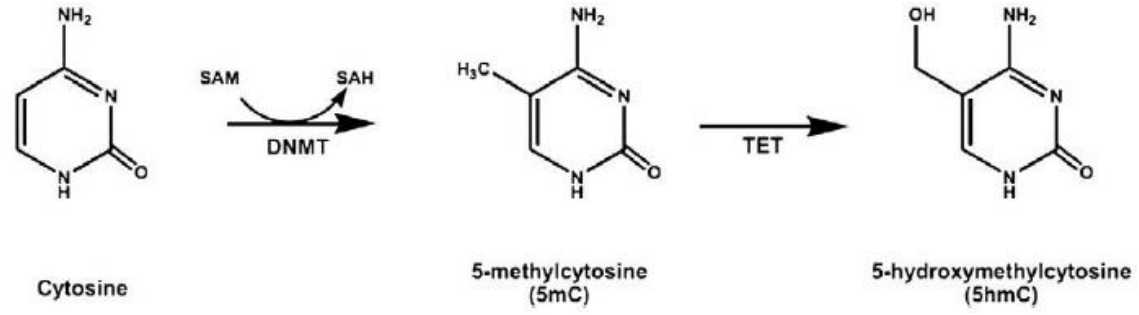

Figure 1.9: Cytosine methylation and hydroxymethylation. Abbreviations: DNMT, DNA methyltransferase; SAH, S-Adenosyl Homocysteine; SAM, S-Adenosyl Methionine; TET, Ten-Eleven translocation methylcytosine dioxygenase.

1.5.3 DNA methyltransferases

The DNMT family of enzymes catalyse the transfer of a methyl group to DNA. DNA methylation serves a wide variety of biological functions, and all the known DNA methyltransferases use SAM as the methyl donor. DNMTs can be divided into three different groups on the basis of the chemical reactions they catalyse:

- m6A, that generate N6-methyladenine
- m4C, that generate N4-methylcytosine
- m5C, that generate C5-methylcytosine

The first two groups of methyltransferases (m6A and m4C) are only found in prokaryotes and will not be discussed. On the other hand, C-5 cytosine-specific DNA methyltransferases (m5C) are found in some lower eukaryotes, in most plants, and in animals. These methyltransferases can specifically methylate the C-5 carbon of cytosines in DNA to produce C5-methylcytosine[86]. Three active DNMTs have been identified in mammals: DNMT1, DNMT3A, and DNMT3B. A fourth enzyme of the same family, previously known as DNMT2, is not a DNA methyltransferase as it does not have enzymatic activity[87]. DNMT3A and DNMT3B are “de novo” methyltransferases and can methylate unmethylated cytosines. These enzymes are mainly expressed in early embryonic development and set up the pattern of methylation[88]. DNMT1 is the most abundant DNA methyltransferase in mammalian cells, and considered to be the key maintenance methyltransferase in mammals[89]. This maintenance methyltransferase adds methylation to DNA when one strand is already methylated. DNMT1 works throughout the life of the organism to maintain the methylation pattern that had been established by the de novo methyltransferases.

1.5.4 DNMT1 in mitochondria

Recently, Shock et al[90] reported the presence of 5-hydroxymethylcytosine (5hmC), as well as revealing a 5' flanking genomic DNA sequence upstream of the published transcription start sites[91] for both human and mouse DNMT1 which was in-frame with the highly conserved amino acid sequence of DNMT1. This upstream sequence includes two additional in-frame codons for methionine (ATG), each in a moderate context for ribosome binding. Overexpression of this 1st-to-3rd ATG sequence (both mouse and human sequence) in NIH/3T3 cells resulted in mitochondrial localisation of this leader peptide, however the study did not attempt to overexpress the full length DNMT1 cDNA with the 1st-to-3rd ATG sequence[90]. Furthermore, following a tandem affinity purification (TAP) experiment and isolation of mitochondrial fraction, they performed qPCR with mtDNA specific primers and showed that DNMT1 can bind mtDNA and change the transcription of mitochondrial-encoded proteins such as ND1 (NADH dehydrogenase subunit 1) and ND6 (NADH dehydrogenase subunit 6)[90]. Finally, this study confirmed the absence of other DNMTs, such as DNMT3A or DNMT3B, in the mitochondrial environment.

1.5.5 Mitochondrial epigenetics and cardiovascular diseases

From an era of identifying genetic markers to predicting risk of an individual for cardiac disease, genomic research has been heading toward understanding the pathophysiology of cardiovascular diseases (CVDs). CVDs are influenced by several genetic and environmental factors[92], and contribution by epigenetic mechanisms is known to be involved in the pathogenesis of several CVDs, including atherosclerosis[93,94], cardiac hypertrophy[95], arrhythmias and heart failure[96,97].

Several studies have shown that mtDNA is susceptible to 5mC and 5hmC modification[51,90,98-101], and since unmethylated mtDNA is partially responsible for triggering a TLR9-mediated inflammatogenic response, control over its methylation appears to be a potential therapeutic target for heart failure. The mitochondrial genome has already been used in studies of molecular evolution and, based on mtDNA mutations, as a biomarker[101,102]. Additionally, regulation of mitochondrial epigenetics (mitoepigenetics) has shown to have applications in diagnostics, and could also contribute to therapeutics as a predictor of response to therapy[103].

In conclusion, it is becoming apparent that research in the field of mitochondrial epigenetics has the tools to improve our understanding of the role of epigenetics in the complex mechanisms of regulation of inflammation and cardiovascular diseases, and it is expected that mitoepigenetics will provide a new conceptual vantage point to view mitochondria not only as an integral part of cell biology, but also as a key player in epigenetic interactions of an organism with these pathologies.

1.6 Research hypothesis and aims

The hypothesis of this study is that DNMT1 might affect mtDNA methylation patterns, thus affecting stimulation of TLR9 by mtDNA containing unmethylated CpG motifs and production of proinflammatory cytokines. Therefore, the aim of this study is to elucidate the role of a DNA methyltransferase, DNMT1, at a mitochondrial level. To achieve this aim, my objectives were to:

1. Obtain DNMT1 overexpression plasmids with different features.
2. Confirm DNMT1 ability to localise at a mitochondrial level.
3. Investigate the methylation status of mtDNA following DNMT1 overexpression.
4. Develop and refine new tools for DNMT1 overexpression
5. Investigate DNMT1 interaction with other DNMTs and other potential co-factors.

Chapter 2 : General materials and methods

2.1 Cell culturing

2.1.1 HEK293A cells

Human embryonic kidney cells (HEK293A, Invitrogen Life Technologies®) were cultured in 75 cm^2 "T75" flasks (Thermo Fisher Scientific®, 178905) with Dulbecco's modified eagle medium (DMEM, Sigma-Aldrich® D6546) containing 10% foetal bovine serum (FBS, Gibco®, 10270-106) and 1% L-Glutamine-Penicillin-Streptomycin solution (PSG, Sigma-Aldrich®, G1146). Cells were incubated at 37ºC with 5% CO_2 and passaged at approximately 80% confluency. To passage cells, media was aspirated off the flask, and 5 ml phosphate buffered saline (PBS, Sigma-Aldrich®, D8537) was used to rinse the cells. 5 ml 0.5 M Ethylenediaminetetraacetic acid (EDTA) was added to the cells, which were then incubated for 5 minutes at 37ºC. Then, 5 ml culture medium were added and the suspended cell solution was collected in a 15 ml Falcon™ conical centrifuge tube (Fisher Scientific®, 339650) and centrifuged at 100 g for 5 minutes. The supernatant was discarded and the pellet of cells was resuspended in 10 ml of pre-warmed culture medium. Finally, 2 ml of cell mixture was diluted with 8 ml of culture medium and seeded into a new T75 flask.

2.1.2 H9C2 cells

Rattus norvegicus cardiomyoblasts (H9C2, ATCC® CRL-1446™) were cultured in 75 cm^2 "T75" flasks with DMEM containing 10% FBS and 1% PSG. Cells were incubated at 37ºC with 5% CO_2 and passaged at approximately 80% confluency. To passage cells, media was aspirated off the flask and 5 ml PBS was used to rinse the cells. 1ml Trypsin-EDTA solution (Sigma-Aldrich®, T4049) was diluted in 4 ml PBS and added to the cells, which were then incubated for 5 minutes at 37ºC. Then, 5 ml culture medium were added and the suspended cell solution

was collected in a 15 ml Falcon™ conical centrifuge tube and centrifuged at 100 g for 5 minutes. The supernatant was discarded and the pellet of cells was resuspended in 10 ml of pre-warmed culture medium. Finally, 2 ml of cell mixture was diluted with 8 ml of culture medium and seeded into a new T75 flask.

2.1.3 MCE cells

Mouse cardiac endothelial cells (MCEC, CEDARLANE®, CLU510) were cultured in 175 cm^2 "T175" flasks (Thermo Fisher Scientific®, 178883) with DMEM containing 5% FBS, 1% 200mM L-Glutamine solution (Sigma-Aldrich®, G7513) and 1% 1M 4-(2-hydroxyethyl)-1-piperazineethanesulfonic acid (HEPES, Gibco®, 15630080). Cells were incubated at 37°C with 5% CO_2 and passaged at approximately 80% confluency. To passage cells, media was aspirated off the flask and 10 ml PBS was used to rinse the cells. 2ml Trypsin-EDTA solution were diluted in 8 ml PBS and added to the cells, which were then incubated for 5 minutes at 37°C. Then, 10 ml culture medium were added and the suspended cell solution was collected in a 50 ml Falcon™ conical centrifuge tube (Fisher Scientific®, 339650) and centrifuged at 100 g for 5 minutes. The supernatant was discarded and the pellet of cells was resuspended in 10 ml of pre-warmed culture medium. Finally, 2 ml of cell mixture was diluted with 18 ml of culture medium and seeded into a new T175 flask.

2.2 Molecular cloning and subcloning principles and methods

Molecular cloning is an umbrella term that is defined as a set of experimental methods of molecular biology that are used to assemble recombinant DNA molecules and to direct their replication within host organisms (i.e. bacteria). Subcloning is a technique used to move a particular DNA sequence from a parent vector to a destination vector. Restriction enzymes are used to excise the gene of interest (the insert) from the parent. The insert is then purified in order to isolate it from other DNA molecules. The same restriction enzymes can also be used to digest (cut) the destination. The idea behind using the same restriction enzymes is to create complementary sticky ends, which will facilitate ligation later on. Below follows the list of the cloning techniques that have been used to obtain the plasmid vectors:

- Bacterial transformation
- Mini and maxi preparations
- Enzyme digestion
- DNA gel electrophoresis
- DNA gel extraction
- DNA ligation
- DNA sequencing

2.2.1 Bacterial transformation

Bacterial transformation was performed using MAX Efficiency® DH5α™ competent cells (Thermo Fisher Scientific®, 18258012) in order to amplify the

constructs at the end of each cloning step. Briefly, DH5α™ cells were thawed on ice for 2 minutes, then 1-2 µl of sample (corresponding to 50-500 ng of construct) was added to the cells, and the mixture was incubated on ice for another 10-30 minutes. After this, in order to allow the construct to enter the bacterial membrane, heat shock at 42ºC was applied for 45 second. Then the cells were put on ice for another 3 minutes, resuspended in 1 ml S.O.C. Medium (Thermo Fisher Scientific®, 15544034) and incubated at 37ºC for 1 hour. Finally, the cells were spinned at 8000 rpm for 3 minutes, 900 µl of supernatant was discarded and the pellet was resuspended in the remaining 100 µl, plated onto LB agarose plates with antibiotic selection (depending on the construct) and incubated overnight at 37ºC.

The antibiotic allows for positive selection of colonies formed from single cells carrying the construct of interest which is expressing the antibiotic resistance gene and therefore allows the cells to survive. The next day, colonies were harvested with a toothpick and incubated in 2 ml LB medium (with antibiotic selection) overnight at 37ºC. LB agarose plate and LB medium composition are shown (**Table 2.1** and **Table 2.2**).

Table 2.1: LB plates reagents. All reagents were added in a 500 ml heat-resistant glass bottle and autoclaved. Then, after cooling down, antibiotic was added and the mixture was poured into sterile petri-dish and stored at 4ºC.

LB Plates	Amount
LB Broth powder (Sigma Aldrich®, L3522)	12.5 g
Bacto Agar (BD®, 214010)	7.5 g
dH_2O	500 ml

Table 2.2: LB Broth reagents. All reagents were added in a 500 ml heat-resistant bottle and autoclaved. Then, after cooling down, the bottle was stored at 4ºC. For better antibiotic preservation, 50 ml working stocks were created.

LB liquid	Amount
LB Broth powder (Sigma Aldrich®, L3522)	12.5 g
dH_2O	500 ml

2.2.2 Mini preparations (Miniprep)

The plasmids were extracted from the cells using QIAprep® Spin Miniprep Kit (Qiagen®, 27106). A benchtop centrifuge (Eppendorf®, 5415R) was used for all the centrifuging steps.

For each colony, 1 ml of the LB medium containing DH5α™ cells was collected in a 1.5 ml Eppendorf tube and centrifuged at 8000 rpm for 3 minutes. Supernatant was discarded. The pellet was resuspended in 250 µl Buffer P1 with RNase A (100 µg/ml) and lysed with 250 µl Buffer P2. Then, to release the plasmid DNA, 350 µl of precipitation Buffer N3 were added to the samples and centrifugation at 13,000 rpm for 10 minutes was performed. Supernatant containing the plasmid DNA was applied to a QIAprep 2.0 spin column by pipetting and centrifuged at 13,000 rpm for 1 minute in order to bind it to the column. The column was then washed with 750 µl Buffer PE and centrifuged twice at 13,000 rpm for 1 minute to remove the residua wash buffer. Finally, 30 µl of dH_2O were applied onto the column and the DNA was eluted and collected in a clean 1.5 microcentrifuge tube through incubation at room temperature for 5 minutes and centrifugation at 13,000 rpm for 1 minute. The DNA concentration of the sample was measured through a NanoDrop 2000 UV-Vis Spectrophotometer (Thermo Scientific®), then the sample was stored at -20ºC or used for the next subcloning steps.

2.2.3 Enzyme digestion

Every subcloning step was performed by digesting the sequence of interest with the following conditions:

- Up to 1/10 ratio of digestion enzymes in 20 µl final volume
- 200-500 µg of DNA
- 2 µl of digestion buffer (New England Biolabs)
- 1.5 hrs incubation at 37ºC

2.2.4 DNA gel electrophoresis

Following DNA digestion, DNA gel electrophoresis was performed running the samples at 120V for 30 minutes with Tris/borate/EDTA (TBE) buffer (**Table 2.3**) in 1% agarose gel using PowerPac™ Basic Power Supply (Bio-Rad™, 1645050).

Table 2.3: 10X TBE buffer solution reagents.

TBE buffer solution reagents	Amount
Trizma base	108 g
Boric acid	55 g
0.5M EDTA	40 ml
dH_2O	960 ml

2.2.5 DNA gel extraction

DNA was extracted from the gel using a QIAquick™ gel extraction kit (Qiagen®, 28704). Relevant DNA bands were visualized under UV light, cut from the gel and weighed. Then, 3 volumes of Buffer QG were added and the mixture was incubated at 50ºC for 10 minutes. Following incubation, 1 volume of isopropanol

was added to the sample, and the mixture was applied to a QIAquick spin column and centrifuged at 13,000 rpm for 1 minute, capturing the DNA fragments on the column. The column was then washed with 750 µl Buffer PE and centrifuged twice at 13,000 rpm for 1 minute. Finally, the DNA was eluted from the column by adding 30 µl water and centrifuging at 13,000 rpm for 1 minute. The DNA sample was then stored at -20ºC, or used for ligation.

2.2.6 DNA ligation

DNA ligation steps were performed using a T4 DNA ligase kit (Takara®, 2011) (**Table 2.4**). After mixing all reagents together, standard ligation was achieved through overnight incubation at 16ºC. The final DNA sample was then used for the next cloning step, starting from DH5α transformation once again. Sequencing steps have been performed by Source BioScience Labs (Cambridge).

Table 2.4: Reaction mixture for DNA ligation.

Reagent	Amount
T4 DNA ligase	4 µl
DNA insert	3 µl
DNA plasmid	1 µl

2.2.7 Maxi preparations (Maxiprep)

After obtaining the final constructs, they were amplified through maxi preparations (maxiprep) in order to obtain enough DNA amounts for overexpression experiments. Maxiprep was performed according to QIAGEN Plasmid Maxi Kit protocol (QIAGEN®, 12165), using a Sorvall® Legend RT large bench centrifuge (Sorval®, 75004373) and a high-speed Sorvall® RC-6 Plus

centrifuge (Sorvall®, 46910) with a Sorvall® SA-600 rotor (Sorvall®, SO-SA600). The high-speed centrifuge step was performed at 16500g by using Nalgene™ Oak Ridge High-Speed PPCO centrifuge tubes with sealing cap (Thermo Fisher Scientific®, 3139-0050).

2.2.8 Cloning vector: pBluescript II KS(+) features

All the subcloning steps have been performed using a pBluescript II KS (+) (**Figure 2.1**), which is a cloning vector that was designed to simplify commonly used cloning and sequencing procedures (determining expression and developing genomic libraries are some applications for which it can be used).

It contains a multiple cloning site sequence (MCS) with 18 unique restriction enzyme recognition sites and an antibiotic (ampicillin) resistance sequence for selection. Since this vector does not have a mammalian origin of replication, it cannot be used as an expression vector in mammalian cells.

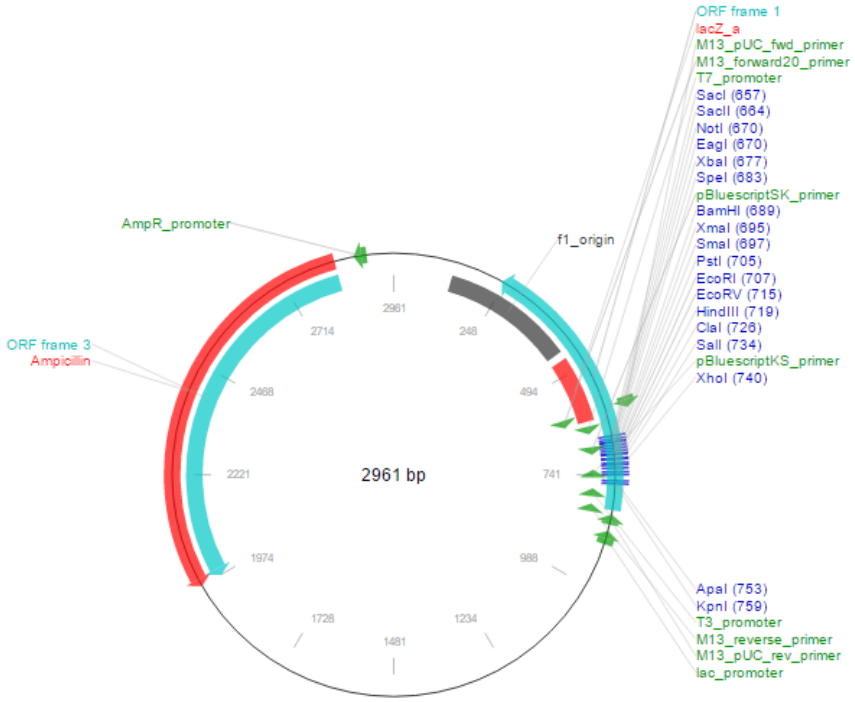

Figure 2.1: pBluescript II KS(+) features. The vector contains a gene for ampicillin resistance and a MCS, as well as M13 and T7 sites for sequencing. Figure taken from Addgene.

2.2.9 Expression vector: pCMV-SPORT6 features

The backbone vector that was used for expressing the different DNMT1 isoforms in mammalian cells is pCMV-SPORT6 (**Figure 2.2**). This vector can be directly used for expression of genes under the control of CMV promoter in mammalian cells, and it's a gateway-adapted mammalian expression vector. In pCMV-SPORT6, the expression of the insert is driven by the CMV promoter. In the sequence there is also a MCS with 16 unique restriction enzyme recognition sites and an antibiotic (ampicillin) resistance gene for screening.

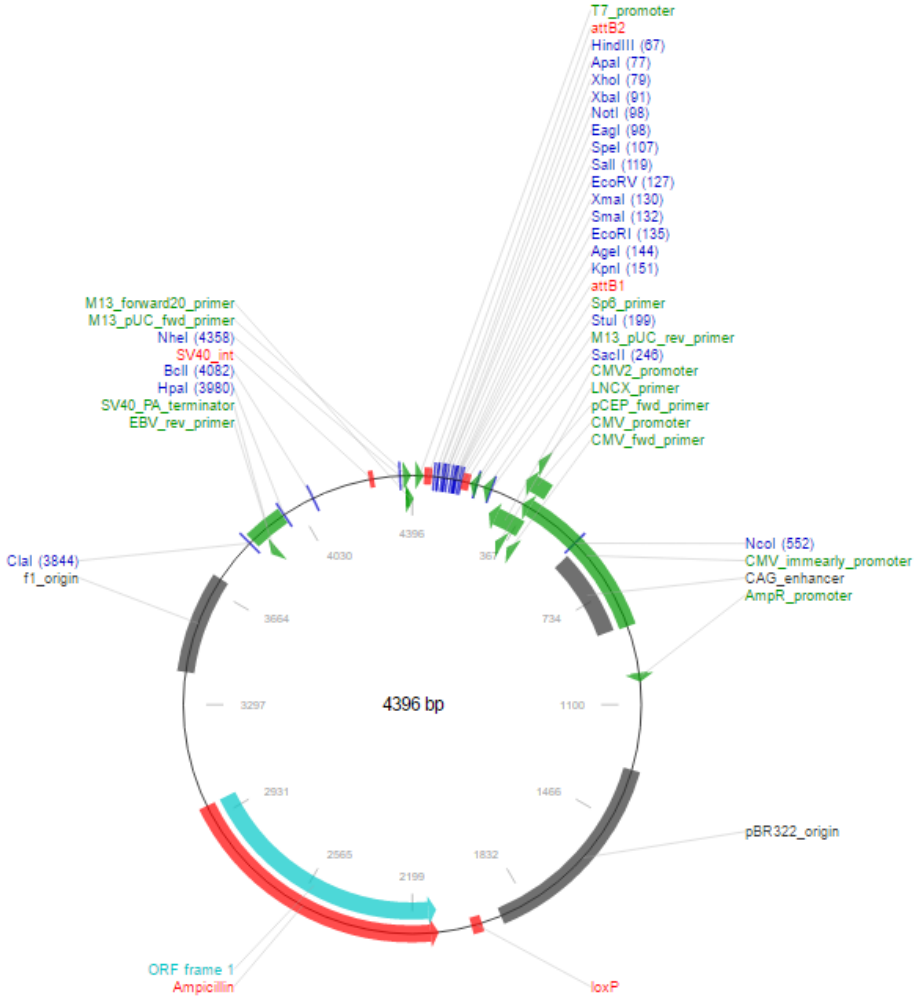

Figure 2.2: pCMV-SPORT6 features. The vector contains a gene for ampicillin resistance and a MCS, as well as M13 and T7 sites for sequencing. Furthermore, a CMV promoter for mammalian overexpression is also present. Figure taken from Addgene.

2.2.10 Original Nuclear DNMT1 vector features

An expression vector containing the mouse sequence for nuclear Dnmt1 was received from Japan, courtesy of Prof. Tajima (University of Osaka). The plasmid vector carries a CAG promoter, which is a strong synthetic promoter frequently used to drive high levels of gene expression in mammalian expression vectors, and the full length mouse nuclear DNMT1 cDNA sequence (which also carries a predicted internal nuclear localisation signal, NLS) with Myc-tag and a NLS at 5' region. The mouse nuclear cDNA DNMT1 sequence contains EcoRI sites at both 5' and 3' ends (**Figure 2.3**) which have been modified by introducing two single nucleotide mutations in the internal EcoRI digestion sites (**Figure 2.4**), but the amino acid sequence was not changed from these mutations.

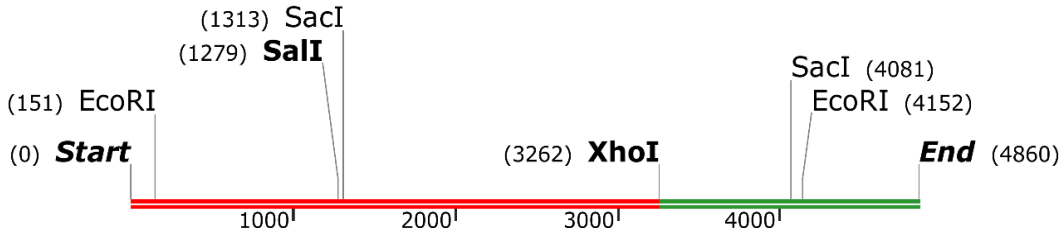

Figure 2.3: Restriction enzyme map from Mus musculus (mouse) DNMT1 original cDNA sequence. EcoRI mutations were performed at 150 bp and 4152 bp. 5' and 3' fragments are highlighted (red and green) and separated by an XhoI site, which has been used for further cloning steps.

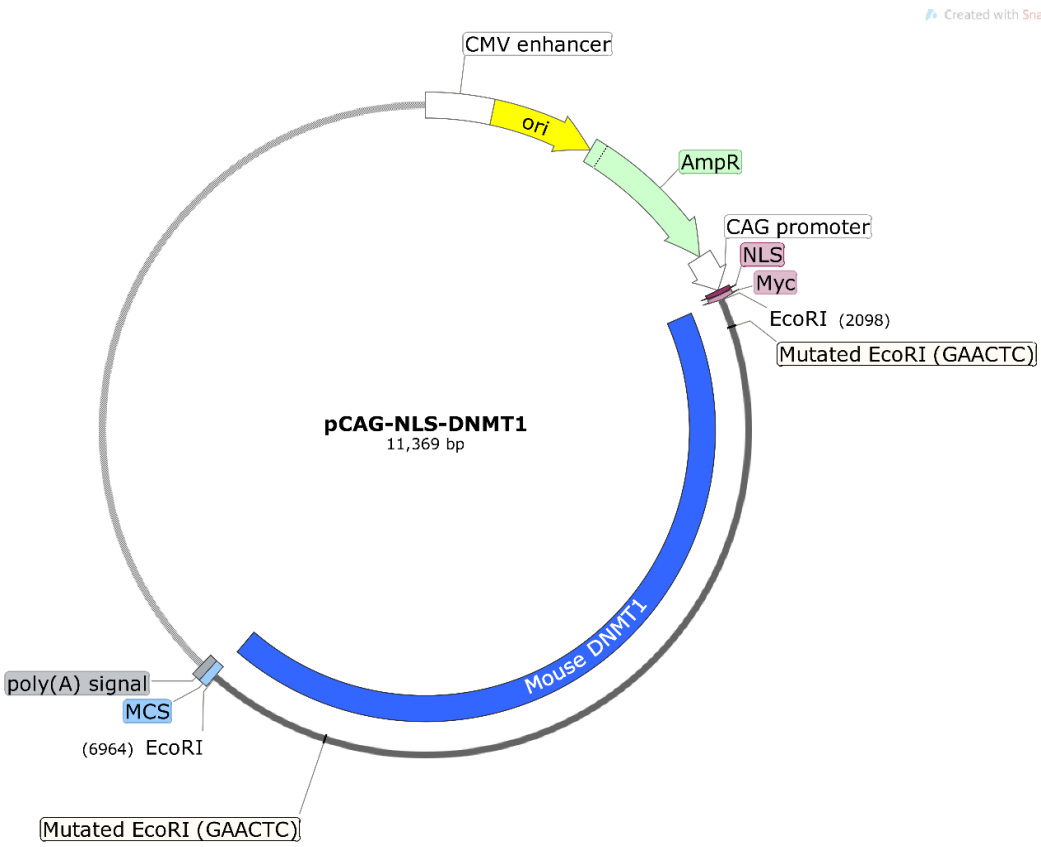

Figure 2.4: Overview of Prof. Tajima's cloning strategy. The vector contains a gene for ampicillin resistance and a MCS, as well as the mouse DNMT1 sequence. Furthermore, a CMV enhancer and CAG promoter for mammalian overexpression are also present.

2.3 Plasmid DNA transfection

2.3.1 Calcium phosphate protocol

Cells were seeded on 15 cm^2 Cellstar® tissue culture dishes (VWR®, 82050-598) and transfected at about 60-70% confluence. Two dishes were used for each transfection condition. The reagents used for the 2xBBS solution for calcium phosphate transfection are shown (**Table 2.5**).

Table 2.5: 2xBBS Solution reagents.

2X BBS Solution reagents	
NaCl (Sigma-Aldrich®, S7653)	1.6 g
Na_2HPO_4 (Sigma-Aldrich®, S7907)	0.021 g
BES (Sigma-Aldrich®, B4554)	1.1 g
dH_2O	To 100 mL

Briefly, 32 µg of DNA was resuspended in a tube containing 248 µl of 2M Calcium chloride ($CaCl_2$) solution (Sigma-Aldrich®, 449709) and 1.72 ml of dH_2O. Then, the solution was resuspended dropwise in 2 ml of 2x BBS solution and incubated at room temperature for 15 minutes. Following incubation, the final solution was poured dropwise onto the 15 cm^2 tissue culture dishes (2 ml per dish), then the dishes were incubated at 37ºC, 5% CO_2 for 48 hours prior to subcellular fractioning, with a change of culture medium 18 hours after transfection.

2.3.2 FuGene HD® protocol

For immunocytochemistry purposes, HEK293A cells were seeded in 12 well Corning® Costar® cell culture plates (Sigma Aldrich®, CLS3513). A collagen coated cover slip was added to the wells, then 20,000 cells/well were seeded in 1 ml DMEM 10% FBS, 1% PSG per well, and incubated overnight at 37ºC with 5% CO_2. Subsequently, cells were transfected with 1 µg of DNA for each well by adding 50 µg of transfection complex (8.8 µg DNA in 414 µl dH_2O and 26 µl FuGENE HD®) and incubated for 24 hours at 37ºC with 5% CO_2.

2.4 Immunocytochemistry and imaging

2.4.1 Staining, fixation and antibody incubation

Following transfection, the medium was removed from the wells, and each well was incubated for 15 minutes at 37ºC with 500 µl of culture medium with 250 nM MitoTracker® Red CMXRos staining solution (Thermo Fisher Scientific®, M7512). Staining solution was then removed and cells were fixed with a 4% paraformaldehyde PBS solution and incubated for 15 minutes at 37ºC. PBS solution was then removed and cells were washed three times with a PBS-G solution (PBS with 100mM Glycine). After removing PBS-G solution, cells were incubated for 15 minutes at room temperature with 300 µl per well of 0.2% Triton-X PBS solution.

Prior to antibody incubation, cells were incubated with 500 µl per well of 2% Bovine Serum Albumin (BSA, Sigma-Aldrich®, A7906) PBS blocking solution for 1 hour at room temperature. After removing the blocking solution, cells were incubated overnight at 4ºC with an HA-tag antibody (Cell Signalling Technology®, C29F4 Rabbit mAb #3724) diluted 1:1000 in a 2% BSA PBS solution. Subsequently, cells were washed three times with 1 ml per well of PBS solution with MgCa and incubated in the dark with 100 µl of a 1:1000 Alexa Fluor® 488 Goat Anti-Rabbit IgG secondary antibody PBS solution with 0.1% BSA for 1 hour at room temperature. Finally, wells were washed with 1 ml PBS, and cover slips were removed for mounting.

2.4.2 Mounting and cell imaging

Cover slips were labelled and mounted with VECTASHIELD® Mounting Medium with DAPI (Vector Laboratories, H1200), and cell imaging was performed using Eclipse Ti-E Inverted microscope (Nikon®) with CSU-X1 Spinning Disk Confocal

and Andor Ixon3 EM-CCD camera. Following confocal microscopy experiments, mounted slides were stored at 4ºC with light shielding.

2.5 Subcellular fractioning

The protocol for subcellular fractioning was taken from Wieckowski et al (Nature Protocols, 2009) and modified as explained below.

2.5.1 Buffers

After obtaining primary (**Table 2.6**) and fractioning buffers (**Table 2.7**), they were stored at 4 ºC. Fractioning buffers were used within 1 month to avoid degradation of mannitol and sucrose.

Table 2.6: Primary buffers for cell fractioning.

Buffer	Reagents
0.5 M Hepes	5.96 g HEPES 40 ml dH_2O
1M Tris	6.07 g Trizma base 30 ml dH_2O
0.1M EGTA	3.8 g EGTA 70 ml dH_2O

Table 2.7: Fractioning buffers for cell fractioning.

Buffer	Reagents
IB-1	50 ml IB-2 buffer 20 ul 0.1 M EGTA

IB-2	4.1 g mannitol 2.6 g sucrose 3 ml 1M Tris 80 ml dH_2O
MRB	2.28 g mannitol 500 ml 0.5M HEPES 40 mL dH_2O
STM	4.28 g sucrose 2.5 ml 1M Tris-HCl 125 µl 2M $MgCl_2$ 47.5 ml dH_2O
NET	2 ml 0.5M HEPES 37.5 µl 2M $MgCl_2$ 25 ml 1M NaCl 20 µl 0.5M EDTA 10 ml 100% glycerol 5 ml 10% Triton-X 8 ml dH_2O

2.5.2 Measurement of pH

Buffers IB-1, IB-2 and MRB were equilibrated to pH 7.4 using a BASIC pH Meter (Denver Instrument).

2.5.3 Initial fractioning protocol

After removing the culture medium from the tissue culture dishes, the cells were washed in ice-cold PBS (10 ml for each 15 cm^2 tissue culture dish). PBS was

then aspirated and cells were scraped and collected in a 50 ml falcon tube with 10 ml ice-cold PBS. Subsequently, samples were centrifuged for 5 minutes at 600g (4ºC), PBS was withdrawn from the falcon tubes, and cell pellets underwent another cycle of resuspension and centrifuging. Finally, PBS was withdrawn from the falcon tubes and the cell pellets were resuspended in 400 µl IB-1 buffer, and homogenized with a Teflon-glass homogenizer-potter system undergoing 10x 2 seconds-long stroke/pause cycles at 1000 rpm.

Homogenized cells were moved into a new 1.5 ml Eppendorf tube (tube #1), where 10 up-and-down pipetting cycles with a 1 ml tip were performed. After that, samples were centrifuged for 3 minutes at 500g (4ºC), and supernatant was moved to a fresh 1.5 ml Eppendorf tube (tube #2). Pellet from tube #1 was resuspended in 350 µl IB-1 buffer with 20 up-and-down pipetting cycles using a 1 ml tip, and centrifuged for 3 minutes at 500g (4ºC). Supernatant was added to tube #2. Again, remaining pellet from tube #1 was resuspended in 300 µl IB-1 buffer with 20 up-and-down pipetting cycles using a 1 ml tip, and centrifuged for 3 minutes at 500g (4ºC). Supernatant was added to tube #2. Then, final pellet from tube #1 was used to isolate nuclear fraction.

2.5.4 Mitochondrial fractioning

Tube #2 was centrifuged for 5 minutes at 600g (4ºC) and supernatant was moved to a fresh 1.5 ml Eppendorf tube (tube #3). Tube #3 was then centrifuged for 10 minutes at 7000g (4ºC), supernatant was discarded and the remaining pellet was resuspended in 500 µl IB-2 buffer and centrifuged for 10 minutes at 7000g (4ºC). Supernatant was discarded once more, and the remaining pellet containing the purified mitochondrial fraction was resuspended in 50 µl MRB buffer and moved to a fresh 1.5 ml Eppendorf tube.

2.5.5 Nuclear Fractioning

Pellet from tube #1 was resuspended in 500 µl STM buffer with protease inhibitors (PI) (Sigma-Aldrich®, P8340) and centrifuged for 15 minutes at 800g (4ºC). The supernatant was discarded, and the remaining pellet was resuspended in 300 µl STM buffer with PI, vortexed for 15 seconds, and centrifuged 15 minutes at 500g (4ºC). Again, supernatant was discarded and pellet was resuspended in 300 µl STM buffer with PI, vortexed for 15 seconds, and centrifuged for 15 minutes at 1000g (4ºC). Supernatant was discarded once more, and pellet was resuspended in 200 µl NET buffer with PI, vortexed for 15 seconds, and let rest on ice for 30 minutes. After that, solution was sonicated for 15 seconds and centrifuged for 30 minutes at 9000g (4ºC). Finally, the supernatant containing the nuclear fraction was moved to a new 1.5 ml Eppendorf tube.

2.6 Protein extraction from whole cell lysates

Cells were cultured in 6 well Corning® Costar® cell culture plates (Sigma-Aldrich, CLS3516). Lysis buffer containing a protease inhibitor (PI) cocktail was prepared (**Table 2.8**). Culture medium was aspirated and the wells were washed with 1 ml ice-cold PBS each. Cells were then scraped, collected in a fresh 1.5 ml Eppendorf tube and centrifuged at 13000 rpm and 4ºC for 5 minutes. Supernatant was discarded, and the pellet was resuspended in 50 µl cold lysis buffer. Samples were sonicated for 10 seconds using a SFX 150 Branson Sonifier® (Emerson®) and centrifuged at 13000 rpm and 4ºC for 5 minutes. Then, the supernatant containing the protein fraction was moved to a new 1.5 ml Eppendorf tube and stored at -80ºC.

Table 2.8: Lysis buffer reagents.

Reagent	Final concentration
Tris-HCl (pH7.4)	50 mM
NaCl	150 mM
EDTA	1 mM
EGTA	1 mM
Na Orthovanadate	2.5 mM
Na Pyrophosphate	2.5 mM
Na β-glycerophosphate	1 mM
TritonX-100	1%
PMSF	1 mM
Protease Inhibitors	1:1000

2.7 Protein quantification

Protein quantification was performed using a Pierce™ BCA Protein Assay Kit (Thermo Fisher Scientific®, 23225). Briefly, 10 µl of each protein sample were diluted 5 fold in lysis buffer with protease inhibitors (PI). Then, 20 µl of 1:5 samples were incubated with 160 Pierce™ Reagent A/Reagent B working solution at 37ºC for 30 minutes, using a 96 well Corning® Costar® cell culture plate (Sigma-Aldrich®, CLS3595). BCA standards were used for comparison.

Then, the 562 nm absorbance was measured using an Infinite® 200 PRO absorbance reader (Tecan Life Sciences), and the samples' values were then interpolated with the standard values in order to determine the protein concentration of each sample.

2.8 Western blotting

2.8.1 Sample preparation and SDS-PAGE

After measuring the protein concentration, 20-30 µg of protein sample was mixed with 5x sample buffer (**Table 2.9**) with 5% 2-mercaptoethanol (2-ME, Sigma-Aldrich®, M3148). Samples were either heated to 95ºC for 5 minutes, then loaded onto 7.5% and 10% Sodium dodecyl sulphate (SDS) gels (**Table 2.10**) with SDS-PAGE buffer (**Table 2.9**) and Precision Plus Protein Dual Xtra Standards (Bio-Rad®, 161-0377) and Sodium dodecyl sulphate-Polyacrylamide gel electrophoresis (SDS-PAGE) was performed for 80 minutes at 120 V.

Table 2.9: List of solutions used for sample preparation and Western blotting.

Buffer	Reagents
Sample buffer (5X)	10 ml 0.1% bromophenol blue 5 ml 1M sodium phosphate (pH 7.0) 50 ml glycerol 2 g SDS powder dH_2O to 100 ml
SDS-PAGE buffer	3 g Tris 14.5 g glycine 1 g SDS powder dH_2O to 1 l
Transfer buffer	2.9 g Tris 14.5 g glycine 200 ml methanol dH_2O to 1 l

TBS	2.42 g Tris 8 g NaCl HCl to pH 7.4 dH_2O to 1 l
TBS-T	TBS with 0.1% Tween20

Table 2.10: List of gels for Western blotting

Gel type	Reagent
7.5% SDS-Page	1.5 ml 30% acrylamide 1.5 ml 1.5 M Tris HCl (pH 8.8) 30 µl 20% SDS 45 µl 10% ammonium persulfate 15 µl TEMED dH_2O to 6 ml
10% SDS-Page	2 ml 30% acrylamide 1.5 ml 1.5 M Tris HCl (pH 8.8) 30 µl 20% SDS 45 µl 10% ammonium persulfate 15 µl TEMED dH_2O to 6 ml
Stacking gel	0.9 ml 30% acrylamide 1.5 ml 0.5 M Tris HCl (pH 6.8) 30 µl 20% SDS 45 µl 10% ammonium persulfate 20 µl TEMED dH_2O to 6 ml

2.8.2 Wet transfer and densitometric analysis

Proteins were transferred from SDS-PAGE onto nitrocellulose membrane (Thermo Fisher Scientific®, 15269794) at 0.2 A for 2 hours with transfer buffer (Table 2.9). After transfer, the membrane was rinsed twice with TBS (Table 2.9) and blocked for 1 hour at room temperature using Odyssey® blocking buffer (LI-COR Biosciences®, 927-40000). After blocking, membranes were incubated overnight at 4ºC with the primary antibody diluted in the blocking reagent. Next day, the membranes were washed as described earlier, followed by secondary antibody incubation at room temperature for 1 hour. Membranes were washed as before and developed using the Odyssey Clx imager (LI-COR Biosciences®). Image Studio Lite software version 5.2 (LI-COR Biosciences®) was used to analyse images and perform densitometric analysis. Primary and secondary antibodies used for Western blotting are listed (**Table 2.11**).

Table 2.11: List of antibodies used for Western blotting.

Antibody	Dilution (in blocking buffer)	Company and catalogue number
Rabbit anti-mouse/human DNMT1	1:1000	CST, 5032
Rabbit anti-mouse/human DNMT3A	1:1000	CST, 2160
Rabbit anti-HA tag	1:1000	CST, 3724
Mouse anti-mouse/human αtubulin	1:5000	CST, 3873
Mouse anti-human lamin A/C 4C11	1:2000	CST, 4777
Rabbit anti-mouse/human VDAC	1:1000	CST, 4661
Goat anti-rabbit IRDye 800CW	1:15000	Li-Cor, 925-32211
Goat anti-mouse IRDye 680RD	1:15000	Li-Cor, 925-68070

2.9 Sequencing

Miniprep samples were resuspended in UltraPure™ DNase/RNase-free distilled water (Thermo Fisher Scientific®, 10977-35) in a final concentration of 100 ng/µl, then labelled and shipped to a Source BioScience facility where Sanger sequencing was performed overnight. Sequencing data was received through email, and analysed using BioEdit Sequence Alignment Editor Software.

2.10 Software for plasmid design

All figures of plasmid have been created using SnapGene® software (from GSL Biotech; available at snapgene.com).

Chapter 3 : DNMT1 cloning and DNMT1 localisation studies in HEK293A cells

3.1 Introduction

3.1.1 DNA (cytosine-5)-methyltransferase 1 (DNMT1) overview and methylation features

The DNA of vertebrates contains tissue-specific patterns of methylated cytosine residues, which are transmitted though the activity of DNA (cytosine-5)-Methyltransferase 1 (DNMT1) on hemimethylated DNA[104]. DNMT1 is the most abundant DNA methyltransferase in mammalian cells, and considered to be the key maintenance methyltransferase in mammals[89]. Maintenance methyltransferases add methylation to DNA when one strand is already methylated, and work throughout the life of the organism to maintain the methylation pattern that had been established by the de novo methyltransferases (DNMT3A and DNMT3B)[88]. The crystal structures of both mouse and human DNMT1 protein have been solved. These two proteins share 85% sequence identity and similar structure, which suggest a common mechanism of action[105]. Mouse DNMT1 is a 1620 residue multimodular protein composed of a replication foci-targeting domain (RFD), a DNA-binding CXXC domain, a pair of bromo-adjacent homology (BAH1 and BAH2) domains, and a C-terminal catalytic domain with methyltransferase activity that also contains a Target recognition domain (TRD) [105] (**Figure 3.1** and **Figure 3.2**).

The first 1,100 amino acids constitute the regulatory domain of the enzyme, and the remaining residues constitute the catalytic domain. Both domains are required for the catalytic function of DNMT1. All sequence specific contacts with DNA are made via the CXXC domain (residues 650-699), which targets both the major and minor groove of the DNA over a CpG-containing 4-bp footprint. A loop segment (Arg684 -Ser685 -Lys686 -Gln687) from the CXXC domain penetrates into the major groove and forms base-specific and phosphodiester intermolecular

interactions. Lys686 and Gln687 contact the guanine bases in the CpG dinucleotide, whereas Ser685 Lys686 interact with the cytosine bases. However, these are not the only interactions made with the DNA, as the CXXC domain also contains recognition sites of salt bridges from arginines to the phosphodiester backbone of the DNA. The CXXC domain shares similarities with CXXC domains of histone methyltransferases[106,107], and although it has been reported to specifically bind unmethylated CpG dinucleotides [107-109], it has been shown that the DNA is anchored by the CXXC domain in a position that is distant from the active site of DNMT1. This is the result of an auto inhibitory CXXC-BAH1 linker. Unmethylated DNA is excluded from the active site of mDNMT1 by the binding of the CXXC domain, whereas the presence of the acidic auto inhibitory CXXC-BAH1 linker positioned directly between the DNA and the active site prevents entrance of DNA into the catalytic pocket; furthermore, the BAH2-TRD loop anchors the TRD in a retracted position and prevents it from binding in the DNA major groove. The CXXC domain also aids in the control of not interacting with methylated CpG sites by steric hindrance. If a methyl group were present on the CpG dinucleotide, it would unfavourably interact with Arg684 -Ser685 -Lys686 residues due to steric interference with nearby peptide atoms. The BAH1 and BAH2 domains of mDNMT1 are connected by an α-helix (BAH linker) and are arranged in a dumbbell configuration, both physically associated with the methyltransferase domain.

The methyltransferase domain of mouse DMNT1 is the main catalytic domain of the protein and folds into two subdomains, the TRD, and the catalytic core, which are separated by a large cleft in the protein, which is occupied by the DNA.

Maintenance methylation is tightly coupled to DNA replication[110], and unmethylated CpG sites are protected from de novo methylation through binding

by the CXXC domain as CpG dinucleotides emerge from the replication complex, thus increasing the efficiency of maintenance methylation through inhibition of de novo methylation.

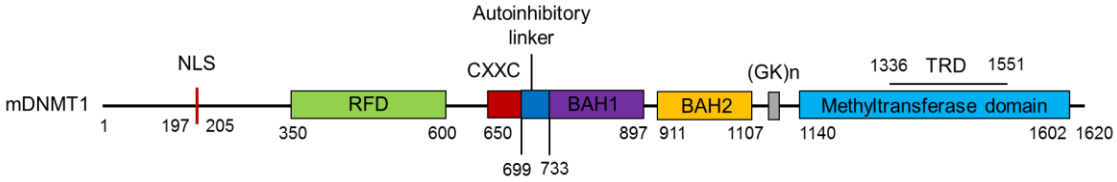

Figure 3.1: Structural overview of mDNMT1. The CXXC, BAH1, BAH2, and methyltransferase domain are coloured in red, light purple, orange and light blue, respectively. Adapted from *Structure of DNMT1-DNA complex reveals a role for autoinhibition in maintenance DNA methylation*, Song J et al, Science, 2011[105].

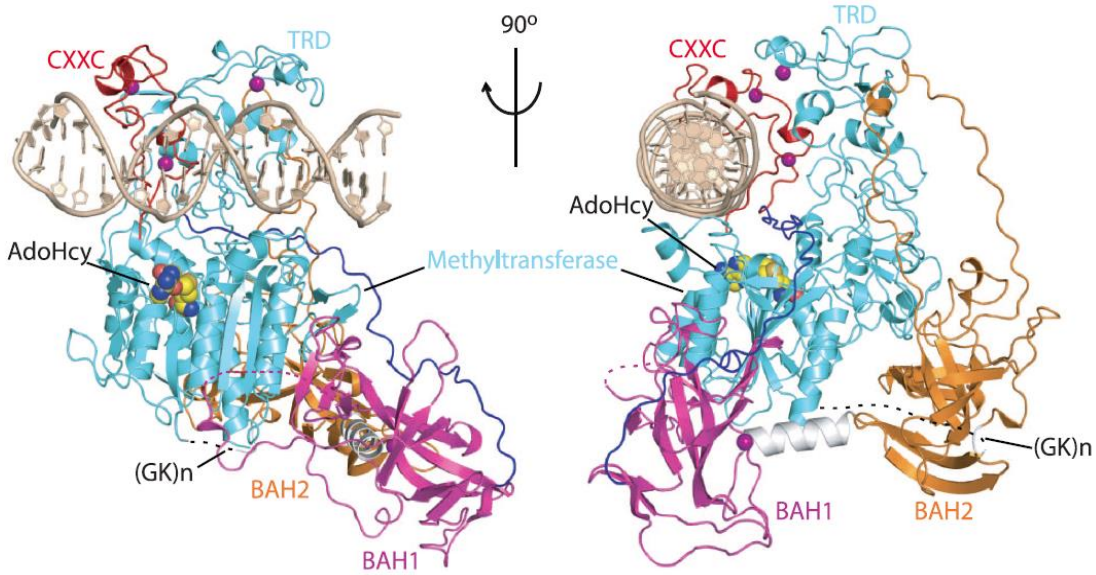

Figure 3.2: Ribbon representation of mouse DNMT1- S-adenosyl homocysteine (AdoHcy) complex in two orthogonal views. DNA and zinc ions are coloured in light brown and dark purple, respectively; CXXC-BAH1 linker in dark blue, BAH1-BAH2 linker in silver, (GK)n-containing BAH2-methyltransferase linker in black, and bound AdoHcy as in space-filling representation. Figure taken from *Structure of DNMT1-DNA complex reveals a role for autoinhibition in maintenance DNA methylation*, Song J. et al, Science, 2011[105].

3.1.2 Protein transport mechanism in mitochondria

Mitochondria have a retained complete genetic system in the matrix, however only ~1% of mitochondrial proteome is encoded by the mitochondrial genome and synthesized in the matrix[111]. Mitochondrion-encoded proteins form a few subunits of the respiratory chain complexes and are typically inserted into the inner membrane by an export and assembly machinery, called the oxidase assembly (OXA) machinery. The remaining 99% of the more than 1000 proteins constituting the mitochondrial proteome is encoded by nuclear genes, and includes genes that were transferred from the endosymbiont to the nucleus as well as genes for new mitochondrial proteins that arose during eukaryotic evolution; nucleus-encoded mitochondrial proteins are synthesized as precursors proteins on cytosolic ribosomes and imported into the organelle[112]. These proteins possess targeting signals that are recognized by receptors on the mitochondrial surface and direct the precursors to their functional destination in the mitochondrial sub compartment. Two main groups of targeting signals can be distinguished[38,112,113]: the first group is the amino-terminal extensions of precursors which represent the classical mitochondrion-targeting signals[114-116], whilst other precursor proteins are not synthesized with cleavable extensions but contain internal targeting signals which remain part of the protein even after mitochondrial localisation.

Precursor proteins are translated in the cytosol and are imported in mitochondria through 5 protein import pathways (**Figure 3.3**), with the translocase of the outer membrane (TOM) complex functioning as the main mitochondrial entry gate for both cleavable preproteins and most non-cleavable precursors, except for outer-membrane proteins with α-helical transmembrane segments which are imported through the mitochondrial import (MIM) complex[117]. The classic import pathway

is termed “the presequence pathway”, in which the preproteins are imported by the TOM and translocase of the inner membrane (TIM23) complexes[118,119]. Then, the presequence translocase-associated motor (PAM) drives protein translocation into the matrix[120] where the mitochondrial processing peptidase (MPP) cleaves off the presequences[121].

The four other protein import pathways are only used for precursor proteins with internal targeting signals. Depending on the nature of the internal targeting signal, the proteins can be internalised by carrier translocase of the inner membrane (TIM22)[122], inserted into the outer membrane by the sorting and assembly machinery (SAM) proteins[123] (for β-barrel proteins), or imported via the mitochondrial import and assembly (MIA) machinery of the intermembrane space[124] (Cys-rich proteins).

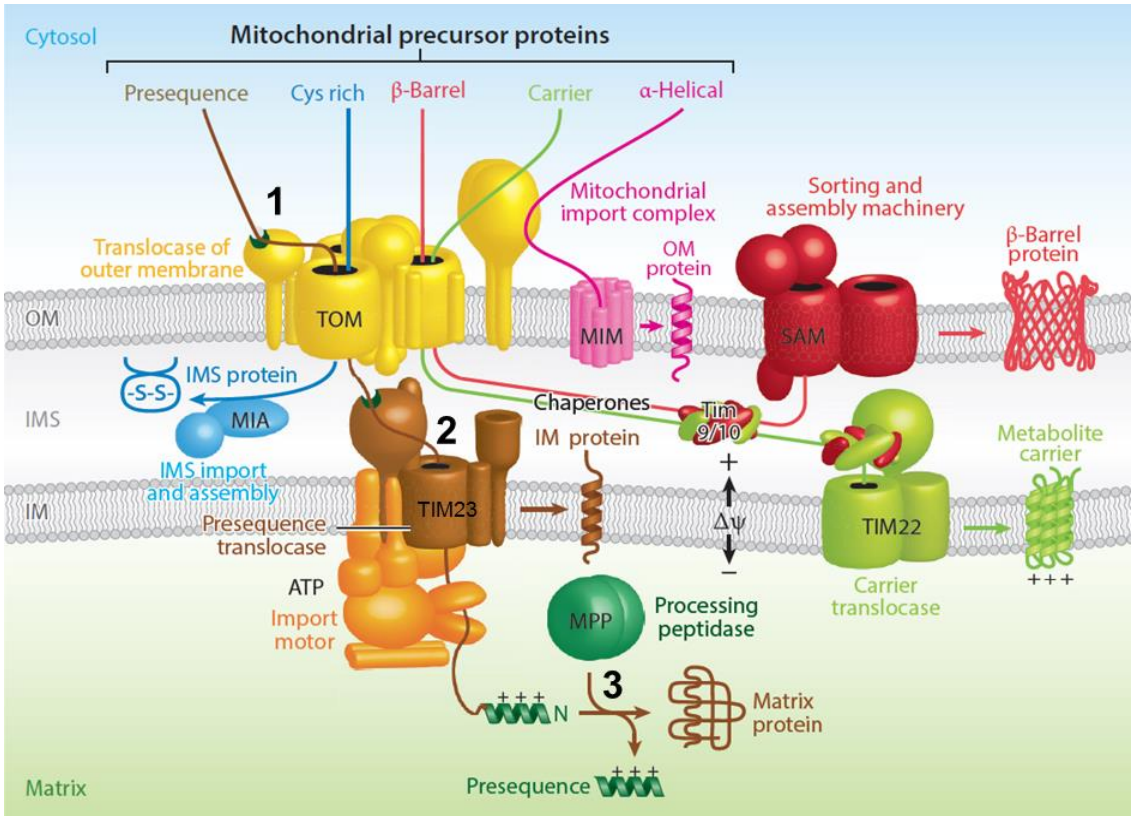

Figure 3.3: Overview of the five major protein import pathways of mitochondria. The presequence pathway starts with the recognition of the presequence protein by the TOM. Following internalisation in the IMS, the protein gets translocated to the matrix after interaction with the TIM23 complex. Once inside the matrix, the presequence is cleaved from the protein by the MPP. Abbreviations: TOM, translocase of the outer membrane; TIM23, translocase of the inner membrane; MPP, mitochondrial processing peptidase. Figure taken from *Mitochondrial machineries for protein import and assembly* Wiedemann N. et al. Nature, 2017[125].

3.2 Aims

The aims of this chapter were to examine whether the full length DNMT1 cDNA containing 1st-to-3rd ATG sequence can localise at a mitochondrial level. To investigate this hypothesis, several plasmid constructs (including a construct carrying a DNMT1 cDNA with a mutated consensus sequence for nuclear localisation) were generated and overexpressed in HEK293 cells.

3.3 Methods

3.3.1 Materials for pCMV-SPORT6-nuclear DNMT1 construct

To generate the expression vector of nuclear DNMT1 cDNA under the control of CMV promoter, the DNMT1 cDNA was digested from the pCAG-NLS-myc-DNMT1 vector and further modified in order to obtain a pCMV-SPORT6 vector carrying the nuclear DNMT1 sequence with an HA-tag at 5' region.

3.3.1.1 Primer sets for de novo PCR synthesis of HA-tag

A de novo PCR synthesis of the KpnI-SalI 5' region was performed, including the synthesis of an HA tag. The primers used for De novo PCR are shown (**Table 3.1**).

Table 3.1: PCR primers for de novo PCR of KpnI to SalI sequence with HA-tag. The KpnI is underlined, whilst the start codon is indicated in bold.

Primer	Sequence
Forward	5'- AAGGTACCACC**ATG**GCTTACCCATACGATGTTCCAGATTA CGCTATGCCAGCGCGAACAGCTCC-3'
Reverse	5'-CATGAATTGCTTTGGCACAC-3'

3.3.1.2 -De novo PCR synthesis conditions for KpnI-SalI DNMT1 fragment and cloning strategy

After obtaining the KpnI-SalI PCR product with HA-tag, it was inserted in an empty pBluescript II KS+ vector through KpnI-SalI digestion. Then, its sequence was checked. Subsequently, the KpnI-SalI PCR product was inserted in pCMV-SPORT6, along with SalI-XhoI and XhoI-HindIII fragments of the original DNMT1

sequence. Reagents for De novo PCR are listed (**Table 3.2**) and PCR conditions are shown (**Figure 3.4**).

Table 3.2: PCR reagents for De novo PCR synthesis.

Reagent	Quantity (µl)
2x Extreme Buffer	12.5
2 mM dNTPs	5
dH_2O	0.5
10 µM Forward Primer	0.75
10 µM Reverse Primer	0.75
Template (mouse genomic DNA) 10 µg/µl	5
KOD Xtreme DNA Polymerase	0.5

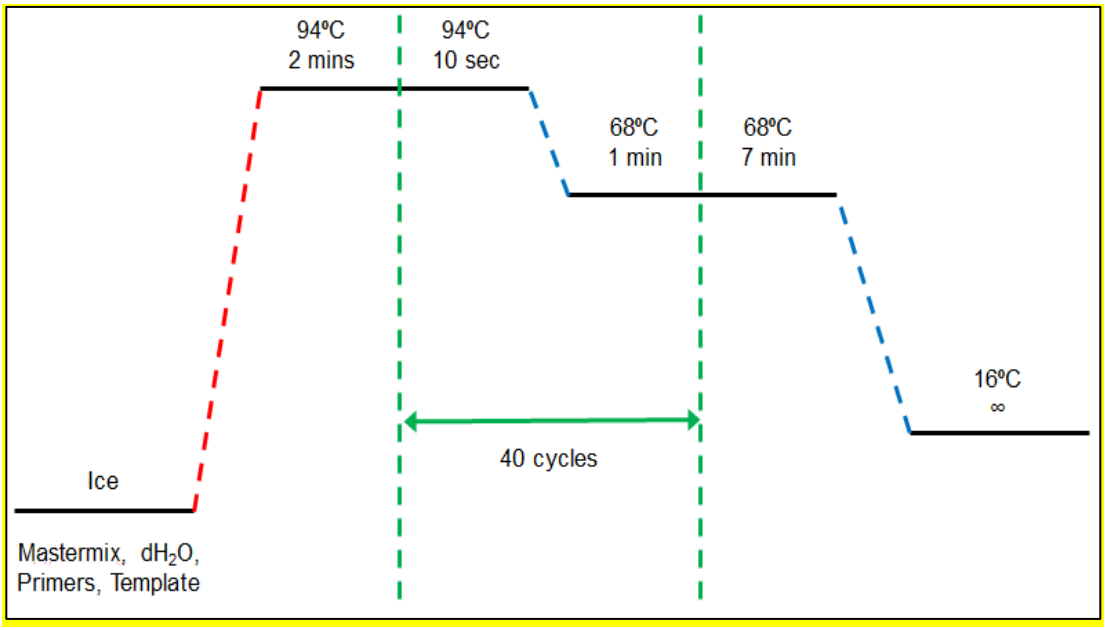

Figure 3.4: De novo PCR synthesis scheme.

3.3.2 Materials for pCMV-SPORT6-whole DNMT1 construct

First of all, the cDNA of DNMT1 was modified by adding the predicted mitochondrial localisation signal (MLS) 1st-to-3rd ATG sequence, coupled with an

HA-tag (derived from the Human influenza hemagglutinin surface glycoprotein, corresponding to amino acids 98-106), in order to obtain a protein that could effectively localise at both mitochondrial and nuclear level. Two different strategies in terms of HA-tag positioning were planned. In the first strategy, the primers have been designed so that the HA-tag with Kozak sequence would be positioned before the 1st ATG, whereas the second strategy had the HA-tag positioned right before the 3rd ATG (**Figure 3.5**).

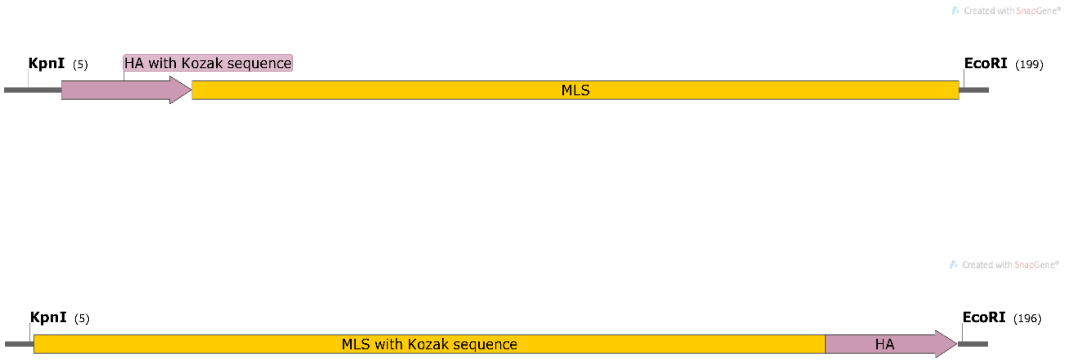

Figure 3.5: General scheme for final 1st-to-3rd ATG sequences carrying the MLS, HA-tag and Kozak sequence.

3.3.2.1 Primer sets for de novo PCR synthesis of MLS

De novo PCR synthesis was performed in order to obtain these fragments.

The sequences of primer sets used are shown (**Table 3.3**).

Table 3.3: Primers for 1st-to-3rd ATG sequences with HA-tag. The Kozak sequences are underlined, whilst the start codons are highlighted in bold. The KpnI site is highlighted in red, whilst the EcoRI site is highlighted in green.

Primer	Sequence
Strategy #1 Forward	5'-AAAGCGGCCGCGGTACC**ATG**GCTTACCCATACGATGTTCCAGATTACGCTATGCGCACTCCCTTCGGGCATAGCATGGTC-3'
Strategy #1 Reverse	5'-AAAGAATTCCTTGCAGGTTGCAGACGACAGAACAGCTCT-3'
Strategy #2 Forward	5'AAAGGTACC**ATG**GCTCGCACTCCCTTCGGGCATAGCATGGTCTTC3'
Strategy #2 Reverse	5'AAAGAATTCAGCGTAATCTGGAACATCGTATGGGTACTTGCAGGTTGCAGACGACAGAACAGCTCT-3'

3.3.2.2 De novo PCR synthesis conditions for MLS fragments

The final PCR products from strategy #1 and #2 carrying a KpnI site at 5' and an EcoRI site at 3' were subcloned in pBluescript II KS+ vector and sequenced to check for mutations, respectively. Then, they were inserted into pCMV-SPORT6 along with the rest of DNMT1 sequence (EcoRI-XhoI 5' fragment and XhoI-EcoRI 3' fragment). Reagents for De novo PCR are listed (**Table 3.4**), and PCR conditions are illustrated (**Figure 3.6**).

Table 3.4: PCR reagents for De novo PCR synthesis.

Reagent	Quantity (µl)
2x Extreme Buffer	12.5
2 mM dNTPs	5
dH_2O	0.5
10 µM Forward Primer	0.75
10 µM Reverse Primer	0.75
Template (mouse genomic DNA) 10 µg/µl	5
KOD Xtreme DNA Polymerase	0.5

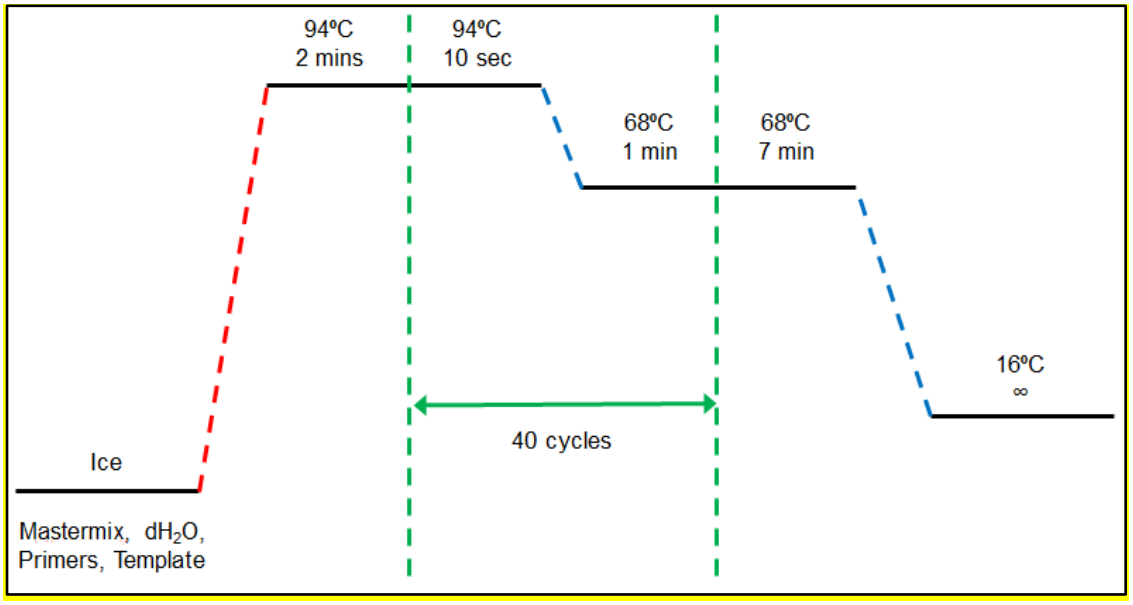

Figure 3.6: De novo PCR synthesis scheme.

3.3.2.3 Mitochondrial localisation probability analysis

After obtaining the 2 different 1st-to-3rd ATG sequences, the chances of mitochondrial localisation of the two different DNMT1 cDNAs was calculated through Mitoprot II software analysis (http://ihg.gsf.de/ihg/mitoprot.html).

3.3.3 Materials for pCMV-SPORT6-mitochondrial DNMT1 construct

Starting from the pCMV-SPORT6-whole DNMT1 construct, a DNMT1 cDNA was modified in order to allow the protein to only localise at a mitochondrial level. To achieve this, the NLS was disrupted through mutation.

3.3.3.1 Uniprot analysis

In order to identify the predicted site for the NLS, mouse DNMT1 protein sequence was analysed using Uniprot website (http://www.uniprot.org/uniprot/). The results were then used to plan which residues to mutate, and PCR primers for mutagenesis were designed accordingly.

3.3.3.2 Mutagenesis of NLS

Mutations of the NLS was performed using Geneart® site-directed mutagenesis Kit (Invitrogen Life Technologies®, A13282), and involved the disruption of NLS by replacing some Arginine (R) and Lysine (K) residues of the sequence with the amino acid Alanine. Arginine and Lysine possess positively charged side chains that allow for nuclear translocation, however mutation with Alanine would disrupt this mechanism as Alanine has uncharged side chains. Furthermore, Alanine is the smallest of the 21 proteinogenic amino acids, so using Alanine ensured that the mutation would not disrupt the secondary structure of the protein due to steric hindrance.

Since the kit is only capable of mutating a maximum of 15 nucleotides for each reaction, the complete mutagenesis was performed in two steps. The general scheme of the mutagenesis procedure (**Figure 3.7**) and primers' sequences (**Table 3.5**) are reported. The mutagenesis kit starts with the template DNA getting methylated and then amplified with the primers for mutations. Then, it is

transformed in a specific strain of DH5α cells that will digest the methylated template, thus only incorporating the mutated PCR product. The first step of mutation introduced a SacII digestion site to use as mutagenesis control along with the sequencing. Following each mutation step, the DNA sample was transformed in DH5α cells, extracted through miniprep and checked through both DNA gel electrophoresis after enzyme digestion (SacII) and then sequencing for the second mutation step. After confirming the sequence following the first mutation step, the second step of the mutagenesis was performed. Again, the DNA sample has been transformed in DH5α cells, extracted through miniprep and checked through sequencing. Finally, the 1.1 kbp mutated fragment was inserted into pCMV-SPORT6 carrying the 5' fragment of nuclear DNMT1. The changes in the amino acidic sequence after mutation are also reported (**Figure 3.8**).

Table 3.5: PCR primers for mutation reactions. Residues marked in bold represent mutation sites that will convert amino acids to Alanine. SacII (CCGCGG) and NotI (GCGGCCGC) sites are underlined.

Primer	Sequence
Mutation step #1 Forward	5'-TTCACGAAGGGCCCCACC**GCGGCCGCT**CCCAAGGAAGAGTCGGA-3'
Mutation step #1 Reverse	5'-TCCGACTCTTCCTTGGG**AGCGGCCGC**GGTGGGGCCCTTCGTGAA-3'

Mutation step #2 **Forward**	5'- GGAGAGAGACCAGGA**T<u>GCGGCCGC</u>TGC**TGTTGTAG ACACAGAGA-3'
Mutation step #2 **Reverse**	5'- TCTCTGTGTCTACAACA**GCAGCGGCCGCA**TCCTGG TCTCTCTCC-3'

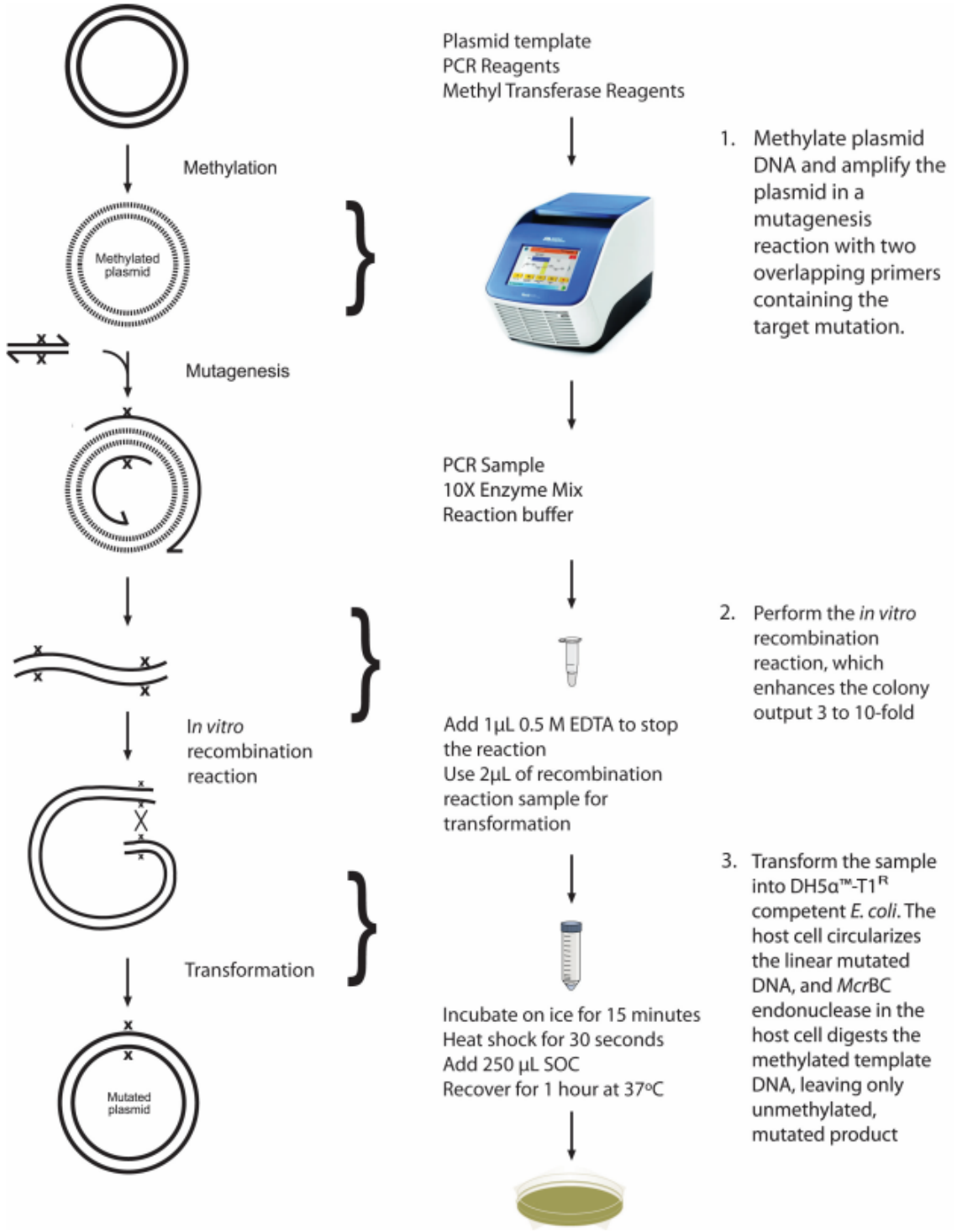

Figure 3.7: General workflow of Geneart site-directed mutagenesis kit. Figure taken from Invitrogen Life Sciences®.

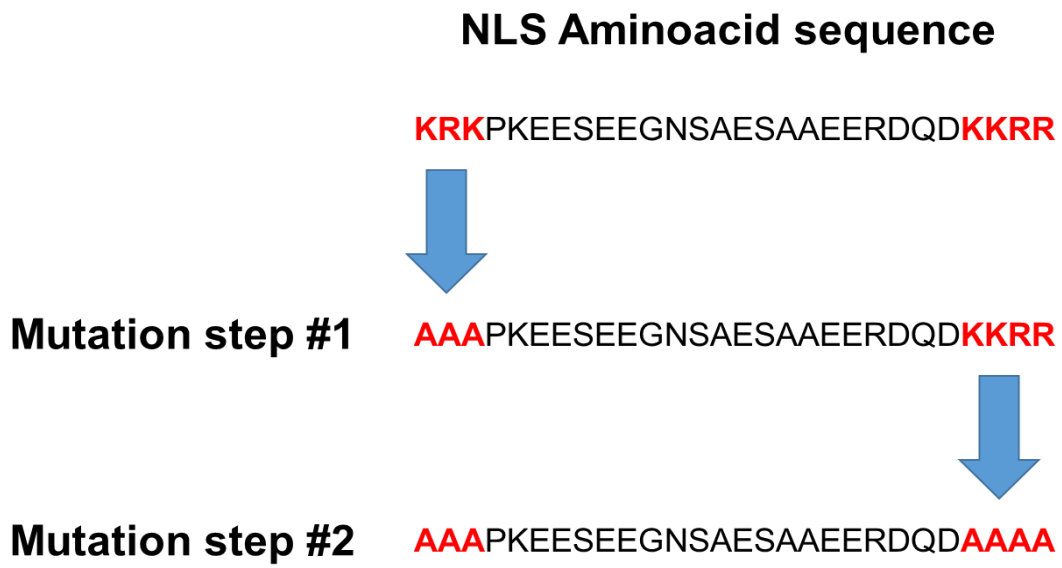

Figure 3.8: Changes in NLS amino acidic sequence.

3.3.4 Establishment of overexpression systems for the different DNMT1 isoform

3.3.4.1 Immunocytochemistry and cell imaging after overexpression

HEK293A cells were seeded in a 12-well plate with a collagen coated cover slip in each well, and transfected with FuGene HD (as described in subchapter 2.3.2). Following transfection, immunocytochemistry on HEK293A cells was performed (as described in subchapter 2.4). Five different transfection conditions were investigated: an empty pCMV-SPORT6 (used as a negative control), and pCMV-SPORT6-nuclear DNMT1, pCMV-SPORT6-whole DNMT1 (from strategy #1), pCMV-SPORT6-whole DNMT1 (from strategy #2), and pCMV-SPORT6-mitochondrial DNMT1.

Following fixation and mounting of cover slips, the first session of pictures was taken using an Andor Ixon3 EM-CCD camera connected to an Eclipse Ti-E Inverted microscope (Nikon®) with CSU-X1 Spinning Disk Confocal. Then, to further confirm localisation, another set of experiments was performed using another confocal microscope.

3.3.4.2 Western blotting after overexpression and cell fractioning

Following FuGene HD transfection and overexpression of the different DNMT1 cDNAs, HEK293A cells were harvested and fractioning was performed (as described in subchapter 2.5). Four different transfection conditions were investigated: empty pCMV-SPORT6 (negative control), pCMV-SPORT6-nuclear DNMT1, pCMV-SPORT6-whole DNMT1 (from strategy #2), and pCMV-SPORT6-mitochondrial DNMT1.

Western blotting of both whole cell lysates and nuclear and mitochondrial fractions was performed. Membranes were probed for DNMT1, HA-tag, αTubulin (whole cell housekeeping), Lamin A/C (nuclear housekeeping) and VDAC (mitochondrial housekeeping), using rabbit and mouse fluorescent secondary antibodies. Specifications of primary and secondary antibodies used are reported (**Table 2.11** in subchapter 2.8.2).

3.4 Results

3.4.1 Confirmation of pCAG-NLS-DNMT1 vector

To confirm the DNMT1 cDNA sequence in the pCAG-NLS-DNMT1 vector (**Figure 3.9**), enzyme digestion by EcoRI and XhoI and DNA gel electrophoresis were performed. Initially, the EcoRI and XhoI restriction sites were investigated through digestion and DNA gel electrophoresis (**Figure 3.10**). The expected bands, such as 5' region of DNMT1 cDNA [DNMT1 EcoRI-XhoI (5')], 3' region of DNMT1 cDNA [DNMT1 XhoI-EcoRI (3')] and pCAG vector region, were observed. The DNMT1 EcoRI-XhoI (5') was inserted in pCMV-SPORT6 (pCMV-SPORT6-DNMT1 5') (**Figure 3.11**). And the sequence, including start codon and modification of 5' internal EcoRI site, was confirmed.

The DNMT1 XhoI-EcoRI (3') was also inserted in pBluescript II KS(+) [pBS II KS(+)-DNMT1 3'] (**Figure 3.12**). The sequence, including 3' internal EcoRI site and stop codon, was confirmed. The vectors, pCMV-SPORT6-DNMT1 5' and pBS II KS(+)-DNMT1 3', were used for obtaining the pCMV-SPORT6 overexpression vectors as shown in the next sections.

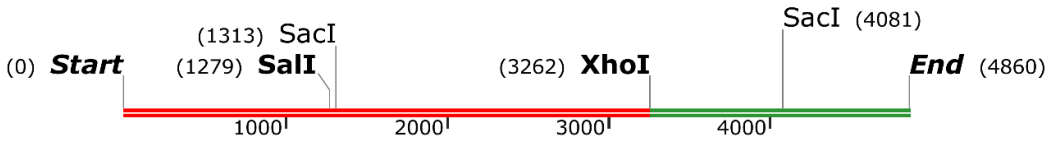

Figure 3.9: Restriction enzyme map from Mus musculus (mouse) DNMT1 cDNA sequence after Tajima's modifications. The internal EcoRI sites have been disrupted while still maintaining the same amino acid sequence. 5' and 3' fragments are highlighted (red and green) and separated by an XhoI site, which was used for cloning steps.

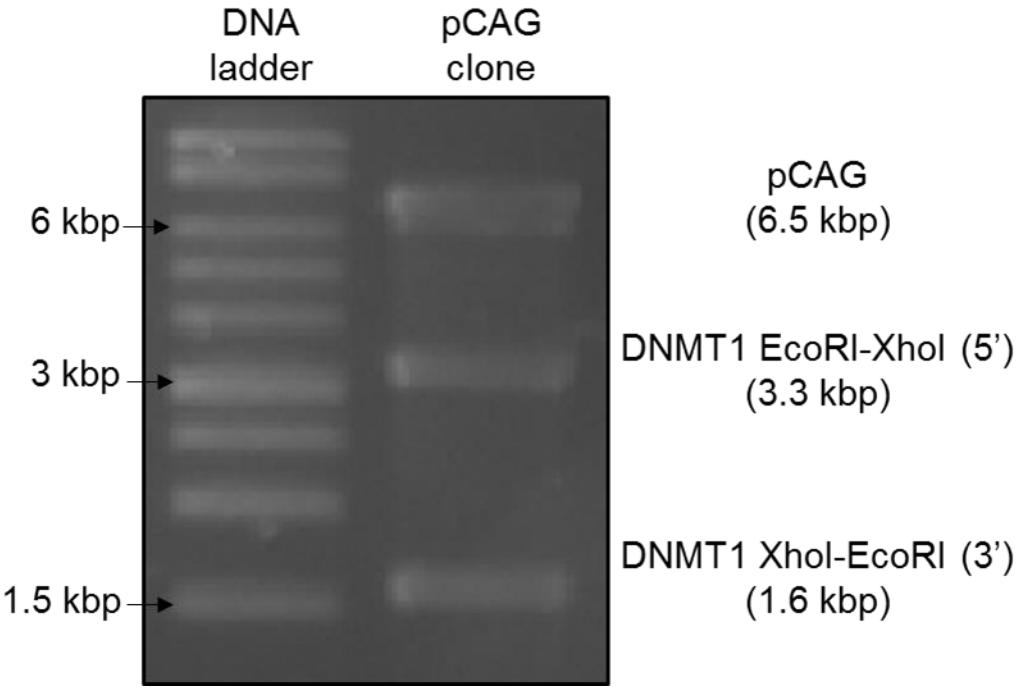

Figure 3.10: DNA gel electrophoresis of a pCAG-NLS-DNMT1 clone digested with EcoRI and XhoI. The 5' and 3' fragments have been used for the next cloning steps. The highest band represents pCAG vector (6.5 kbp).

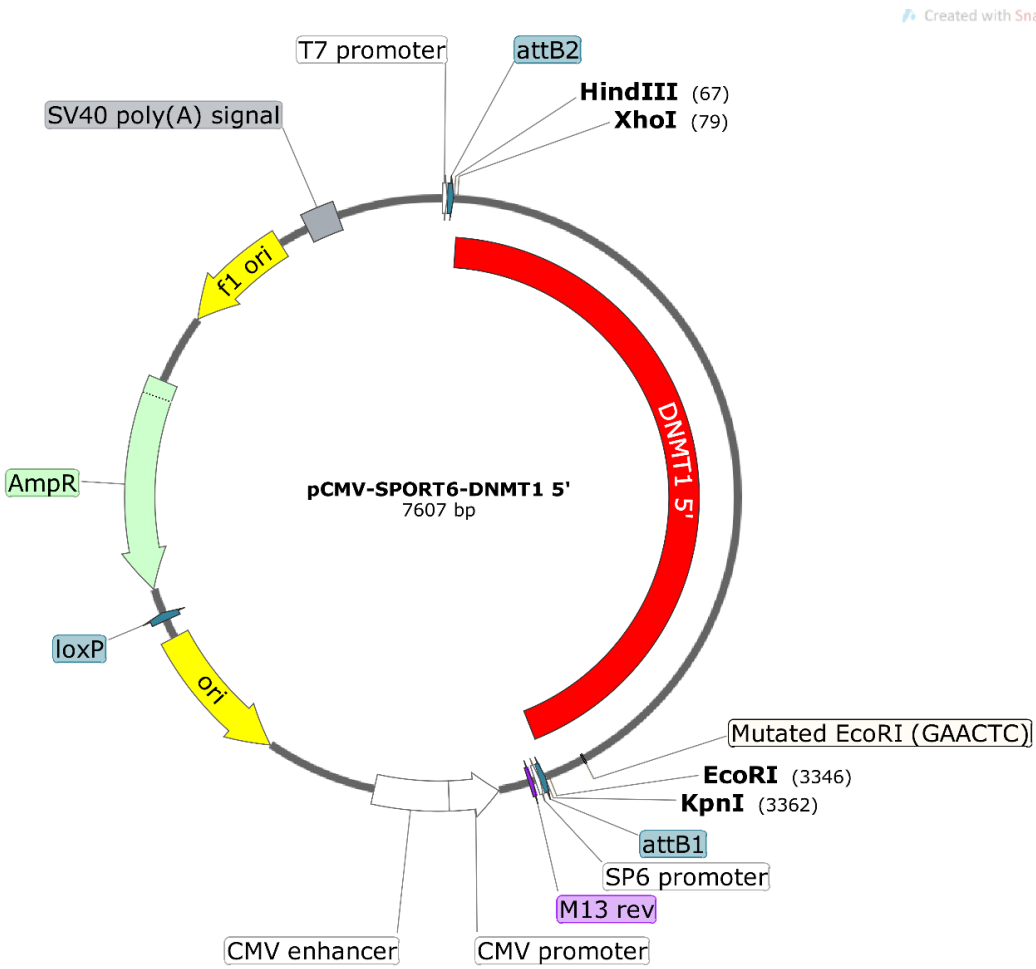

Figure 3.11: DNMT1 5' fragment insertion in pCMV-SPORT6 vector.

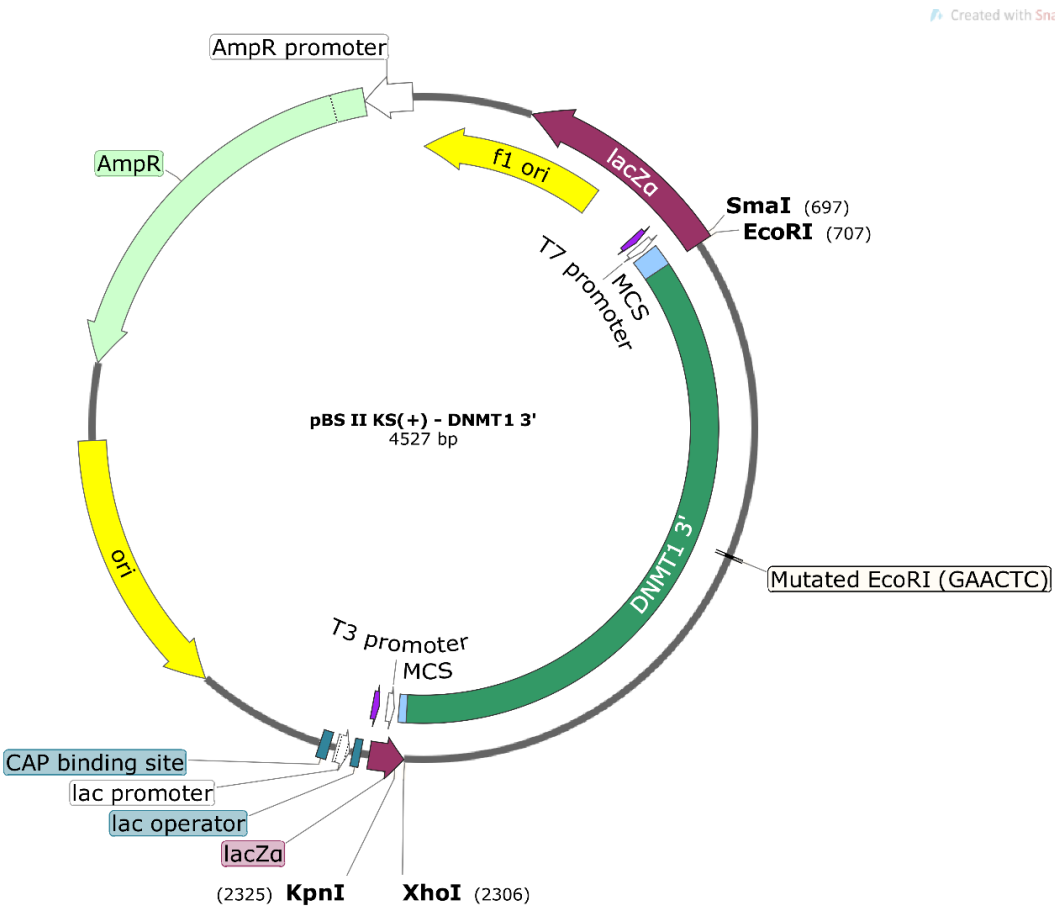

Figure 3.12: DNMT1 3' fragment insertion in pBluescript II KS(+).

3.4.2 Generation of pCMV-SPORT6-nuclear DNMT1 construct

To facilitate the following cloning steps, a HindIII site was created at SmaI site of 3' MCS in pBS II KS(+)-DNMT1 3' using HindIII linker (5'-CAAGCTTG-3') ligation (**Figure 3.13**). To investigate the expression and localization of the overexpressed DNMT1, HA tag sequence was inserted at 5' region of DNMT1 cDNA. PCR was performed to generate the 5' region of DNMT1 with an HA tag using the primers (shown in **Table 3.3**), then the PCR product digested by KpnI and SalI was inserted in pBluescript II KS(+) and the sequence was confirmed (Figure 3.14).

To generate the nuclear DNMT1 plasmid, the XhoI-HindIII (3') fragment was digested from pBS II KS(+)-DNMT1 3' (**Figure 3.12**) and inserted in pCMV-SPORT6-DNMT1 5' (**Figure 3.11**). Then, the KpnI-SalI PCR product was extracted from pBS II KS(+) - DNMT1 5' KpnI-SalI (**Figure 3.14**) and inserted in the pCMV-SPORT6-DNMT1 KpnI-HindIII vector digested with KpnI-SalI (**Figure 3.15**) and a digestion check after maxiprep was performed (**Figure 3.16**). Of note, the EcoRI site in the MCS next to KpnI was removed through de novo PCR synthesis of KpnI-SalI fragment.

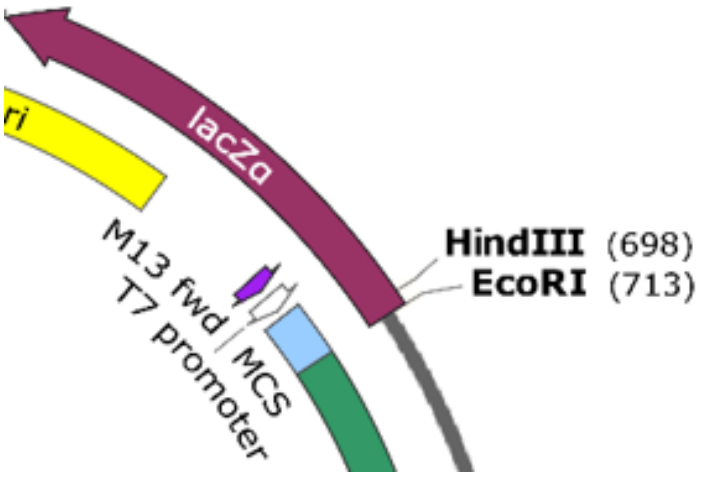

Figure 3.13: SmaI disruption and HindIII insertion in pBluescript II KS (+) - DNMT1 3'.

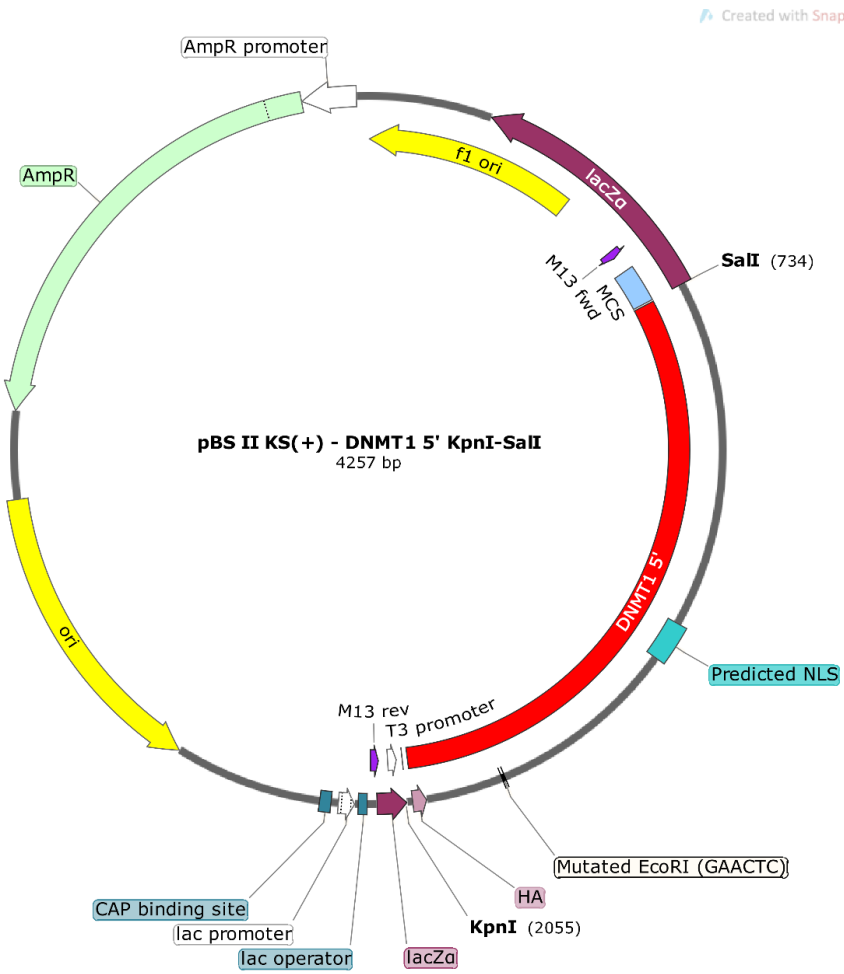

Figure 3.14: pBluescript II KS(+) vector with DNMT1 5' KpnI-SalI PCR product.

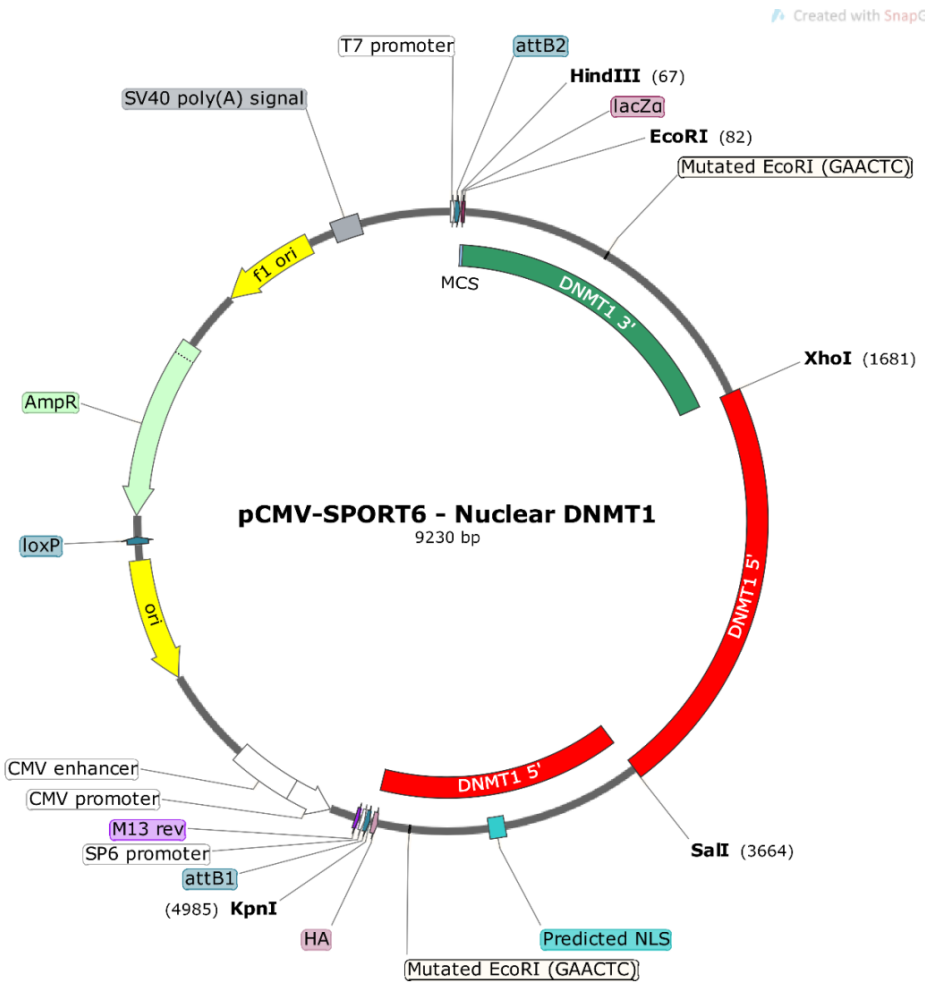

Figure 3.15: Final pCMV-SPORT6 – Nuclear DNMT1 overexpression vector.

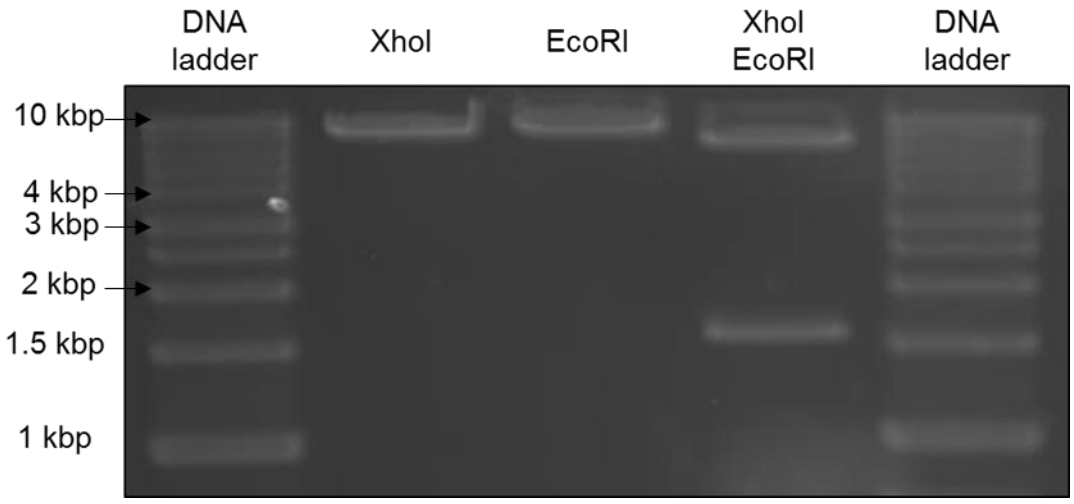

Figure 3.16: DNA gel electrophoresis of final pCMV-SPORT6-nuclear DNMT1 maxiprep sample. Several digestion patterns were checked and all proved to be consistent with the restriction enzyme map (Figure 3.15). Since the EcoRI site next to KpnI site is not present anymore, a single 9.2 kbp band is produced through both EcoRI-only and XhoI-only digestion.

However, 7.6 kbp and 1.6 kbp bands are obtained through EcoRI-XhoI double digestion, indicating a correct digestion pattern.

3.4.3 Generation of pCMV-SPORT6-whole DNMT1 construct

3.4.3.1 pCMV-SPORT6-whole DNMT1 cloning steps

To add the predicted MLS (coupled with an HA tag) in the 1st-to-3rd ATG sequence to the cDNA of DNMT1, two different strategies in terms of HA-tag positioning were planned: strategy #1 (HA tag before the 1st-to-3rd ATG sequence) and strategy #2 (HA tag after the 1st-to-3rd ATG sequence). The PCR products from strategy #1 and #2 (**Table 3.3**) were digested by KpnI and EcoRI. The enzyme-digested fragments were inserted in pBluescript II KS+ vector and confirmed by sequencing, respectively (pBSII KS(+)-Strategy #1 and pBSII KS(+)-Strategy #2) (**Figure 3.17** and **Figure 3.18**). After confirming the sequence of the MLS fragments, both of them were subcloned in pCMV-SPORT6- DNMT1 5' using KpnI and EcoRI restriction sites, respectively (pCMV-SPORT6-MLS-5' DNMT1 #1, **Figure 3.19**) (pCMV-SPORT6-MLS-5' DNMT1 #2, **Figure 3.20**).

The 3' fragment of DNMT1 was extracted from pBS II KS(+) - DNMT1 3' HindIII by XhoI and HindIII and was subcloned in pCMV-SPORT6-MLS-5'DNMT1 #1 or pCMV-SPORT6-MLS-5'DNMT1 #2 vector (**Figure 3.21** and **Figure 3.22**). Finally, two whole-cell DNMT1 overexpression vectors were obtained, with the only difference being in the positioning of the HA-tag (5' for strategy #1, before 3rd ATG for strategy #2). After having obtained the final vectors, they have been transformed in DH5α cells and a maxiprep was performed. Several DNA digestion reactions were performed to check for the final constructs, referring to the internal endonucleases digestion sites of DNMT1 (**Figure 3.23**). The final maxiprep samples have been used for all overexpression experiments in HEK293A cells (**Figure 3.24** and **Figure 3.25** show the DNA restriction checks).

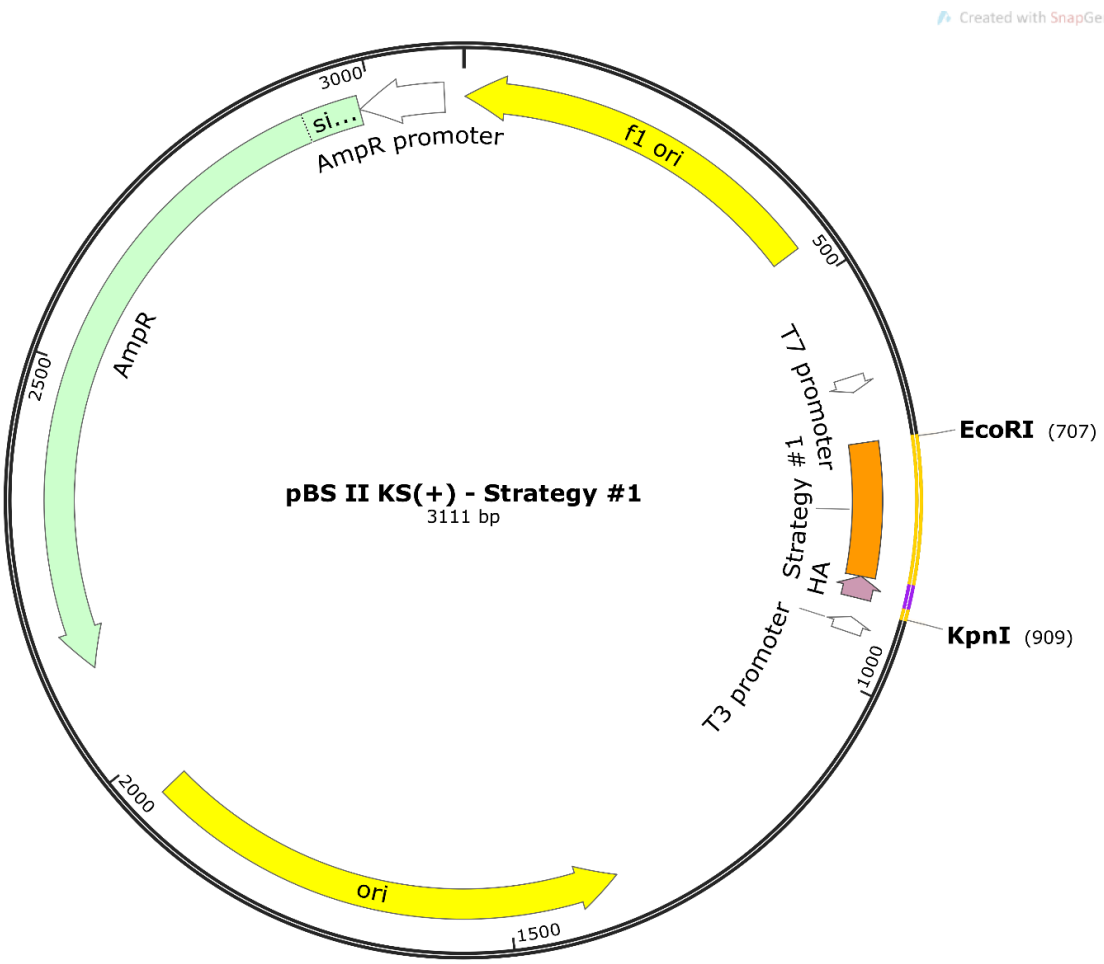

Figure 3.17: Insertion of HA tag-1st-to-3rd ATG sequence from strategy #1 in pBluescript II KS(+) for sequencing.

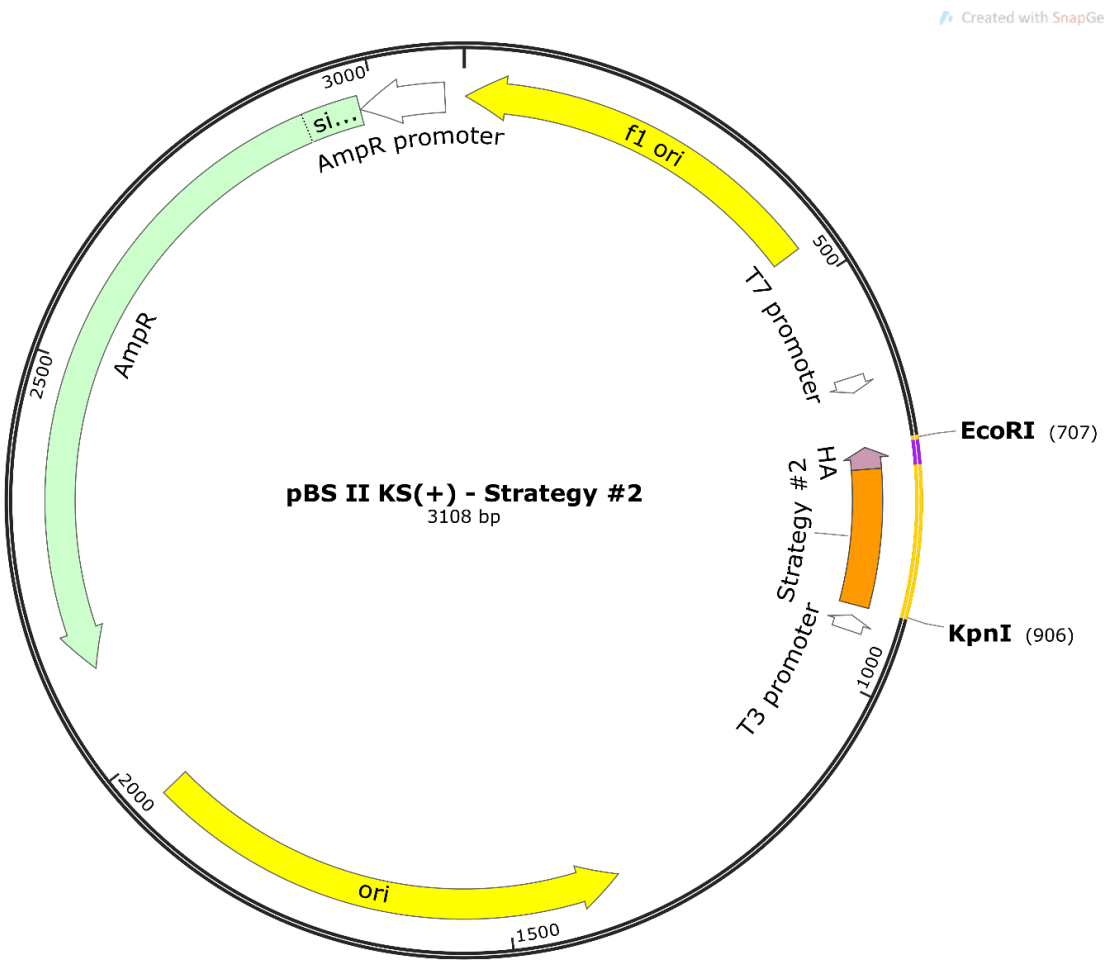

Figure 3.18: Insertion of 1st-to-3rd ATG sequence-HA tag from strategy #2 in pBluescript II KS(+) for sequencing.

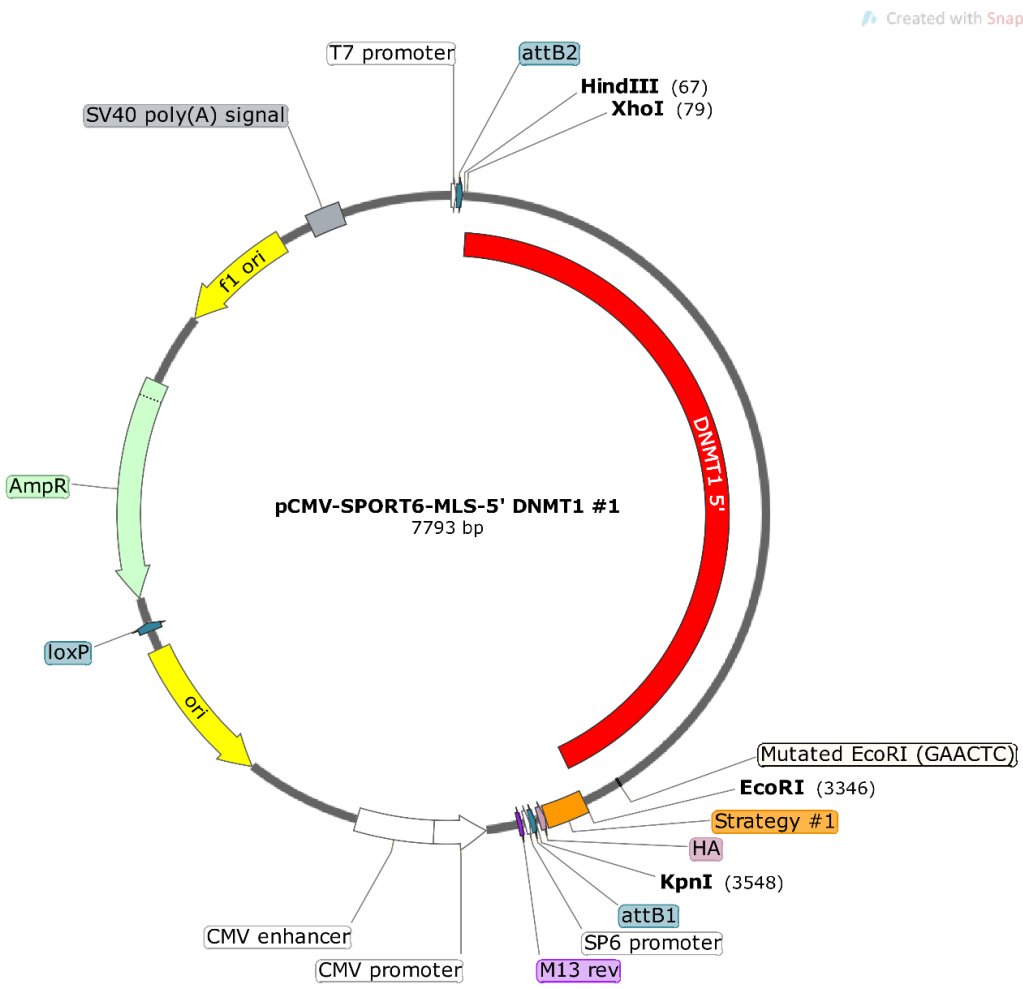

Figure 3.19: Insertion of the Strategy #1 PCR product in pCMV-SPORT6 vector carrying the 5' DNMT1 fragment.

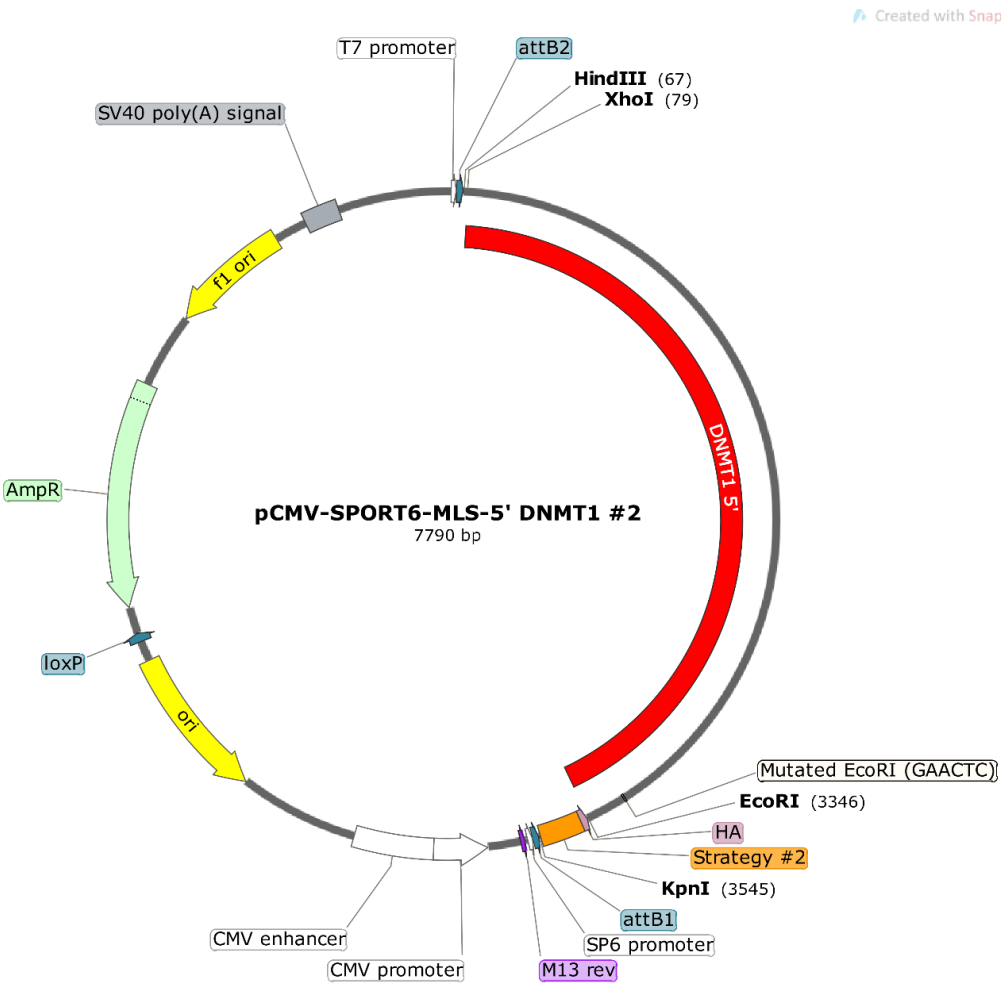

Figure 3.20: Insertion of the Strategy #2 PCR product in pCMV-SPORT6 vector carrying the 5' DNMT1 fragment.

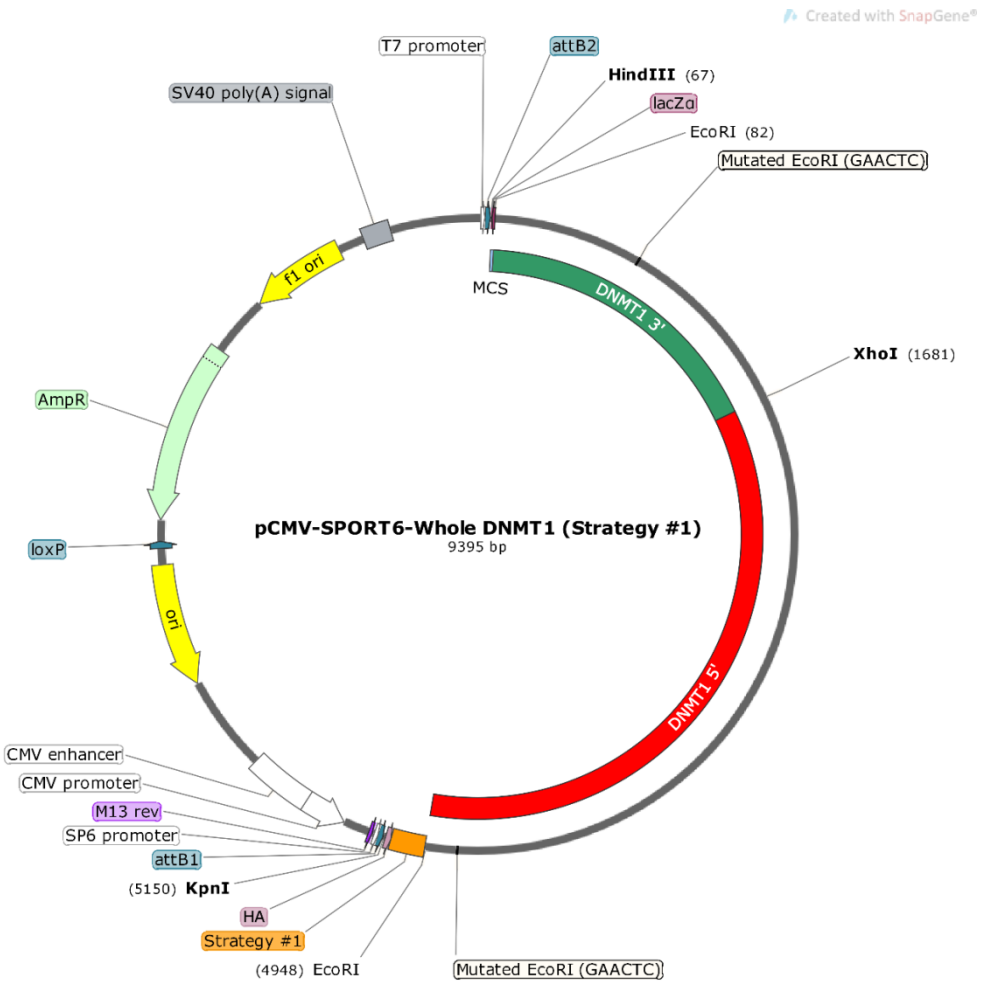

Figure 3.21: Insertion of DNMT1 3' fragment in the final pCMV-SPORT6-whole DNMT1 vector (Strategy #1).

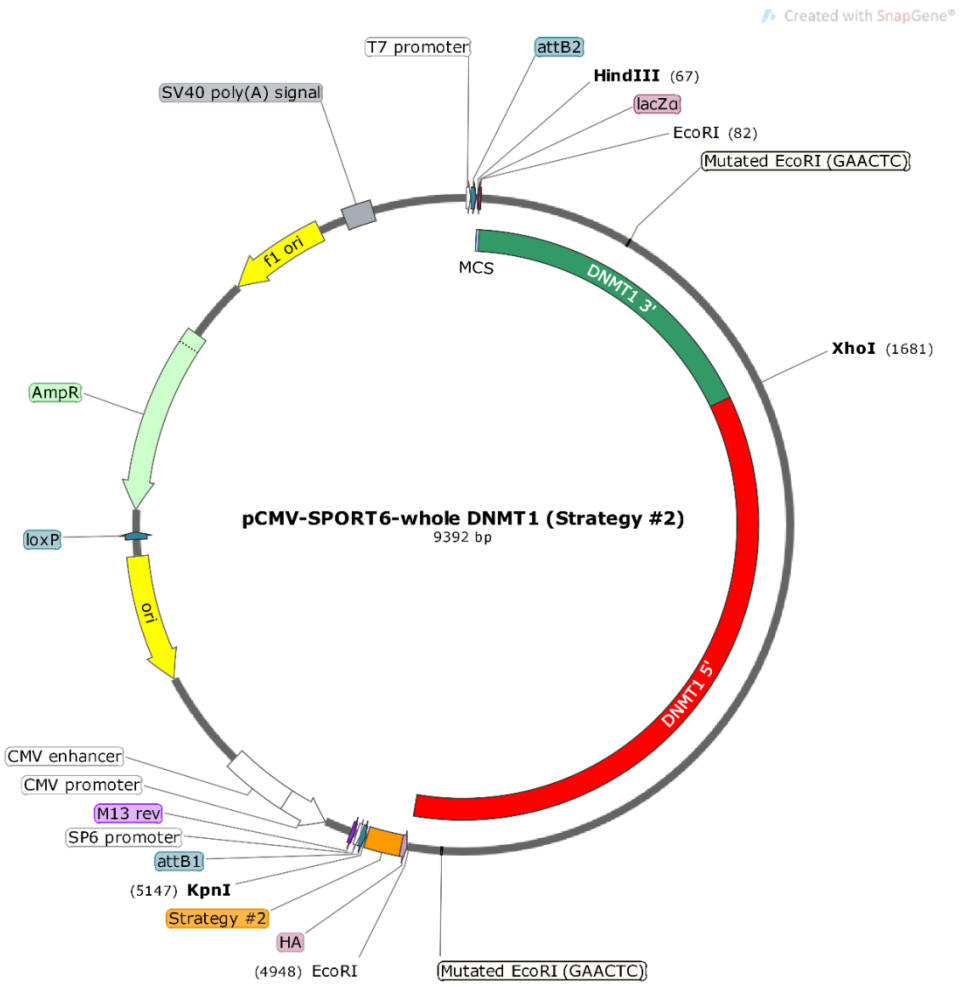

Figure 3.22: Insertion of DNMT1 3' fragment in the final pCMV-SPORT6-whole DNMT1 vector (Strategy #2).

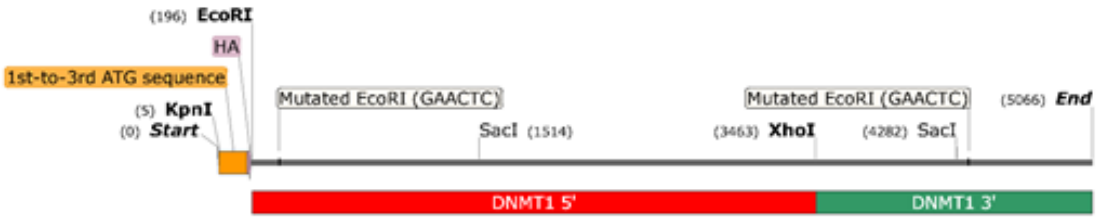

Figure 3.23: General scheme of DNMT1 digestion sites. Strategy #2 cDNA is shown.

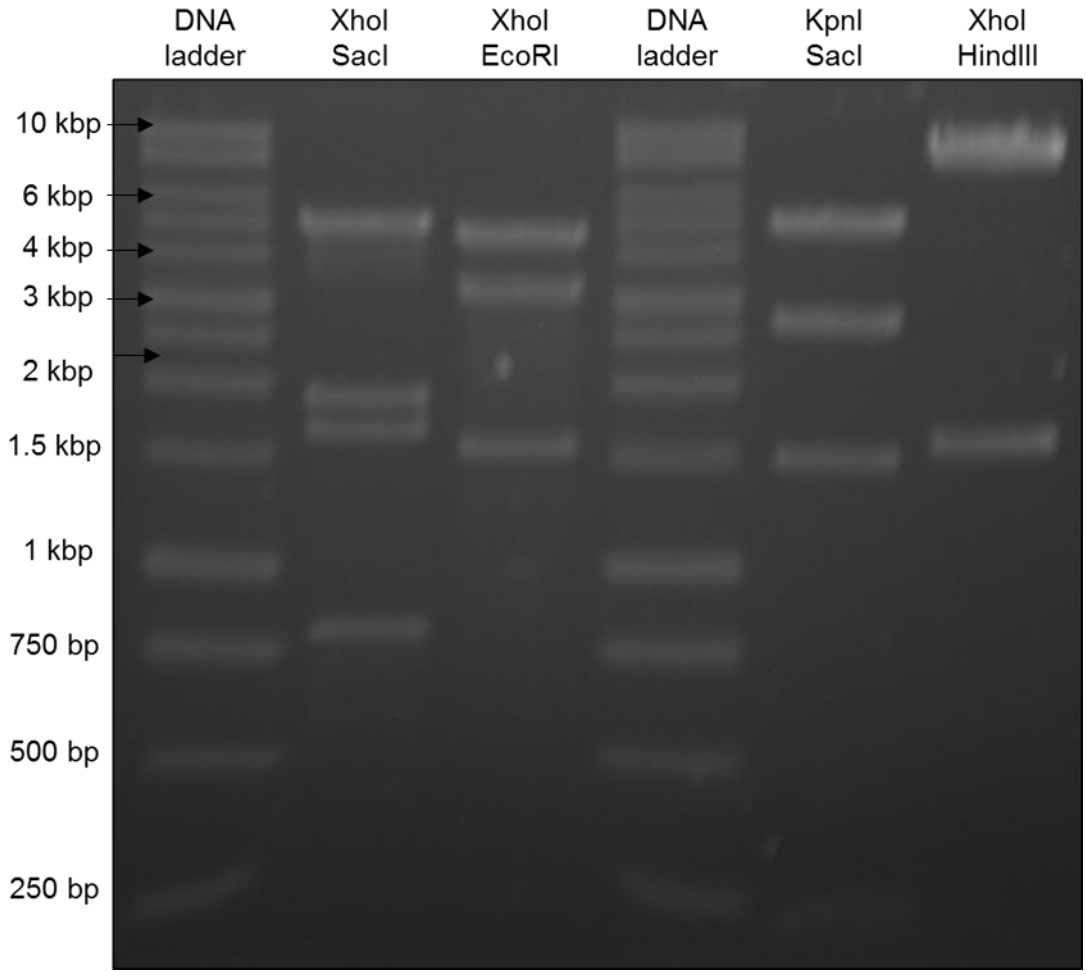

Figure 3.24: DNA gel electrophoresis of final pCMV-SPORT6-whole DNMT1 Maxiprep sample (strategy #1). Several digestion patterns were checked and all proved to be consistent with the restriction enzyme map (Figure 3.23).

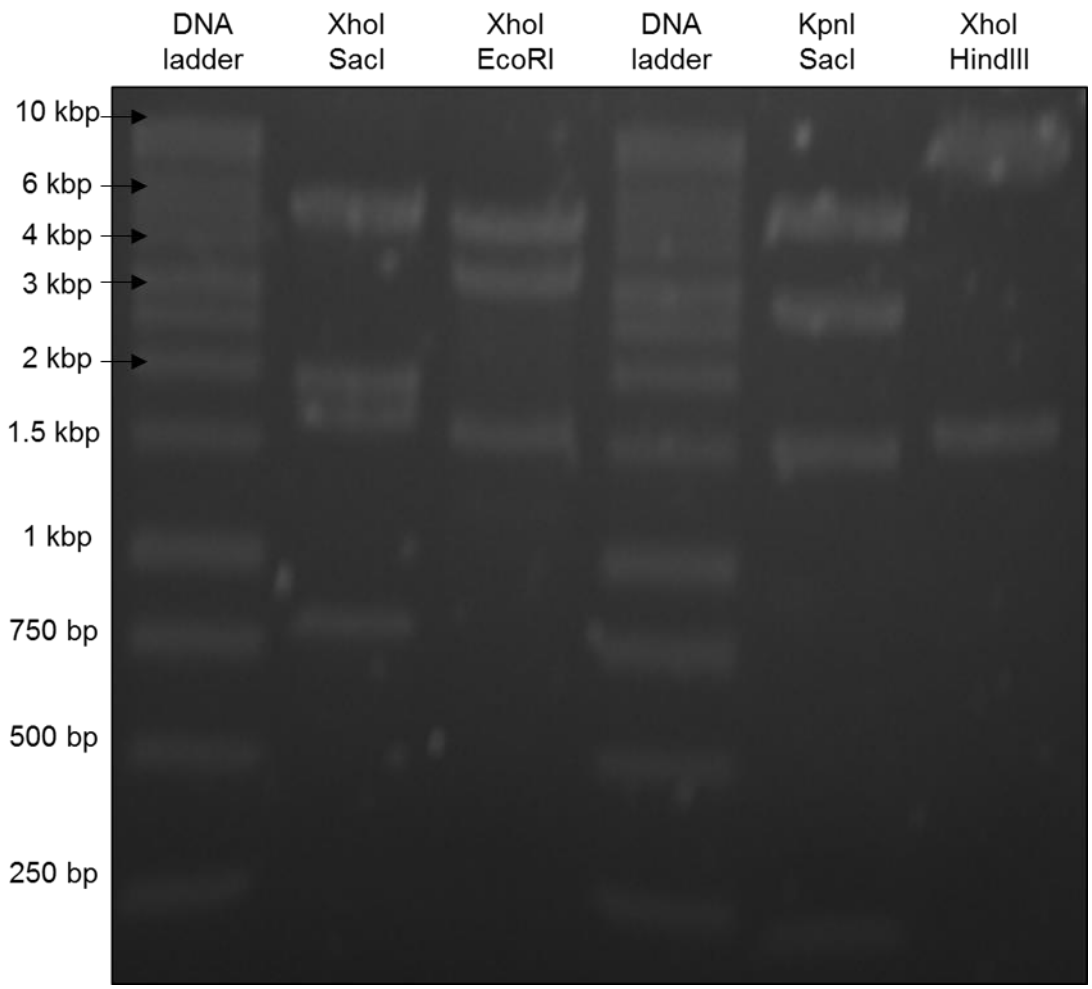

Figure 3.25: DNA gel electrophoresis of final pCMV-SPORT6-whole DNMT1 Maxiprep sample (strategy #2). Several digestion patterns were checked and all proved to be consistent with the restriction enzyme map (Figure 3.23).

3.4.3.2 Prediction of mitochondrial localisation using mitoprot II software

Full lenght DNMT1 cDNAs from strategy #1 and #2 were investigated for mitochondrial localisation using mitoprot II software. The cleavage site sequence of final strategy #1 could not be calculated (**Figure 3.26**), whereas the cleavage site of final strategy #2 could be identified by the software (**Figure 3.27**), predicting mitochondrial localisation of the DNMT1 cDNA with 1st-to-3rd ATG sequence -HA tag from strategy #2..

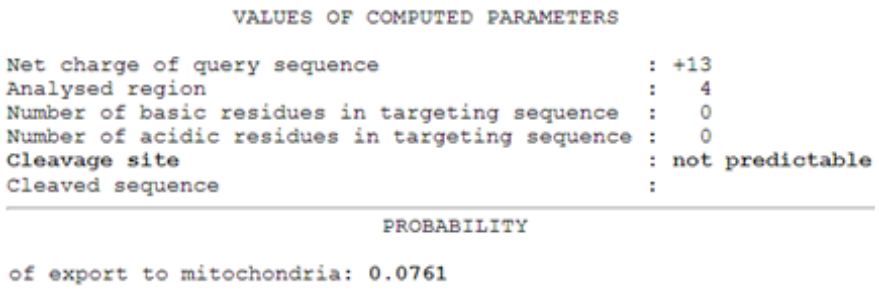

Figure 3.26: Mitochondrial localisation probability for full length DNMT1 sequence (Strategy #1).

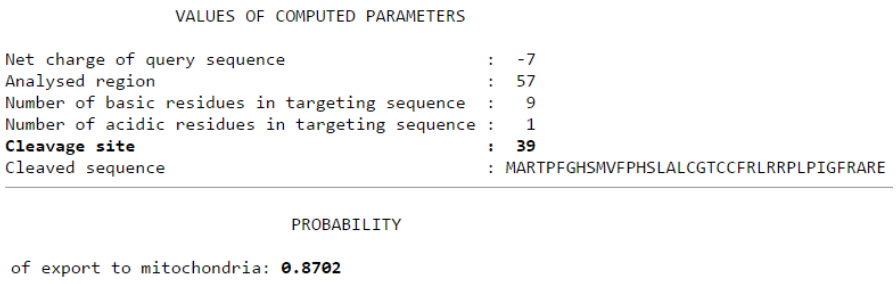

Figure 3.27: Mitochondrial localisation probability for full length DNMT1 sequence (Strategy #2).

3.4.4 Generation of pCMV-SPORT6-mitochondrial DNMT1 construct

3.4.4.1 Prediction of nuclear localisation signal using Uniprot analysis

Analysis of DNMT1 sequence through Uniprot (**Figure 3.28**) predicted the NLS site between residues 175-202 of the nuclear sequence. The mutagenesis was

performed at the region to obtain the mitochondrion-specific DNMT1 overexpression vector, and will be described in the following section.

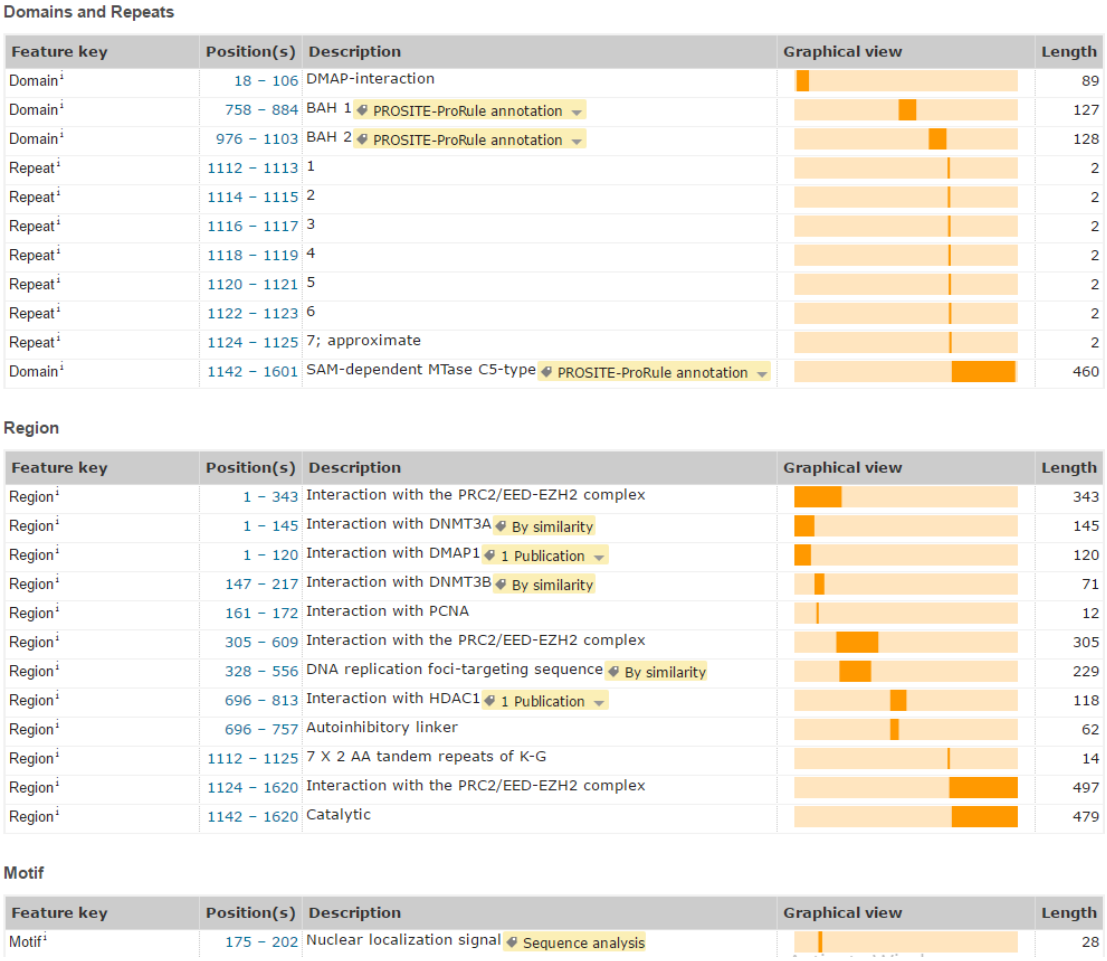

Domains and Repeats

Feature key	Position(s)	Description	Graphical view	Length
Domain	18 – 106	DMAP-interaction		89
Domain	758 – 884	BAH 1 PROSITE-ProRule annotation		127
Domain	976 – 1103	BAH 2 PROSITE-ProRule annotation		128
Repeat	1112 – 1113	1		2
Repeat	1114 – 1115	2		2
Repeat	1116 – 1117	3		2
Repeat	1118 – 1119	4		2
Repeat	1120 – 1121	5		2
Repeat	1122 – 1123	6		2
Repeat	1124 – 1125	7; approximate		2
Domain	1142 – 1601	SAM-dependent MTase C5-type PROSITE-ProRule annotation		460

Region

Feature key	Position(s)	Description	Graphical view	Length
Region	1 – 343	Interaction with the PRC2/EED-EZH2 complex		343
Region	1 – 145	Interaction with DNMT3A By similarity		145
Region	1 – 120	Interaction with DMAP1 1 Publication		120
Region	147 – 217	Interaction with DNMT3B By similarity		71
Region	161 – 172	Interaction with PCNA		12
Region	305 – 609	Interaction with the PRC2/EED-EZH2 complex		305
Region	328 – 556	DNA replication foci-targeting sequence By similarity		229
Region	696 – 813	Interaction with HDAC1 1 Publication		118
Region	696 – 757	Autoinhibitory linker		62
Region	1112 – 1125	7 X 2 AA tandem repeats of K-G		14
Region	1124 – 1620	Interaction with the PRC2/EED-EZH2 complex		497
Region	1142 – 1620	Catalytic		479

Motif

Feature key	Position(s)	Description	Graphical view	Length
Motif	175 – 202	Nuclear localization signal Sequence analysis		28

Figure 3.28: Uniprot analysis of DNMT1 cDNA sequence. Full sequence analysis is available at: http://www.uniprot.org/uniprot/P13864

3.4.4.2 Disruption of NLS and cloning of mtDNMT1 into pCMV-SPORT6

According to the result in section 3.4.3.2 using Mitoprot II analysis, the 5' region of DNMT1 was digested from pCMV-SPORT6-whole DNMT1 (Strategy #2) by EcoRI and SalI and was inserted into pBluescript II KS (+) (pBS II KS(+) – DNMT1 5' EcoRI –SalI, **Figure 3.29**). To disrupt the predicted NLS (as shown in Figure 3.8), the first step of mutation was performed using mutation step #1 primer set (Table 3.5). The clone generated from the first step was named as pBS II (KS+)-

NLS Mutagenesis #1 (**Figure 3.30**). Since the SacII site was generated by the mutagenesis, DNA gel electrophoresis after EcoRI-SacII digestion was performed (**Figure 3.31**). Then, the second step of mutation was performed using mutation step #2 primer set (**Table 3.5**). After mutagenesis, the sequence of whole 5' region was confirmed (pBS II KS(+)-NLS Mutagenesis #2, **Figure 3.32**). The EcoRI-SalI fragment with mutated NLS was inserted into EcoRI-SalI digested pCMV-SPORT6-MLS 5' DNMT1 #2 containing KpnI-EcoRI fragment (with MLS and HA tag) and SalI-XhoI fragment (**Figure 3.33**). The DNMT1 XhoI-HindIII 3' fragment from pCMV-SPORT6-whole DNMT1 (Strategy #2) (**Figure 3.22**) was inserted in pCMV-SPORT6-DNMT1 5' mutated NLS and finally mitochondrial-specific DNMT1 overexpression vector (pCMV-SPORT6-mitochondrial DNMT1) was obtained (**Figure 3.34**). Then, several DNA digestion reactions were performed from maxiprep sample to confirm the right digestion pattern (**Figure 3.35**), referring to the internal digestion sites of DNMT1 (**Figure 3.23**).

The mitochondrial-specific DNMT1 cDNA sequence was analysed by Mitoprot II. The probability is 0.8674 (**Figure 3.36**). The maxiprep sample of pCMV-SPORT6-mitochondrial DNMT1 has been used for all overexpression experiments, as shown in the following sections.

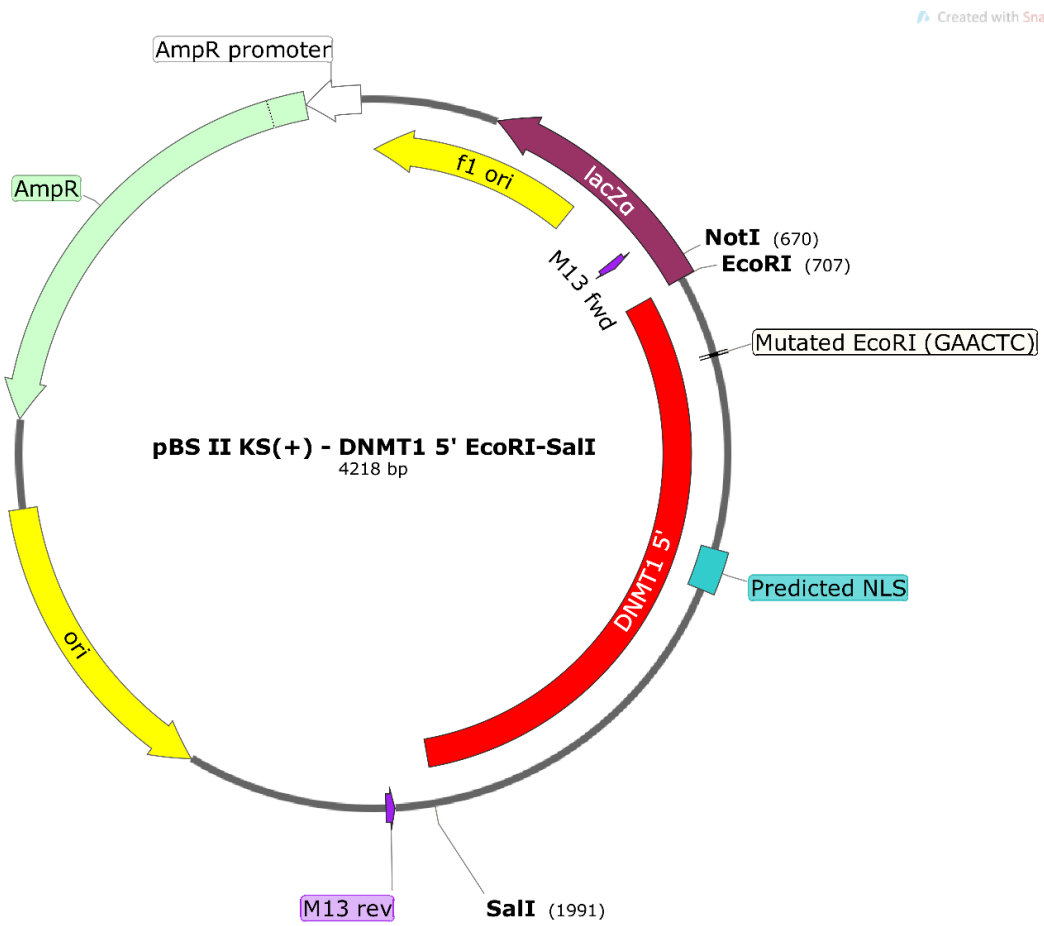

Figure 3.29: Subcloning of EcoRI-SalI DNMT1 fragment in pBluescript II KS(+) for NLS mutation.

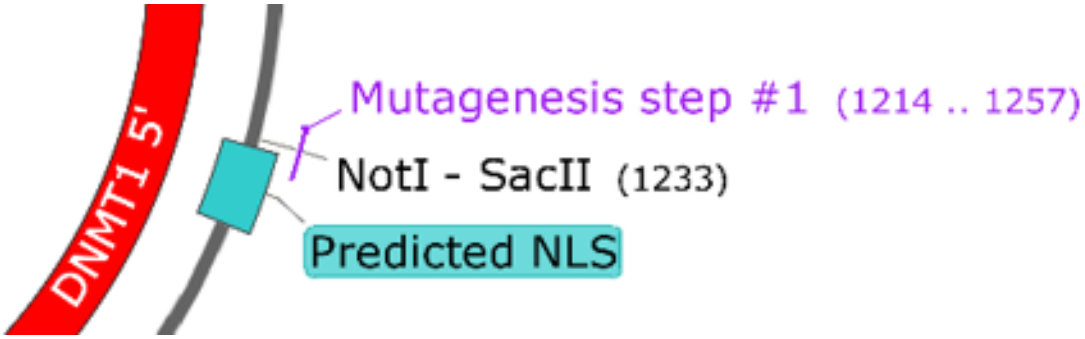

Figure 3.30: First step of NLS mutagenesis.

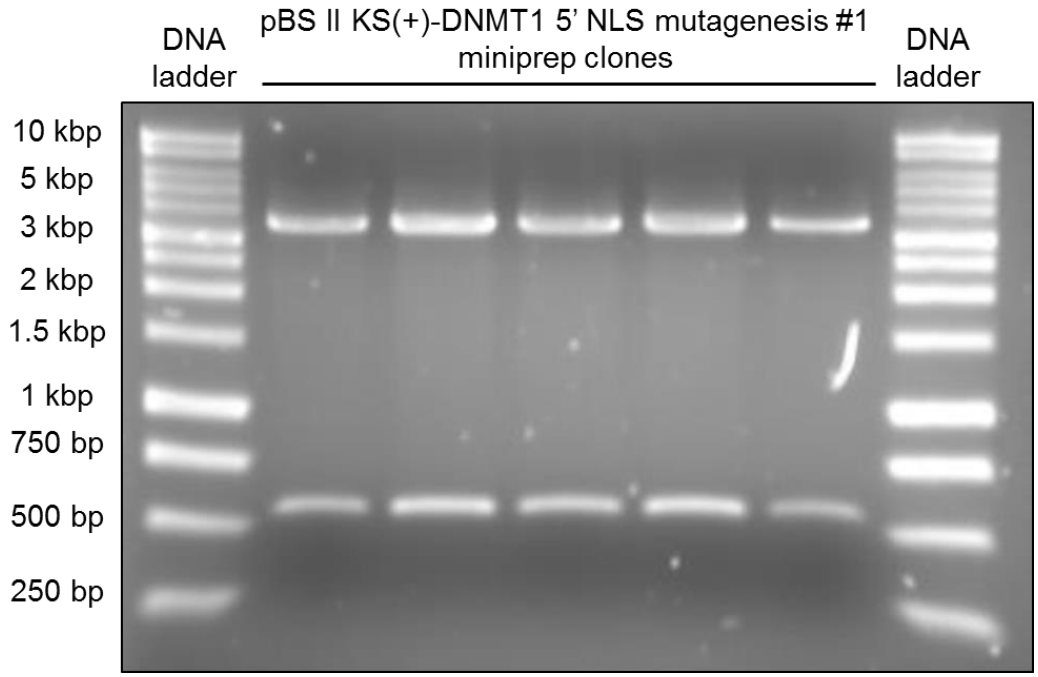

Figure 3.31: DNA gel electrophoresis after the first mutagenesis step. The mutagenesis was confirmed for all clones through EcoRI-SacII digestion.

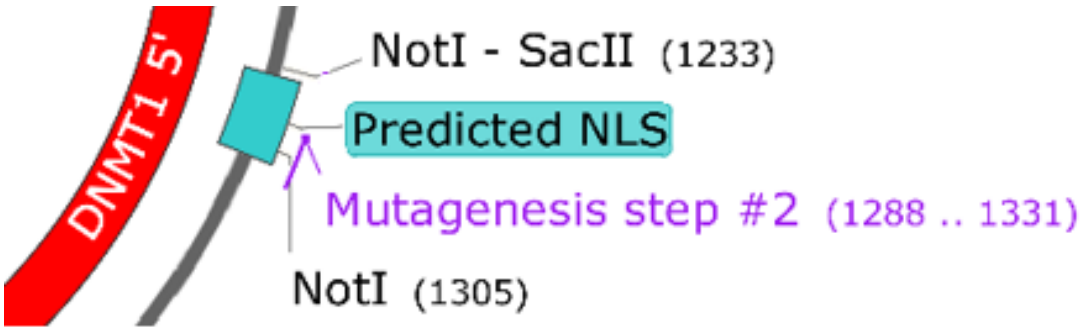

Figure 3.32: Second step of NLS mutagenesis.

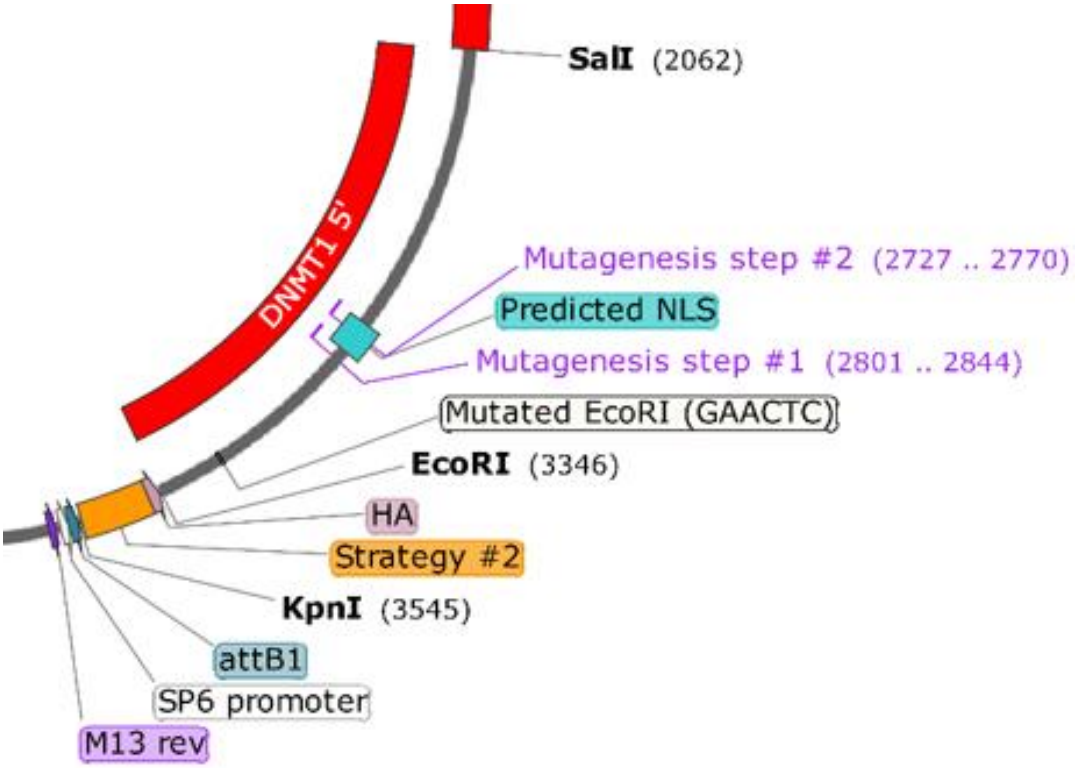

Figure 3.33: Insertion of 5' fragment with mutated NLS in pCMV-SPORT6.

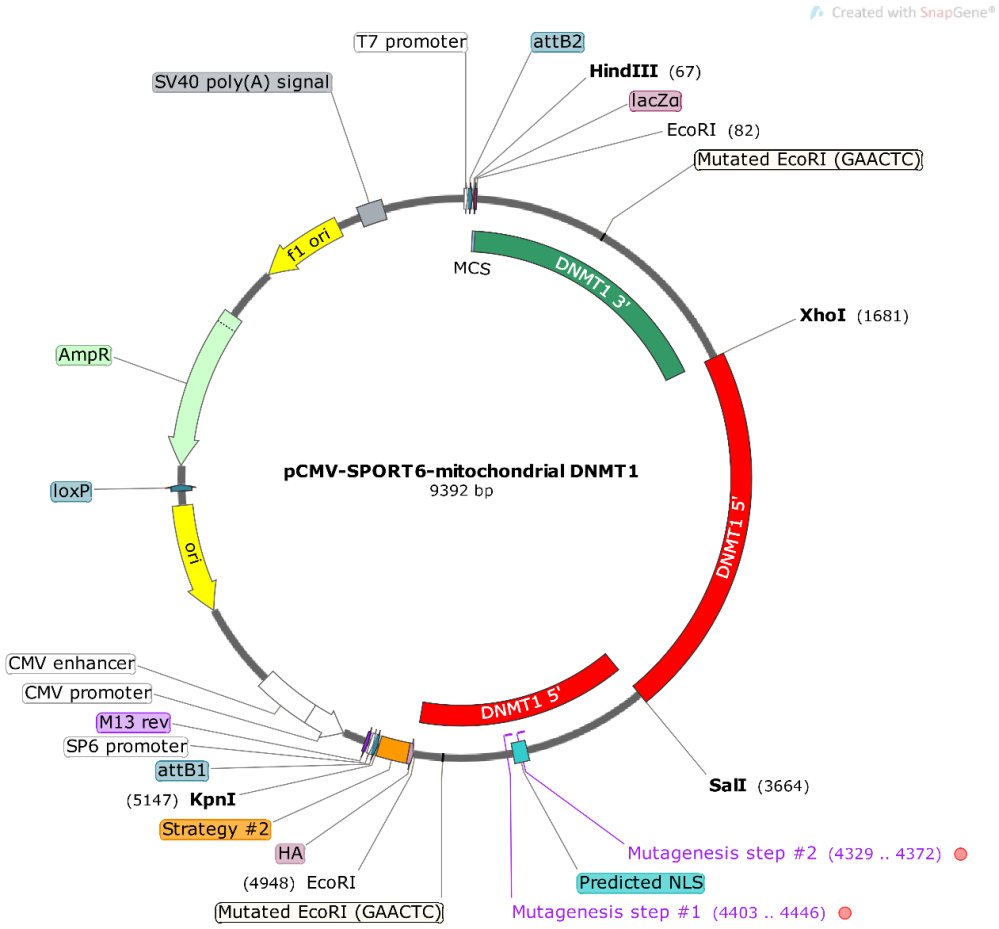

Figure 3.34: Final pCMV-SPORT6-mitochondrial DNMT1 with mutated NLS. The vector contains the MLS and HA-tag from strategy #2.

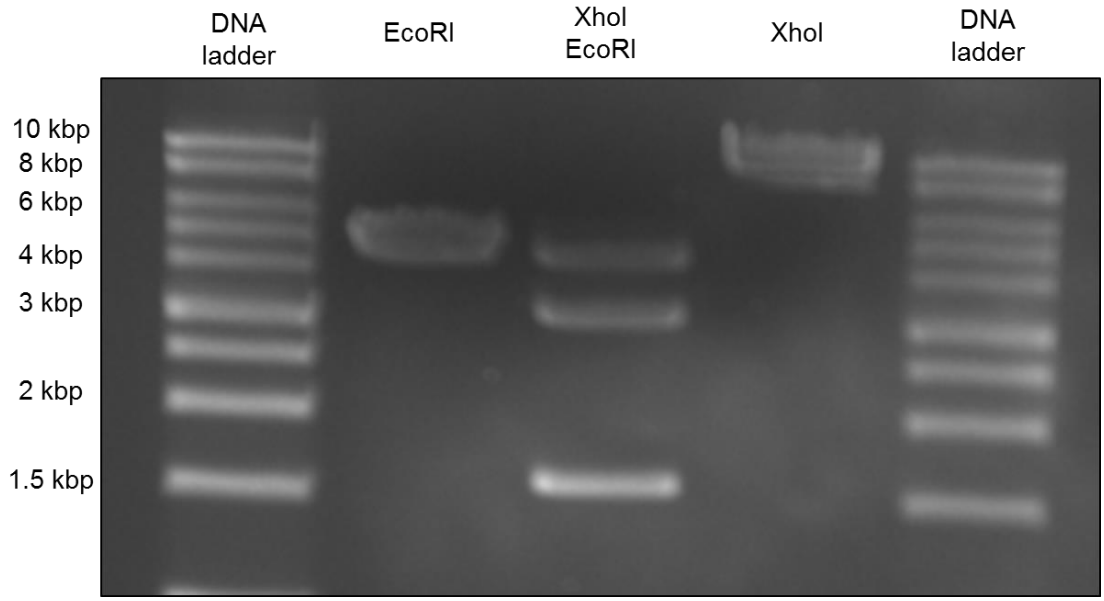

Figure 3.35: DNA gel electrophoresis of final pCMV-SPORT6-mitochondrial DNMT1 maxiprep sample. Several digestion patterns were checked and all proved to be consistent with the restriction enzyme map (Figure 3.27). Though the EcoRI digestion seems to show a single band, the signal actually comes from 2 separate bands of similar size (4.4 kbp and 4.8 kbp), i.e. the pCMV-SPORT6 vector and mitochondrial DNMT1 cDNA. This was confirmed through XhoI digestion, which shows a single band of about 10 kbp.

VALUES OF COMPUTED PARAMETERS

Net charge of query sequence	:	-9
Analysed region	:	57
Number of basic residues in targeting sequence	:	9
Number of acidic residues in targeting sequence	:	1
Cleavage site	**:**	**39**
Cleaved sequence	:	MARTPFGHSMVFPHSLALCGTCCFRLRRPLPIGFRARE

PROBABILITY

of export to mitochondria: **0.8674**

Figure 3.36: Mitoprot II analysis of full length mtDNMT1 sequence with mutated NLS. The probability of mitochondrial localisation is high, and the sequence has a clear cleavage site.

3.4.5 Subcellular localisation of DNMT1 isoforms

The subcellular localisation of DNMT1 isoforms was investigated through both confocal microscopy and western blotting.

3.4.5.1 Confocal microscopy of SPORT6-DNMT1 vectors

For this experiment, all the plasmids generated as described in subchapters 3.4.2, 3.4.3 and 3.4.4, as well as empty pCMV-SPORT6 (as a negative control), were used. For all transfection condition, pictures of each channel (DAPI for nuclear staining, HA-tag for overexpressed DNMT1 and Mitotracker Red for mitochondrial staining) were taken. After this, a merged image of the 3 channels was created. Larger pictures of the slides were also taken.

3.4.5.1.1 Empty pCMV-SPORT6 localisation

Nuclear and mitochondrial staining were successful. As expected, no signal was obtained from the staining of HA-tag antibody (**Figure 3.37** and **Figure 3.38**), suggesting that HA-tag staining is indeed useful for investigating DNMT1 localisation.

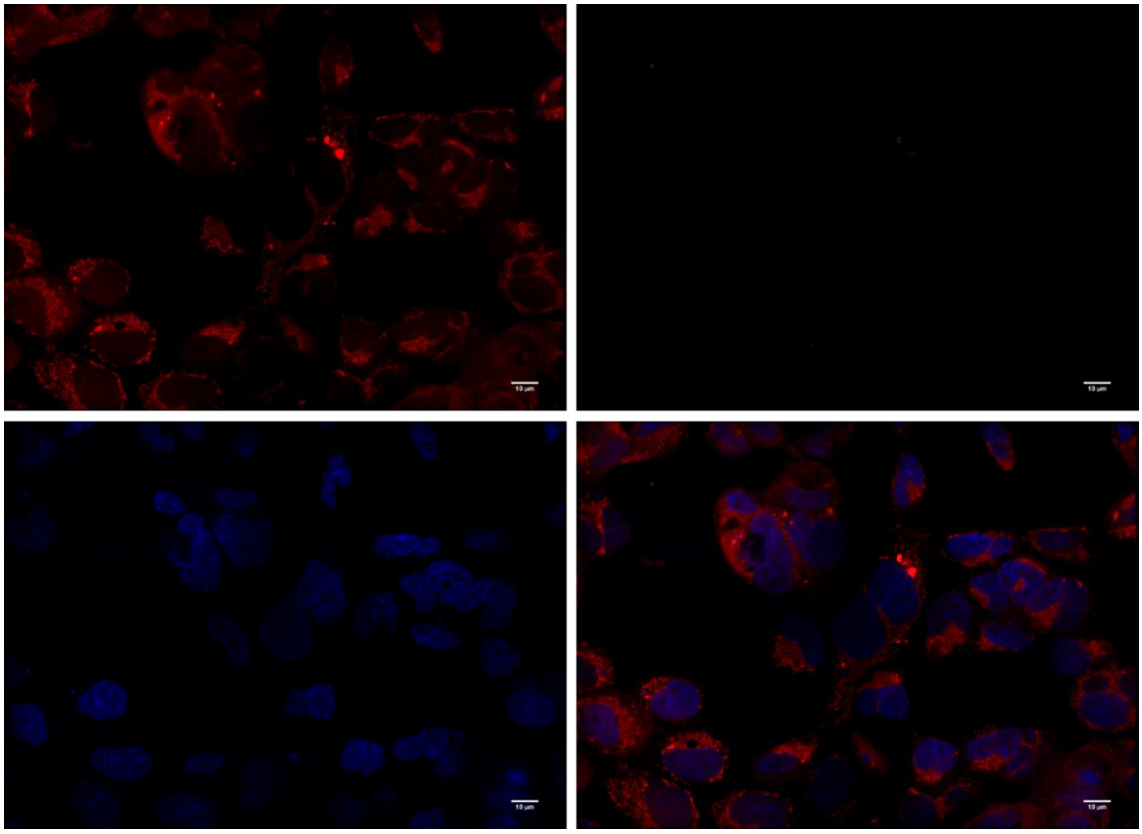

Figure 3.37: Confocal microscopy after IC of HEK293A cells transfected with empty pCMV-SPORT6 (low magnification). Multiple images were taken, then stitched together. Cells have been stained for mitochondria (Mitotracker red, top left), HA-tag (Alexafluor 488, top right) and nuclei (DAPI, bottom left). Bottom right is a merged image of all channels. Scale bar = 10 µm.

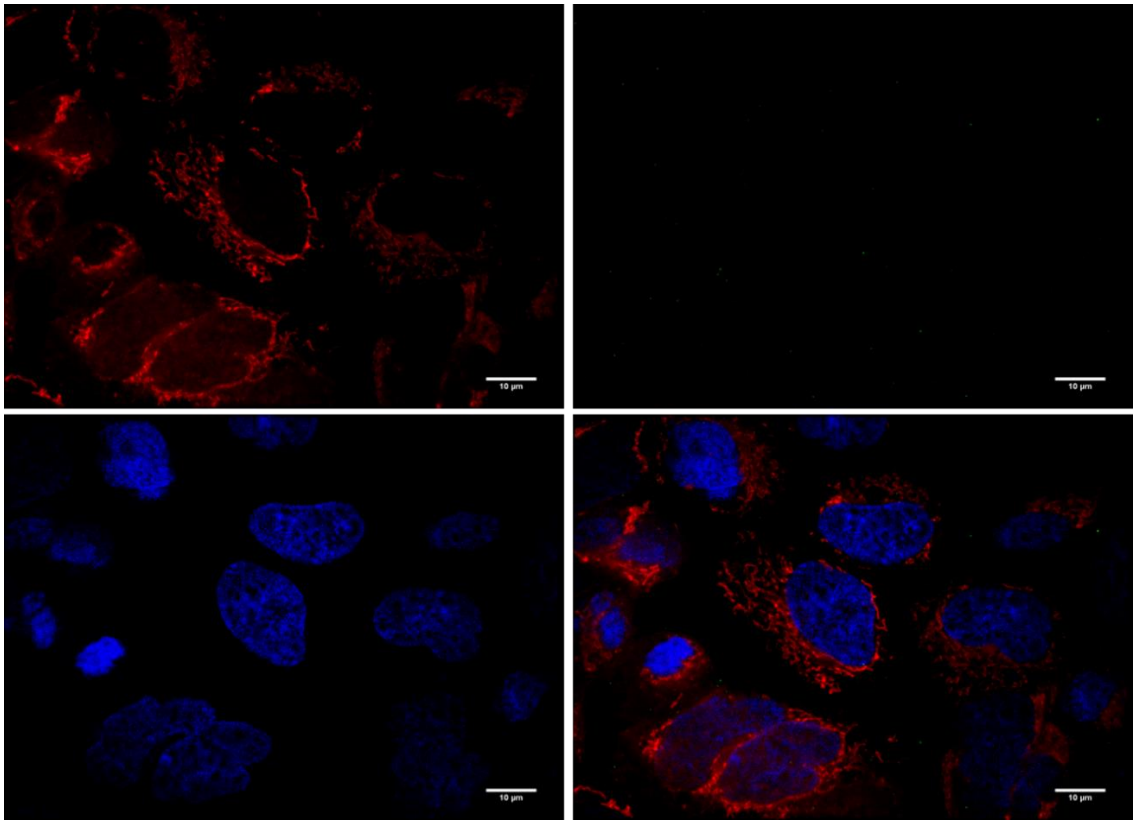

Figure 3.38: Confocal microscopy after IC of HEK293A cells transfected with empty pCMV-SPORT6 (high magnification). Cells have been stained for mitochondria (Mitotracker red, top left), HA-tag (Alexafluor 488, top right) and nuclei (DAPI, bottom left). Bottom right is a merged image of all channels. Scale bar = 10 µm.

3.4.5.1.2 pCMV-SPORT6-nuclear DNMT1 localisation

Localisation of DNMT1 protein overexpressed by pCMV-SPORT6-nuclear DNMT1 was examined. The protein stained with HA-tag antibody was successfully expressed in the nucleus (**Figure 3.39** and **Figure 3.40**).

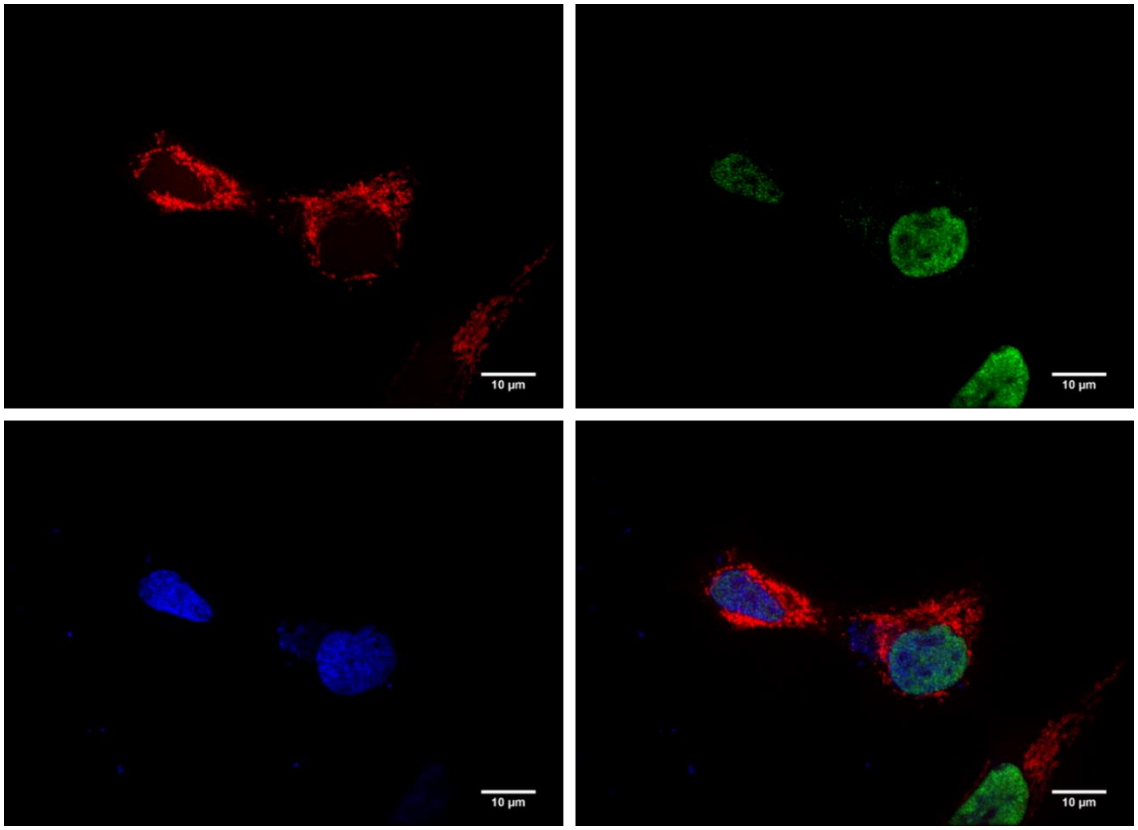

Figure 3.39: Confocal microscopy after IC of HEK293A cells transfected with pCMV-SPORT6-nuclear DNMT1 (high magnification). Cells have been stained for mitochondria (Mitotracker red, top left), HA-tag (Alexafluor 488, top right) and nuclei (DAPI, bottom left). Bottom right is a merged image of all channels. Scale bar = 10 µm.

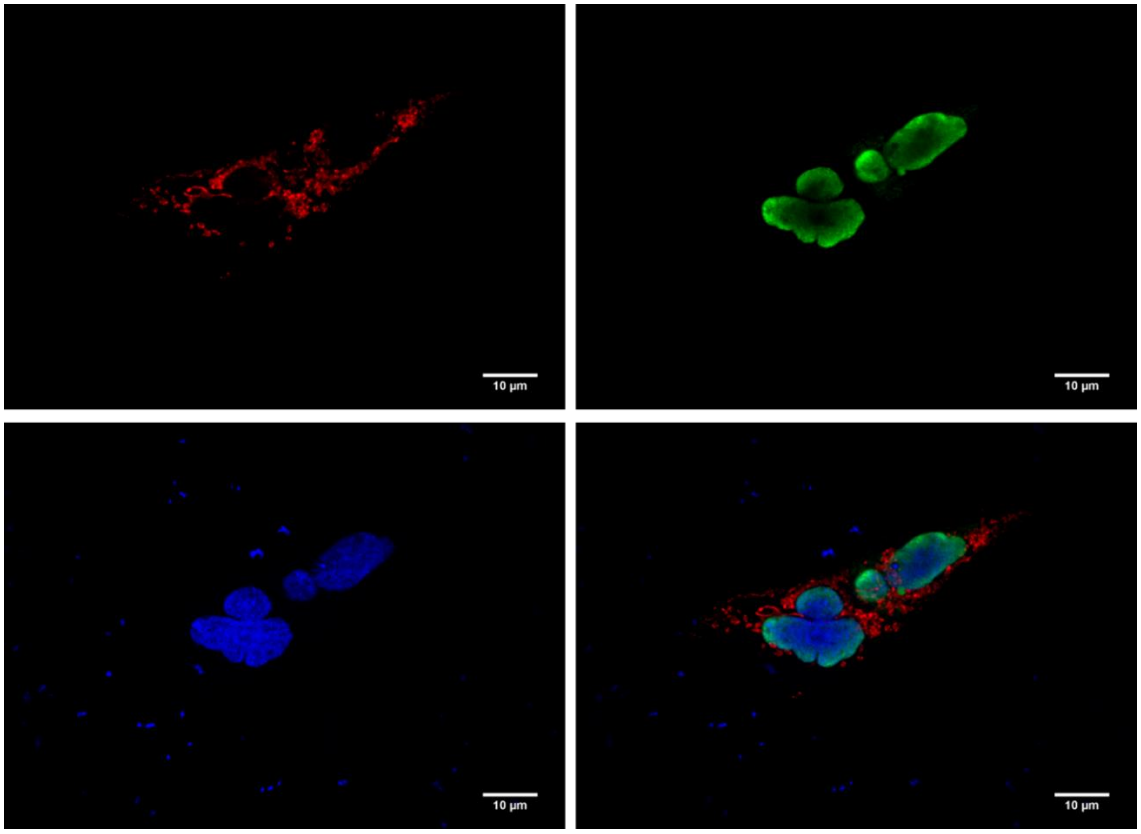

Figure 3.40: Confocal microscopy after IC of HEK293A cells transfected with pCMV-SPORT6-nuclear DNMT1 (high magnification). Cells have been stained for mitochondria (Mitotracker red, top left), HA-tag (Alexafluor 488, top right) and nuclei (DAPI, bottom left). Bottom right is a merged image of all channels. Scale bar = 10 µm.

3.4.5.1.3 pCMV-SPORT6-whole DNMT1 localisation

Localisation of whole DNMT1 proteins overexpressed by pCMV-SPORT6-whole DNMT1 (Strategy #1) and pCMV-SPORT6-whole DNMT1 (Strategy #2) was examined. As expected from Mitoprot II prediction, the protein expressed by pCMV-SPORT6-whole DNMT1 (Strategy #1) could not localise at a mitochondrial level, as only nuclear signal coming from the HA-tag antibody was detected. Strong cytosolic signal was also observed in some cells (**Figure 3.41** and **Figure 3.42**).

According to Uniprot and Mitoprot II predictions, the protein expressed by pCMV-SPORT6-whole DNMT1 (Strategy #2) was observed in both nuclear and mitochondrial regions in HEK293A cells (**Figure 3.43** and **Figure 3.44**). Even though the pattern of localisation was not homogeneous (**Figure 3.45**), all pCMV-SPORT6-whole DNMT1 (Strategy #2) transfected cells showed a good mixture of nuclear and mitochondrial localisation, indicating that the 1st-to-3rd ATG sequence acts as a MLS for DNMT1.

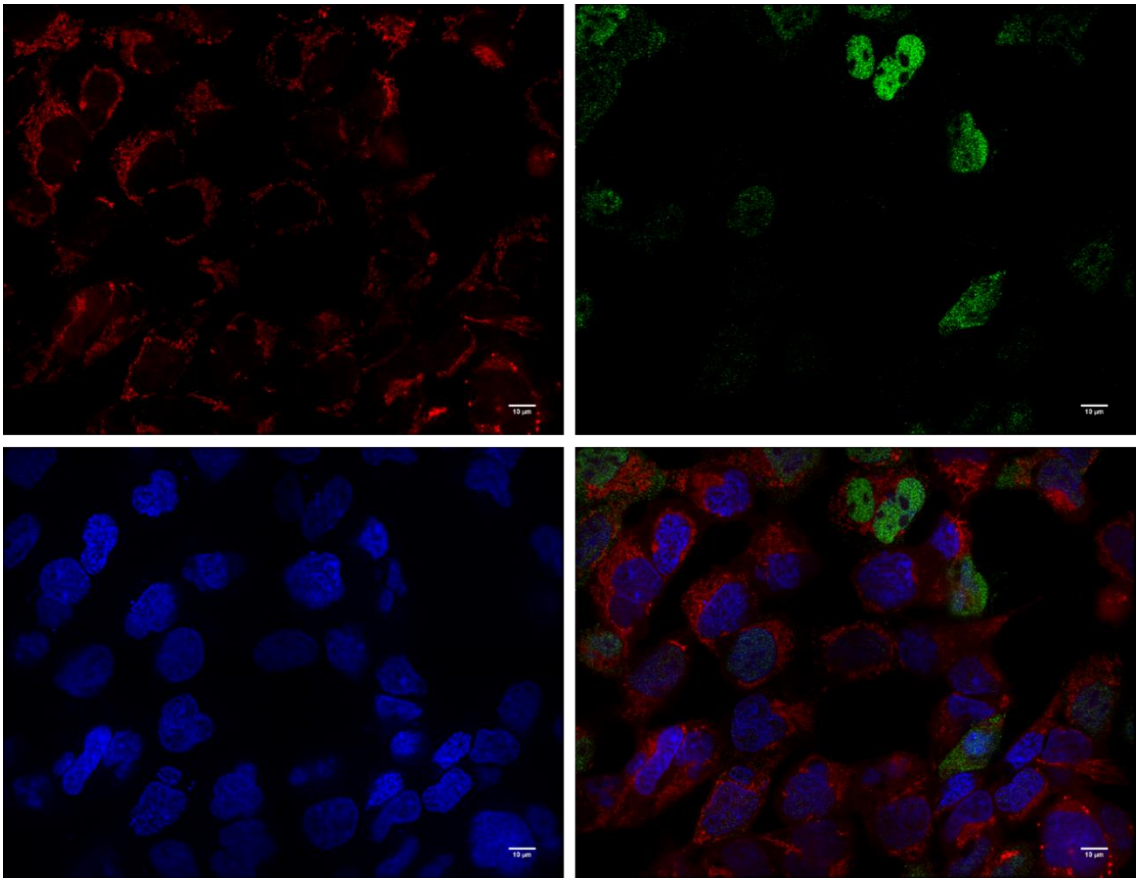

Figure 3.41: Confocal microscopy after IC of HEK293A cells transfected with pCMV-SPORT6-whole DNMT1 (Strategy #1) (low magnification). Multiple images were taken, then stitched together. Cells have been stained for mitochondria (Mitotracker red, top left), HA-tag (Alexafluor 488, top right) and nuclei (DAPI, bottom left). Bottom right is a merged image of all channels. Scale bar = 10 µm.

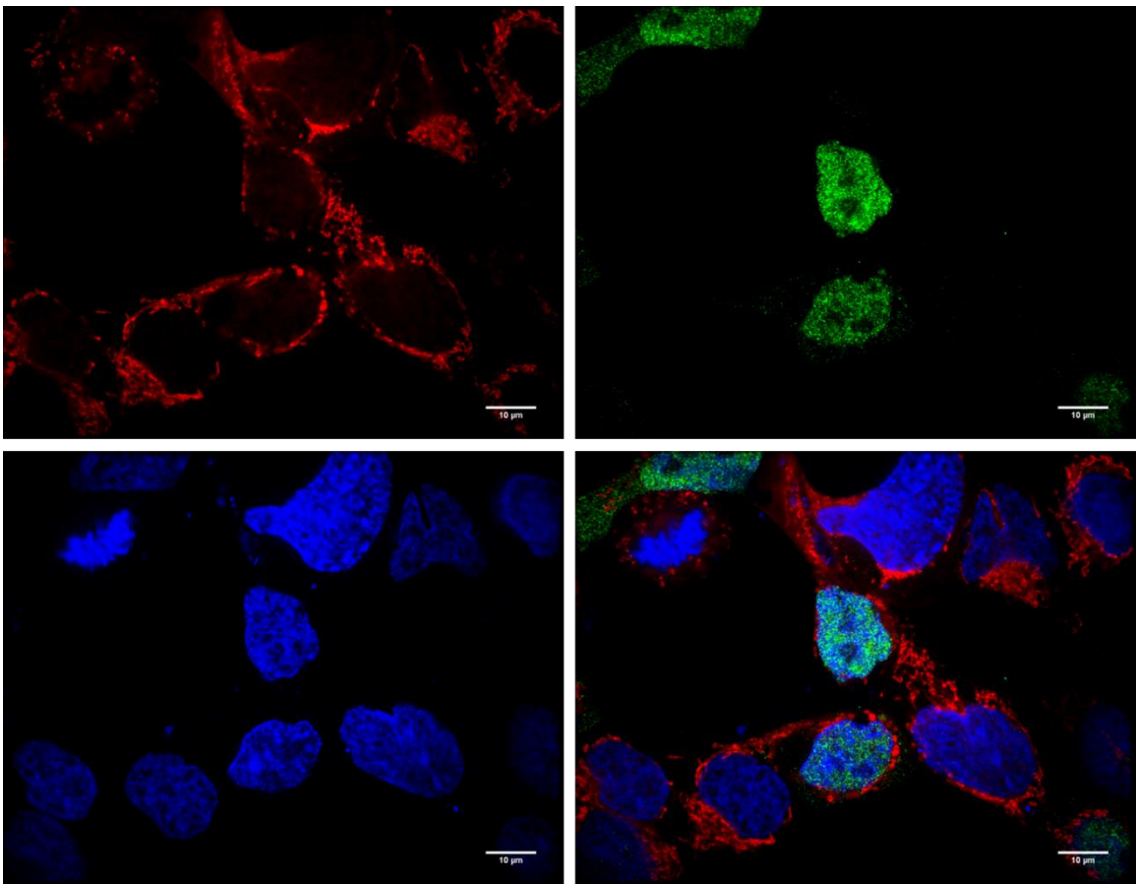

Figure 3.42: Confocal microscopy after IC of HEK293A cells transfected with pCMV-SPORT6-whole DNMT1 (Strategy #1) (high magnification). Cells have been stained for mitochondria (Mitotracker red, top left), HA-tag (Alexafluor 488, top right) and nuclei (DAPI, bottom left). Bottom right is a merged image of all channels. Scale bar = 10 µm.

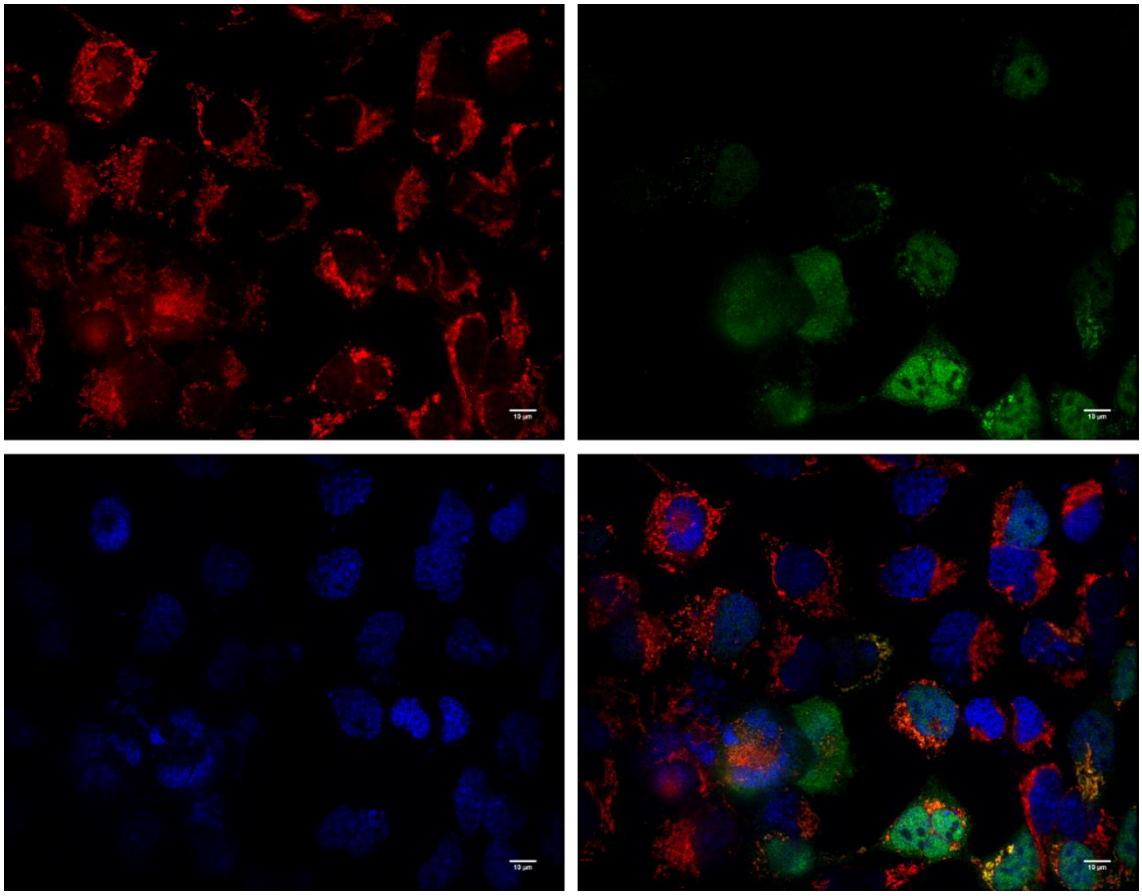

Figure 3.43: Confocal microscopy after IC of HEK293A cells transfected with pCMV-SPORT6-whole DNMT1 (Strategy #2) (low magnification). Multiple images were taken, then stitched together. Cells have been stained for mitochondria (Mitotracker red, top left), HA-tag (Alexafluor 488, top right) and nuclei (DAPI, bottom left). Bottom right is a merged image of all channels. Scale bar = 10 µm.

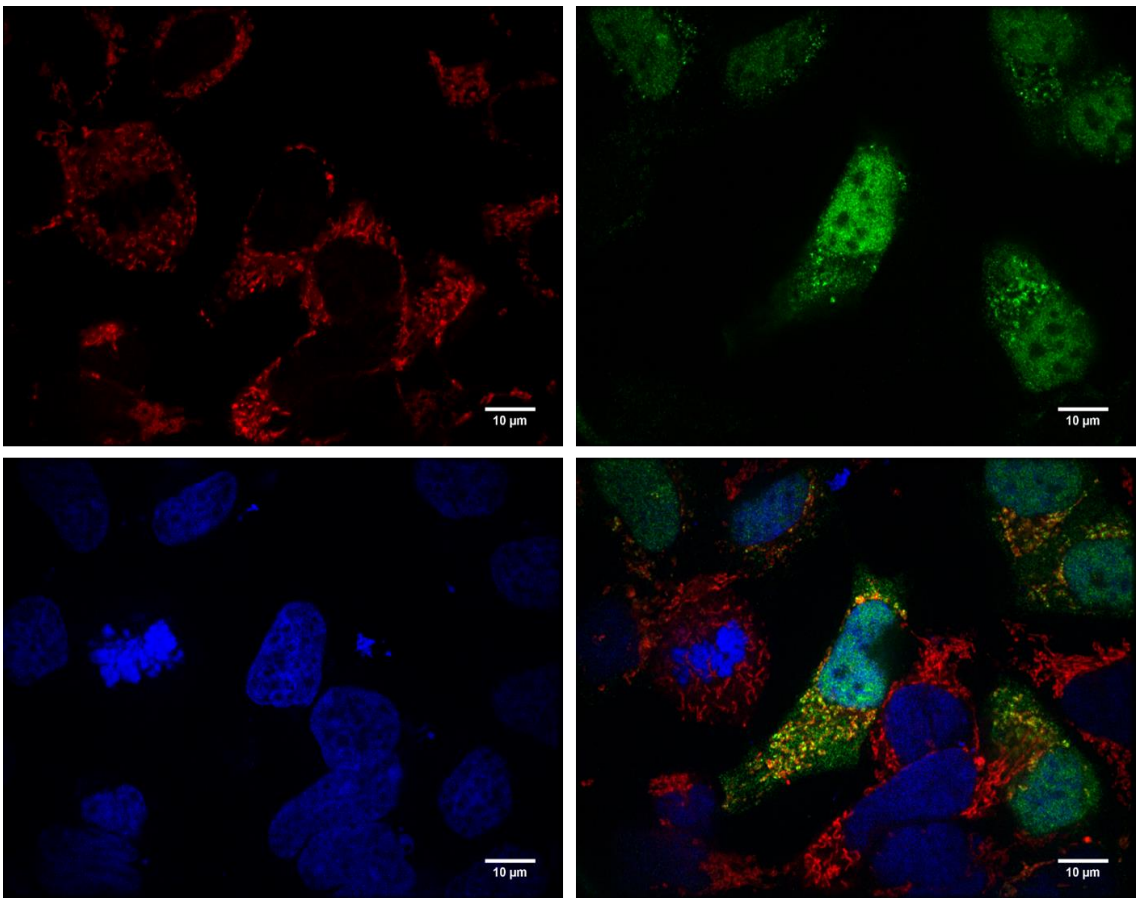

Figure 3.44: Confocal microscopy after IC of HEK293A cells transfected with pCMV-SPORT6-whole DNMT1 (Strategy #2) (high magnification). Cells have been stained for mitochondria (Mitotracker red, top left), HA-tag (Alexafluor 488, top right) and nuclei (DAPI, bottom left). Bottom right is a merged image of all channels. Scale bar = 10 µm.

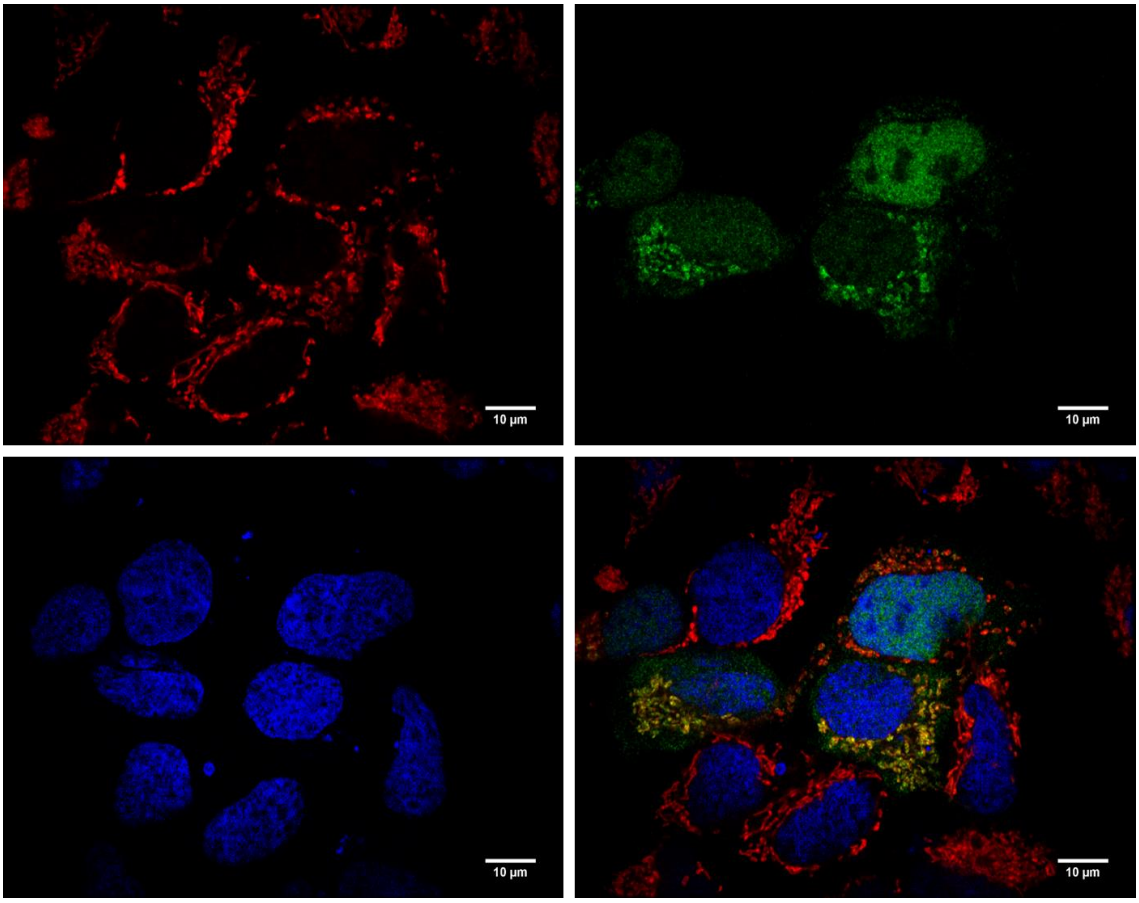

Figure 3.45: Confocal microscopy after IC of HEK293A cells transfected with pCMV-SPORT6-whole DNMT1 (Strategy #2) (high magnification). Cells have been stained for mitochondria (Mitotracker red, top left), HA-tag (Alexafluor 488, top right) and nuclei (DAPI, bottom left). Bottom right is a merged image of all channels. Scale bar = 10 µm.

3.4.5.1.4 pCMV-SPORT6-mitochondrial DNMT1 localisation

Localisation of overexpressed mitochondrial DNMT1 with mutated NLS by pCMV-SPORT6-mitochondrial DNMT1 was examined. No HA-tag antibody signal from nuclei of successfully transfected cells was observed. Furthermore, a clear mitochondrial localisation pattern was observed in all successfully transfected cells (**Figures 3.46**, **3.47** and **3.48**) indicating that the 1st-to-3rd ATG sequence acts as a mitochondrial localisation signal and the predicted nuclear localisation signal allows DNMT1 to localise at a nuclear level.

By disrupting the NLS through mutation it has been possible to obtain a DNMT1 isoform that may only interact with mitochondrial DNA due to the nature of its localisation features, and its effects on mtDNA methylation will be investigated in chapter 4.

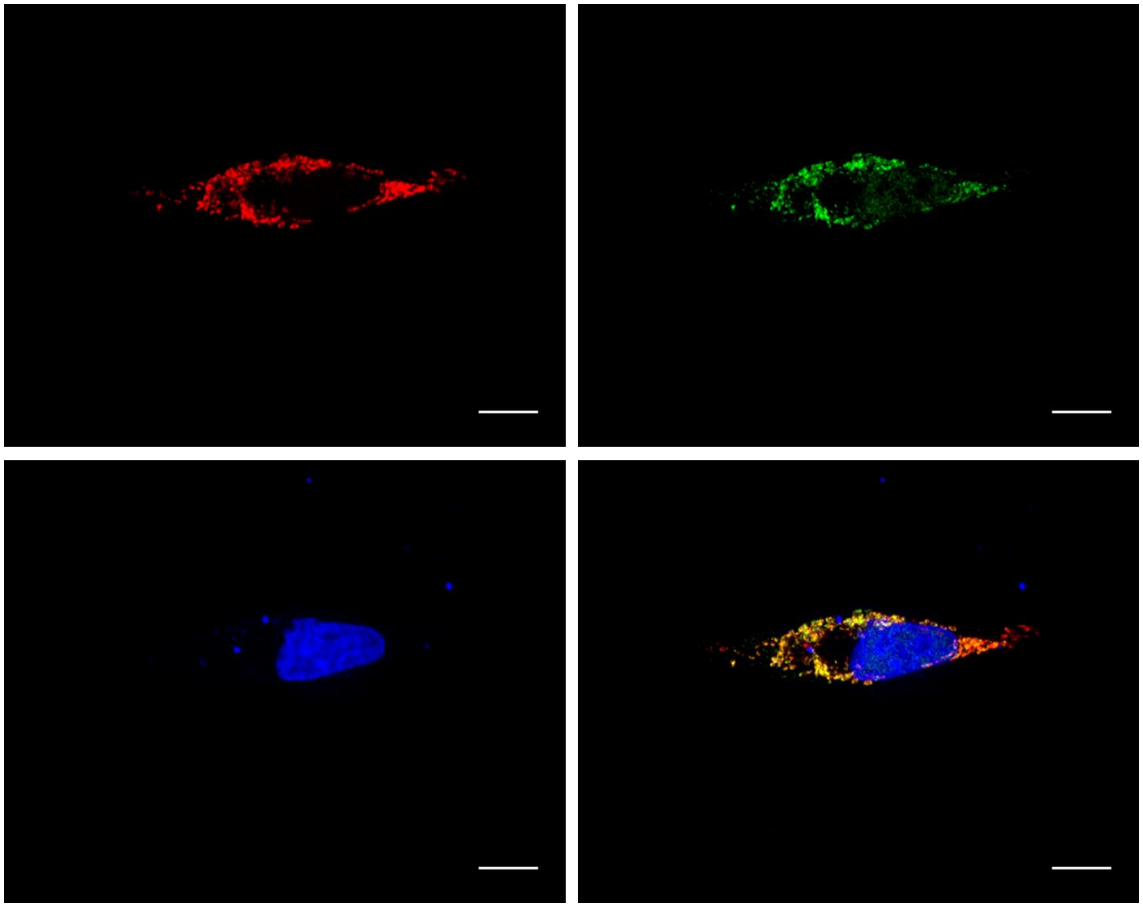

Figure 3.46: Confocal microscopy after IC of HEK293A cells transfected with pCMV-SPORT6-mitochondrial DNMT1 (high magnification). Cells have been stained for mitochondria (Mitotracker red, top left), HA-tag (Alexafluor 488, top right) and nuclei (DAPI, bottom left). Bottom right is a merged image of all channels. Scale bar = 10 µm.

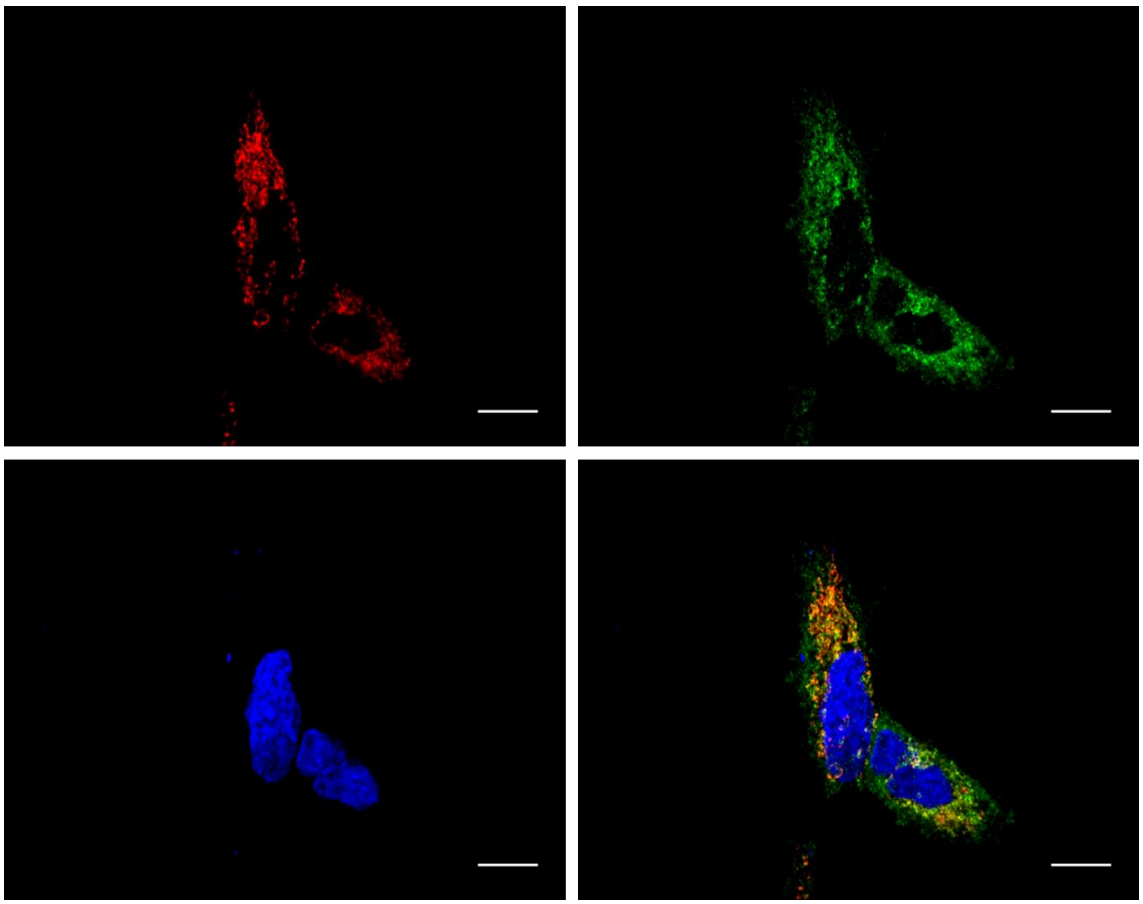

Figure 3.47: Confocal microscopy after IC of HEK293A cells transfected with pCMV-SPORT6-mitochondrial DNMT1 (high magnification). Cells have been stained for mitochondria (Mitotracker red, top left), HA-tag (Alexafluor 488, top right) and nuclei (DAPI, bottom left). Bottom right is a merged image of all channels. Scale bar = 10 µm.

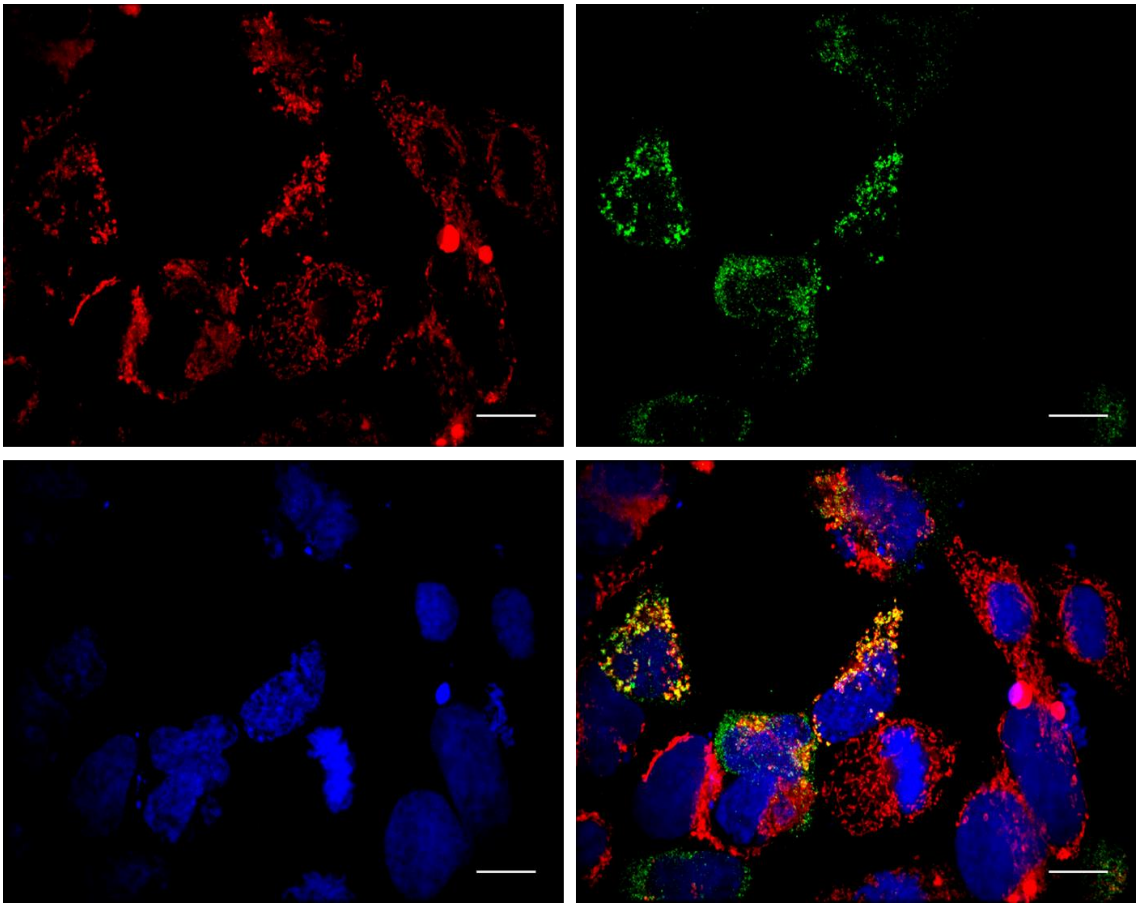

Figure 3.48: Confocal microscopy after IC of HEK293A cells transfected with pCMV-SPORT6-mitochondrial DNMT1 (high magnification). Cells have been stained for mitochondria (Mitotracker red, top left), HA-tag (Alexafluor 488, top right) and nuclei (DAPI, bottom left). Bottom right is a merged image of all channels. Scale bar = 10 µm.

3.4.5.2 Western blotting after fractioning of HEK293A cells

Several protocols for transfection and fractioning were performed in order to find the best conditions. The final protocols are described in subchapters 2.3 and 2.5. The samples were incubated with antibodies for DNMT1 and HA-tag, respectively. A certain degree of overexpression was observed in all of the samples transfected with plasmids containing DNMT1 sequence compared with the proteins transfected with empty SPORT6 vector (**Figure 3.49**). The samples incubated with the antibody for DNMT1 show a faint band in the control sample, whereas the other samples show very clear bands. The negative control transfected with empty pCMV-SPORT6 vector incubated with the HA-tag antibody, as expected, did not show any bands, whereas clear bands could be seen in nuclear DNMT1, whole DNMT1 and mitochondrial DNMT1 transfected samples.

Then, the Western blotting using the fractionated samples transfected with plasmids containing DNMT1 sequence was then performed. The blots showed a good degree of separation after fractioning, with clear Lamin A/C bands in the nuclear fraction (with no VDAC clear bands detectable) and clear VDAC bands in the mitochondrial fraction (with little to no Lamin A/C bands). However, the DNMT1 expression in mitochondrial fraction is low, and Lamin A/C signal was observed, suggesting contamination from the nuclear fraction (**Figure 3.50**).

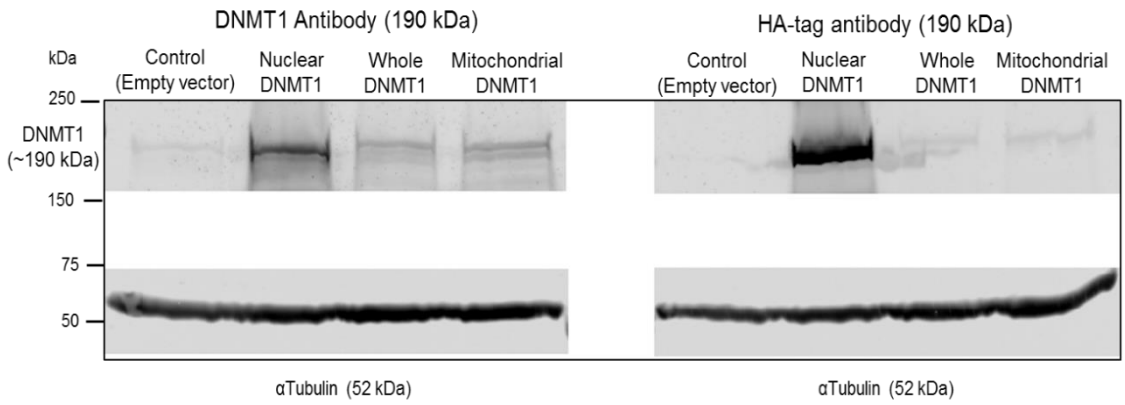

Figure 3.49: Western blotting of HEK293A cells following DNMT1 overexpression. Empty pCMV-SPORT6 as a negative control. Membranes were probed with both DNMT1 and HA-tag antibodies. αTubulin was used as an housekeeping control for protein expression.

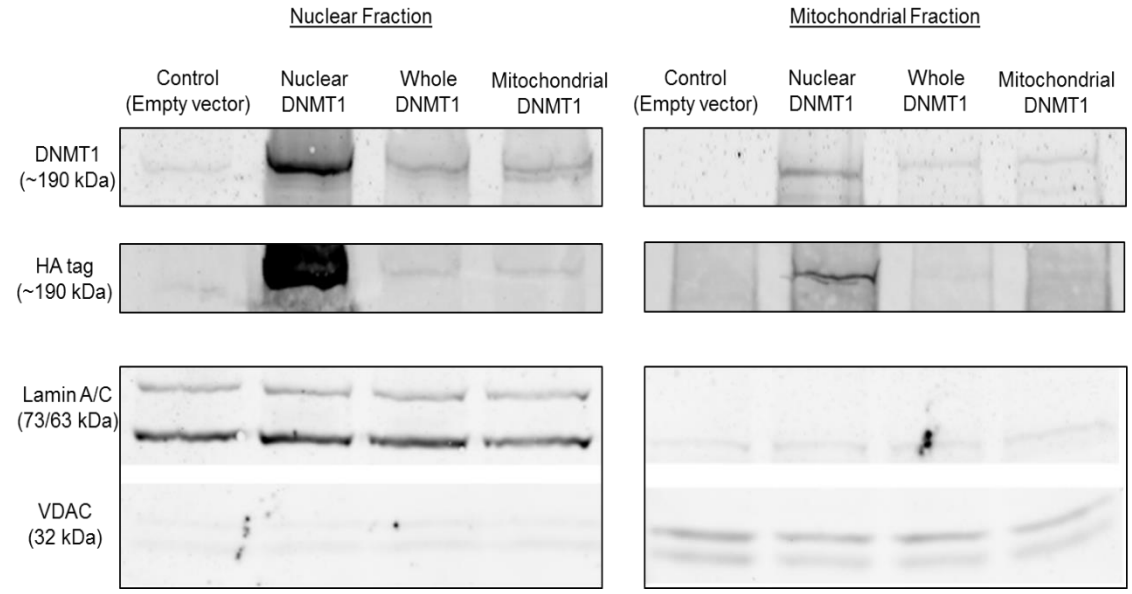

Figure 3.50: Western blotting of HEK293A cells nuclear and mitochondrial fractions following DNMT1 overexpression. Empty pCMV-SPORT6 as a negative control. Membranes were probed with both DNMT1 and HA-tag antibodies. Lamin A/C was used as an housekeeping control for the nuclear fraction, whereas Voltage-dependent anion channel protein (VDAC) was used as an housekeeping control for the mitochondrial fraction.

3.5 Discussion

Starting from a pCAG-NLS-DNMT1 construct obtained from Prof. Tajima (Japan), four constructs for the overexpression of DNMT1 were generated. The first construct (pCMV-SPORT6-nuclear DNMT1) was generated to serve as an overexpression vector for nuclear DNMT1, thereby replacing it. Furthermore, by obtaining this vector it has been possible to replace the Myc-tag and EcoRI external restriction site with an HA tag and a KpnI external restriction site. Additionally, this cloning strategy resulted in excision of the external NLS site, allowing me to examine the localization features of DNMT1 cDNA (carrying the internal NLS site) under the control of a CMV promoter.

Immunocytochemistry analysis following overexpression showed a nuclear-only localisation, thereby confirming the efficacy of the internal NLS and of the plasmid.

To obtain a plasmid that could overexpress DNMT1 in both mitochondria and nuclei, the predicted MLS sequence (that is, the 1st-to-3rd ATG sequence reported by Shock L. et al[101]) was cloned along with an HA-tag, and inserted at 5' of the nuclear DNMT1 cDNA. In this regard, two different strategies were adopted for the creation of this construct, leading to the creation of two separate plasmids. The pCMV-SPORT6-whole DNMT1 (Strategy#1) and pCMV-SPORT6-whole DNMT1 (Strategy #2) construct were created by adding the MLS sequence, and only differed in the positioning of the HA-tag. The first construct (pCMV-SPORT6-whole DNMT1 (Strategy #1)) created would carry the HA tag before the MLS, whereas the second construct (pCMV-SPORT6-whole DNMT1 (Strategy #2)) would carry it right before the 3rd ATG. These constructs would localise in the mitochondrial matrix through the recognition of a cleavage site by the presequence translocase complex within the inner membrane[111,113]. The

cleavage site and chances of mitochondrial localisation of the two DNMT1 sequences were investigated by using Mitoprot II software. No cleavage site could be predicted for pCMV-SPORT6-whole DNMT1 (strategy #1) and the chances of mitochondrial localisation were very low (~7.6%). Conversely, analysis of pCMV-SPORT6-whole DNMT1 (strategy #2) resulted in identification of a cleavage site and high chances of mitochondrial localisation (~87%), suggesting that whole DNMT1 (strategy #2) can localise to mitochondria.

To confirm the mitochondrial localisation, immunocytochemistry after single overexpression of the two plasmids was performed, and pCMV-SPORT6-whole DNMT1 (Strategy #1) plasmid was therefore abandoned. Furthermore, pCMV-SPORT6-whole DNMT1 (Strategy #2) could successfully overexpress HA-tagged DNMT1 in both nuclear and mitochondrial compartments, suggesting that the 1st-to-3rd ATG region indeed acts as a MLS and that DNMT1 is localised to mitochondria via recognition of the MLS and the presequence pattern, and confirming the importance of the NLS site for nuclear localisation. Since pCMV-SPORT6-whole DNMT1 (Strategy #1) was abandoned, the pCMV-SPORT6-whole DNMT1 (Strategy #2) plasmid will now be referred to as pCMV-SPORT6-whole DNMT1.

Finally, a fourth construct was generated by modifying the pCMV-SPORT6-whole DNMT1 overexpression vector; a mutation of the predicted NLS in the DNMT1 cDNA was performed, and the sequence was analysed through Mitoprot II. Software analysis showed a similar cleavage site as pCMV-SPORT6-whole DNMT1, with similar chances of mitochondrial localisation (~87%). Immunocytochemistry results proved this vector to be able to successfully localize in the mitochondrial compartment, but not in the nuclear compartment. These results further confirm the importance of a conserved NLS sequence for

nuclear localisation[126]. To date, this is the first study to demonstrate the functionality of the predicted NLS as the only sequence required for DNMT1 nuclear localisation, and presents new opportunities for setting up mitochondria-specific DNMT1 overexpression systems.

After obtaining these vectors, Western blotting experiments were performed to identify the best transfection protocol as well as a mean to refining the cell fractioning protocol. Clear DNMT1 and HA-tag bands were found in whole cell lysates of transfected samples, and results of the different housekeeping genes used (α-tubulin for whole cell lysates, VDAC for mitochondria and Lamin A/C for nuclei) showed that the fractioning protocol is suitable for successful isolation of the different cell compartments. However, nuclear and mitochondrial transfected samples failed to show proper localization of DNMT1 as per the immunocytochemistry studies. Moreover, no HA-tag bands were found in pCMV-SPORT6-whole DNMT1 or pCMV-SPORT6-mitochondrial DNMT1 transfected samples. This could be due to some experimental issues with the fractioning protocol[127], as a certain degree of cross-contamination between the two fractions appears to be unavoidable.

To conclude, these results altogether confirm the importance of a conserved nuclear localisation sequence for nuclear localisation and demonstrate the ability of the 1st-to-3rd ATG sequence to act as an MLS. Both these sequences proved to be important to achieve proper DNMT1 localization, thereby confirming the results predicted in the papers by Song J. et al[105] (for NLS) and Shock et al (for MLS)[90]. In the next chapter, the methylation status of HEK293A mtDNA sequences after DNMT1 overexpression will be investigated.

Chapter 4 : Methylation analysis of mtDNA sequences, DNMT3A cloning and establishment of DNMT1-DNMT3A double overexpression

4.1 Introduction

4.1.1 Methylation of mitochondrial DNA

The epigenetic regulation of mtDNA has been an infrequently studied topic and remained an open question for a long time. Early studies from the 1970s reported controversial results, claiming that there was no methylation of mtDNA in either mouse or human cells[128,129], and finding methylation in mtDNA from beef heart[130]. Studies conducted between the 1980s and the 1990s reported low levels of methylation restricted to CpG dinucleotides in mitochondria of both mouse[51] and human cells[131], or even similar levels of CpG suppression to that of nuclear DNA[52].

Since then, even though there has been increasing number of reports confirming the presence of methylation at mitochondrial level[132-134], and mitochondria have been shown to contain the machinery required to epigenetically modify mtDNA[135,136], the presence of methylation in mtDNA has remained controversial[99,102,137-139]. Moreover, mitochondrial DNA has been linked to heart failure[36] and its epigenetic regulation has been suggested as a next-generation biomarker for diseases[103,140].

4.1.2 Interaction between DNMT1 and other DNMTs

It has been reported that the human de novo enzymes hDNMT3A and hDNMT3B form complexes with the maintenance enzyme hDNMT1, as interaction sites exist in their sequence[141] (**Figure 4.1**). Interaction sites for DNMT3A and DNMT3B are localised on the N-terminal of DNMT1 sequence, with the DNMT3B site overlapping part of the NLS, and both DNMT3A and DNMT3B possess overlapping interaction sites for the other DNMTs. Furthermore, functional

cooperation between hDNMT1 and hDNMT3B has been shown in a human colorectal carcinoma line[142].

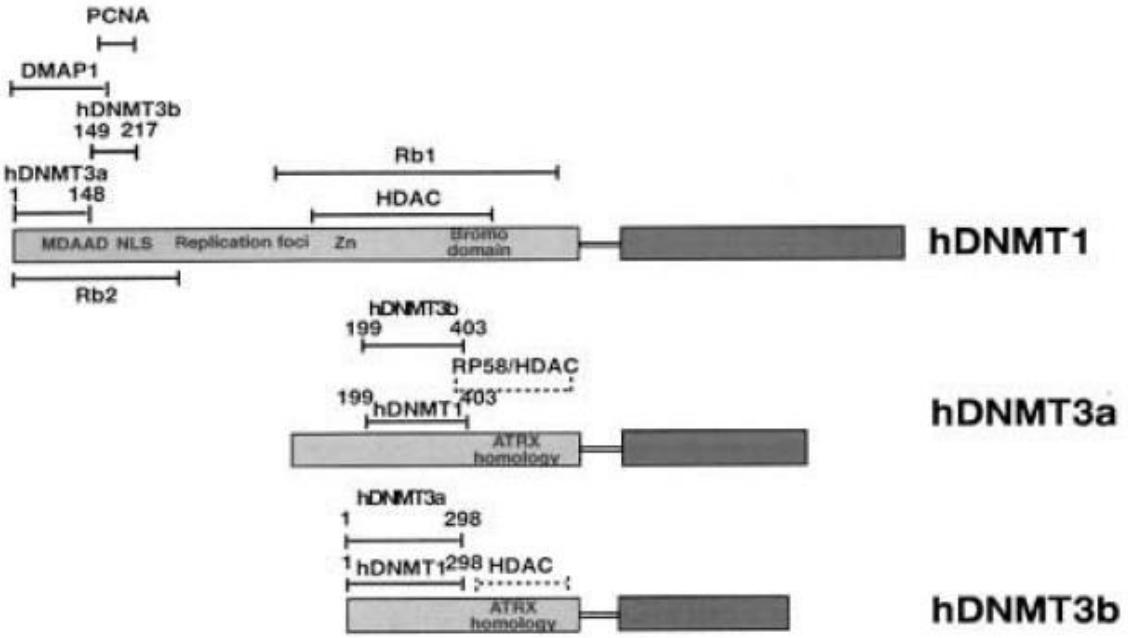

Figure 4.1: Summary of the interaction sites of the human DNMTs. Amino acid residues for protein-protein interactions are indicated underneath the interacting protein's name (i.e. hDNMT3A 1-148). Figure taken from *Co-operation and communication between the human maintenance and de novo DNA (cytosine-5) methyltransferases*, Kim et al, 2002[141].

4.1.3 DNMT3A overview and methylation features

DNMT3A is involved in de novo methylation of cytosine residues, especially for de novo methylation of the CpG dinucleotides in the repeated DNA sequences which are present in the pericentric satellite regions of chromosomes[88,143]. Knock-out of the Dnmt3a gene has been shown to cause embryonic lethality similar to the Dnmt1$^{-/-}$ mouse model[88]. The structure of DNMT3A includes 3 main parts: an N-terminal regulatory domain, a C-terminal catalytic domain and a central linker region[144,145]. The DNMT3A sequence does not contain an MLS.

4.1.4 Bisulphite sequencing principles

DNA modification by bisulphite conversion is a well-established protocol that can be performed for DNA methylation analysis. The fundamental principle behind bisulphite conversion is that sulphite can be reversibly added to cytosine to mediate the deamination of cytosine to uracil. The mechanism by which this process is driven was discovered many years ago[146-148], and since then methods based around bisulphite conversion of DNA account for the majority of new data on DNA methylation.

The protocol begins with the nucleophilic addition of bisulphite to the C-6 position of cytosine, which allows the rapid deamination of cytosine into 5,6-dihydrouracil-6-sulfonate. Subsequent treatment with an alkaline solution swiftly eliminates the sulfonate group and regenerates the double bond, yielding uracil. Unmodified cytosines (C) are deaminated to uracil (U), and read as thymines (T) when sequenced. Cytosines that are methylated are resistant to the bisulphite conversion, and therefore are still read as cytosines when sequenced[149] (**Figure 4.2**).

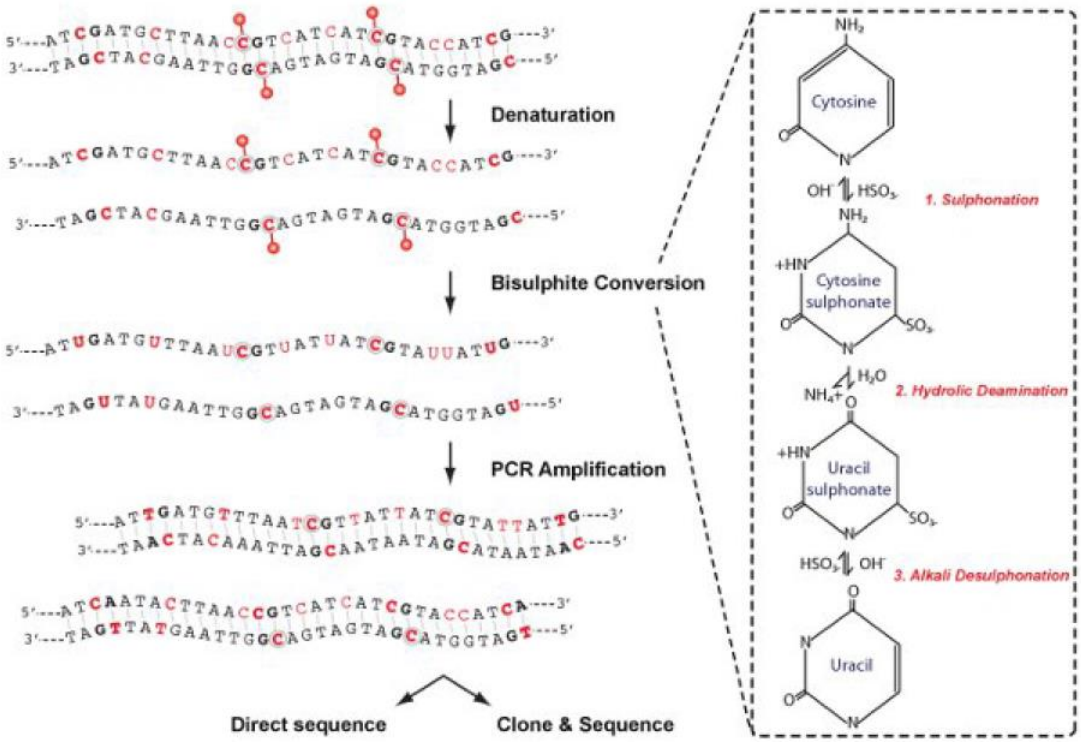

Figure 4.2: Schematic of bisulphite conversion. The bisulphite treatment conversion is divided in sulphonation, hydrolic deamination and alkali desulphonation. After this, the DNA strands are amplified and sequenced. Figure taken from *DNA Methylation: Bisulphite Modification and Analysis*, Patterson et al, 2011[149].

4.2 Aims

The aims of the studies in this chapter were to measure methylation changes of mtDNA sequences following overexpression of DNMT1, to obtain a DNMT3A overexpression construct, test the hypothesis that DNMT1 can interact with DNMT3A and allow it to localise at a mitochondrial level, and finally to establish a double overexpression system for DNMT1 and DNMT3A and investigate whether this could impact the epigenetic status of mtDNA sequences.

4.3 Methods

4.3.1 Measurement of methylation changes of mtDNA

In order to assess the effects of overexpression of the different DNMT1 isoforms on the methylation status of mitochondrial DNA genes, sequencing analysis following bisulphite treatment was performed. Depending of the region of interest, three different transfection conditions were investigated: empty pCMV-SPORT6, pCMV-SPORT6-whole DNMT1 (strategy #2), and pCMV-SPORT6-mitochondrial DNMT1.

4.3.1.1 DNA isolation and bisulphite treatment

4.3.1.1.1 Bisulphite treatment on circular mtDNA

For each transfection condition, a total of 400,000 HEK293A cells were seeded in a 10 cm Corning® tissue-culture treated culture dish (Sigma Aldrich®, CLS430167). The next day, transfection with FuGene HD was performed, and DNA was isolated 48 hours after transfection using a QIAamp DNA Blood Mini Kit (Qiagen®, 51104). Protocol from Appendix J (Protocol for Crude Cell Lysates and Other Samples) was used.

The DNA including circular mtDNA underwent bisulphite conversion using a EZ-DNA Methylation Gold Kit (Zymo Research®, D5005). The kit guarantees a conversion rate of over 99%. Briefly, 400 ng of DNA from each sample was added to 130 µl of CT conversion reagent, and the mixtures were then incubated in a thermocycler where they underwent a single cycle of 98º C for 10 minutes, 64º C for 150 minutes and cooldown to 4º C. Then, the samples were loaded onto a Zymo-Spin ™ IC column with 600 µl of M-Binding Buffer, and centrifuged at 13,000 rpm for 30 seconds. Flow-through was discarded and column were washed with 100 µl M-Wash buffer and centrifuged at 13,000 rpm for 30 seconds.

200 µl M-Desulphonation buffer was added to the columns, which were then incubated at room temperature for 20 minutes. Following incubation, columns were centrifuged at 13,000 rpm for 30 seconds. Flow-through was discarded and columns were washed with 200 µl M-wash buffer and centrifuged at 13,000 rpm for 30 seconds. Finally, columns were placed into a fresh 1.5 ml Eppendorf tube, and samples were eluted by applying 10 µl M-Elution buffer directly to the column matrix and centrifuging at 13,000 rpm for 30 seconds. A general scheme of bisulphite conversion through EZ-DNA Methylation Gold Kit is shown (**Figure 4.3**).

4.3.1.1.2 Bisulphite treatment with linearised mtDNA

Following the first round of results, an additional step was introduced. Following DNA isolation after transfection, isolated DNA was quantified through Nanodrop analysis, and 2 µg of each sample were digested overnight at 37ºC using 2 µl HindIII high concentration restriction enzyme (New England BioLabs®, R0104T). This step was introduced in order to digest and linearise mtDNA and allow the bisulphite conversion kit to successfully convert mtDNA residues. Digested DNA was then extracted through phenol extraction-ethanol precipitation.

Briefly, samples were resuspended in dH_2O (200 µl final volume), then 100 µl of phenol and 100 µl of chloroform-isoamyl alcohol (24:1) were added. Samples were vortexed for 30 seconds and then centrifuged at 13,000 rpm for 5 minutes. The supernatant was then moved to a new 1.5 eppendorf tube, 20 µl of 3M of sodium acetate (NaAc) were added and the samples were vortexed. Then, 2.5 volumes of 100% ethanol solution (EtOH) were added, the samples were incubated on ice for 30 minutes and then centrifuged at 13,000 rpm for 5 minutes. Supernatant was discarded. Pellets were washed with 1 ml of 70% EtOH solution,

centrifuged at 13,000 rpm for 5 minutes twice (surnatant was removed after both centrifuge steps). Pellets were then dried up and resuspended in 30 µl dH_2O, and DNA was quantified using Nanodrop and used for bisulphite treatment.

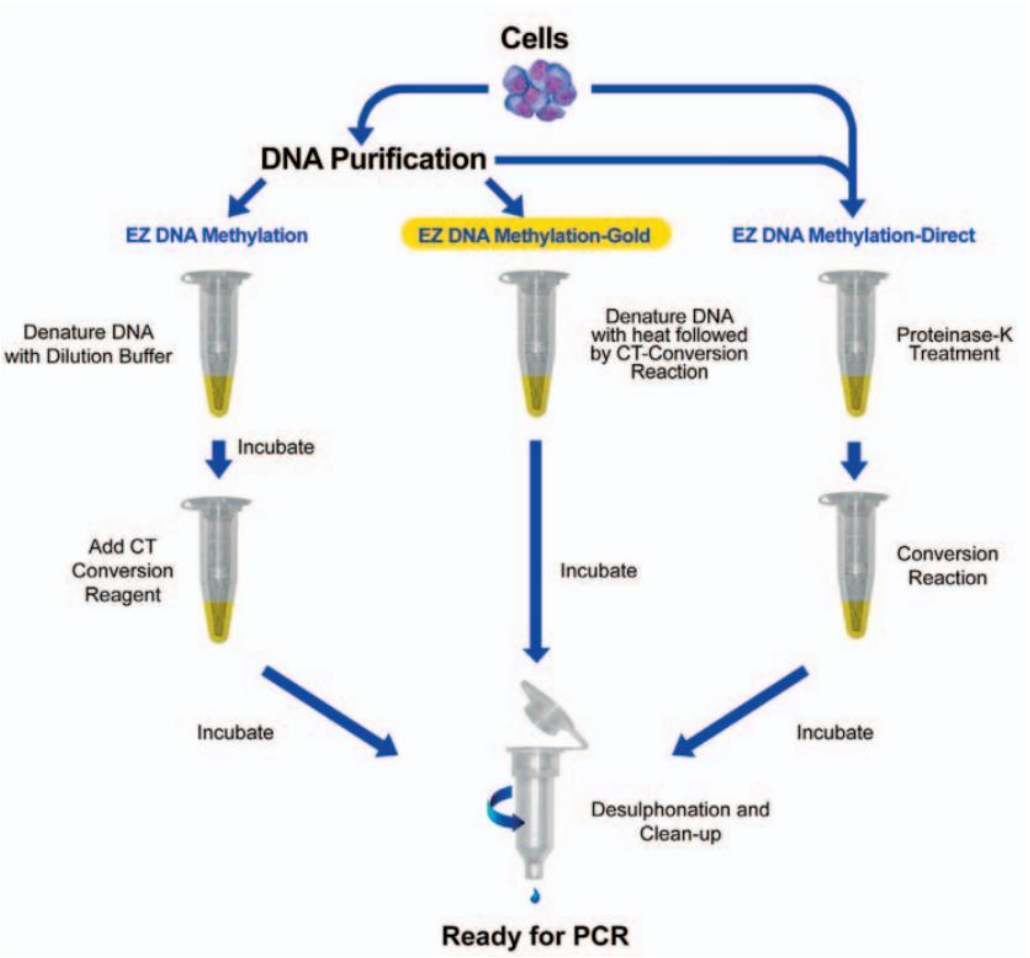

Figure 4.3: Bisulphite treatment workflow. For this project, the EZ DNA Methylation Gold Kit was used. Figure taken from Zymo Research®.

4.3.1.2 PCR for mtDNA sequences

Eluted DNA was used as a template for PCR reactions aiming to amplify given mtDNA sequences. For this study, COX2 and the first 215 base pairs of the top (light) strand of the D-Loop have been chosen as mitochondrial targets for investigation. A 10-bp tag (marked in bold) was added to the 5′- ends of the L-strand primers in order to increase the annealing temperature of the A–T enriched primer sequences. Primers' sequences (**Table 4.1**) and PCR conditions (**Figure 4.4**) are reported. PCR products were run on a 2% agarose gel to confirm the size of the amplicons.

Table 4.1: Primer sets for PCR of mitochondrial genes after bisulphite treatment.

Primer	Sequence	Company
COX2 Forward	5'-ATTGGTTATTAATGGTATTGAATTTA-3'	IDT
COX2 Reverse	5'-CTCCACAAATTTCAAAACATTAAC-3'	IDT
D-Loop Forward	5'-**AGGAAGAGAG**GATTTTAATTTAAATTATT-3'	IDT
D-Loop Reverse	5'-**AGGAAGAGAG**ACTATACTTACTTAT-3'	IDT

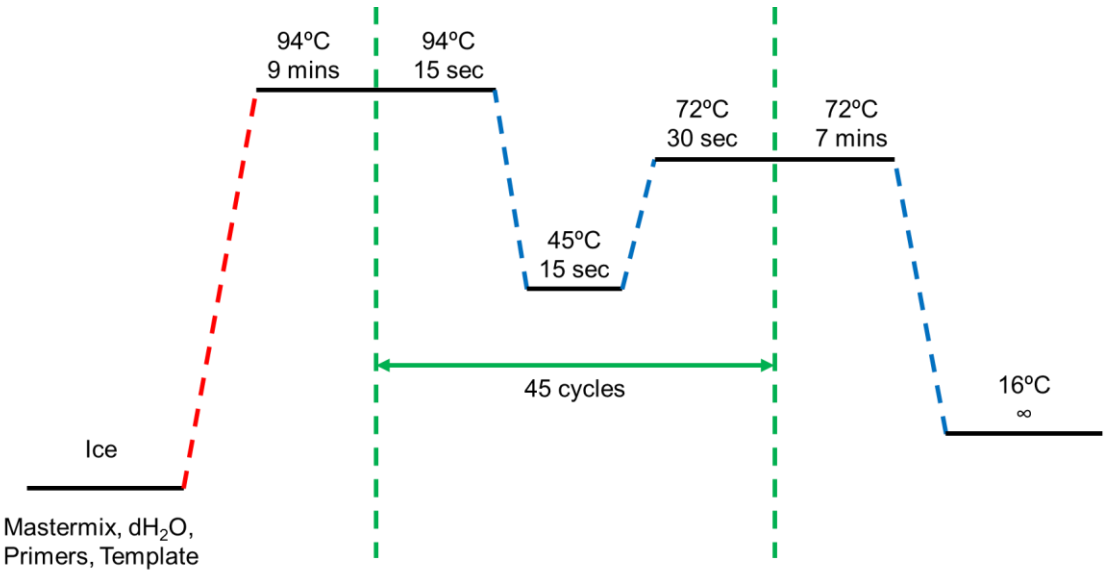

Figure 4.4: PCR conditions for COX2 and D-Loop primer sequences.

4.3.1.3 TOPO cloning of PCR products

Following PCR, PCR products were inserted in a TOPO vector using TOPO® TA Cloning® Kit for Subcloning (Thermo Fisher Scientific®, 450641). Briefly, 4 µl of PCR product were mixed with 1 µl pCR 2.1-TOPO vector (**Figure 4.5**) and 1 µl salt solution (200 mM NaCl; 10 mM $MgCl_2$), and incubated at 23º C for 15 minutes. Then, the final vector carrying the PCR product was transformed in DH5α cells (according to the protocol described in subchapter 3.3.1.1), colonies were picked and DNA was isolated through miniprep. Successful insertion of PCR products was confirmed by digesting the samples with EcoRI (New England BioLabs®, R0101L) and running them on a 2% agarose gel.

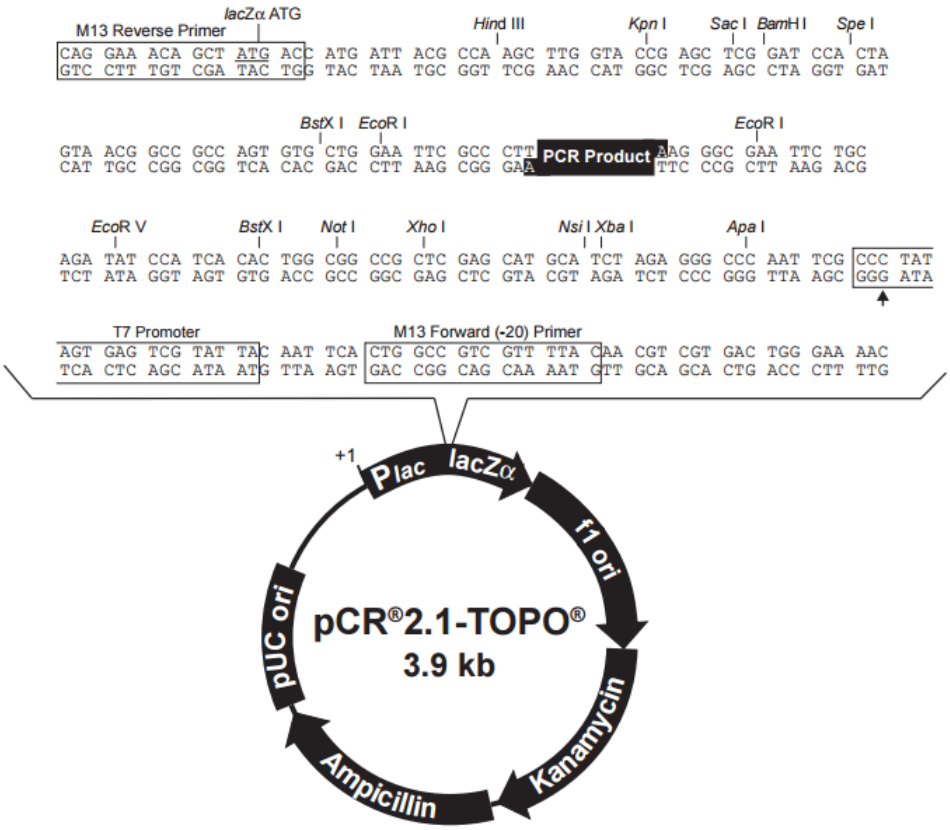

Figure 4.5: pCR 2.1-TOPO vector map. The vector contains sequences for Ampicillin as well as Kamanycin selection. The PCR product is inserted between 2 EcoRI restriction sites, and then sequenced using M13 reverse and forward primers. Taken from Thermo Fisher Scientific®.

4.3.1.4 Methylation analysis

Miniprep samples with the insert were then submitted for sequencing, and the sequencing data was analysed using Bisulphite Primer Seeker tool from Zymo Research® (http://www.zymoresearch.com/tools/bisulphite-primer-seeker).

4.3.2 Methods for pCMV-SPORT6-DNMT3A construct

To investigate whether DNMT1-DNMT3A interaction would allow DNMT3A to localise at a mitochondrial level and methylate mtDNA, a new cloning strategy for a mouse DNMT3A overexpression vector for double overexpression studies was planned. The pBluescript II KS(+) vector was used as cloning vector for subcloning and sequencing steps, whereas the pCMV-SPORT6 vector was used as an expression vector.

The first step involved PCR of the 5' fragment, sequence digestion by EcoRI-SacI and insertion into pBluescript II KS(+) for sequencing analysis, and insertion into pCMV-SPORT6. The second step involved PCR of the 3' fragment, sequence digestion by SacI-XhoI and insertion into pBluescript II KS(+) for sequencing analysis, and then insertion into pCMV-SPORT6. To facilitate cloning steps, an EcoRI site was created in the forward primer for the 5' fragment, as well as an XhoI site in the reverse primer of the 3' fragment. Moreover, a Myc-tag sequence was added to the 5' forward primer in order to facilitate detection of the protein after overexpression (**Figure 4.6**).

Figure 4.6: Final DNMT3A sequence with Myc-tag and EcoRI-XhoI restriction sites.

4.3.2.1 Primer sets for de novo PCR synthesis of DNMT3A fragments

Using C57BL/6 mouse genomic DNA as a template, PCR primers for the 5' fragment and 3' fragment of mouse DNMT3A synthesis were designed (**Table 4.2**). PCR reagents are reported (**Table 4.3**).

Table 4.2: Primer sets for DNMT3A de novo PCR synthesis. The starting codons for forward primer #1 are marked in bold, whereas the Myc tag sequence is underlined.

Primer	Sequence
DNMT3A Forward #1	5'-AAAAAGAATTCACC**ATG**GAGCAGAAGCTGATCTCAGAGGAGGACCTG**ATG**CCCTCCAGCGGCCCCGGGGACACCAG - 3'
DNMT3A Reverse #1	5'- CTCCTTGACCTTAGGTTTCTCTGTTGTGCT -3'
DNMT3A Forward #2	5'- GGCAAGTTCTCAGTGGTGTGTGTGGAGAA - 3'
DNMT3A Reverse #2	5'-AAAACTCGAGTTACACACAAGCAAAATATTCCTTCAGCGG - 3'

Table 4.3: Reagents for DNMT3A de novo PCR synthesis.

Reagent	Quantity (µl)
2x Extreme Buffer	12.5
2 mM dNTPs	5
dH_2O	0.5
10 µM Forward Primer	0.75
10 µM Reverse Primer	0.75
Template (mouse cDNA) 10 µg/µl	5
KOD Xtreme DNA Polymerase	0.5

4.3.2.2 De novo PCR synthesis conditions for DNMT3A fragments

PCR conditions for DNMT3A 5' fragment (**Figure 4.7**) and 3' fragment (**Figure 4.8**) are reported.

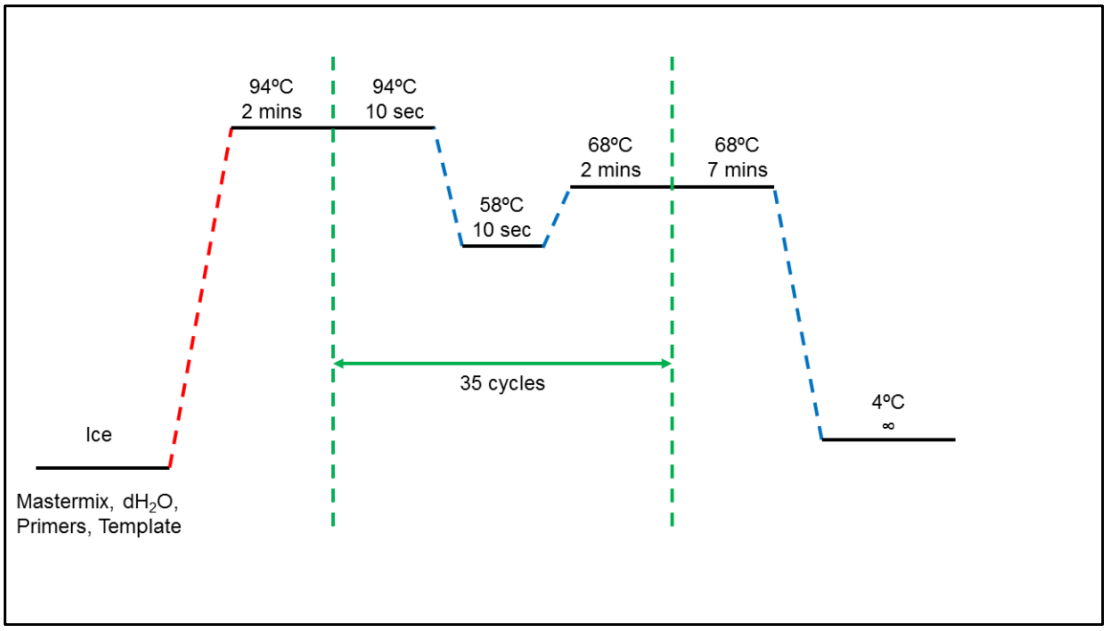

Figure 4.7: Conditions for de novo PCR synthesis of DNMT3A 5' fragment.

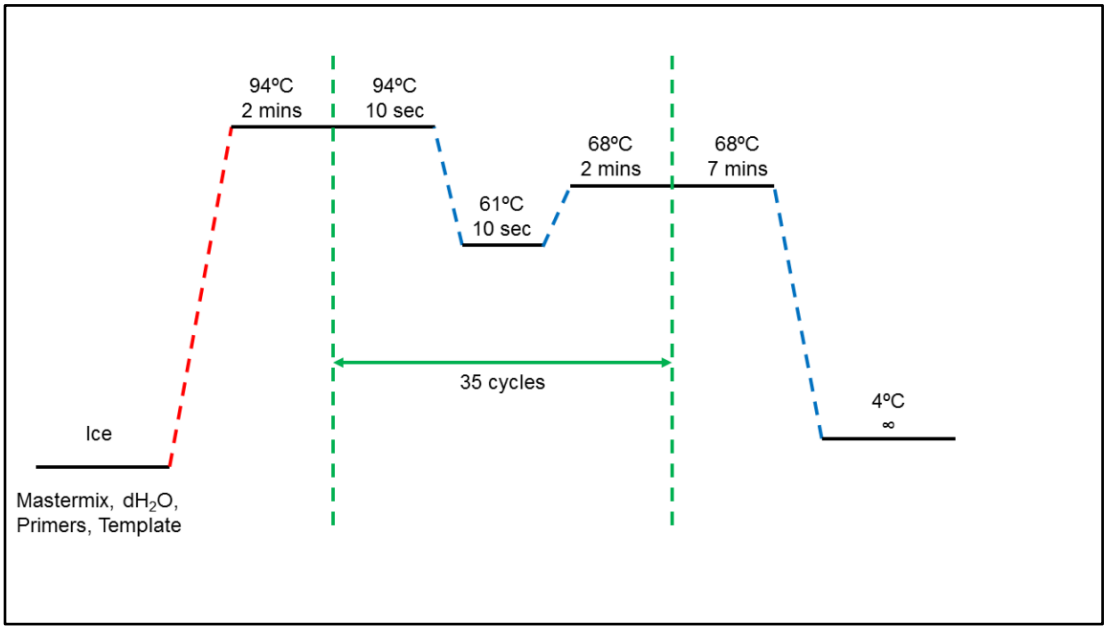

Figure 4.8: Conditions for de novo PCR synthesis of DNMT3A 3' fragment.

4.3.3 Establishment of double overexpression in HEK293A cells

To establish a DNMT1-DNMT3A double overexpression system in HEK293A cells for methylation analysis experiments, HEK293A cells were initially transfected with pCMV-SPORT6-DNMT3A plasmid alone for 48 hours, using the FuGene HD transfection protocol described in subchapter 2.2.2. Following

transfection, proteins were harvested and Western blotting for DNMT3A and Myc-tag was performed, using the protocol described in subchapter 2.7. A samples of HEK293A cells transfected with empty pCMV-SPORT6 was used as a negative control, and αTubulin was used as housekeeping gene. DNMT3A, Myc-tag and αTubulin primary antibodies are listed in Table 2.7 from subchapter 2.7.2.

After confirming single DNMT3A overexpression with both antibodies, a DNMT1-DNMT3A double transfection was performed. The usual FuGene HD protocol was performed using half of the DNA amount from pCMV-SPORT6-mitochondrial DNMT1 vector and half from pCMV-SPORT6-DNMT3A vector. Moreover, 3 other transfection conditions were used for this experiment: empty pCMV-SPORT6 as negative control, half pCMV-SPORT6-whole DNMT1/half empty pCMV-SPORT6, and half pCMV-SPORT6-DNMT3A/half empty pCMV-SPORT6. The vector pCMV-SPORT6-whole DNMT1 was chosen over pCMV-SPORT6-mitochondrial DNMT1 in order to investigate the interactions of DNMT3A with the full lenght DNMT1 sequence. After 48 hours of transfection, proteins were harvested and western blotting for DNMT1 and DNMT3A was performed.

4.3.4 HEK293A immunocytochemistry after DNMTs double overexpression

To verify localisation of overexpressed DNMT3A and whether DNMT1-DNMT3A interaction would happen at cytosolic or nuclear level, two separate sets of transfection and immunocytochemistry experiments were performed. Cells were seeded, transfected, fixed and stained according to the protocol described in subchapter 2.2 and 2.3.

In the first set of experiments, cells were transfected with 4 different conditions: empty pCMV-SPORT6, pCMV-SPORT6-mitochondrial DNMT1, pCMV-

SPORT6-DNMT3A and finally pCMV-SPORT6-mitochondrial DNMT1 and pCMV-SPORT6-DNMT3A altogether.

In the second set of experiments, cells were once again transfected with 4 different conditions: empty pCMV-SPORT6, pCMV-SPORT6-whole DNMT1, pCMV-SPORT6-DNMT3A, and finally pCMV-SPORT6-whole DNMT1 and pCMV-SPORT6-DNMT3A altogether. For both sets of experiments, imaging was performed using a TCS SP5 confocal microscope (Leica Microsystems®).

4.3.5 Bisulphite treatment and methylation analysis of mtDNA sequences after DNMT3A and whole DNMT1-DNMT3A overexpression in HEK293A cells

After establishing DNMT3A and whole DNMT1-DNMT3A overexpression, HEK293A cells were harvested and their DNA was isolated according to the protocol described in subchapter 4.3.1.1. Then, DNA was digested with HindIII restriction enzyme (New England BioLabs®, R0104T) and bisulphite treatment was performed according to the protocol described in subchapter 4.3.1.1.1. After purifying bisulphite treated-DNA, PCR for mtDNA sequences was performed. For this set of experiments, COX2 and D-Loop Light fragment sequences were investigated. The list of primers is reported in subchapter 4.3.1.2.

4.4 Results

4.4.1 Methylation analysis of mtDNA sequences after overexpression of DNMT1 isoforms

In this section, the results of methylation analysis of mtDNA sequences following overexpression of DNMT1 isoforms are reported. The subchapters have been divided by gene of interest.

4.4.1.1 COX2 methylation status after mitochondrial DNMT1 overexpression

The methylation analysis of COX2 gene was investigated with or without linearization of mtDNA.

4.4.1.1.1 Methylation analysis of circular mtDNA (COX2)

After performing bisulphite conversion of DNA samples from transfected cells (empty pCMV-SPORT6 or pCMV-SPORT6-mitochondrial DNMT1), the sequence of interest (COX2) was amplified through PCR using bisulphite-converted DNA as a template. Several annealing temperatures were tested in order to obtain the best PCR conditions. The PCR products were ran on a 2% agarose gel (**Figure 4.9**).

After confirming the proper size of the PCR products, they were amplified through TOPO-cloning and DH5α transformation. The clones obtained were then screened for successful insertion through EcoRI digestion and DNA gel electrophoresis (**Figure 4.10** and **Figure 4.11**) and clones incorporating the PCR product were sequenced. The sequencing data was then analysed for bisulphite conversion.

At first, the methylation pattern of both the negative control and the pCMV-SPORT6-mitochondrial DNMT1 transfected sample showed a high percentage of methylation of CpG and non-CpG motifs alike (**Table 4.4** and **Table 4.5**). However, mitochondrial DNA has long been known to have little to no methylation at all, at basal conditions. This result prompted the hypothesis that the circular nature of mtDNA would shield it from bisulphite treatment.

4.4.1.1.2 Methylation analysis of linearised mtDNA (COX2)

A new set of experiments was planned. This time, the DNA samples have been digested with a high concentration of HindIII restriction enzyme in order to linearise the mtDNA prior to bisulphite treatment and PCR. Then, the methylation status of samples transfected with pCMV-SPORT6 or pCMV-SPORT6-mitochondrial DNA was investigated (**Table 4.6** and **Table 4.7**).

The total percentage of converted C residues in both the pCMV-SPORT6 and the pCMV-SPORT6-mitochondrial DNMT1 transfected samples was increased to 99.7%, compared to the previously obtained 13.27% (for circular pCMV-SPORT6) and 11.1% (for circular pCMV-SPORT6-mitochondrial DNMT1) values. The percentage of both converted CpG and non-CpG motifs was also similar, with 99.5% and 99.7% conversion, respectively.

This result proved that without proper digestion of mtDNA samples, the circular form of the DNA can introduce a bias during bisulphite treatment, granting reduced efficacy of the treatment and creating artefact results. This result also proved that overexpression of mitochondrial DNMT1 does not impact COX2 gene epigenetic regulation in HEK293A cells. Following this result, the HindIII digestion step has been added to the protocol and performed before each bisulphite treatment.

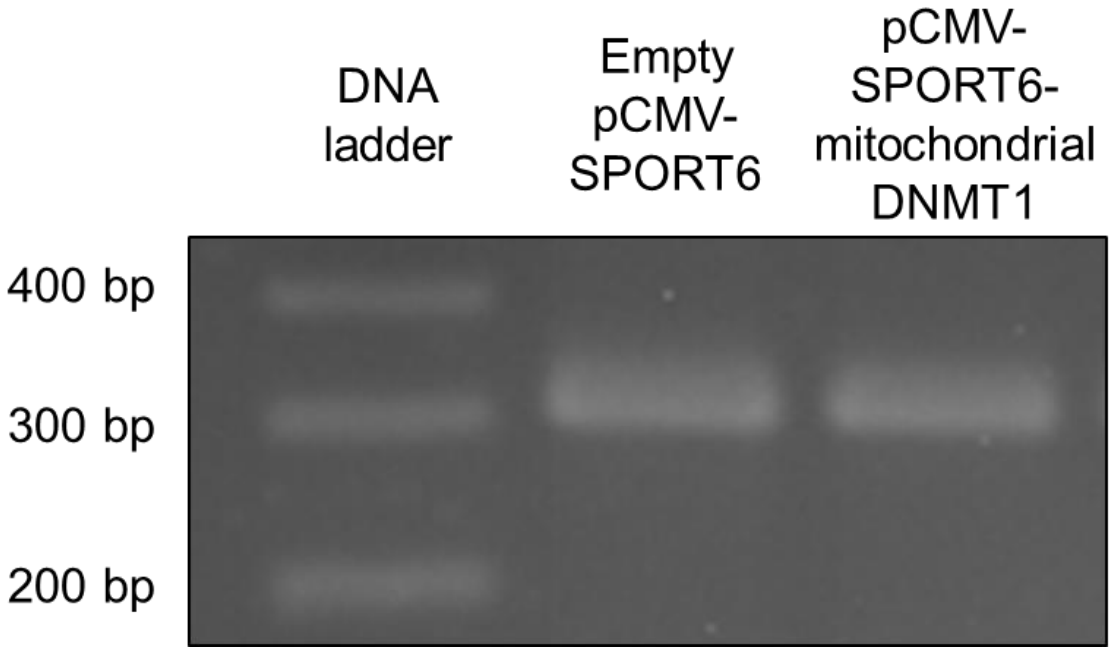

Figure 4.9: DNA gel electrophoresis of COX2 PCR samples (300 bp) Empty pCMV-SPORT6- or pCMV-SPORT6-mitochondrial DNMT1-transfected DNA samples were used as template.

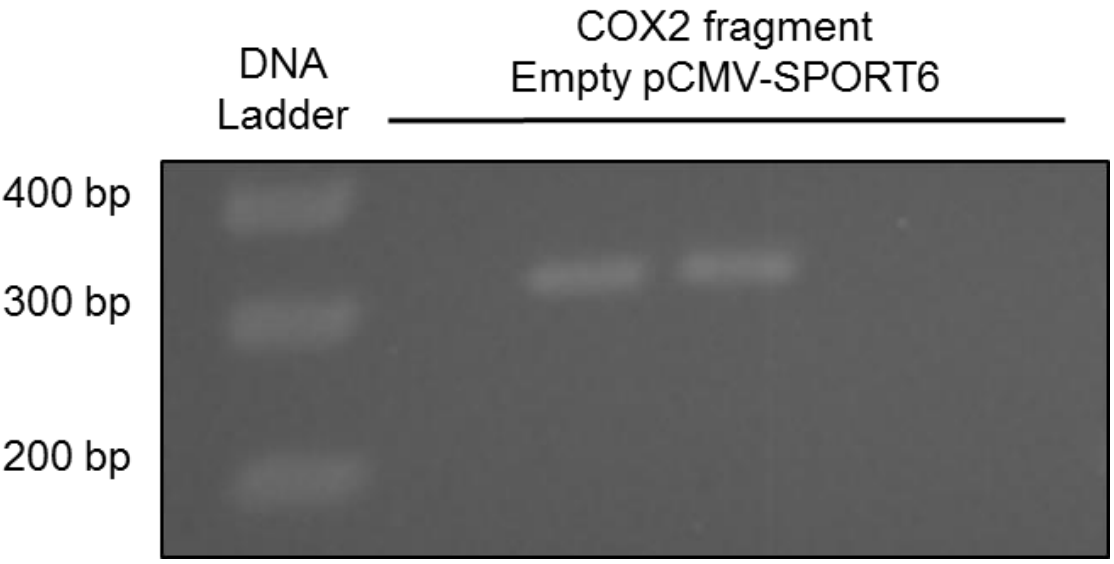

Figure 4.10: Representative DNA gel electrophoresis of TOPO-COX2 miniprep samples from empty pCMV-SPORT6 transfected DNA.

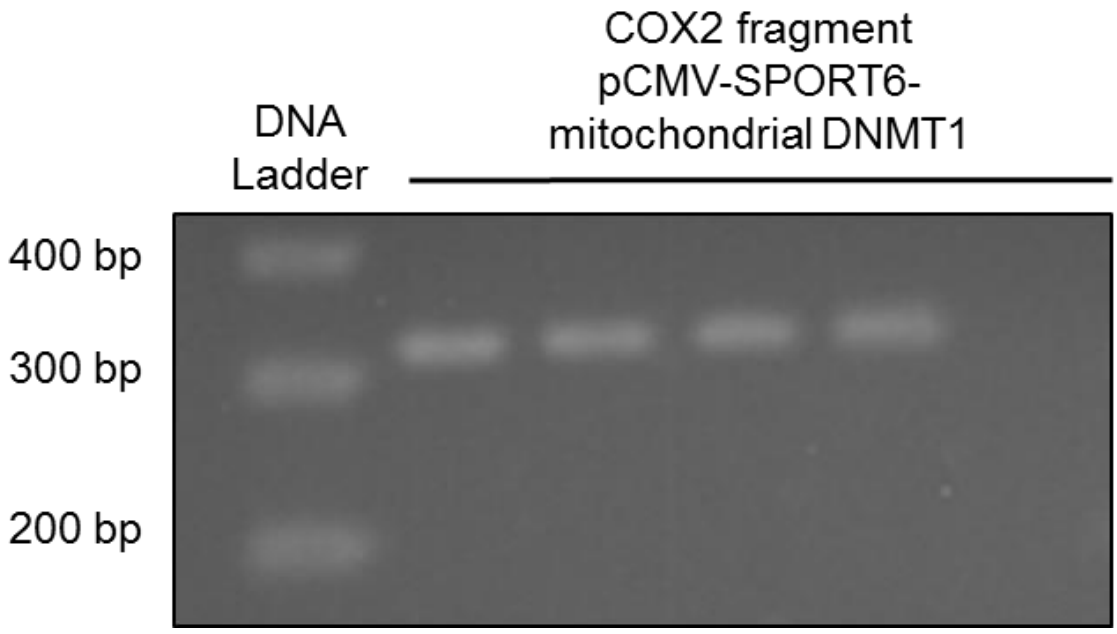

Figure 4.11: Representative DNA gel electrophoresis of TOPO-COX2 miniprep samples from pCMV-SPORT6-mitochondrial DNMT1 transfected DNA.

Table 4.4: Methylation status analysis of COX2 sequences from pCMV-SPORT6 transfected samples (negative control). N = 12.

Vector	Target							
pCMV-SPORT6	COX2							
Sample name	length (bp)	Total C residues	Converted C	total CpG motifs	total converted CpG motifs	total non-CpG motifs	total converted non-CpG motifs	percent of identity
Empty_COX2_1	257	81	20	17	6	64	14	100.00%
Empty_COX2_2	257	81	5	17	2	64	3	100.00%
Empty_COX2_3	257	81	8	17	1	64	7	100.00%
Empty_COX2_4	257	81	7	17	2	64	5	100.00%
Empty_COX2_5	257	81	14	17	4	64	10	100.00%
Empty_COX2_6	257	81	5	17	3	64	2	100.00%
Empty_COX2_7	257	81	5	17	2	64	3	100.00%
Empty_COX2_8	257	81	18	17	2	64	16	100.00%
Empty_COX2_9	257	81	13	17	3	64	10	100.00%
Empty_COX2_10	257	81	9	17	3	64	6	100.00%
Empty_COX2_11	257	81	13	17	2	64	11	100.00%
Empty_COX2_12	257	81	12	17	4	64	8	100.00%
total	3084	972	129	204	34	768	95	
		total C converted rate	**13.27%**	**total CpG converted rate**	**16.6%**	**total nonCpG converted rate**	**12.4%**	

Table 4.5: Methylation status analysis of COX2 sequences from pCMV-SPORT6-mitochondrial DNMT1 transfected samples. N = 12.

Vector	Target							
pCMV-SPORT6-mitochondrial DNMT1	COX2							
Sample name	length (bp)	Total C residues	Converted C	total CpG motifs	total converted CpG motifs	total non-CpG motifs	total converted non-CpG motifs	percent of identity
Mito_COX2_1	257	81	4	17	2	64	2	100.00%
Mito_COX2_2	257	81	6	17	2	64	4	100.00%
Mito_COX2_3	257	81	8	17	4	64	4	100.00%
Mito_COX2_4	257	81	24	17	10	64	14	100.00%
Mito_COX2_5	257	81	8	17	2	64	6	100.00%
Mito_COX2_6	257	81	5	17	1	64	4	100.00%
Mito_COX2_7	257	81	10	17	3	64	7	100.00%
Mito_COX2_8	257	81	9	17	3	64	6	100.00%
Mito_COX2_9	257	81	8	17	2	64	6	100.00%
Mito_COX2_10	257	81	6	17	1	64	5	100.00%
Mito_COX2_11	257	81	9	17	3	64	6	100.00%
Mito_COX2_12	257	81	11	17	6	64	5	100.00%
total	2827	972	108	187	39	704	69	
		total C converted rate	**11.1%**	**total CpG converted rate**	**20.8%**	**total nonCpG converted rate**	**9.8%**	

Table 4.6: Methylation status analysis of COX2 sequences from pCMV-SPORT6 transfected samples (linearised). Samples were linearised with HindIII digestion prior to bisulphite treatment. N = 12.

Vector	Target							
pCMV-SPORT6	COX2							
Sample name	length (bp)	Total C residues	Converted C	total CpG motifs	total converted CpG motifs	total non-CpG motifs	total converted non-CpG motifs	percent of identity
Empty_COX2_1	257	81	81	17	17	64	64	100.00%
Empty_COX2_2	257	81	80	17	17	64	63	100.00%
Empty_COX2_3	257	81	81	17	17	64	64	100.00%
Empty_COX2_4	257	81	81	17	17	64	64	100.00%
Empty_COX2_5	257	81	81	17	17	64	64	99.99%
Empty_COX2_6	257	81	81	17	17	64	64	100.00%
Empty_COX2_7	257	81	80	17	16	64	64	100.00%
Empty_COX2_8	257	81	81	17	17	64	64	100.00%
Empty_COX2_9	257	81	81	17	17	64	64	100.00%
Empty_COX2_10	257	81	81	17	17	64	64	100.00%
Empty_COX2_11	257	81	81	17	17	64	64	100.00%
Empty_COX2_12	257	81	80	17	17	64	63	100.00%
total	3084	972	969	204	203	768	766	
		total C converted rate	**99.7%**	**total CpG converted rate**	**99.5%**	**total nonCpG converted rate**	**99.7%**	

Table 4.7: Methylation status analysis of COX2 sequences from pCMV-SPORT6-mitochondrial DNMT1 transfected samples (linearised). Samples were linearised with HindIII digestion prior to bisulphite treatment. N = 12.

Vector	Target							
pCMV-SPORT6-mitochondrial DNMT1	COX2							
Sample name	length (bp)	Total C residues	Converted C	total CpG motifs	total converted CpG motifs	total non-CpG motifs	total converted non-CpG motifs	percent of identity
Mito_COX2_1	257	81	81	17	17	64	64	99.98%
Mito_COX2_2	257	81	81	17	17	64	64	100.00%
Mito_COX2_3	257	81	81	17	17	64	64	100.00%
Mito_COX2_4	257	81	81	17	17	64	64	100.00%
Mito_COX2_5	257	81	81	17	17	64	64	100.00%
Mito_COX2_6	257	81	81	17	17	64	64	100.00%
Mito_COX2_7	257	81	81	17	17	64	64	100.00%
Mito_COX2_8	257	81	81	17	17	64	64	100.00%
Mito_COX2_9	257	81	78	17	16	64	62	99.98%
Mito_COX2_10	257	81	81	17	17	64	64	100.00%
Mito_COX2_11	257	81	81	17	17	64	64	100.00%
Mito_COX2_12	257	81	81	17	17	64	64	100.00%
total	3084	972	969	204	203	768	766	
		total C converted rate	**99.7%**	**total CpG converted rate**	**99.5%**	**total nonCpG converted rate**	**99.7%**	

4.4.1.2 D-Loop sequence fragment methylation status after mitochondrial DNMT1 overexpression

The D-Loop represents the regulatory region of mtDNA, where all mRNAs originate, so this would represent a good candidate for epigenetic regulation at mitochondrial level. Investigation of part of the D-Loop sequence (residues 1-181) was performed through bisulphite sequencing and sequencing analysis. After optimising the PCR conditions in order to amplify the right sequence (**Figure 4.12**), the methylation status of mtDNA samples originated from cells transfected with either pCMV-SPORT6 (negative control) (**Figure 4.13** and **Table 4.8**) or pCMV-SPORT6-mitochondrial DNMT1 (**Figure 4.14** and **Table 4.9**) was investigated.

No methylation was found in the CpG motifs of pCMV-SPORT6 transfected samples, with a conversion rate of 100%, and a 99.3% conversion rate was obtained for non-CpG motifs. Similar conversion rates were also obtained for pCMV-SPORT6-mitochondrial DNMT1 transfected samples, with 100% conversion rate for CpG motifs and 98.9% conversion rate for non-CpG motifs.

This result indicated that there is no methylation in residues 1-181 of the D-Loop during basal conditions, and that mitochondrial DNMT1 overexpression has no impact of the epigenetic regulation of this area of mtDNA in HEK293A cells. The result also prompted discussion in regards of DNMT3 isoforms, which do not have a mitochondrial localisation signal in their sequence but possess De novo methylation features.

Since DNMT1 sequence contains DNMT3A and DNMT3B interaction sites, the possibility of DNMT1 acting as a chaperone for DNMT3A mitochondrial localisation will be investigated.

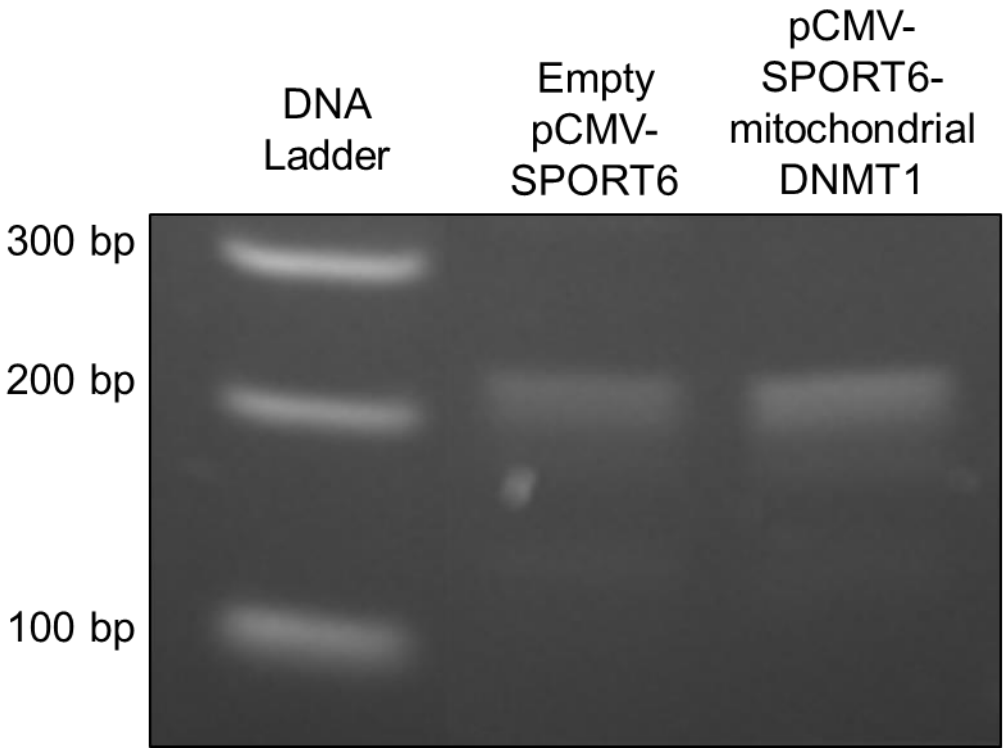

Figure 4.12: DNA gel electrophoresis of D-Loop fragment PCR samples. Empty pCMV-SPORT6- of pCMV-SPORT6-mitochondrial DNMT1-transfected DNA samples were used as template.

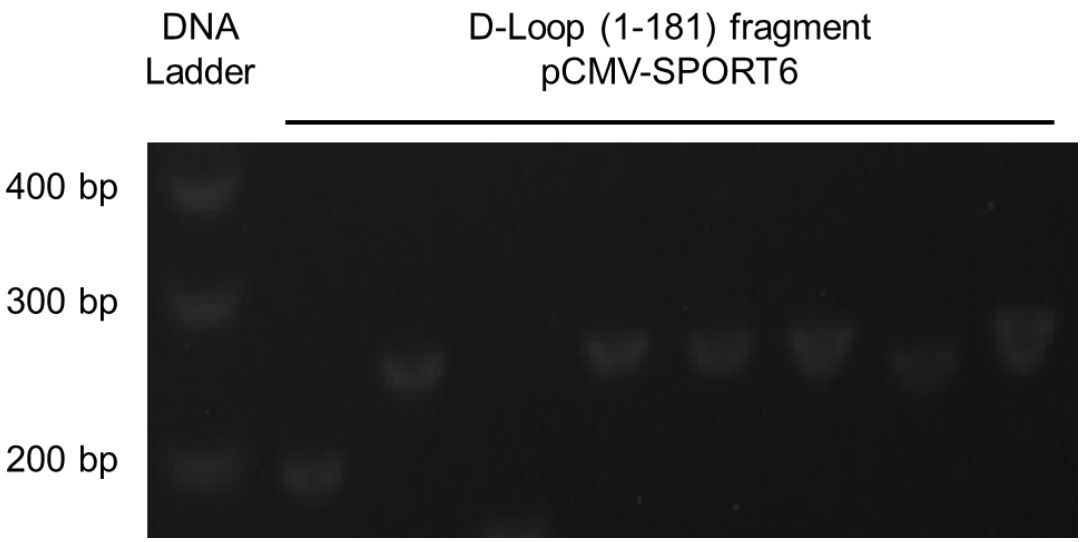

Figure 4.13: Representative DNA gel electrophoresis of TOPO-D-Loop (1-181) miniprep samples (pCMV-SPORT6-transfected DNA).

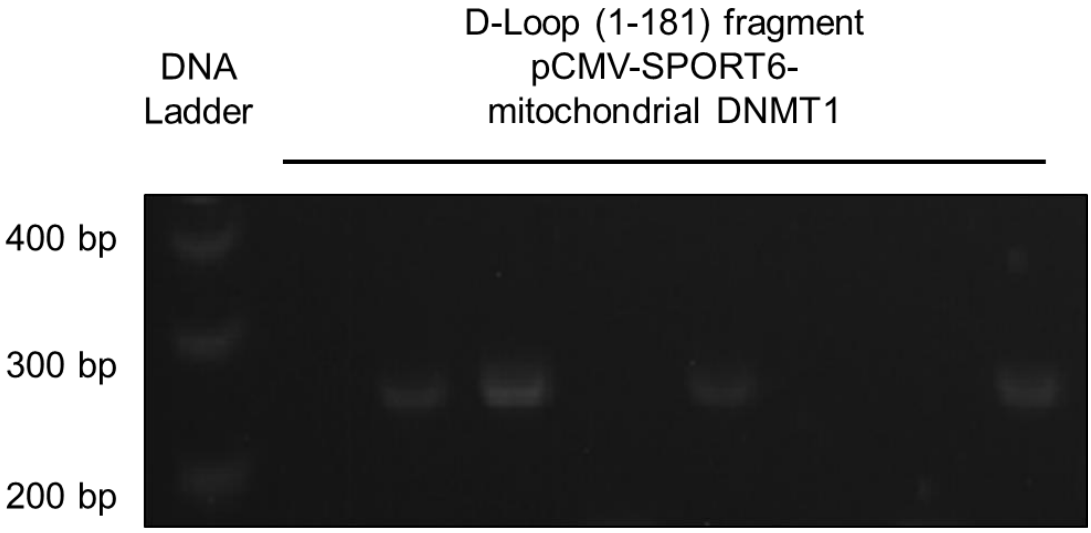

Figure 4.14: Representative DNA gel electrophoresis of TOPO-D-Loop (1-181) miniprep samples (pCMV-SPORT6-mitochondrial DNMT1-transfected DNA).

Table 4.8: Methylation status analysis of D-Loop (1-181) sequences from pCMV-SPORT6 transfected samples (linearised). Samples were linearised with HindIII digestion prior to bisulphite treatment. N = 12.

Vector	Target							
pCMV-SPORT6	D-Loop (1-181)							
name	target length	total C	Converted C	total CpG	total converted CpG	total nonCpG	total converted nonCpG	percent of identity
Empty_Light1_1	181	55	53	3	3	52	50	100.00%
Empty_Light1_2	181	55	55	3	3	52	52	100.00%
Empty_Light1_3	181	55	55	3	3	52	52	100.00%
Empty_Light1_4	181	55	55	3	3	52	52	100.00%
Empty_Light1_5	181	55	54	3	3	52	51	100.00%
Empty_Light1_6	181	55	55	3	3	52	52	100.00%
Empty_Light1_7	181	55	55	3	3	52	52	100.00%
Empty_Light1_8	181	55	54	3	3	52	51	100.00%
Empty_Light1_9	181	55	55	3	3	52	52	100.00%
Empty_Light1_10	181	55	55	3	3	52	52	100.00%
Empty_Light1_11	181	55	54	3	3	52	52	100.00%
Empty_Light1_12	181	55	55	3	3	52	52	100.00%
Total	2172	660	655	36	36	624	620	
		total C converted rate	**99.2%**	**total CpG converted rate**	**100.0%**	**total nonCpG converted rate**	**99.3%**	

Table 4.9: Methylation status analysis of D-Loop (1-181) sequences from pCMV-SPORT6-mitochondrial DNMT1 transfected samples (linearised). Samples were linearised with HindIII digestion prior to bisulphite treatment. N = 12.

Vector	Target							
pCMV-SPORT6-Mitochondrial DNMT1	D-Loop (1-181)							
name	target length	total C	Converted C	total CpG	total converted CpG	total nonCpG	total converted nonCpG	percent of identity
Mito_Light1_1	181	55	53	3	3	52	50	100.00%
Mito_Light1_2	181	55	55	3	3	52	52	100.00%
Mito_Light1_3	181	55	55	3	3	52	52	100.00%
Mito_Light1_4	181	55	55	3	3	52	52	100.00%
Mito_Light1_5	181	55	54	3	3	52	51	100.00%
Mito_Light1_6	181	55	55	3	3	52	52	100.00%
Mito_Light1_7	181	55	54	3	3	51	51	100.00%
Mito_Light1_8	181	55	54	3	3	52	51	100.00%
Mito_Light1_9	181	55	53	3	3	52	50	100.00%
Mito_Light1_10	181	55	55	3	3	52	52	99.97%
Mito_Light1_11	181	55	54	3	3	52	51	100.00%
Mito_Light1_12	181	55	55	3	3	52	52	100.00%
Total	2172	660	652	36	36	623	616	
		total C converted rate	**98.8%**	**total CpG converted rate**	**100.0%**	**total nonCpG converted rate**	**98.9%**	

4.4.2 Generation of DNMT3A overexpression vector

Following PCR using primers for DNMT3A (**Table 4.2**), the PCR products were extracted (**Figure 4.15**) and digested with EcoRI and SacI in the case of 5' fragment, or SacI and XhoI in the case of 3' fragment. The two PCR products were then inserted in pBluescript II KS(+) in two separate reactions for sequencing purposes (**Figure 4.16** and **Figure 4.17**). Transformation of DH5α

cells and miniprep were performed and clones with successful insertion were sequenced. Miniprep clones were digested with the relative enzymes, and clones showing successful insertion were sequenced.

After choosing one clone with the right sequence for each fragment, pCMV-SPORT6 vector was digested with EcoRI and XhoI, and a double ligation with the 5' and 3' DNMT3A fragments was performed. This ligation was performed using the same fragment ratio for both fragments (vector : fragment = 1 : 3). A map of the final construct is shown (**Figure 4.18**).

Following ligation, the mixture was transformed in DH5α cells, miniprep was performed and the samples were checked through both endonuclease digestion (EcoRI-XhoI, EcoRI-SacI, SacI-XhoI) and sequencing. A clone with the right sequence was chosen, and DH5α transformation and maxiprep were performed. Finally, the maxiprep sample was sequenced and checked through endonuclease digestion (EcoRI-XhoI, EcoRI-SacI, SacI-XhoI, KpnI) once more (**Figure 4.19**). After confirming the right fragment length for all digestion patterns investigated, the pCMV-SPORT6-DNMT3A maxiprep sample was used for overexpression experiments.

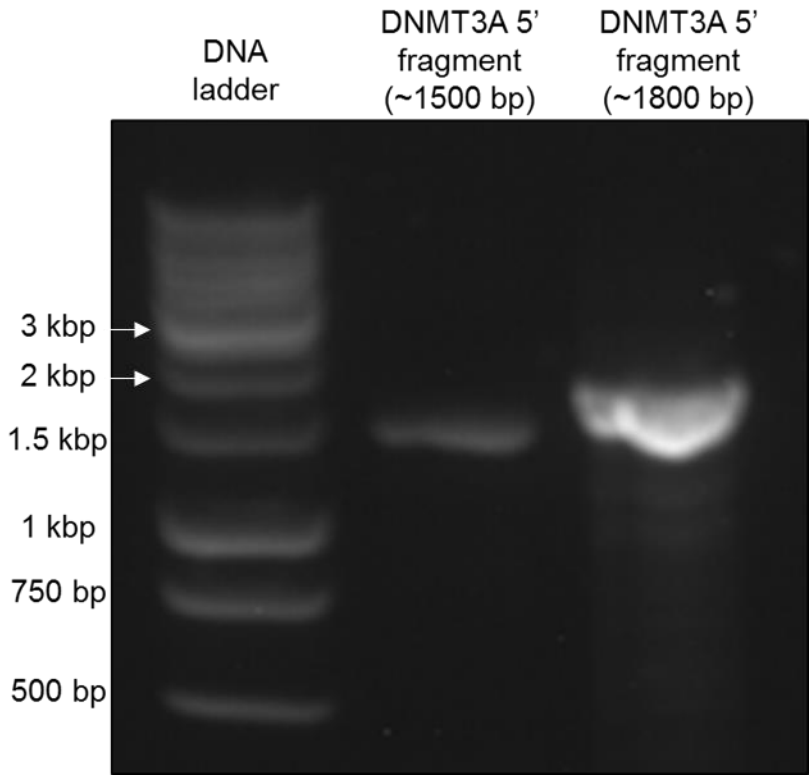

Figure 4.15: DNA gel electrophoresis of DNMT3A 5' and 3' PCR products.

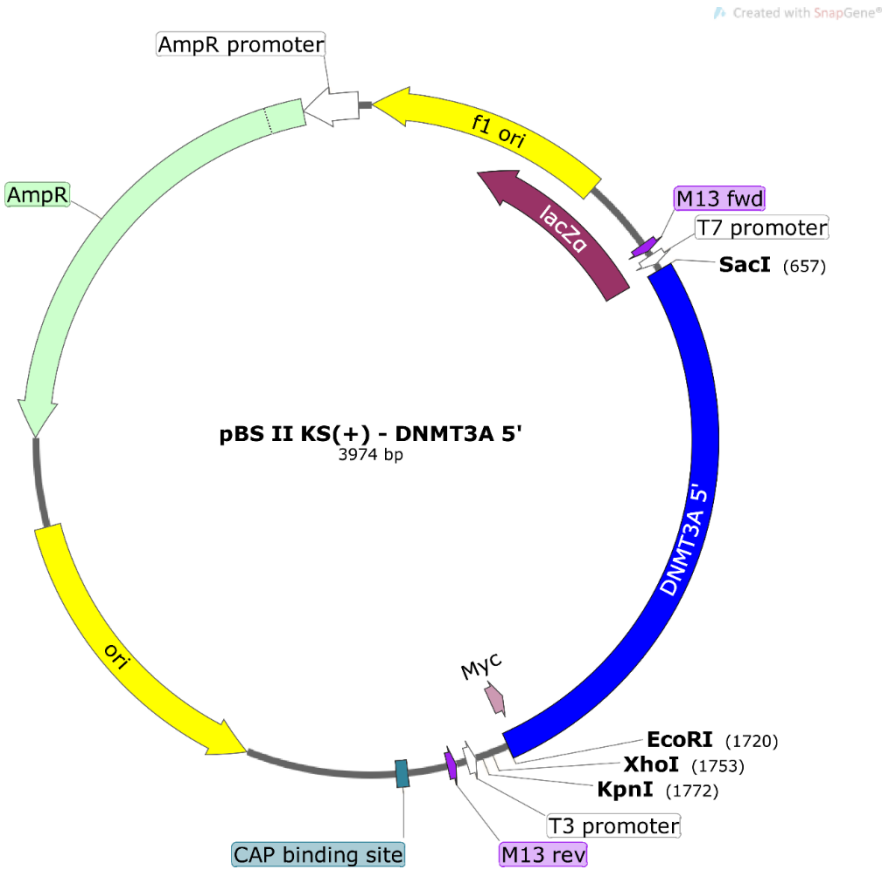

Figure 4.16: Insertion of DNMT3A 5' fragment in pBluescript II KS(+).

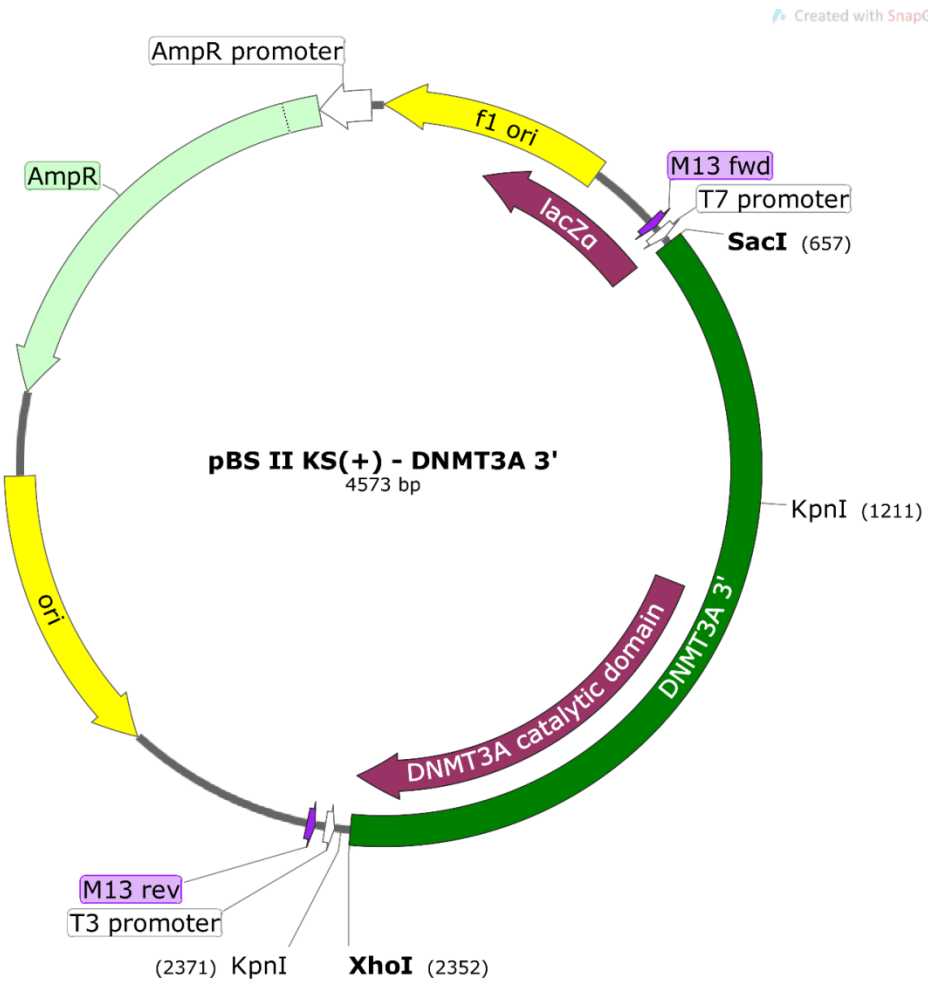

Figure 4.17: Insertion of DNMT3A 3' fragment in pBluescript II KS(+).

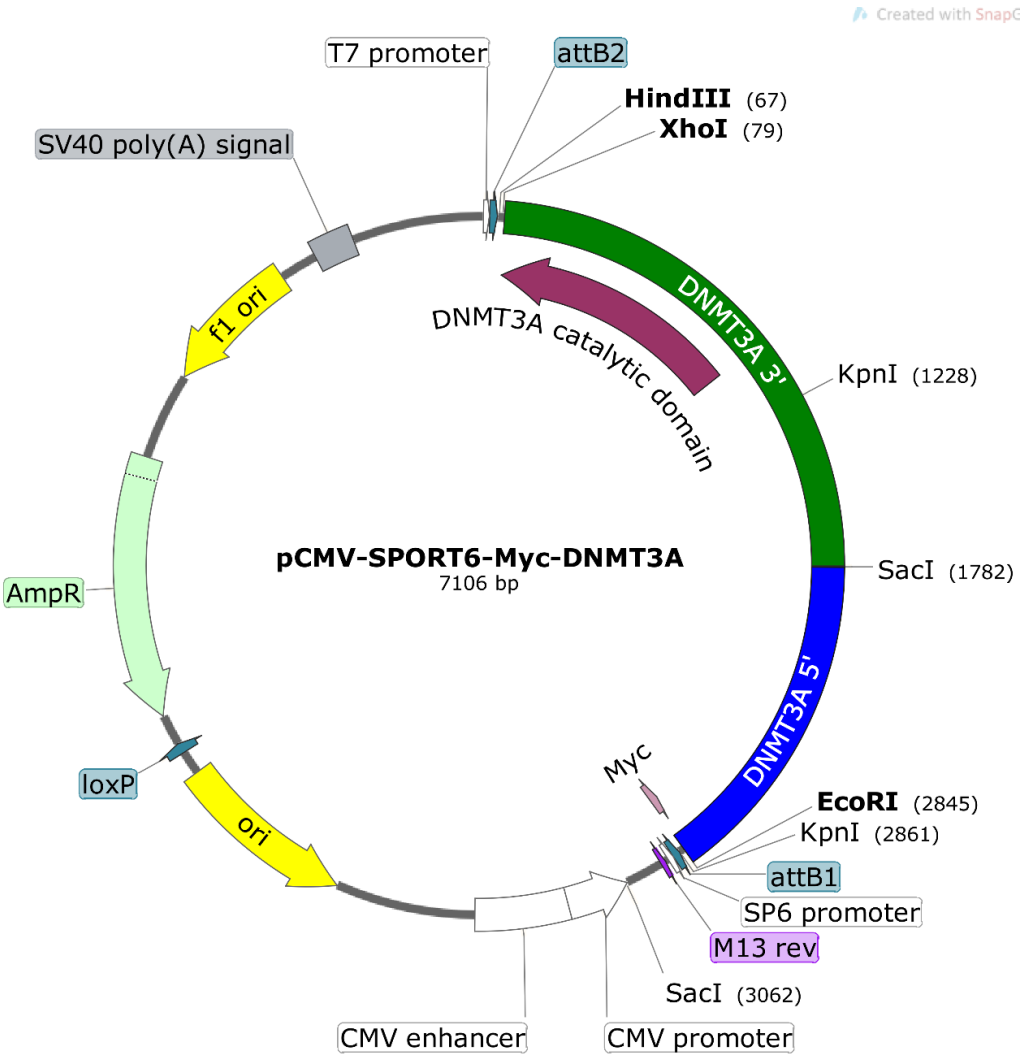

Figure 4.18: Insertion of DNMT3A 5' and 3' fragments in the final pCMV-SPORT6 vector. A double ligation reaction was performed.

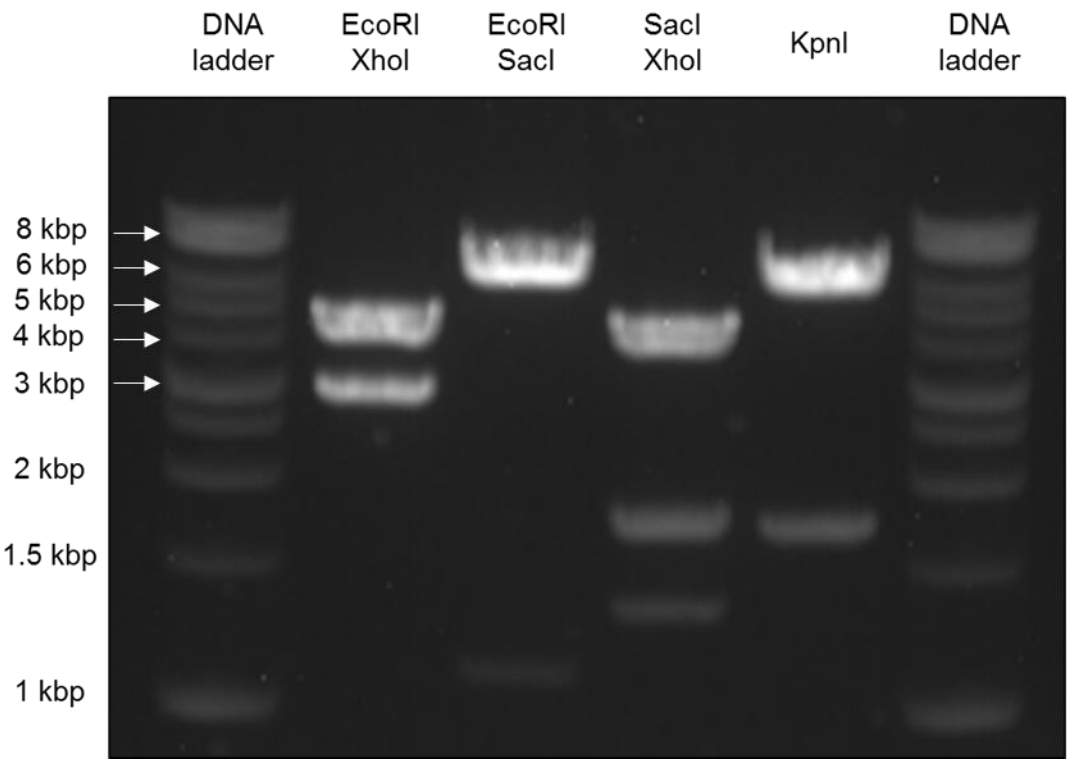

Figure 4.19: DNA gel electrophoresis of DNMT3A maxiprep sample.

4.4.3 Establishment of DNMT1-DNMT3A double overexpression in HEK293A cells

The overexpression and localisation of DNMT3A in the presence or absence of DNMT1 was investigated through both Western blotting and immunocytochemistry.

4.4.3.1 Western blotting after DNMT1-DNMT3A double overexpression

The Western blotting results of DNMT1-DNMT3A overexpression in HEK293A cells (using whole cell lysates) are shown (**Figure 4.20**). To compare the expression, transfection with empty pCMV-SPORT6, pCMV-SPORT6-mtDNMT1 and pCMV-SPORT6-DNMT3A was also performed.

Clear DNMT1 and HA-tag bands were found in both single and double transfection (HA-tag bands are highlighted with red arrows). Moreover, a very strong signal was obtained through DNMT3A and Myc-tag probing of single

DNMT3A and mtDNMT1-DNMT3A transfected samples. This experiment successfully confirmed double overexpression of mtDNMT1 and DNMT3A.

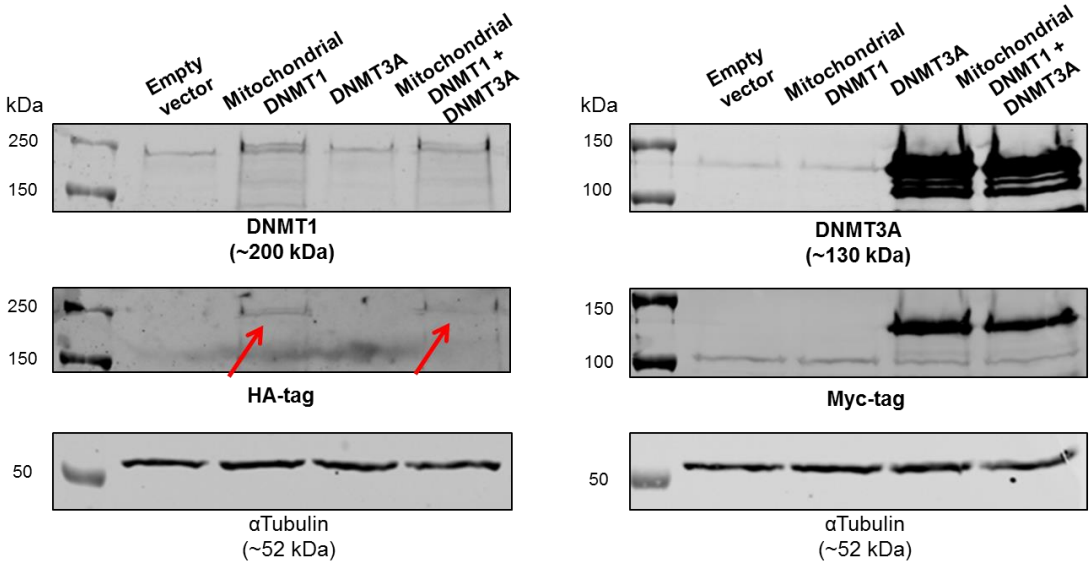

Figure 4.20: Western blotting after overexpression of mitochondrial DNMT1, DNMT3A, and both. αTubulin was used as housekeeping gene.

4.4.3.2 Immunocytochemistry DNMT1-DNMT3A localisation studies

To investigate whether co-overexpression of DNMT1 and DNMT3A could affect DNMT3A localisation, immunocytochemistry was performed. The localisation features of whole DNMT1 and mitochondrial DNMT1 were tested, then a combination of whole DNMT1-DNMT3A and mitochondrial DNMT1-DNMT3A were investigated. Empty pCMV-SPORT6 analysis was also performed (**Figure 4.21** and **Figure 4.22**). No signal from HA-tag staining was obtained.

Staining after overexpression of single whole DNMT1 (**Figure 4.23** and **Figure 4.24**) or mitochondrial DNMT1 (**Figure 4.25** and **Figure 4.26**) confirmed the results obtained in chapter 3: whole DNMT1 was able to localise at both nuclear and mitochondrial level, while mitochondrial DNMT1 showed a mitochondrial-only localisation pattern.

After confirming this result, the localisation of both whole DNMT1 and DNMT3A after whole DNMT1-DNMT3A overexpression was investigated through HA-tag (for DNMT1) (**Figure 4.27** and **Figure 4.28**) or Myc-tag staining (for DNMT3A) (**Figure 4.29** and **Figure 4.30**). Whole DNMT1 showed a whole-cell localisation as predicted, while DNMT3A showed a clear nuclear and cytosolic localisation. No evident signs of mitochondrial localisation of DNMT3A could be observed except for 2 cells (**Figure 4.30**) where the signal from the Myc-tag secondary antibody was very strong. This could be due to photo bleaching or signal from the ATP synthase (red) channel leaking into the Myc-tag (green) channel. However, since this would correlate well with the idea that DNMT3A interaction site within DNMT1 sequence would be critical for DNMT3A localisation at a mitochondrial level. Therefore, this combination of overexpression on the methylation status of mtDNA will be investigated through bisulphite sequencing, and will be discussed in the next subchapter.

Localisation of mitochondrial DNMT1 after double overexpression was investigated through HA-tag (**Figure 4.31** and **Figure 4.32**) and was confirmed to happen only at a mitochondrial level, as previously confirmed. DNMT3A localisation features were also investigated through Myc-tag staining (**Figure 4.33** and **Figure 4.34**). No evident signs of DNMT3A mitochondrial localisation could be detected, while strong nuclear overexpression was observed in all of the successfully transfected cells. Altogether, these results show that DNMT3A localisation is not affected by co-overexpression with mtDNMT1.

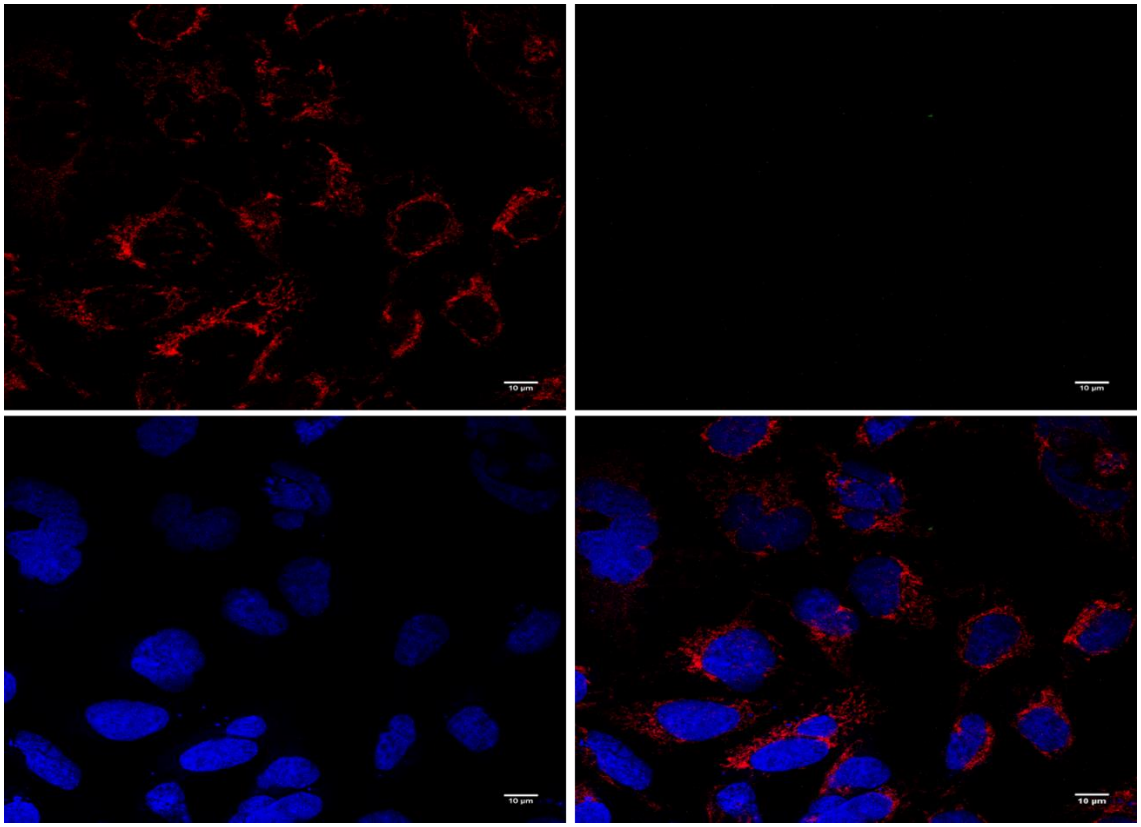

Figure 4.21: Immunocytochemistry of HEK293A cells transfected with empty pCMV-SPORT6. Cells have been stained for mitochondria (ATP synthase, top left), HA-tag (Alexafluor 488, top right) and nuclei (DAPI, bottom left). Bottom right is a merged image of all channels. Scale bar = 10 µm.

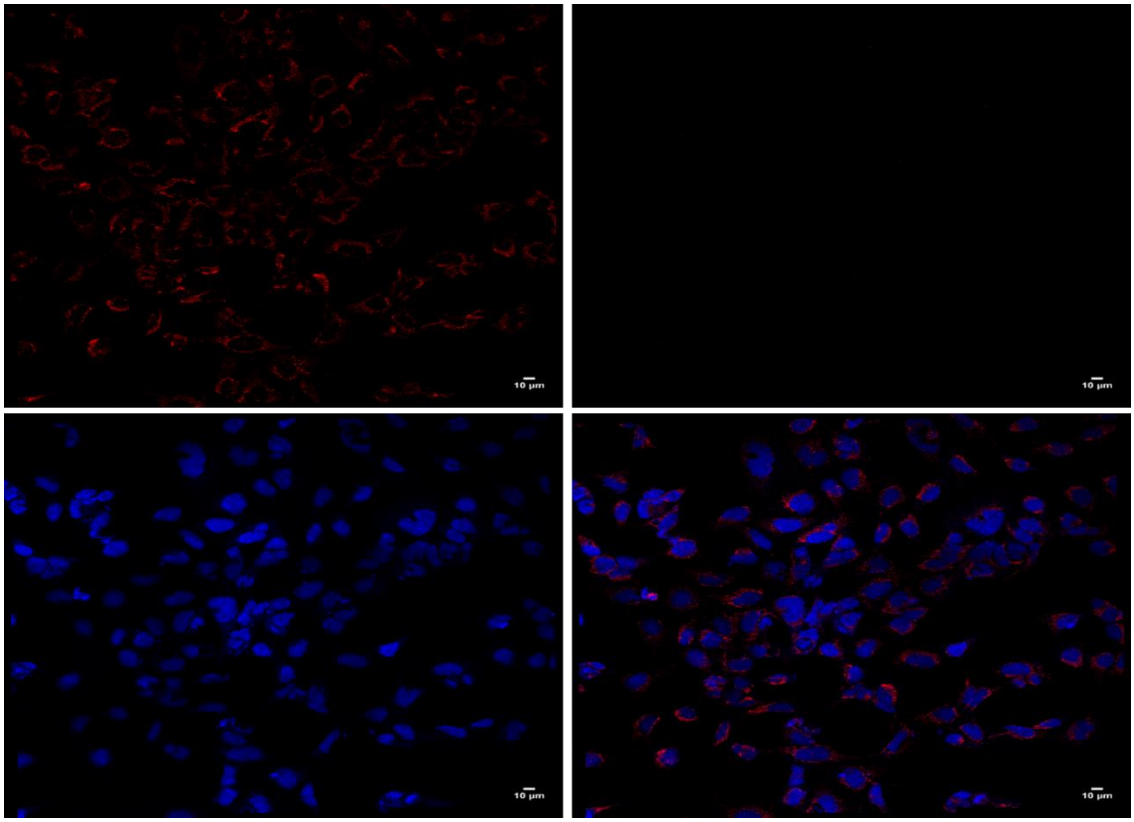

Figure 4.22: Immunocytochemistry of HEK293A cells transfected with empty pCMV-SPORT6 (big picture of 9 images). Cells have been stained for mitochondria (ATP synthase, top left), HA-tag (Alexafluor 488, top right) and nuclei (DAPI, bottom left). Bottom right is a merged image of all channels. Scale bar = 10 µm.

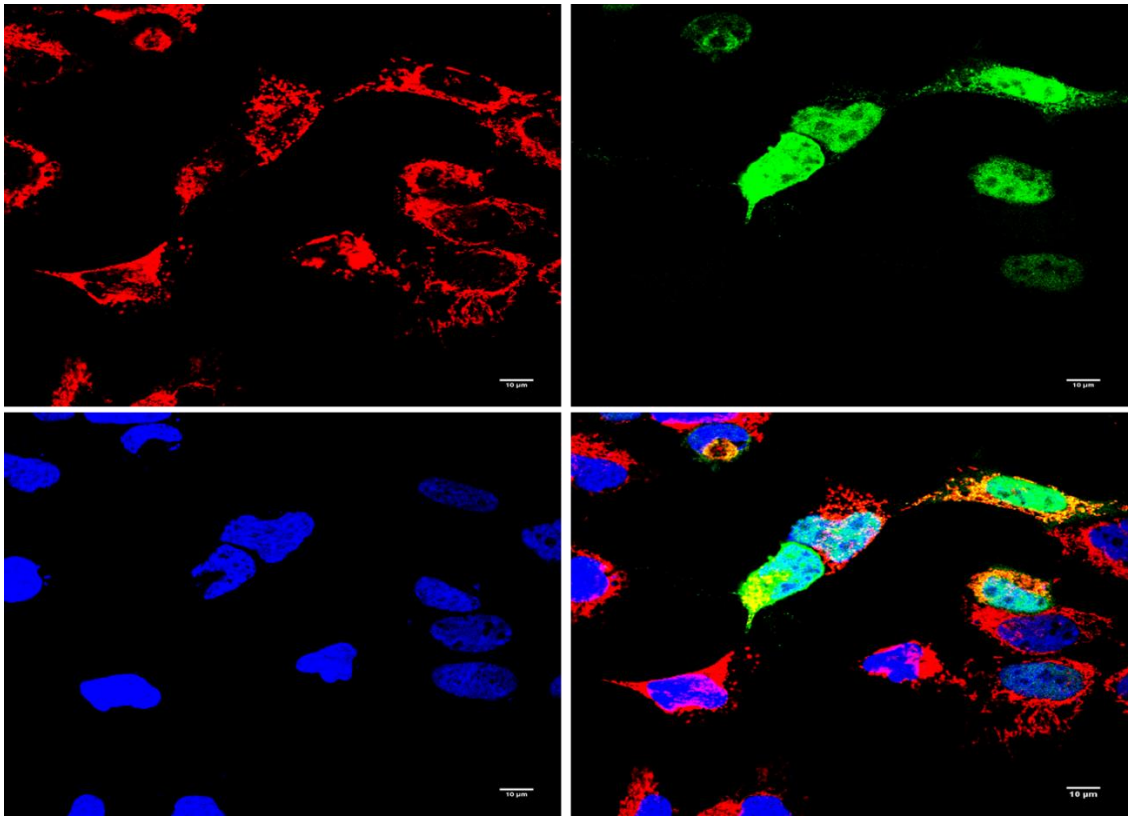

Figure 4.23: Immunocytochemistry of HEK293A cells transfected with pCMV-SPORT6-whole DNMT1. Cells have been stained for mitochondria (ATP synthase, top left), HA-tag (Alexafluor 488, top right) and nuclei (DAPI, bottom left). Bottom right is a merged image of all channels. Scale bar = 10 µm.

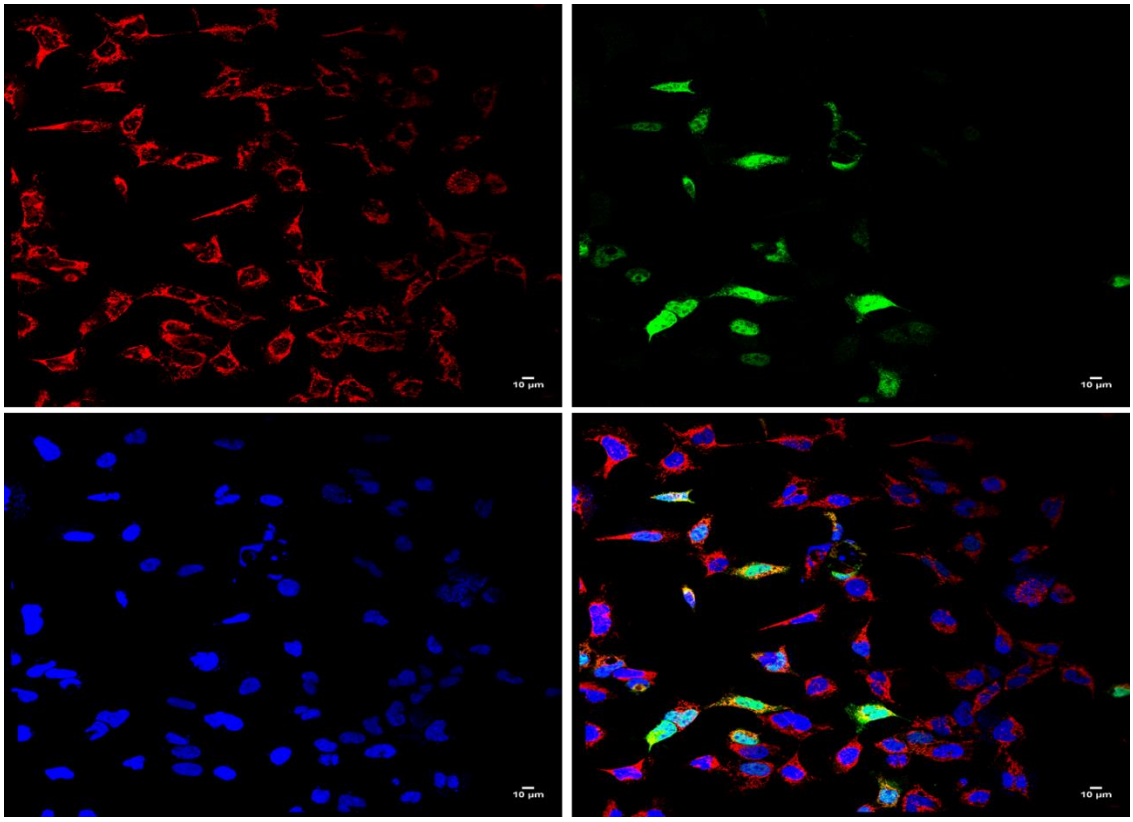

Figure 4.24: Immunocytochemistry of HEK293A cells transfected with pCMV-SPORT6-whole DNMT1 (big picture of 9 images). Cells have been stained for mitochondria (ATP synthase, top left), HA-tag (Alexafluor 488, top right) and nuclei (DAPI, bottom left). Bottom right is a merged image of all channels. Scale bar = 10 µm.

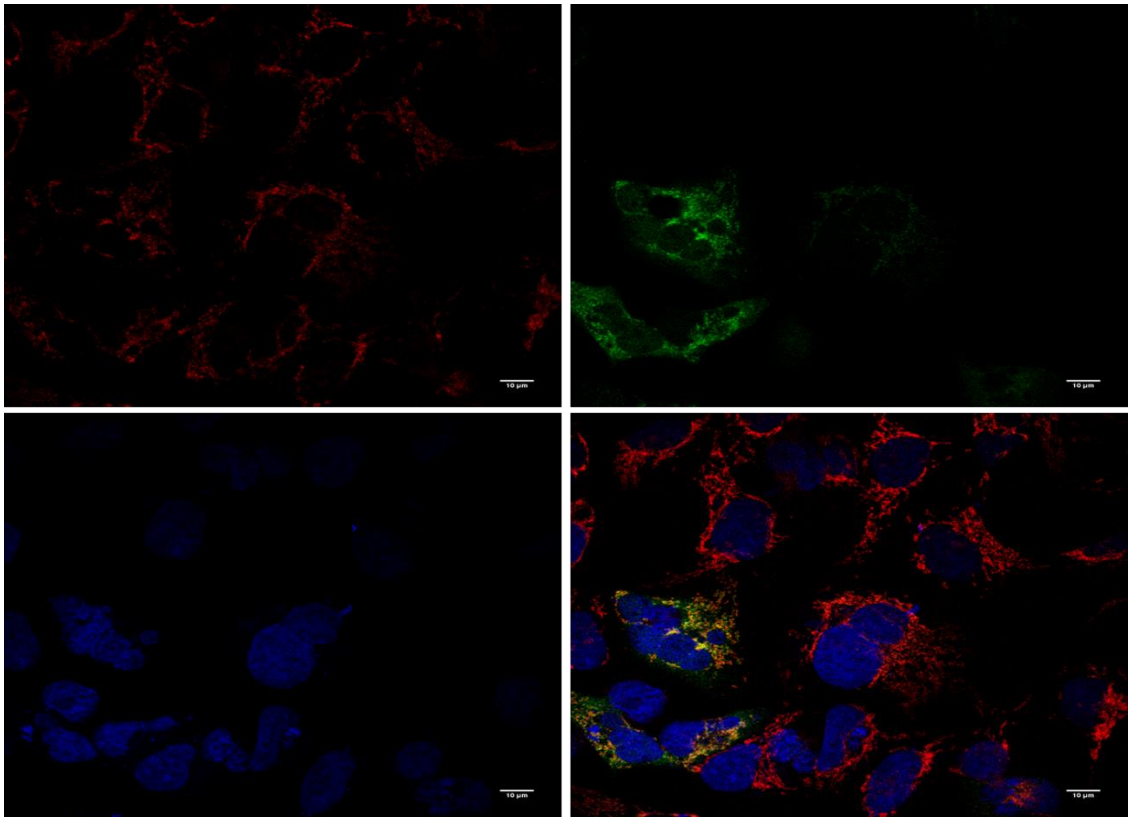

Figure 4.25: Immunocytochemistry of HEK293A cells transfected with pCMV-SPORT6-mitochondrial DNMT1. Cells have been stained for mitochondria (ATP synthase, top left), HA-tag (Alexafluor 488, top right) and nuclei (DAPI, bottom left). Bottom right is a merged image of all channels. Scale bar = 10 µm.

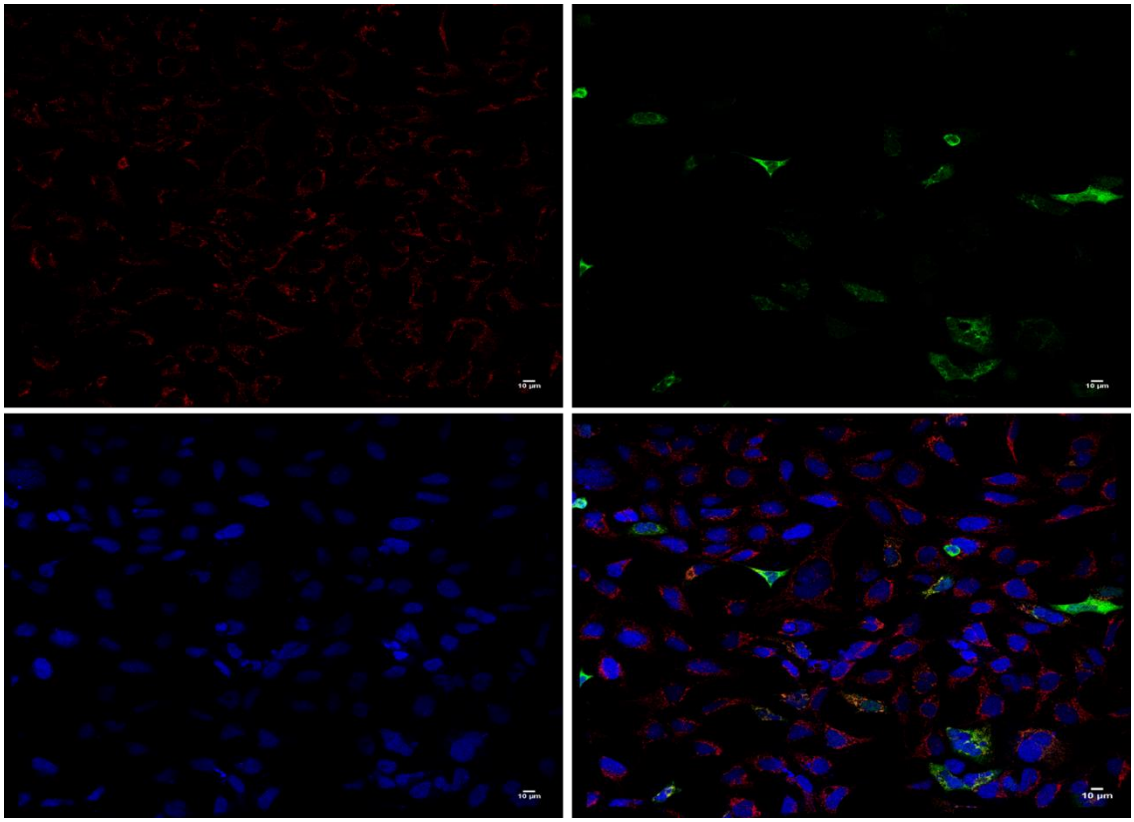

Figure 4.26: Immunocytochemistry of HEK293A cells transfected with pCMV-SPORT6-mitochondrial DNMT1 (big picture of 9 images). Cells have been stained for mitochondria (ATP synthase, top left), HA-tag (Alexafluor 488, top right) and nuclei (DAPI, bottom left). Bottom right is a merged image of all channels. Scale bar = 10 µm.

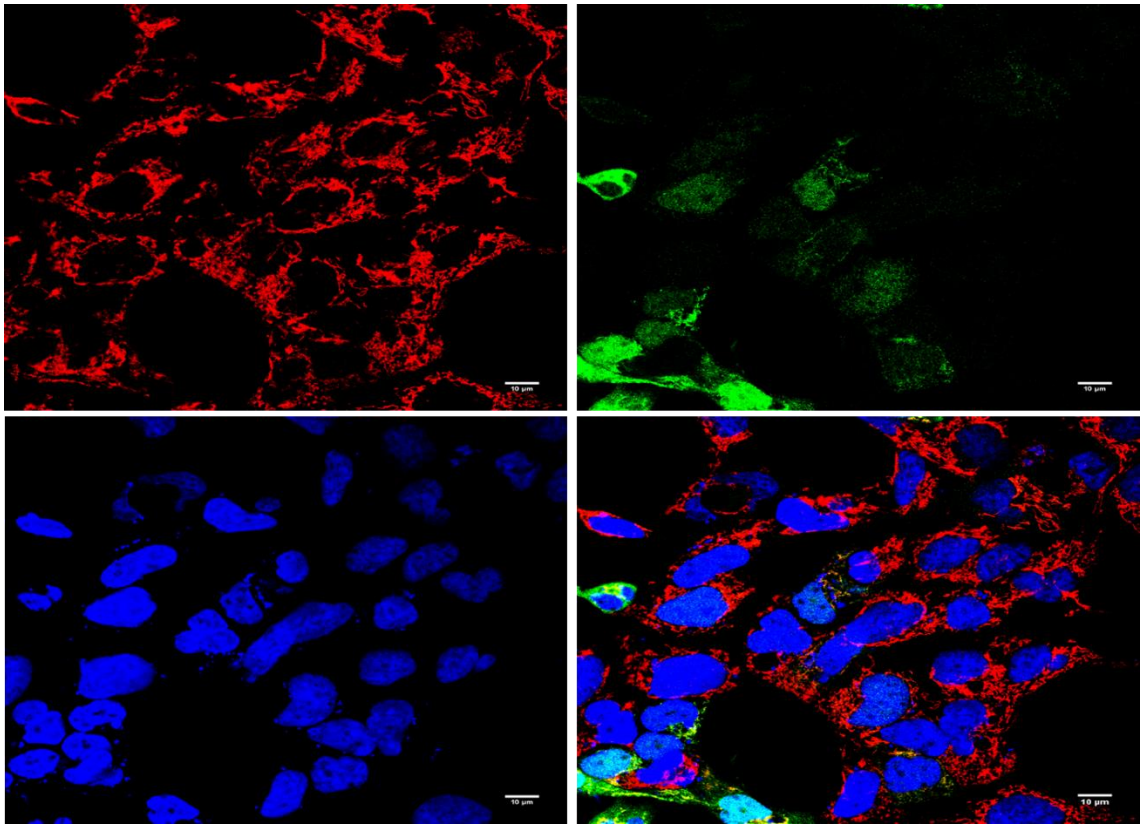

Figure 4.27: Immunocytochemistry of HEK293A cells transfected with pCMV-SPORT6-whole DNMT1 and pCMV-SPORT6-DNMT3A (DNMT1 staining). Cells have been stained for mitochondria (ATP synthase, top left), HA-tag (Alexafluor 488, top right) and nuclei (DAPI, bottom left). Bottom right is a merged image of all channels. Scale bar = 10 µm.

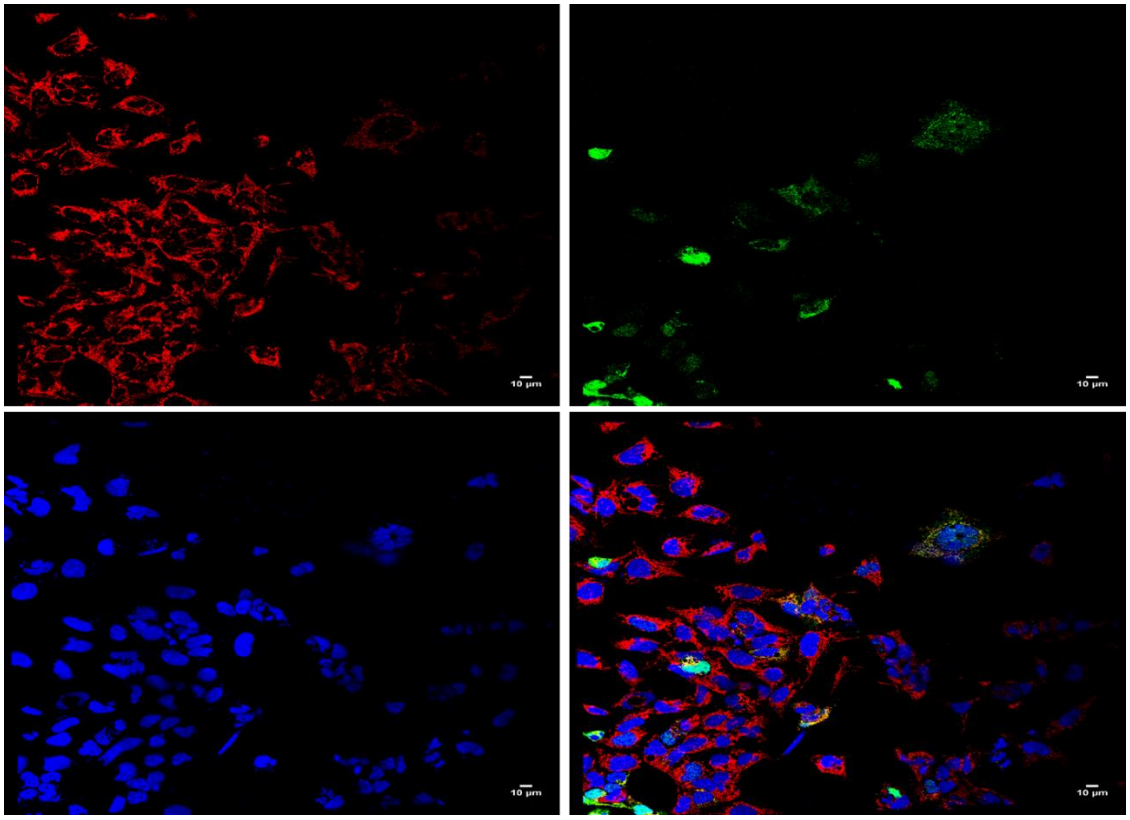

Figure 4.28: Immunocytochemistry of HEK293A cells transfected with pCMV-SPORT6-whole DNMT1 and pCMV-SPORT6-DNMT3A (big picture of 9 images) (DNMT1 staining). Cells have been stained for mitochondria (ATP synthase, top left), HA-tag (Alexafluor 488, top right) and nuclei (DAPI, bottom left). Bottom right is a merged image of all channels. Scale bar = 10 µm.

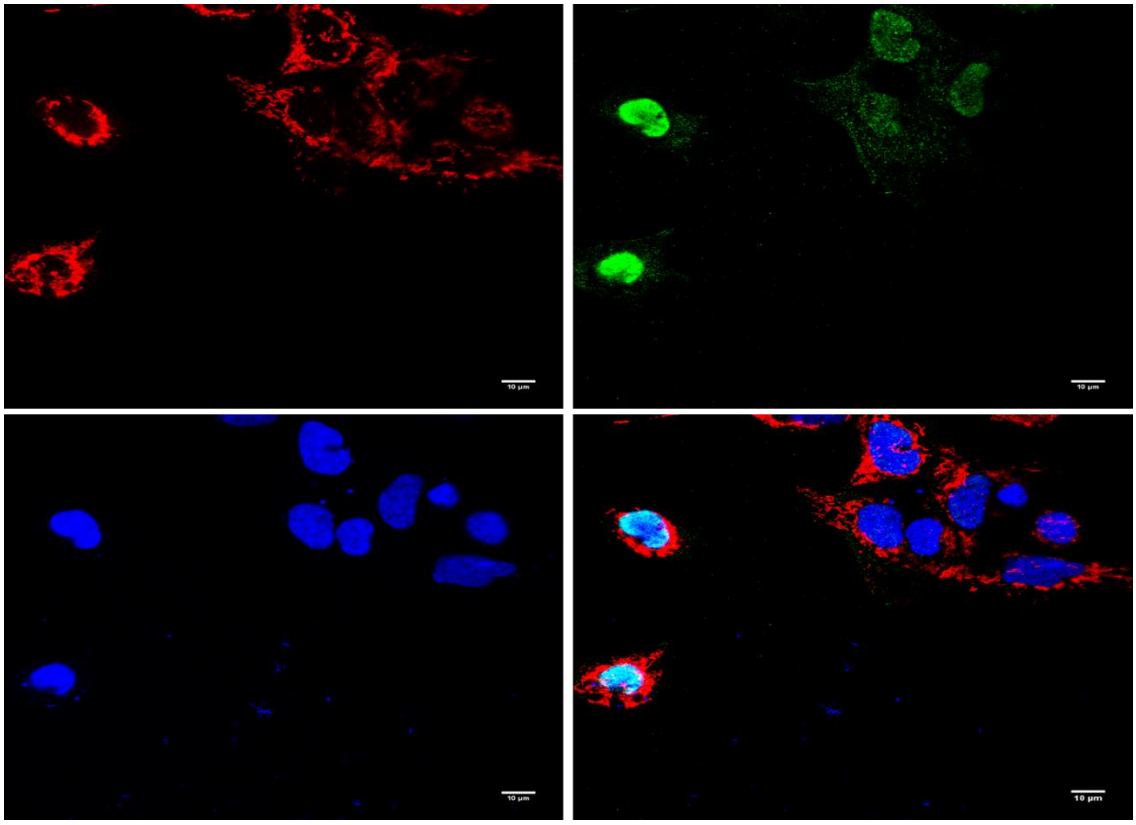

Figure 4.29: Immunocytochemistry of HEK293A cells transfected with pCMV-SPORT6-whole DNMT1 and pCMV-SPORT6-DNMT3A (DNMT3A staining). Cells have been stained for mitochondria (ATP synthase, top left), Myc-tag (Alexafluor 488, top right) and nuclei (DAPI, bottom left). Bottom right is a merged image of all channels. Scale bar = 10 µm.

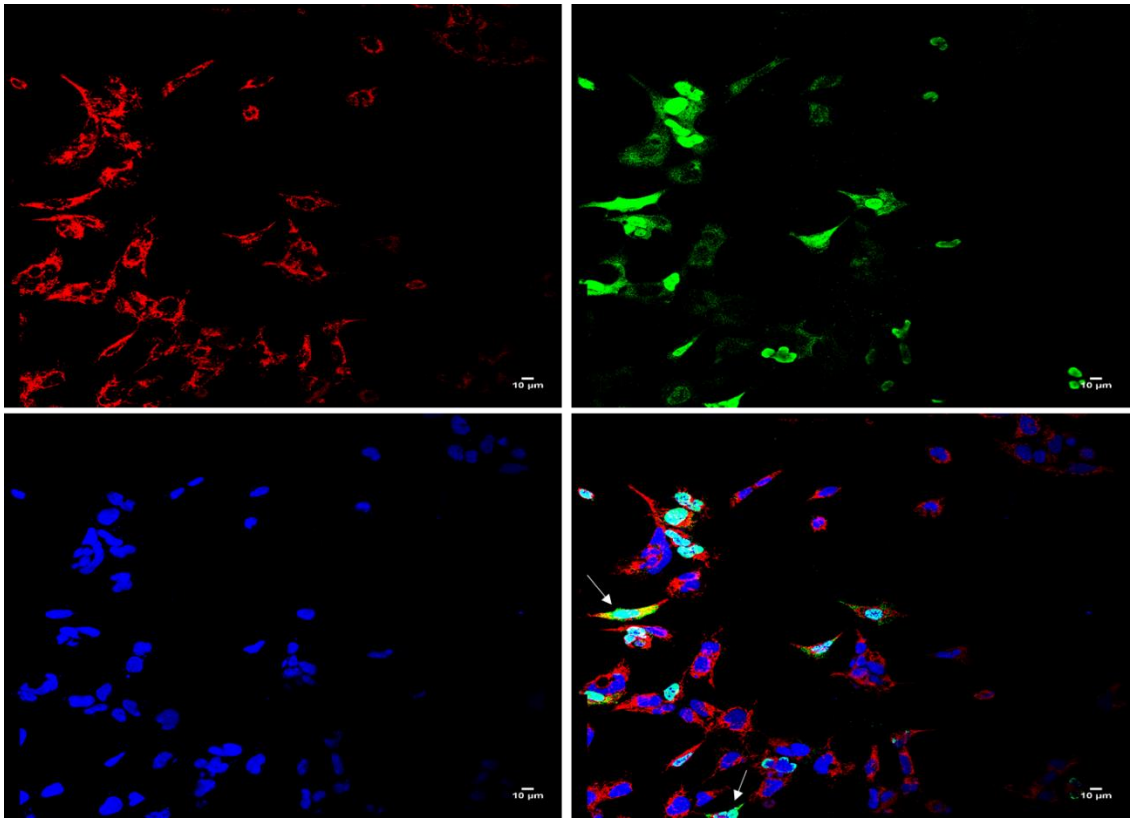

Figure 4.30: Immunocytochemistry of HEK293A cells transfected with pCMV-SPORT6-whole DNMT1 and pCMV-SPORT6-DNMT3A (big picture of 9 images) (DNMT3A staining). Cells have been stained for mitochondria (ATP synthase, top left), Myc-tag (Alexafluor 488, top right) and nuclei (DAPI, bottom left). Bottom right is a merged image of all channels. Scale bar = 10 µm.

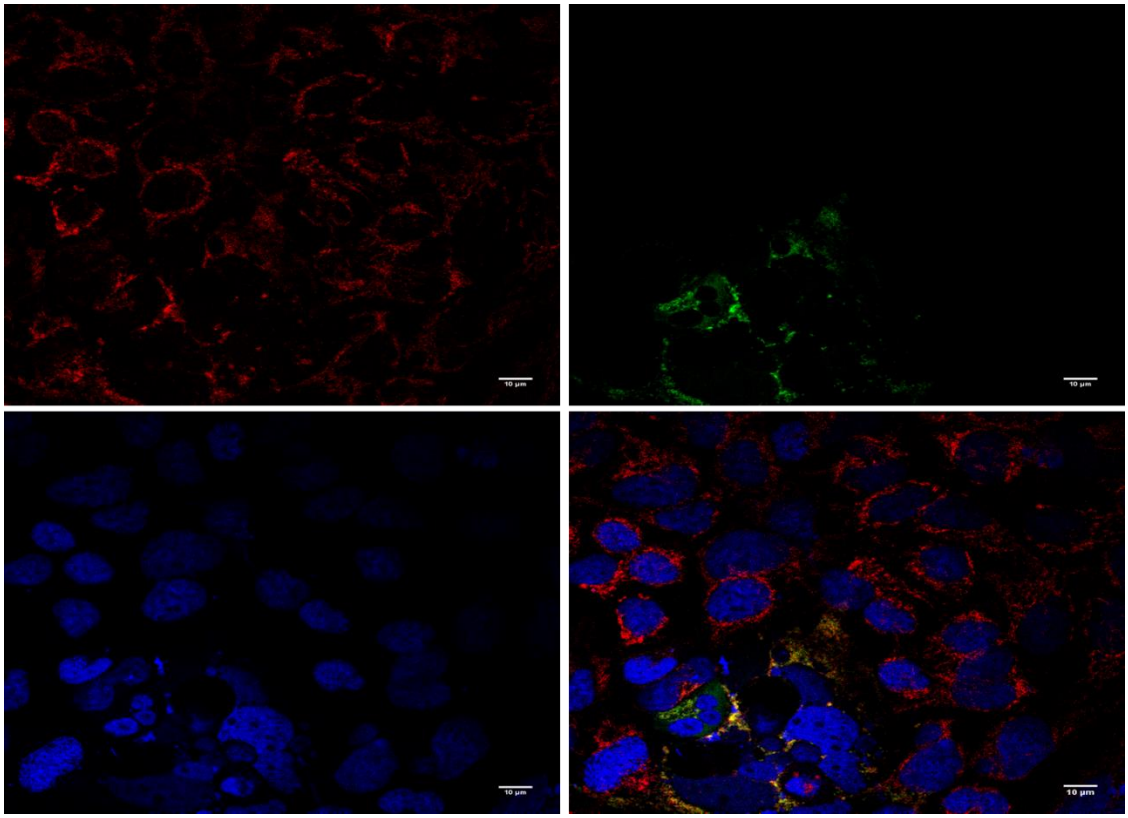

Figure 4.31: Immunocytochemistry of HEK293A cells transfected with pCMV-SPORT6-mitochondrial DNMT1 and pCMV-SPORT6-DNMT3A (DNMT1 staining). Cells have been stained for mitochondria (ATP synthase, top left), HA-tag (Alexafluor 488, top right) and nuclei (DAPI, bottom left). Bottom right is a merged image of all channels. Scale bar = 10 µm.

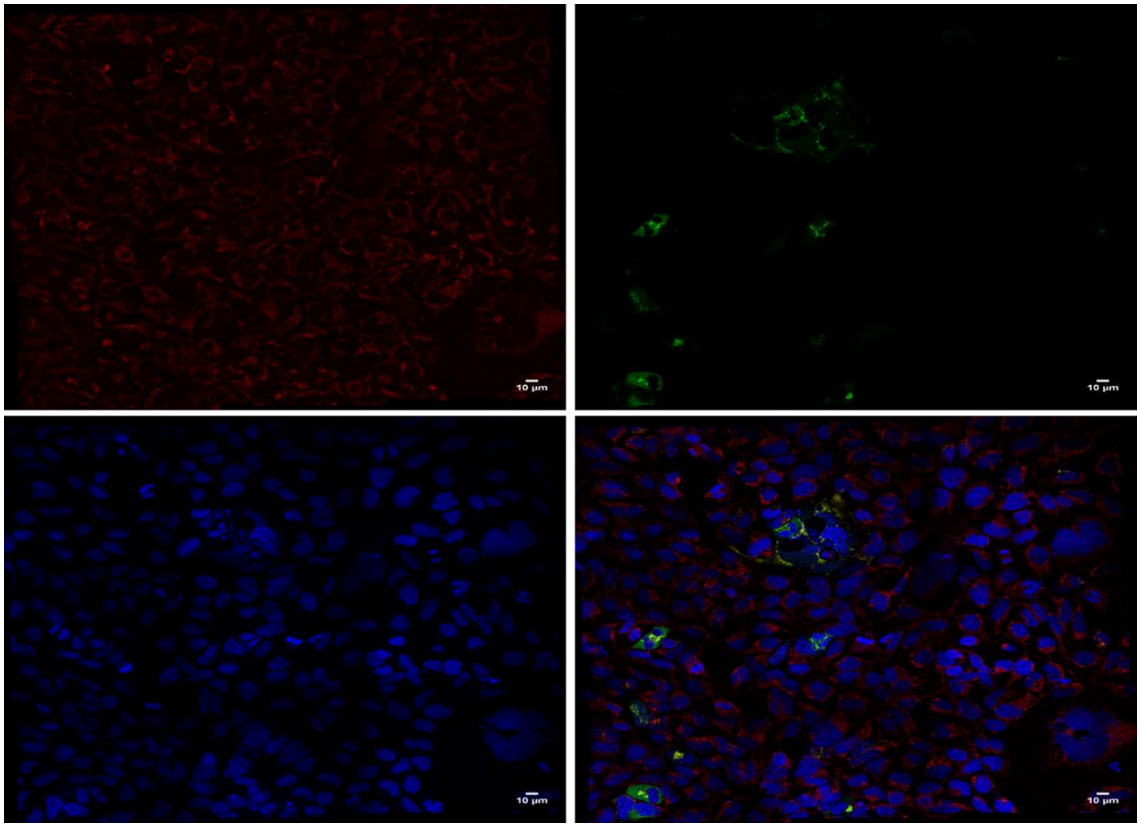

Figure 4.32: Immunocytochemistry of HEK293A cells transfected with pCMV-SPORT6-mitochondrial DNMT1 and pCMV-SPORT6-DNMT3A (big picture of 9 images) (DNMT1 staining). Cells have been stained for mitochondria (ATP synthase, top left), HA-tag (Alexafluor 488, top right) and nuclei (DAPI, bottom left). Bottom right is a merged image of all channels. Scale bar = 10 µm.

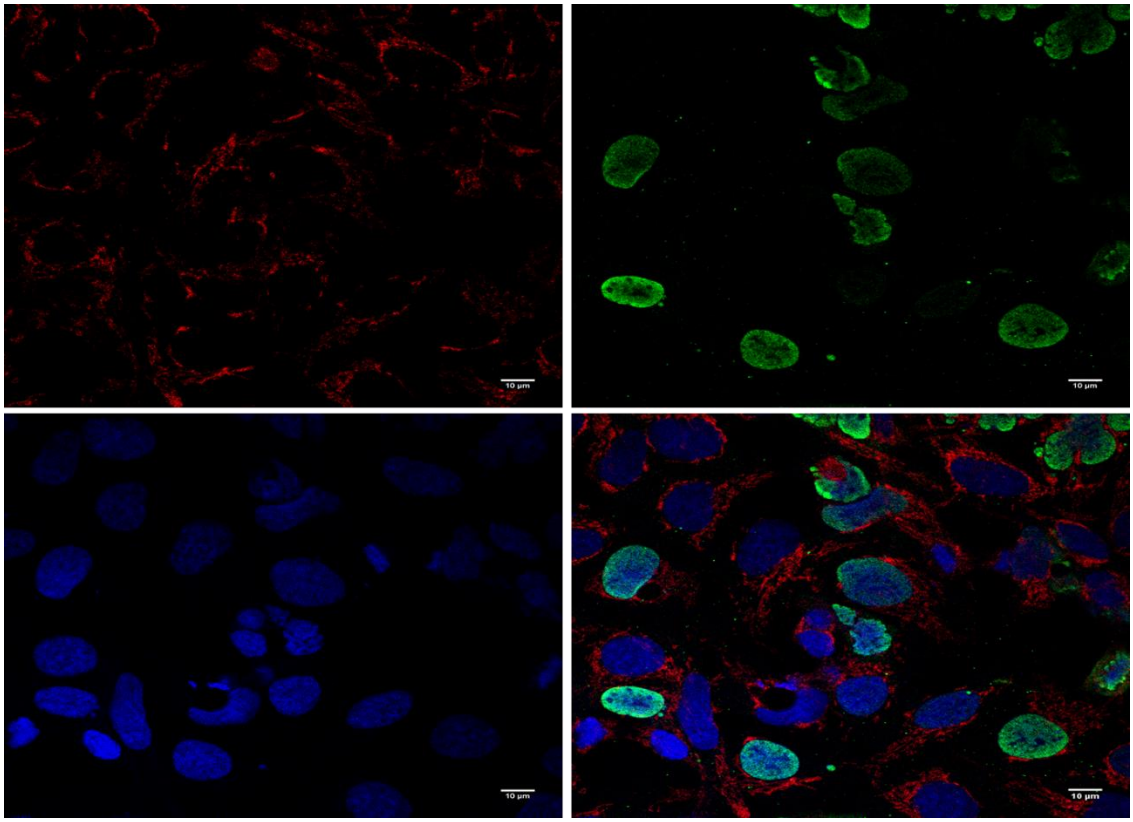

Figure 4.33: Immunocytochemistry of HEK293A cells transfected with pCMV-SPORT6-mitochondrial DNMT1 and pCMV-SPORT6-DNMT3A (DNMT3A staining). Cells have been stained for mitochondria (ATP synthase, top left), Myc-tag (Alexafluor 488, top right) and nuclei (DAPI, bottom left). Bottom right is a merged image of all channels. Scale bar = 10 µm.

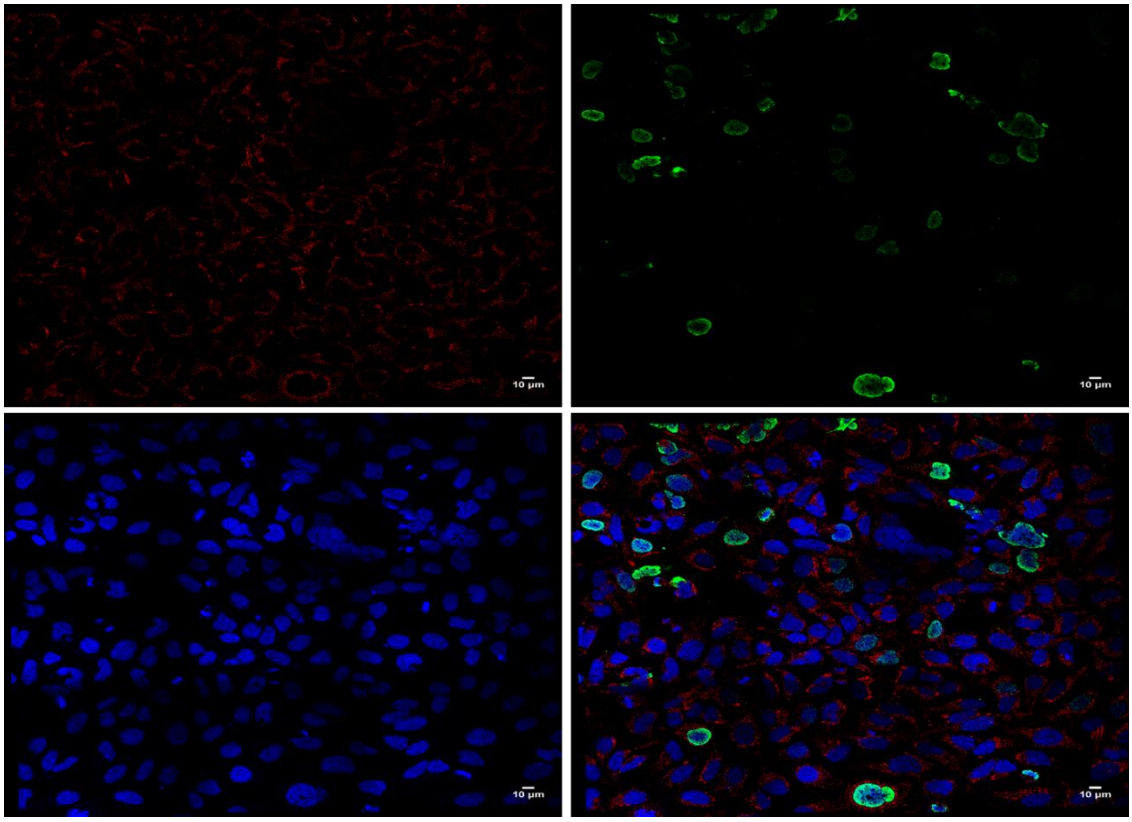

Figure 4.34: Immunocytochemistry of HEK293A cells transfected with pCMV-SPORT6-mitochondrial DNMT1 and pCMV-SPORT6-DNMT3A (big picture of 9 images) (DNMT3A staining). Cells have been stained for mitochondria (ATP synthase, top left), Myc-tag (Alexafluor 488, top right) and nuclei (DAPI, bottom left). Bottom right is a merged image of all channels. Scale bar = 10 µm.

4.4.4 Methylation analysis of mtDNA sequences after DNMT3A overexpression and mitochondrial DNMT1-DNMT3A double overexpression

In this section, the results of methylation analysis of mtDNA sequences following overexpression of DNMT3A and/or mitochondrial DNMT1 and DNMT3A double overexpression are reported. The subchapters have been divided by gene of interest.

4.4.4.1 COX2 methylation status after mitochondrial DNMT1 and DNMT3A overexpression

The methylation status of COX2 was investigated after pCMV-SPORT6-DNMT3A or pCMV-SPORT6-mitochondrial DNMT1 and pCMV-SPORT6-DNMT3A overexpression. First, the PCR conditions for COX2 amplification were checked, using DNA isolated from cells transfected with either conditions (**Figure 4.35**). After successful subcloning of the ~215 bp PCR products in the TOPO-vector (**Figure 4.36** and **Figure 4.37**), the sequencing was performed. The sequencing data was then analysed for bisulphite conversion (**Table 4.10** and **Table 4.11**). Similar results were obtained in both pCMV-SPORT6-DNMT3A and pCMV-SPORT6-mitochondrial DNMT1/pCMV-SPORT6-DNMT3A transfected clones, with a conversion rate of CpG motifs of 99.5% for both conditions, and a conversion rate of non-CpG motifs of 99.9% and 99.8%, respectively. These results indicate that DNMT3A does not play a role in COX2 epigenetic regulation in HEK293A cells, and neither does mitochondrial DNMT1 and DNMT3A double overexpression.

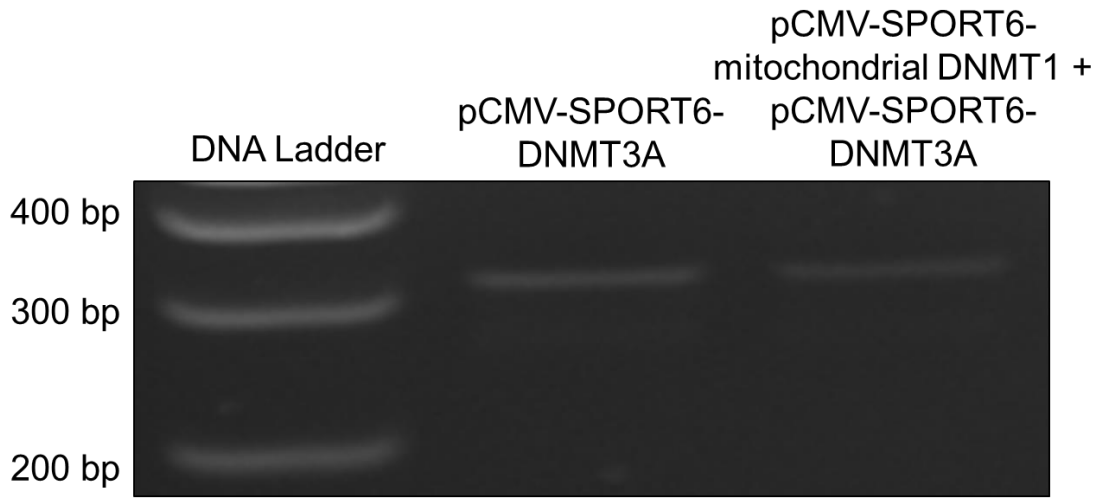

Figure 4.35: DNA gel electrophoresis of COX2 PCR samples using pCMV-SPORT6-DNMT3A, or pCMV-SPORT6-mitochondrial DNMT1 and pCMV-SPORT6-DNMT3A transfected DNA samples as template.

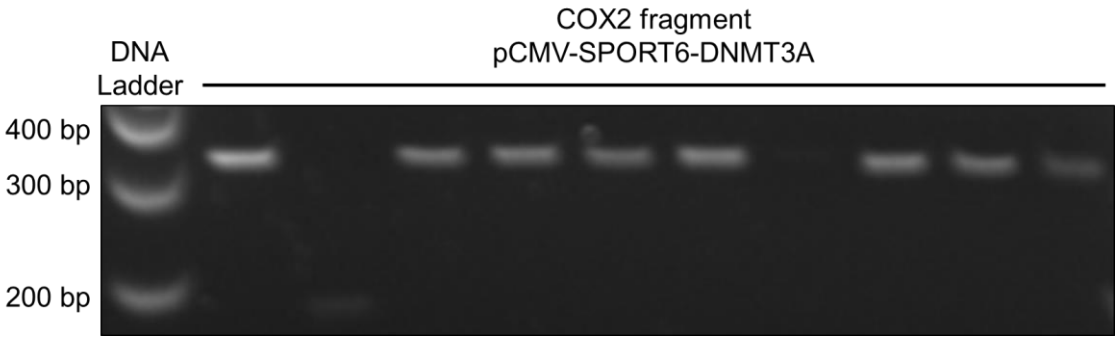

Figure 4.36: Representative DNA gel electrophoresis of TOPO-COX2 miniprep samples from pCMV-SPORT6-DNMT3A-transfected DNA.

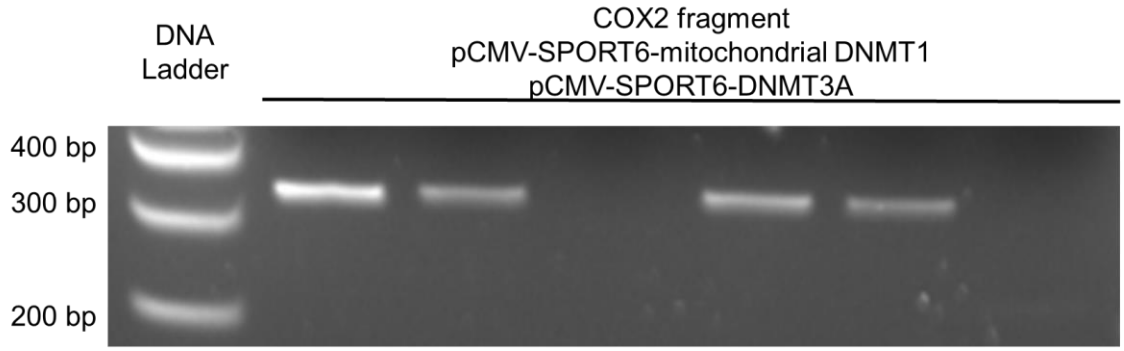

Figure 4.37: Representative DNA gel electrophoresis of TOPO-COX2 miniprep samples from pCMV-SPORT6-mitochondrial DNMT1 and pCMV-SPORT6-DNMT3A transfected DNA.

Table 4.10: Methylation status analysis of COX2 sequences from pCMV-SPORT6-DNMT3A transfected samples. N = 12.

Vector	Target							
pCMV-SPORT6-DNMT3A	COX2							
Sample name	length (bp)	Total C residues	Converted C	total CpG motifs	total converted CpG motifs	total nonCpG motifs	total converted nonCpG motifs	percent of identity
D3A_COX2_1	257	81	81	17	17	64	64	100.00%
D3A_COX2_2	257	81	81	17	17	64	64	100.00%
D3A_COX2_3	257	81	81	17	17	64	64	100.00%
D3A_COX2_4	257	81	81	17	17	64	64	100.00%
D3A_COX2_5	257	81	81	17	17	64	64	100.00%
D3A_COX2_6	257	81	81	17	17	64	64	100.00%
D3A_COX2_7	257	81	81	17	17	64	64	100.00%
D3A_COX2_8	257	81	81	17	17	64	64	100.00%
D3A_COX2_9	257	81	81	17	17	64	64	100.00%
D3A_COX2_10	257	81	80	17	16	64	64	100.00%
D3A_COX2_11	257	81	80	17	17	64	63	100.00%
D3A_COX2_12	257	81	81	17	17	64	64	100.00%
total		972	970	204	203	768	767	100.00%
		total C converted rate	**99.8%**	**total CpG converted rate**	**99.5%**	**total nonCpG converted rate**	**99.9%**	

Table 4.11: Methylation status analysis of COX2 sequences from pCMV-SPORT6-mitochondrial DNMT1 and pCMV-SPORT6-DNMT3A transfected samples. N = 12.

Vector	Target							
pCMV-SPORT6-mitochondrial DNMT1 pCMV-SPORT6-DNMT3A	COX2							
Sample name	length (bp)	Total C residues	Converted C	total CpG motifs	total converted CpG motifs	total nonCpG motifs	total converted nonCpG motifs	percent of identity
D1D3A_COX2_1	257	81	81	17	17	64	64	100.00%
D1D3A_COX2_2	257	81	81	17	17	64	64	100.00%
D1D3A_COX2_3	257	81	81	17	17	64	64	100.00%
D1D3A_COX2_4	257	81	81	17	17	64	64	100.00%
D1D3A_COX2_5	257	81	81	17	17	64	64	100.00%
D1D3A_COX2__6	257	81	81	17	17	64	64	100.00%
D1D3A_COX2__7	257	81	81	17	17	64	64	100.00%
D1D3A_COX2_8	257	81	81	17	17	64	64	100.00%
D1D3A_COX2_9	257	81	80	17	17	64	63	100.00%
D1D3A_COX2_10	257	81	81	17	17	64	64	100.00%
D1D3A_COX2_11	257	81	80	17	16	64	64	100.00%
D1D3A_COX2_12	257	81	81	17	17	64	64	100.00%
total		972	970	204	203	768	767	
		total C converted rate	**99.79%**	**total CpG converted rate**	**99.5%**	**total nonCpG converted rate**	**99.8%**	

4.4.4.2 D-Loop sequence fragment methylation status after mitochondrial DNMT1 and DNMT3A overexpression

Finally, the methylation status of D-Loop (fragment 1-181) was investigated after pCMV-SPORT6-DNMT3A or pCMV-SPORT6-mitochondrial DNMT1 and pCMV-SPORT6-DNMT3A overexpression. The PCR conditions for D-Loop (fragment 1-181) amplification were checked, using DNA isolated from cells transfected with either conditions (**Figure 4.38**). The expected band was obtained (~215 bp), along with another unexpected band of about 180 bp length, even after using stringent PCR conditions. The PCR products were then amplified through TOPO-cloning and DH5α transformation. The clones obtained were then screened for successful insertion through EcoRI digestion and DNA gel electrophoresis (**Figure 4.39** and **Figure 4.40**) and clones incorporating the PCR product as well as the unexpected PCR band were sequenced. The sequencing data was then analysed for bisulphite conversion (**Table 4.12** and **Table 4.13**).

In the samples obtained from pCMV-SPORT6-DNMT3A transfected cells, only 3 clones containing the correct sequence could be found, even after increasing PCR stringency and repeating the whole protocol. After analysis, all these

samples showed a 100% conversion rate of C residues at both CpG and non-CpG motifs.

Additionally, 3 samples containing the unexpected PCR product were sequenced, to check the nature of this insert. The sequencing data showed a sequence that did not have any similarity with the D-Loop fragment sequence. Furthermore, since this DNA was treated with bisulphite sequencing, it was not possible to investigate the nature of this sequence further as all the C residues were converted to U (which is read as a T during sequencing).

None of the clones obtained from samples transfected with pCMV-SPORT6-mitochondrial DNMT1 and pCMV-SPORT6-DNMT3A contained the expected D-Loop fragment sequence. However, 3 clones were investigated. The same unexpected sequence was identified.

At this point, it was concluded that DNMT3A could not modify the methylation status of this D-Loop fragment in HEK293A cells. However, as this DNA methyltransferase has De novo methylation features, it is possible that its overexpression might have caused changes in the epigenetic regulation of nuclear DNA, hence the presence of an unexpected band after PCR of D-Loop fragment.

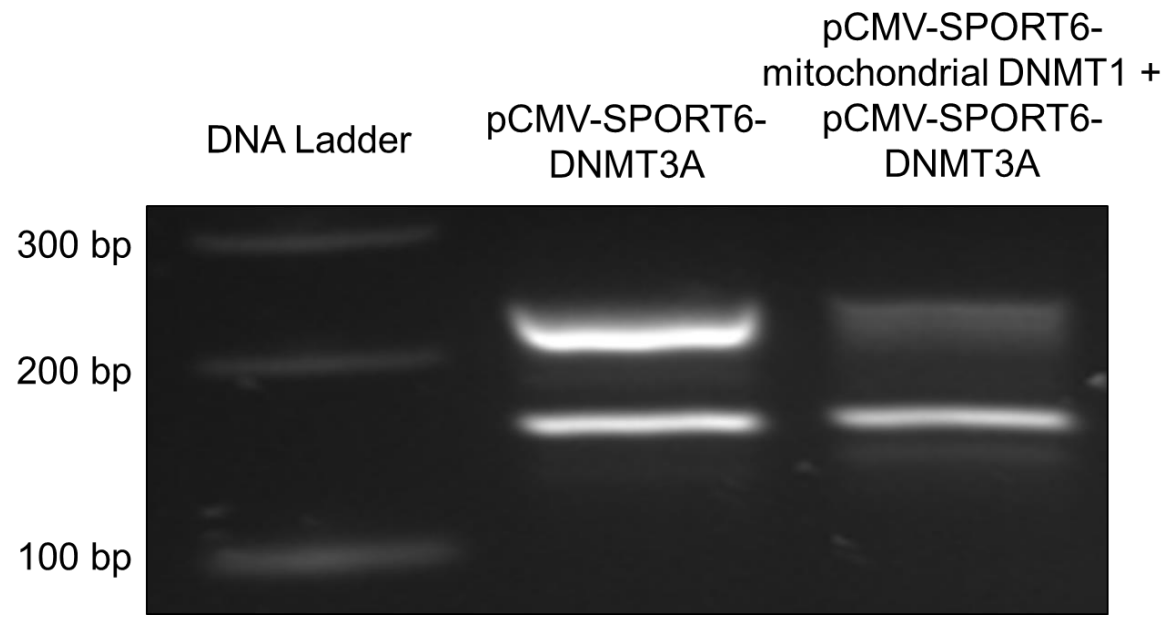

Figure 4.38: DNA gel electrophoresis of D-Loop fragment PCR samples using pCMV-SPORT6-DNMT3A, or pCMV-SPORT6-mitochondrial DNMT1 and pCMV-SPORT6-DNMT3A transfected DNA samples as template.

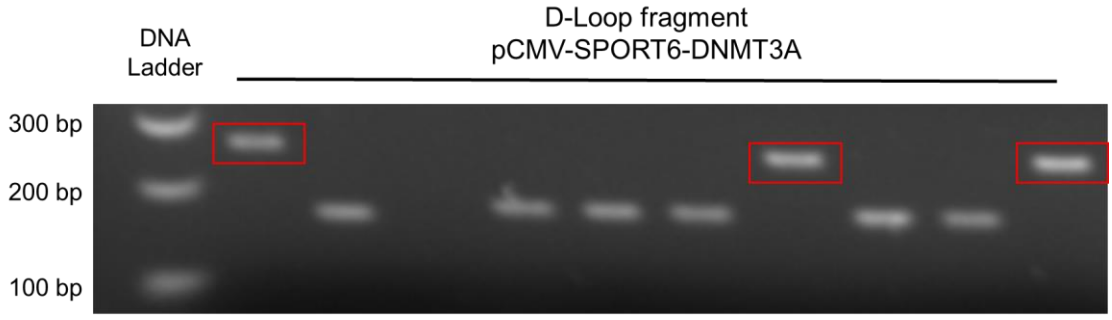

Figure 4.39: Representative DNA gel electrophoresis of TOPO-D-Loop (1-181) miniprep samples originated from pCMV-SPORT6-DNMT3A transfected DNA. The clones containing the expected PCR product are highlighted in red.

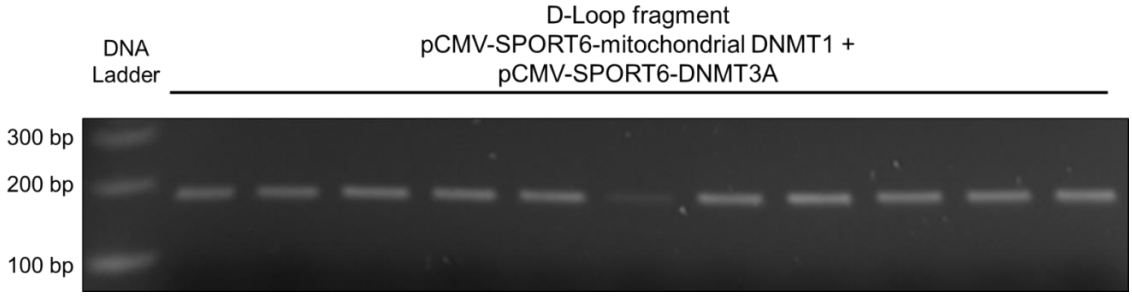

Figure 4.40: Representative DNA gel electrophoresis of TOPO-D-Loop (1-181) miniprep samples originated from pCMV-SPORT6-mitochondrial DNMT1 and pCMV-SPORT6-DNMT3A transfected DNA.

Table 4.12: Methylation status analysis of D-Loop (1-181) sequences from pCMV-SPORT6-DNMT3A transfected samples (linearised). Samples were linearised with HindIII digestion prior to bisulphite treatment. N = 3.

Vector	Target							
pCMV-SPORT6-DNMT3A	D-Loop (1-181)							
Sample name	length (bp)	Total C residues	Converted C	total CpG motifs	total converted CpG motifs	total nonCpG motifs	total converted nonCpG motifs	percent of identity
D3A_L1_1	181	58	58	55	55	3	3	100.00%
D3A_L1_2	181	58	58	55	55	3	3	100.00%
D3A_L1_3	181	58	58	55	55	3	3	100.00%
D3A_L1_4	104							0%
D3A_L1_5	104							0%
D3A_L1_6	104							0%
total		174	174	165	165	9	9	
		total C converted rate	**100%**	**total CpG converted rate**	**100%**	**total nonCpG converted rate**	**100%**	

Table 4.13: Methylation status analysis of D-Loop (1-181) sequences from pCMV-SPORT6-DNMT3A and pCMV-SPORT6-mitochondrial DNMT1 transfected samples (linearised). Samples were linearised with HindIII digestion prior to bisulphite treatment.

Vector	Target							
pCMV-SPORT6-mitochondrial DNMT1 pCMV-SPORT6-DNMT3A	D-Loop (1-181)							
Sample name	length (bp)	Total C residues	Converted C	total CpG motifs	total converted CpG motifs	total nonCpG motifs	total converted nonCpG motifs	percent of identity
D1D3A_L1_1	104							0%
D1D3A_L1_2	104							0%
D1D3A_L1_3	104							0%
total								
		total C converted rate	**n.d.**	**total CpG converted rate**	**n.d.**	**total nonCpG converted rate**	**n.d.**	

4.5 Discussion

In this chapter, methylation analysis of mtDNA following overexpression of DNMTs, generation of a DNMT3A plasmid and localisation studies following overexpression were performed. The protocols performed in this chapter showed some limitations in regards to the output and quality of the data obtained. First of all, the bisulphite sequencing method proved to be very time consuming, and had to be adapted to dealing with mitochondrial DNA in order to yield consistent data. However, some interesting data was obtained.

That is, through comparison of bisulphite sequencing from non-linearized and linearized DNA samples, it has emerged that linearization of mtDNA by restriction enzymes is required in order to avoid protection from bisulphite treatment and reduced conversion rate. By not performing digestion of DNA before bisulphite treatment, a severe bias is introduced in the protocol. Therefore, digestion of the mtDNA samples had to be performed prior to bisulphite sequencing in order to avoid false positives, as mtDNA circular form seemed to be able to protect it from bisulphite treatment, as shown after the first round of sequencing experiments and analysis. This feature of mtDNA has never been investigated in any of the papers where high percentages of mtDNA methylation were shown[51,52,130-133].

To further support this claim, a recent paper[150] by Liu B. et al (published after this study was conducted) demonstrated that the linear mtDNA has significantly higher conversion efficiency compared with circular mtDNA, and that the average methylation levels of 9 different mtDNA regions (including D-Loop) was less than 2% after linearization.

We can therefore rule that the papers claiming high percentages of mtDNA methylation after bisulphite treatment and sequencing were biased, and that the digestion step is crucial for proper mtDNA methylation analysis. However, the

bisulphite sequencing protocol, whilst being able to yield single base resolution for successful sequencing and methylation analysis, cannot discriminate between 5mC and 5hmC, and would not be suitable to understand the actual methylation status of mtDNA if changes in the conversion rate of C residues would have been found.

Another problem was posed by using HEK293A cells. Whilst representing a good candidate for setting up an easy, consistent and reliable overexpression system, these cells do not possess cardiac features nor represent a cardiac-specific cell line. Also, as shown by the immunocytochemistry data, the low transfection efficiency might hinder DNA methylation features of DNMT1 isoforms and DNMT3A. Analysis of COX2 or D-Loop sequences following pCMV-SPORT6-whole DNMT1 or pCMV-SPORT6-mitochondrial DNMT1 overexpression did not show any increase in the methylation of CpG motifs of these sequences, with almost 100% bisulphite conversion rate for all investigated clones. Overall, the results suggest that DNMT1 isoforms can't affect the methylation status of the investigated mtDNA sequences.

Following these results, major efforts were made to obtain a mouse DNMT3A overexpression vector. This vector was obtained using the same initial backbone used to obtain other DNMT1 overexpression constructs, i.e. pCMV-SPORT6. Furthermore, a Myc-tag was added to the original DNMT3A sequence to be used for Western blotting overexpression studies and immunocytochemistry localisation studies. Through this vector (pCMV-SPORT6-DNMT3A), I tested the hypothesis that whole DNMT1 and mitochondrial DNMT1 isoforms could interact with DNMT3A through an interaction site and allow it to localise at a mitochondrial level through their MLS.

First, a double overexpression system for mitochondrial DNMT1 and DNMT3A was set up, as this was the initial condition thought to be able to yield DNMT3A localisation within mitochondria[141]. Western blotting analysis confirmed the transfection protocol as strong bands from both mitochondrial DNMT1 and DNMT3A were observed. Then, localisation of DNMT3A was analysed through immunocytochemistry. No signs of DNMT3A mitochondrial localisation were observed in the mitochondrial DNMT1-DNMT3A transfected samples. Some of the cells transfected with pCMV-SPORT6-whole DNMT1 and pCMV-SPORT6-DNMT3A showed DNMT3A signal coming from mitochondria (Figure 4.30). However, it is possible that the signal was due to bleaching or bleeding of the red channel into the green channel, as no other cell showed DNMT3A mitochondrial localisation and the overall signal was very bright.

After this set of experiments, the methylation status of COX2 mtDNA gene following transfection with pCMV-SPORT6-whole DNMT1 and pCMV-SPORT6-DNMT3A was investigated in HEK293A cells through bisulphite sequencing. No changes in the methylation status of COX2 CpG motifs were detected, so the hypothesis that whole DNMT1 could affect DNMT3A localisation was abandoned, along with the hypothesis that DNMT3A would be able to affect COX2 gene methylation status. These results, along with the aforementioned issues, compelled me to look for more high-throughput and methylation-specific methods for methylation analysis. Furthermore, these results prompted me to investigate methylation features of DNMT1 isoforms, especially mitochondrial DNMT1, in a cardiac-specific environment, using a stronger and more consistent overexpression system as well as a more high-throughput system for detection of methylation changes in mtDNA following overexpression.

In the final chapter of my thesis I attempted to resolve the aforementioned issues through the creation of adenoviral and lentiviral vectors, using a cardiac-specific cell line for overexpression experiments, and establishing a new method for methylation analysis.

Chapter 5 : DNMT1 interaction studies, generation of DNMT1 lentivirus and refinement of MeDIP procedures

5.1 Introduction

5.1.1 Overexpression tools

In this chapter, viral overexpression tools for DNMT1 overexpression were investigated. Specifically, adenoviral vectors were used to setup a transient overexpression system in cell lines other than HEK293 (i.e. MCEC), whereas a lentiviral vector for mtDNMT1 was obtained in order to create a MCEC cell line with stable mtDNMT1 overexpression.

5.1.1.1 Adenoviral vectors

The adenovirus is a 80-100 nm, non-enveloped, icosahedral capsid, double-stranded DNA virus, and it was first isolated from human adenoids in 1953[151]. The adenovirus has over 50 known serotypes[152], with the serotypes 2 and 5 being the most commonly used as a starting point to generate adenoviral vectors[153].

Vectors based on adenovirus are among the most commonly utilized platforms for gene delivery to cells in molecular biology studies and also for gene therapy applications, due to its advantageous characteristics such as high cloning capacity (up to 8 kb), ability to infect a wide variety of cell types and tissues and relative safety due to it remaining episomal in transduced cells.

The first suggestion that adenoviruses (Ad) could be used as a vector system for expression of foreign genes came in the late 1970s[154,155] with the identification of spontaneous recombinants between Ad and SV40 which expressed T antigen fused to and Ad structural protein. However, it was with the creation of cell lines that could complement viruses deleted of the essential early region 1 (E1) that the modern Ad-based vectors were developed[156]. This cell line allowed for the development of Ad-based vectors that could not replicate in most cell lines or tissues, whilst still providing high levels of expression of an exogenous transgene.

Nowadays, the vast majority of studies involving Ad vectors use the simple E1-deleted, first generation Ad vectors. Since E1 is required for virus replication, these vectors do not replicate in most cell lines but can be easily propagated in the E1 complementing cell lines, such as HEK293A cells[156]. Furthermore, most of the first-generation vectors currently in use are also lacking the early region 3 (E3), which is not required for virus replication in culture, and it has been shown that its removal increases the cloning capacity for foreign DNA to ~8 kb[157] (**Figure 5.1**).

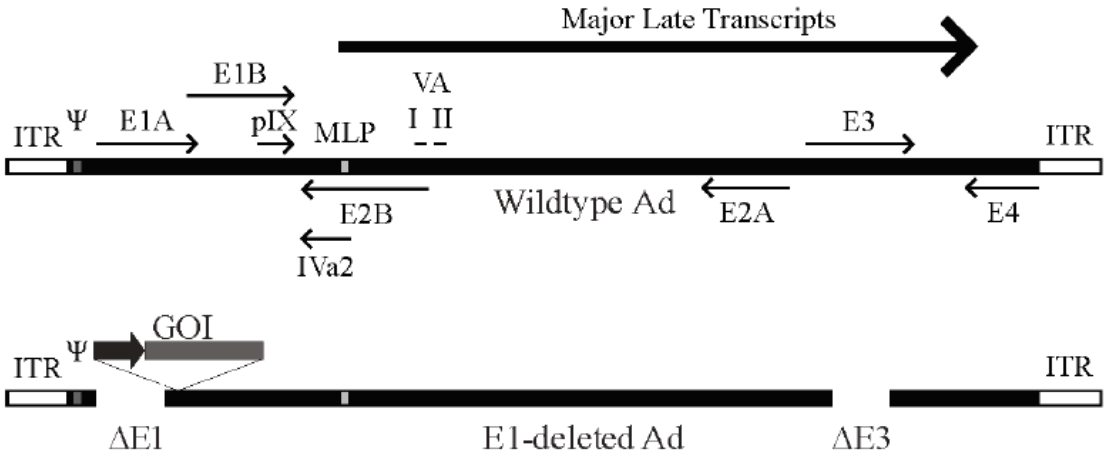

Figure 5.1: Comparison between the wildtype Ad genome (serotype 5) and adenovirus-based Ad vectors. The early genes (E1-E4) and the region from which the major late transcript is produced are shown (transcripts produced from alternative splicing are not shown). In the Ad vectors, the gene of interest is usually introduced to replace the E1 region and is placed under control by a heterologous promoter (dark arrow above ΔE1). Adapted from Wong C.M. et al, *The Role of Chromatin in Adenoviral Vector Function*, Viruses, 2013[153].

5.1.1.2 Lentiviral vectors

Lentiviral vectors are generated from Lentiviruses, which are members of the viral family *Retroviridae* (retroviruses) and are characterized by their use of viral reverse transcriptase (RT) and integrase (IN) for stable insertion of viral genomic information into the host genome. Apart from sustained gene delivery through stable vector integration into the host genome, lentiviral vectors offer several attractive properties as gene-delivery vehicles, including the ability to deliver complex genetic elements, replicate in non-dividing cells[158], broad tissue tropism, no expression of viral proteins after vector transduction, and a relatively easy system for vector manipulation and production. Lentiviral vectors have been used successfully to transduce various cell types, such as neurons, hepatocytes, hematopoietic stem cells, retinal cells, dendritic cells, myocytes and islet cells[159-162].

The majority of lentiviral vectors are based on HIV-1, which has a single-stranded positive-sense RNA genome of approximately 9 kb in length that encodes nine viral proteins. The three major structural genes, Gag, Pol and Env, encode viral core proteins, a set of enzymes required for viral replication (RT, IN) and the viral surface glycoprotein gp160 (which is cleaved into gp120, referred to as the surface subunit or SU, and gp41, which is referred to as the transmembrane subunit or TM), respectively. Additionally, the viral genome also encodes the regulatory proteins Tat and Rev, which activate viral transcription and control the splicing and nuclear exports of viral transcripts, respectively. Each virion contains Gag, Pol and Env proteins, accessory proteins Vif, Vpr and Nef, and two copies of viral genomic RNA.

After infection, the proviral DNA is integrated into the host genome by viral IN[163]. Although there are safety considerations inherent to developing and using

vectors which can integrate into a host genome, and particular consideration must be given to the possibility of generating replication-competent lentiviruses (RCL), these vectors represent a potent tool for basic and translational research. To reduce the likelihood of the production of RCLs in vector preparations, many laboratories have developed a number of 'generations' of lentiviral vectors to reduce this risk.

The first generation of lentiviral vectors is referred to as those vectors that first split the system into three separate plasmids to increase safety, rather than the early replication-competent prototypes of HIV vectors. First generation replication-deficient recombinant HIV-1 vectors are produced from three separate elements: a packaging construct, an Env plasmid encoding a viral glycoprotein and a transfer vector genome construct (**Figure 5.2**)[164]. The packaging construct expresses HIV Gag, Pol and regulatory/accessory proteins from a strong mammalian promoter to generate viral particles, the Env plasmid expresses a viral glycoprotein (usually Vesicular stomatitis virus protein G, VSV-G) to provide the vector particles with a receptor-binding protein, and the transfer vector plasmid contains the transgene(s) and all of the essential elements for packaging, reverse transcription and integration, but expresses no HIV proteins. To increase safety further, second-generation vectors have been developed by removing accessory genes in the system (Vif, Vpu, Vpr and Nef), which are important for HIV as a pathogen but can be depleted in second-generation lentivectors[160] (**Figure 5.2**).

Most currently available lentiviral vectors and packaging constructs, including the ones used in this study, are based on the second-generation lentiviral vectors, but third-generation, as well as further modifications for improved biosafety (i.e. codon optimization for Rev-independent Gag-Pol expression) and vector

performance (i.e. packaging elements from different HIVs for altered vector tropism) also exist[165-167].

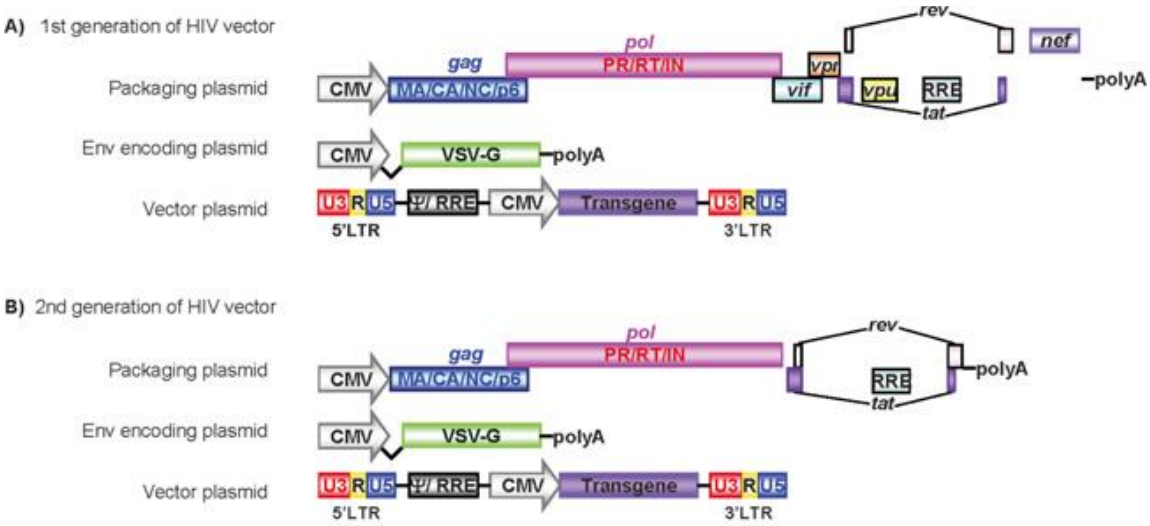

Figure 5.2: First (A) and second (B) generation of HIV-derived lentivectors. The first generation includes all of the viral proteins (except Env) in a packaging plasmid. VSV-G is provided by a different plasmid, and the transgene is expressed under a strong viral promoter such as CMV. For the second generation of vectors, all of the accessory proteins are excluded from the packaging plasmid. Figure adapted from Sakuma T. et al, *Lentiviral vectors: basic to translational*, Biochem J., 2012[164].

5.1.2 Methylated-DNA immunoprecipitation methylation analysis

To investigate the methylation status of mtDNA sequences with a high-throughput approach, a methylated-DNA immunoprecipitation (MeDIP) methylation analysis system was established. MeDIP consists in the immunoprecipitation of methylated DNA fragments using an antibody to 5-methyl cytosine (5-mC)[168] (**Figure 5.3**). The monoclonal antibody against 5-mC allows enrichment for methylated DNA independent of DNA sequence[169], which can then be analysed by a variety of methods: the detection of a gene of interest in the methylated DNA fraction can be done by polymerase chain reaction (PCR), hybridization to genomic arrays, and even high-throughput sequencing[170]. Since the establishment of MeDIP[171], the technique has emerged as one of the most widely used methods in the scientific community, and has been used to derive methylation maps in different organisms[76,172], for epigenetic mapping in cancer[168] and to monitor epigenetic changes upon differentiation of embryonic stem cells[173].

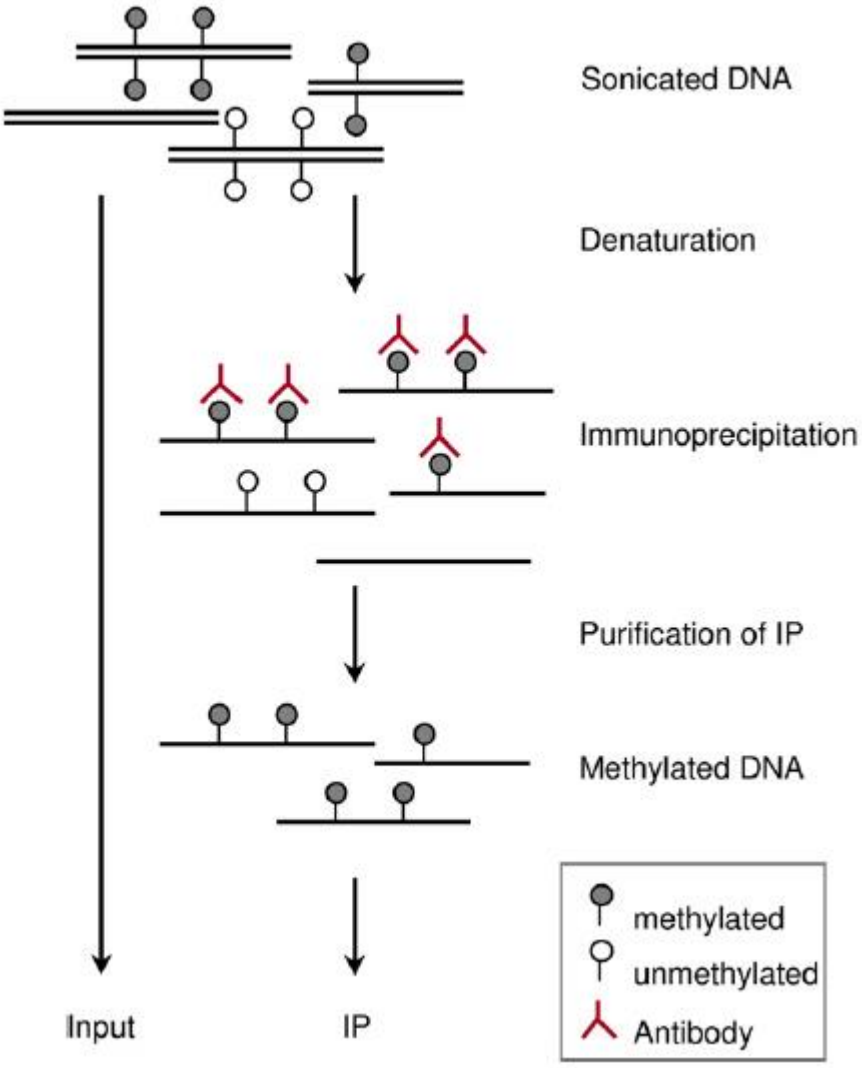

Figure 5.3: MeDIP principles. DNA is fragmented by sonication and denatured. Methylated DNA is precipitated using an antibody against 5mC. Purified methylated DNA (IP) and sonicated control DNA (Input) are then investigated with any of the available downstream applications (qPCR, Microarray, NGS). Figure adapted from Palmke N. et al, *Comprehensive analysis of DNA-methylation in mammalian tissues using MeDIP-chip*, Methods, 2011[174].

5.2 Aims

The aim of this chapter was to generate adenoviral vectors for nuclear DNMT1 and mitochondrial DNMT1, establish DNMT1 overexpression through adenoviral infection, investigate mtDNA methylation through MeDIP and establish MeDIP in London, generate a mtDNMT1 lentivirus and obtain stable mtDNMT1 overexpression in MCE cells, and identify a potential co-factor for increased DNA methylation by DNMT1 at mitochondrial level.

5.3 Methods

5.3.1 Generation of Adenoviral vectors for nDNMT1, mtDNMT1 and DNMT3A

5.3.1.1 Gateway cloning

To increase efficiency of nuclear DNMT1, mitochondrial DNMT1 and DNMT3A overexpression, new adenoviral vectors carrying these sequences were generated. For this purpose, the Gateway® technology (Life Technologies®) was used starting from the nuclear DNMT1, mitochondrial DNMT1 and DNMT3A overexpression vectors (**Figures 5.4**, **5.5** and **5.6**). The Gateway cloning System (Invitrogen™) is a molecular biology method that enables to efficiently transfer DNA-fragments between plasmids using a proprietary set of recombination sequences, the "Gateway att" sites, and two proprietary enzyme mixes, called "LR Clonase", and "BP Clonase". Gateway cloning allows transfer of DNA fragments between different cloning vectors while maintaining the reading frame. A general workflow of the whole protocol is shown (**Figure 5.7**).

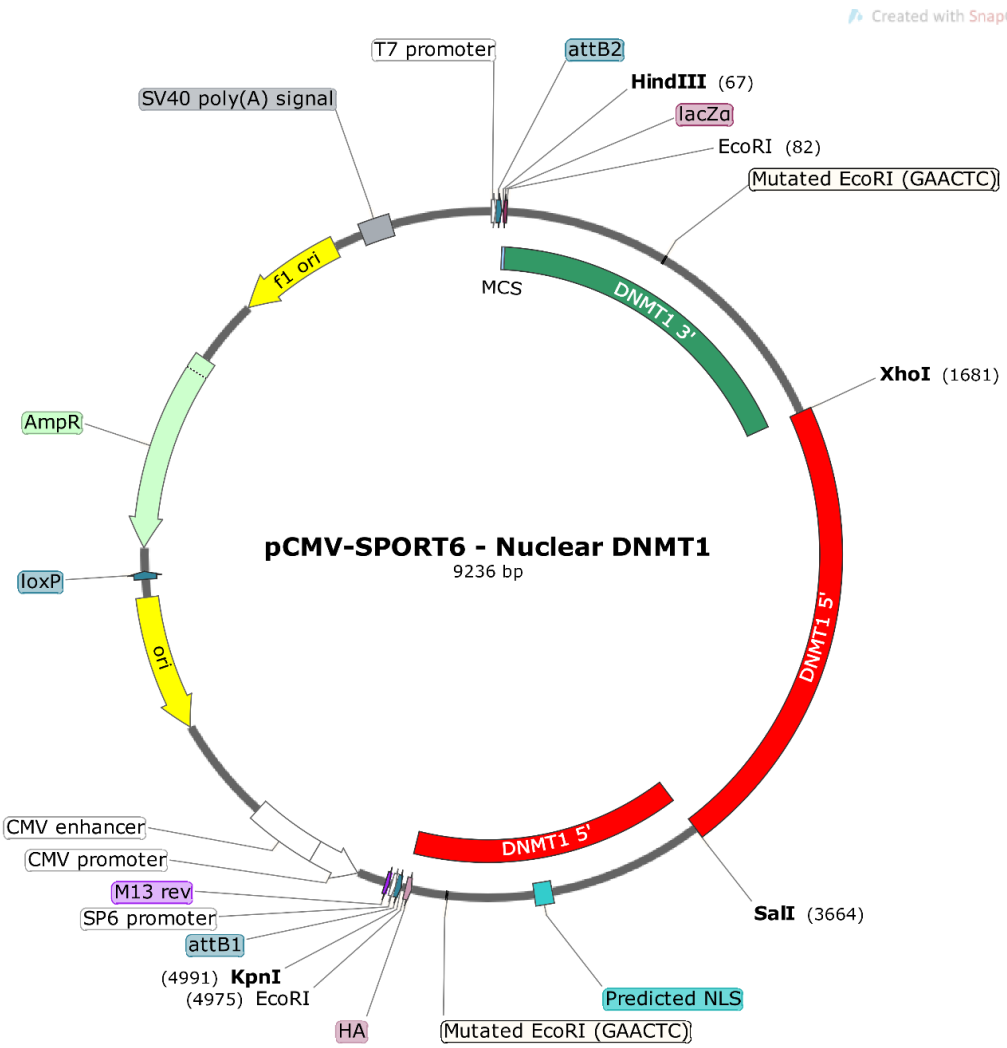

Figure 5.4: Final pCMV-SPORT6-nuclear DNMT1 plasmid.

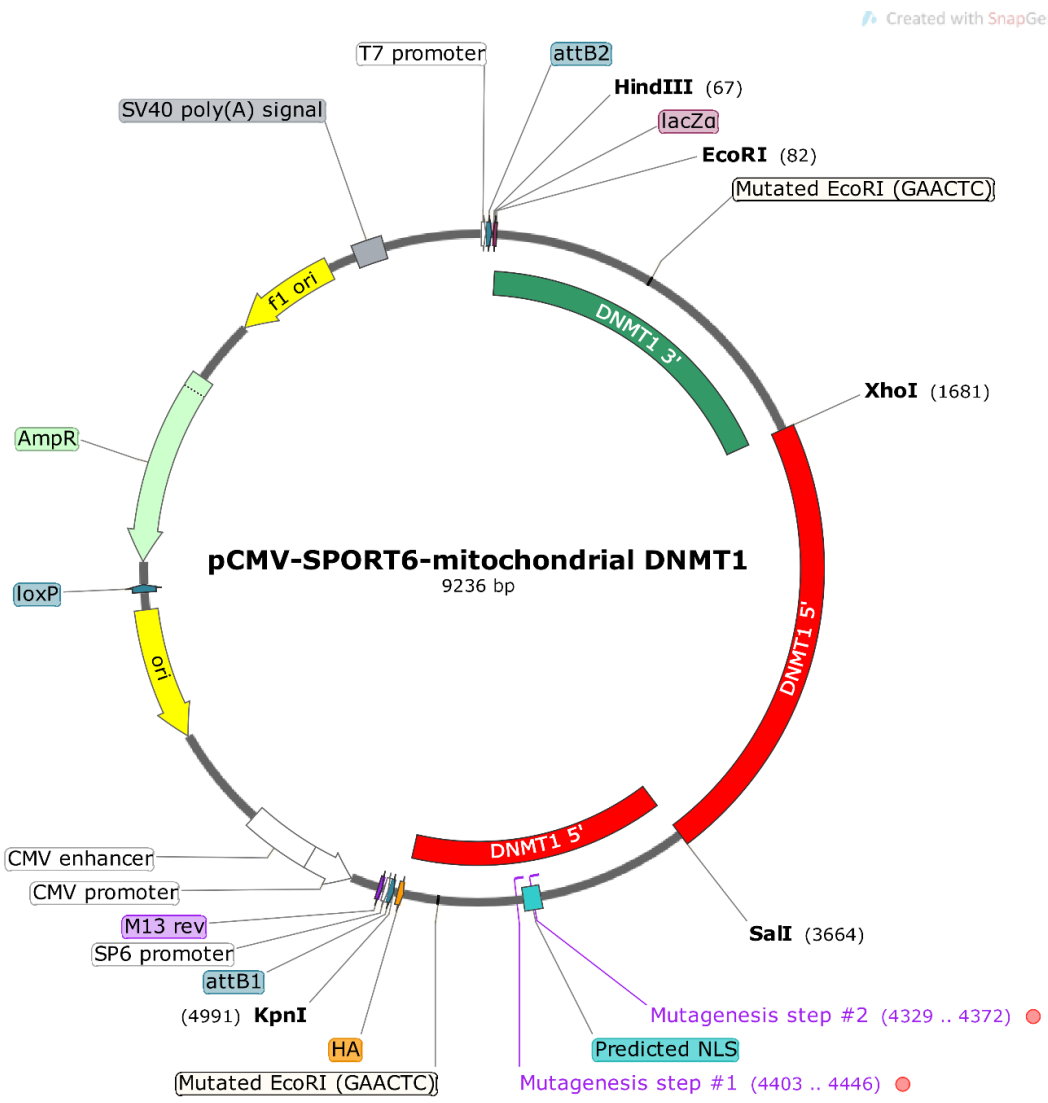

Figure 5.5: Final pCMV-SPORT6-mitochondrial DNMT1 plasmid.

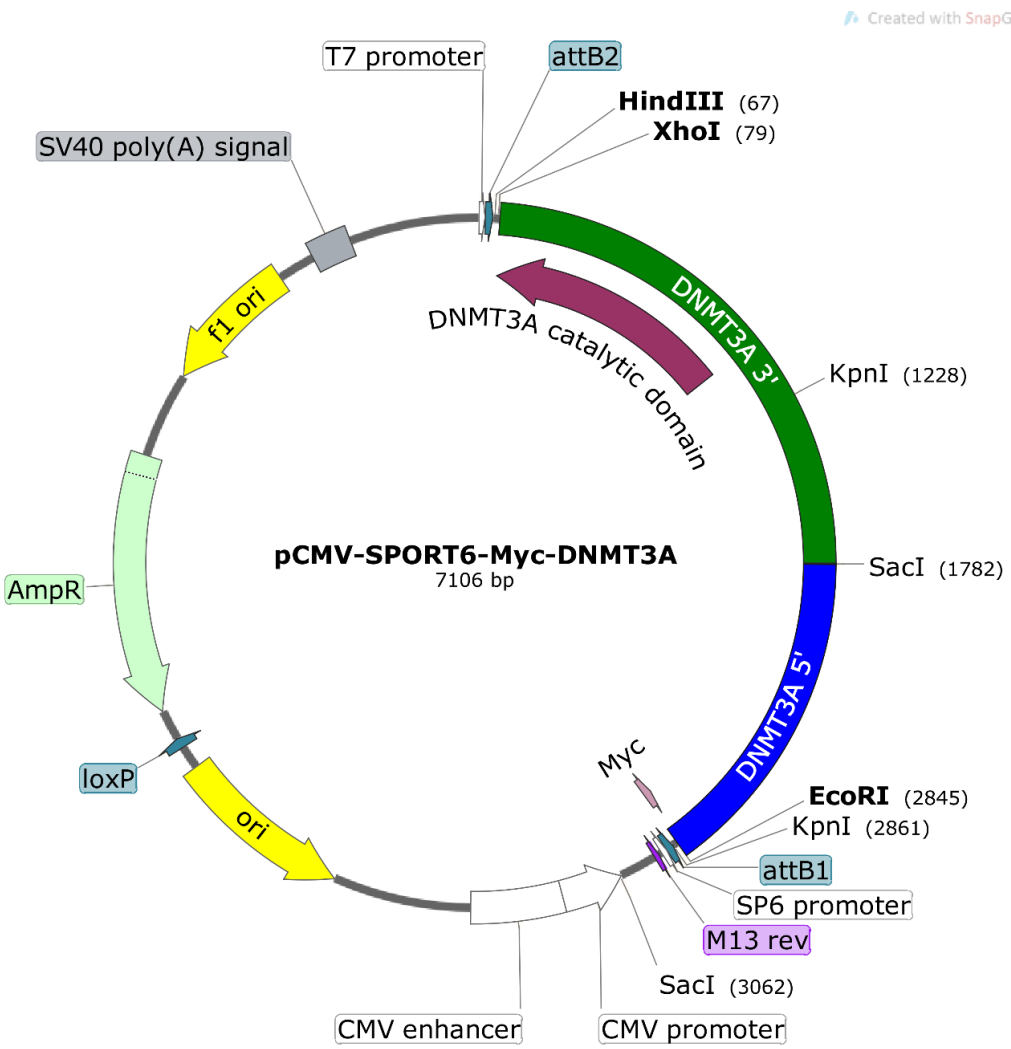

Figure 5.6: Final pCMV-SPORT6-DNMT3A plasmid.

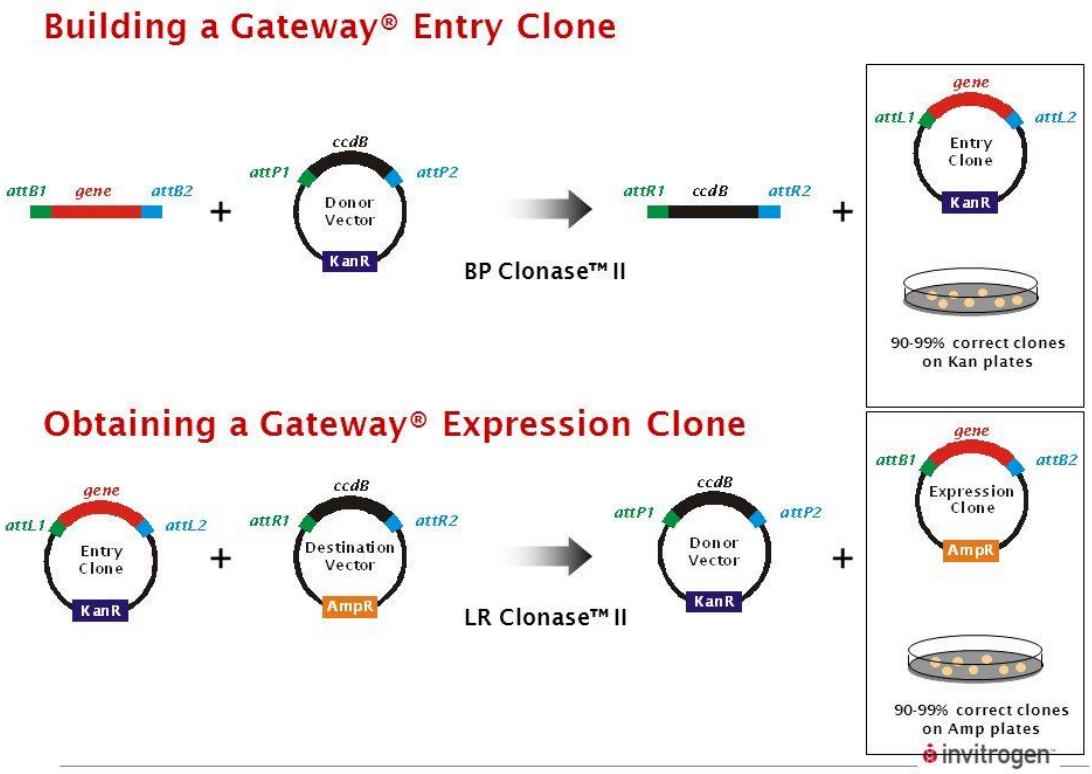

Figure 5.7: Gateway® workflow for creation of adenoviral vectors. The workflow is divided in 2 main steps: in the BP clonase step, the sequence of interest is inserted in an "entry clone" vector and amplified through miniprep. Then, the entry clone plasmid is used in the LR clonase step to obtain the final expression clone. The same workflow was applied for all constructs.

5.3.1.2 BP Clonase reaction

First, insertion of the genes in a donor vector was performed using a BP Clonase™ II kit (Thermo Fisher Scientific®, 11789020). **Figure 5.8** shows pDONR™221 map. Briefly, the vectors were linearized through HpaI digestion (New England BioLabs®, R0105S), which is an enzyme that does not cut DNMT1 or DNMT3A sequences, but has a single restriction site on pCMV-SPORT6.

About 2 µl of the digested samples were ran on a 1% agarose gel to confirm the single cut. Then, the remaining samples were extracted, resuspended in 20 µl TE Buffer and quantified at the NanoDrop. The reaction components (**Table 5.1**) were then added to a 1.5 ml microcentrifuge tube at room temperature and mixed. 2 µl of BP Clonase™ II enzyme mix were added to each sample, then all samples were incubated at 25ºC for 1 hour. After this, 1 µl of Proteinase K solution was added to terminate the reactions, then the samples were incubated at 37ºC for 10 minutes. Reaction mixtures were then transformed into DH5α cells with Kanamycin selection, colonies were picked and miniprep was performed.

The pDONR-nuclear DNMT1 and pDONR-mitochondrial DNMT1 clones were checked through XhoI-HindIII and KpnI-HindIII double digestions, whereas pDONR-DNMT3A clones were checked through SacI-KpnI and EcoRI-XhoI double digestions. Positive clones were then selected for the next step.

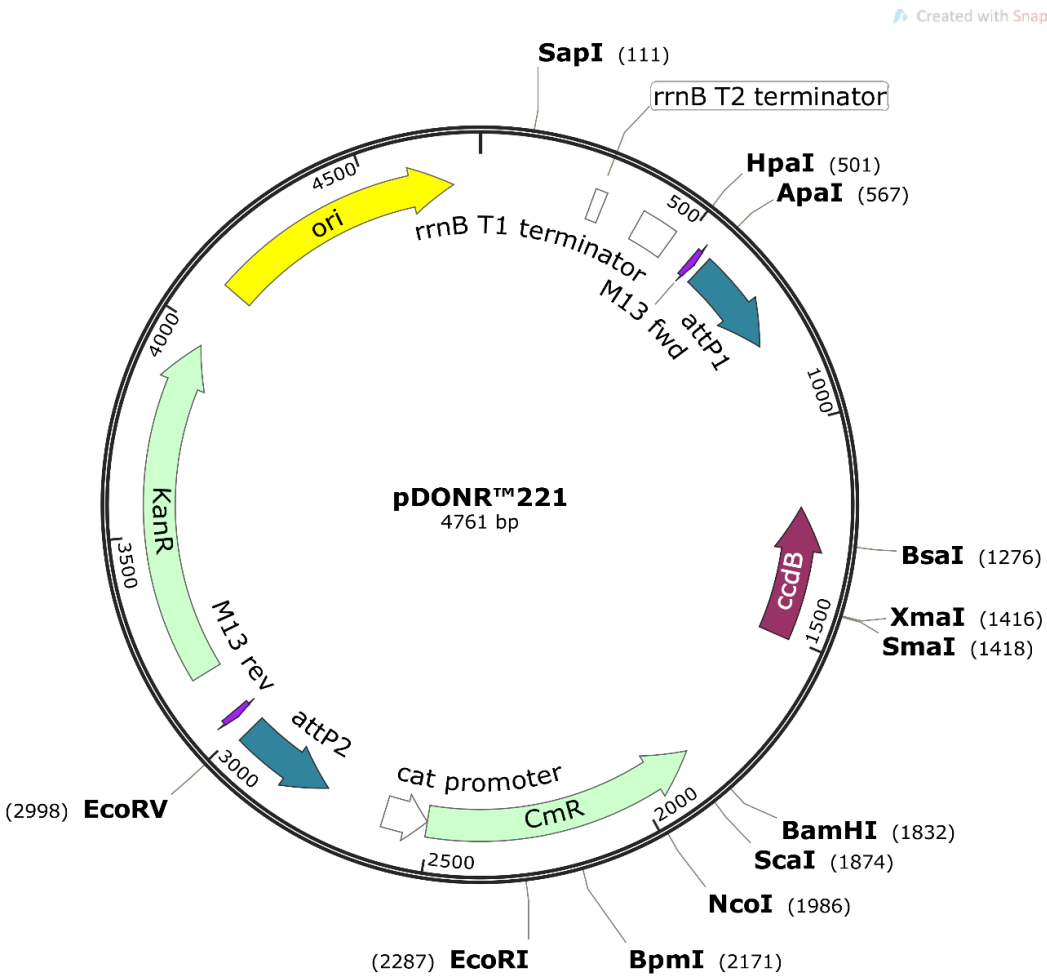

Figure 5.8: pDONR™221 map.

Table 5.1: BP Clonase™ II reaction components.

Reagent	Quantity
attB-PCR product (cut DNMT1/DNMT3A)	1-7 µl (150 ng)
Donor vector (pDONR) (150 ng/µl)	1 µl
1TE Buffer, pH 8.0	to 8 µl

5.3.1.3 LR Clonase reaction

LR Clonase™ II kit (Thermo Fisher Scientific®, 11791020) protocol was then performed. The reaction components (**Table 5.2**) were added to a 1.5 ml microcentrifuge tube at room temperature and mixed. Two µl of LR Clonase™ II enzyme mix were added to each sample, then all samples were incubated at 25ºC for 1 hour. After this, 1 µl of Proteinase K solution was added to terminate the reactions, then the samples were incubated at 37ºC for 10 minutes. Reaction mixtures were then transformed into DH5α cells with Ampicillin selection, colonies were picked and miniprep was performed.

pDEST-nuclear DNMT1, pDEST-mitochondrial DNMT1 and pDEST-DNMT3A clones digestion pattern was investigated using EcoRI, HindIII, KpnI, SacI and XhoI restriction enzymes. Furthermore, in order to better confirm insertion in pDEST V5 (**Figure 5.9**), PCR primers for 5'-end and 3'-end of nuclear DNMT1 and mitochondrial DNMT1 were designed using Primer3 online tool (http://primer3.ut.ee/). The sequence of the primer sets and the reagents used (Table 5.3 and 5.4), as well as the PCR conditions (**Figure 5.10** and **Figure 5.11**) are reported.

Table 5.2: LR Clonase™ II reaction components.

Reagent	Quantity
Entry clone (pDONR-DNMT1/pDONR-DNMT3A)	1-7 µl (150 ng)
Destination vector (pDEST V5) (150 ng/µl)	1 µl
1TE Buffer, pH 8.0	to 8 µl

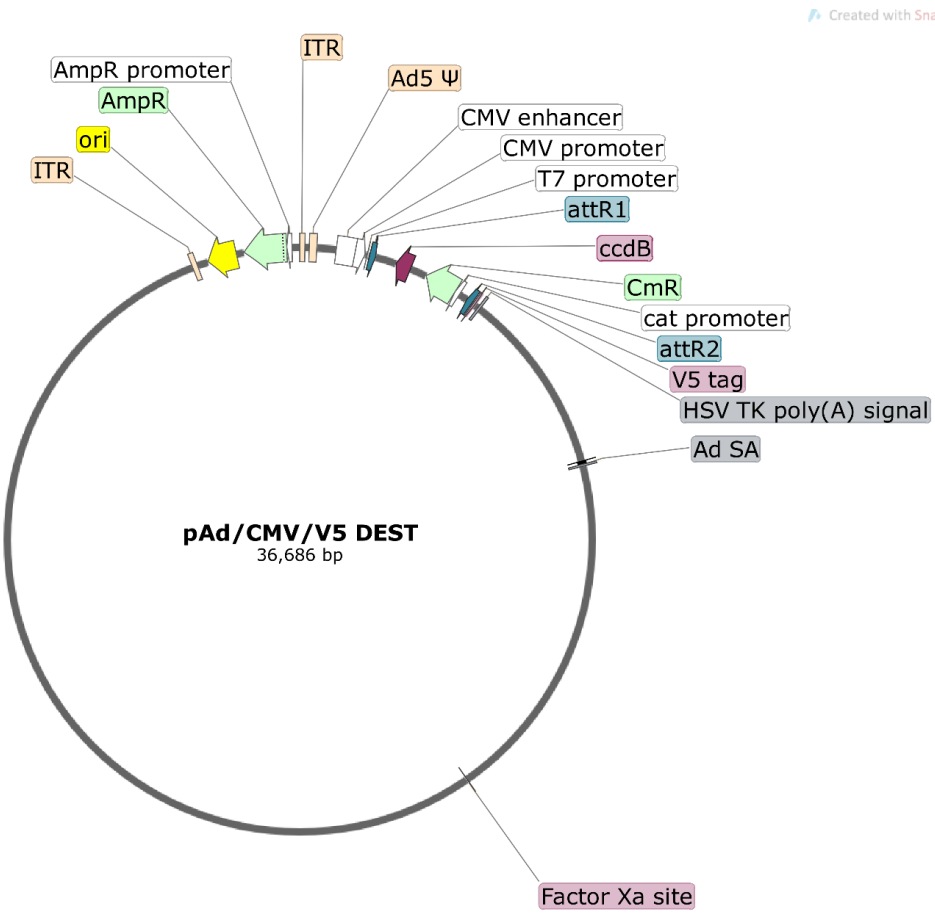

Figure 5.9: pAd/CMV/V5 DEST vector.

Table 5.3: PCR primers for 5'-end and 3'-end DNMT1 sequences.

Primer	Sequence
DNMT1 5' Forward	5'-ATTGGTTATTAATGGTATTGAATTTA-3'
DNMT1 5' Reverse	5'-CTCCACAAATTTCAAAACATTAAC-3'
DNMT1 3' Forward	5'-**AGGAAGAGAG**GATTTTAATTTAAATTATT-3'
DNMT1 3' Reverse	5'-**AGGAAGAGAG**ACTATACTTACTTAT-3'

Table 5.4: Reagents for PCR check of DNMT1 5' and 3' regions.

Reagent	Quantity (µl)
2x Extreme Buffer	12.5
2 mM dNTPs	5
10 µM Forward Primer	1
10 µM Reverse Primer	1
DNA Template (LR clones) (50 ng)	5
KOD Xtreme DNA Polymerase	0.5

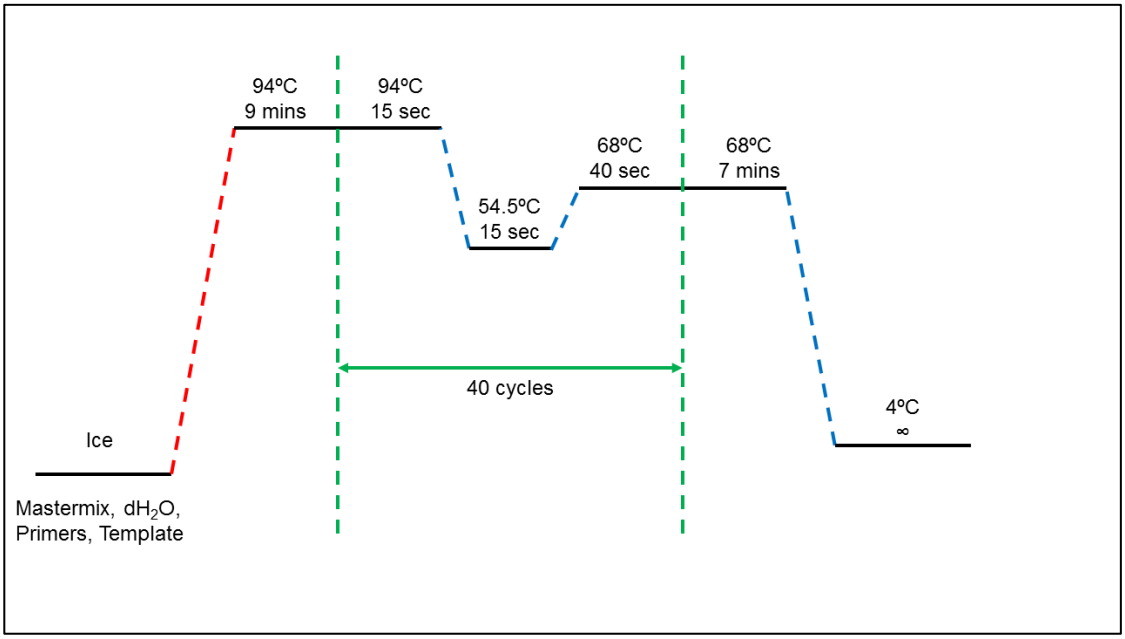

Figure 5.10: PCR conditions for check of DNMT1 5' sequence in LR clones.

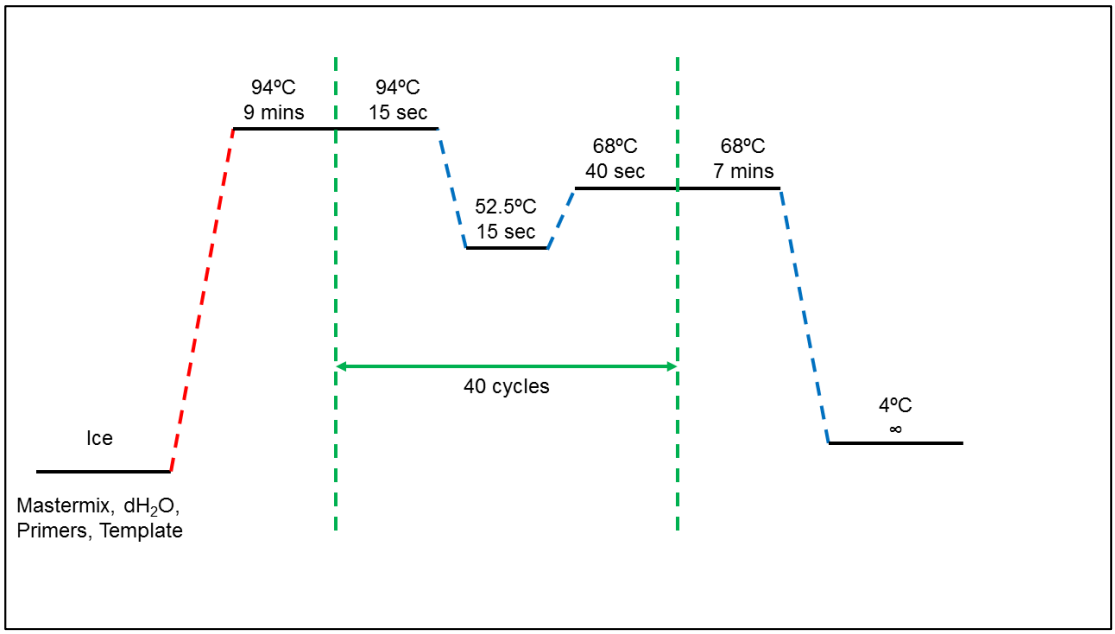

Figure 5.11: PCR conditions for check of DNMT1 3' sequence in LR clones.

5.3.1.4 Generation of adenoviral particles in HEK293A cells

After confirming proper insertion, 8 µg of each of the final clones were linearized with PacI (New England BioLabs®, R0547S) and transfected in HEK293A cells using Lipofectamine™ 3000 (Thermo Fisher Scientific®, L3000008). From this step onwards, a Class II Biosafety Cabinet was used for adenovirus manipulation. HEK293A cells were seeded to be in a 12-well cell culture plate to reach 80% confluence at transfection. The Lipofectamine™, the DNA and the P3000™ reagent were diluted in Opti-MEM™ reduced serum medium (Thermo Fisher Scientific™, 31985070) according to the protocol and incubated at room temperature for 15 minutes, then the DNA-lipid complexes were added to the cells which were then incubated for 2 days at 37ºC. After 2 days, the medium was replaced to 10% FCS DMDM culturing medium, and medium change for performed every 2 days for 2 weeks.

When signs of cell lysis were detected, adenoviruses were extracted from the cells. Medium and cells were collected using a 15 ml falcon tube for each well,

and centrifuged at 1200 rpm for 5 minutes. Then, all but 1 ml of medium was discarded and the cells were resuspended and underwent 3 freeze-thaw cycles (-80ºC for 15 minutes, 37ºC for 5 minutes). The samples from each falcon were moved to a 1.5 ml Eppendorf and centrifuged at 2200 rpm for 10 minutes, the supernatant containing the first generation of adenoviruses was then aliquoted in 100 µl aliquots and stored at -80ºC.

5.3.1.5 Purification of adenoviral vectors

HEK293A cells were seeded in several 15 cm cell culture dishes (2 for each adenovirus), and when they reached 80% confluence they were infected with 20 µl first generation adenovirus for each cell culture dish and incubated at 37ºC for 2 days. The second generation of adenovirus was extracted from the cells following the same protocol as per the first generation, and it was purified using an Adeno MINI Purification ViraKit™ (Virapur, 003059). After equilibrating the purification filters by adding 400 µl of Loading Buffer A and centrifuging at 2200 rpm for 5 minutes, the cell lysates were added on the purification filters and centrifuged at 2200 rpm for 5 minutes. The filters were then washed twice with 400 µl of Wash Buffer B and centrifuged at 2200 rpm for 5 minutes at each wash. The virus were collected in 1.5 ml Eppendorf tubes by elution in 400 µl Elution Buffer C and centrifugation at 2200 rpm for 5 minutes. To optimize storage and cryo-protection, 40 µl of glycerol for each tube were added to the final samples (10% final concentration), and the samples were snap frozen in dry ice and stored at -80ºC.

5.3.1.6 Titration of adenoviral vectors

To obtain the titer of adenoviral vectors for overexpression and methylation analysis studies, Clontech™ Adeno-X™ Rapid Titer Kit (Takara™, 632250) was used. HEK293A cells were seeded in a 24-well cell culture plate in a concentration of 250,000 per well, immediately infected with 100 µl of 10^{-4}, 10^{-5} and 10^{-6} serial dilutions of nuclear DNMT1, mitochondrial DNMT1 and DNMT3A adenoviral stocks and incubated at 37ºC for 48 hours. Then, the medium was aspirated, cells were fixed with 1 ml ice-cold methanol per well and incubated at -20ºC for 10 minutes. After fixation, methanol was aspirated and the wells were rinsed 3 times with 1 ml PBS (1% BSA).

Then, after adding 500 µl of Anti-Hexon antibody (1:1000 in PBS with 1% BSA) to each well, the plate was incubated 1 hour at 37ºC, washed three times with 1 ml PBS (1% BSA) and incubated 1 hour at 37ºC once again with secondary Rat Anti-Mouse antibody (HRP conjugate). After 1 hour, the secondary antibody was aspirated and the wells were washed three times with 1 ml PBS (1% BSA). Finally, wells were stained by incubating them with 250 µl 1X DAB working solution (10X DAB Substrate 1:10 1x Stable Peroxidase Buffer) at room temperature for 10 minutes. Cells with positive hexon protein staining (brown cells) were counted under the microscope and the Infectious units (ifu) were calculated with the formula:

$$\textbf{i.f.u./ml} = \textbf{(10 cells/field)*(313 fields/well) / (0.1 ml)*(}10^{-5}\textbf{/ml)}$$

And according to the instructions reported in the protocol (**Figure 5.12**).

Derivation of Area Counted in Fields/Well						
Objective Lenses	Eyepiece Lenses (10X)			Fields/Well		
	Total Magnification	Field Diameter	Field Area (mm^2)	12-Well Plate area = 3.8 cm^2	24-Well Plate area=2.0 cm^2	96-Well Plate area=0.32 cm^2
4X	40X	5 mm	19.6	19	10	1.6
5X	50X	4 mm	12.5	30	16	2.6
10X	100X	1.8 mm	2.54	150	79	12.6
20X	200X	0.9 mm	0.64	594	313	50

Figure 5.12: Derivation of Area counted in Fields/well. Taken from Adeno-X™ Rapid Titer Kit protocol.

5.3.2 Establishment of DNMT1 overexpression through infection with adenoviral vectors

In order to confirm efficacy of adenoviral vectors, about 300,000 H9C2 cells were seeded in each well of a 6-well cell culture plate with 10% FCS DMEM. The next day, the medium was replaced with serum-free DMEM and infection with 5 different conditions was performed: no infection (negative control), infection with LacZ adenovirus (negative control), infection with nuclear DNMT1 adenovirus, mitochondrial DNMT1 adenovirus and DNMT3A adenovirus. For all adenoviral vectors, 2 different amounts of multiplicity of infection (MOI) were calculated using the titer values and used for infection (MOI 10 and MOI 100). After 24 hours, the medium was replaced with 2 ml serum-free DMEM and the cells were grown for an additional 24 hours. Then, proteins were extracted and western blotting was performed. Western blotting membranes were probed with DNMT1 and DNMT3A primary antibodies, using αTubulin as a housekeeping control.

5.3.3 Cell culturing for mtDNA methylation analysis experiments in Goettingen

The preliminary experiments that led to the first Methylated-DNA immunoprecipitation (MeDIP) results were performed at Universitätsmedizin

Göttingen (UMG) in Elisabeth Zeisberg's lab. To investigate the effects of DNMT1 overexpression on the mtDNA of cardiac-specific cell lines, the MCE (Mouse Cardiac Endothelial) cell line was chosen (Cedarlane®, CLU510). These cells were cultured in DMEM (Sigma-Aldrich®, D5796) with 5% FCS and 1% 4-(2-hydroxyethyl)-1-piperazineethanesulfonic acid (HEPES) (Thermo Fisher Scientific®, 15630080).

5.3.4 MOI calculation for MCEC

To establish the best MOI to use for MCEC infection, MCEC cells were seeded in a Nunc® Lab-Tek® II Chamber Slide™ (Sigma-Aldrich®, C6807) in a concentration of 10,000 cells per well. The next day, the medium was replaced with serum-free DMEM and cells were infected with an Ad-GFP eGFP adenovirus (Vector Biolabs®, #1060) using 3 different MOIs: 5, 10 and 20. Twenty four hours after infection, the medium was replaced once again with 5% FCS DMEM, and positive cells were counted under a bright field microscope with 4x magnification. After comparing the positive cells to the total amount of cells, a percentage of infection efficiency for MCEC was calculated.

5.3.5 Design and validation of D-Loop primers for methylation analysis

To obtain quantitative Real-Time Polymerase Chain Reaction (qRT-PCR) primers that could only amplify for mitochondrial sequences, 2 different online tools were used. First of all, the Mus musculus mitochondrion genome (GenBank: EF108336.1) was investigated in order to obtain the D-Loop sequence (residues 15423-16299). These residues were then divided in 100-250 fragments and used as an input in Primer3 software (http://bioinfo.ut.ee/primer3-0.4.0/primer3/) to obtain primer set candidates. Every primer set candidate was then used as an

input for UCSC In-Silico PCR Tool (https://genome.ucsc.edu/cgi-bin/hgPcr) using the following settings:

- Genome: Mouse
- Assembly: Dec2011 (GRCm38/mm10) (it's the latest one so this should be correct)
- Target: UCSC genes

This additional step was performed in order to select primer sets that could only amplify mitochondrial sequences and not nuclear insertions of mitochondrial origin (NUMTs). After crossing several candidates, 5 primer sets were obtained. These primer sets have been designed to cover the majority of the D-Loop sequence (92.3%), leaving only 85 out of 877 residues uncovered between primer set #3 and #4. Primer sets' sequences are shown (**Table 5.5**).

To validate the affinity of the primers to mouse DNA, PCR and qPCR were performed. For PCR, B6 Mouse genomic DNA from 2 different mice (specimen #233 and #234) was used as a template. Furthermore, a negative control was ran by replacing gDNA with dH2O. After PCR, the samples were ran on a 1% agarose gel and their size was compared to the expected band size (**Table 5.6**). The PCR reagents (**Table 5.7**) as well as the PCR conditions (**Figure 5.13**) are reported. After confirming the size of the bands, primer validation through qPCR was performed using a StepOnePlus™ Real-Time PCR System (Thermo Fisher Scientific®, 4376598). Serial dilutions of B6 mouse gDNA (specimen #233) were used as a template (1:10 initial dilution, then 1:2, 1:4, 1:8, 1:16 and 1:32), then the Ct values for each primer set were plotted and R^2 value was calculated.

Finally, another qPCR was performed where 2 different templates were used, MCEC DNA obtained from the nuclear fraction, and MCEC DNA obtained from the mitochondrial fraction. This was performed in order to confirm the predictions obtained from the UCSC In-silico PCR tool. The qPCR reagents (**Table 5.8**) as well as the qPCR conditions (**Figure 5.14** and **Figure 5.15**) are reported.

Table 5.5: D-Loop PCR primers sequences for qPCR after MeDIP.

Primer	Sequence
D-Loop #1 Forward	5'-CCACCAGCACCCAAAGCT-3'
D-Loop #1 Reverse	5'-TGGTGTATGTCAGATAACACAGA-3'
D-Loop #2 Forward	5'-TCTGTGTTATCTGACATACACCA-3'
D-Loop #2 Reverse	5'-GAGAAGAGGGGCATTGGTGG-3'
D-Loop #3 Forward	5'-ACTATCCCCTTCCCCATTTG-3
D-Loop #3 Reverse	5'-TGTTGGTCATGGGCTGATTA-3
D-Loop #4 Forward	5'-AGTCTAGACGCACCTACGGT-3
D-Loop #4 Reverse	5'-GCATTAAGAGGAGGGGGTGG-3
D-Loop #5 Forward	5'-CCCCCTCCTCTTAATGCCAAA-3
D-Loop #5 Reverse	5'-AGCATTTTCAGTGCTTTGCTT-3

Table 5.6: Expected band sizes for D-Loop primers PCR products.

Primer set	Expected band size (bp)
#1	250
#2	132
#3	232
#4	141
#5	241

Table 5.7: PCR reagents for MeDIP primers check.

Reagent	Quantity (µl)
Taq DNA Polymerase PCR Buffer 10X (Thermo Fisher Scientific®, 18067017)	2.5
MgCl2 1M solution (Thermo Fisher Scientific®, AM9530G)	2.5
dH_2O	14.2
10 µM Forward Primer (#1-#5)	1
10 µM Reverse Primer (#1-#5)	1
Template (B6 mouse gDNA)	2
DMSO (Sigma Aldrich®, D9170)	0.5
dNTP (100 mM) (Thermo Fisher Scientific®, 10297018)	1
Taq DNA Polymerase (Thermo Fisher Scientific®, EP0402)	0.3

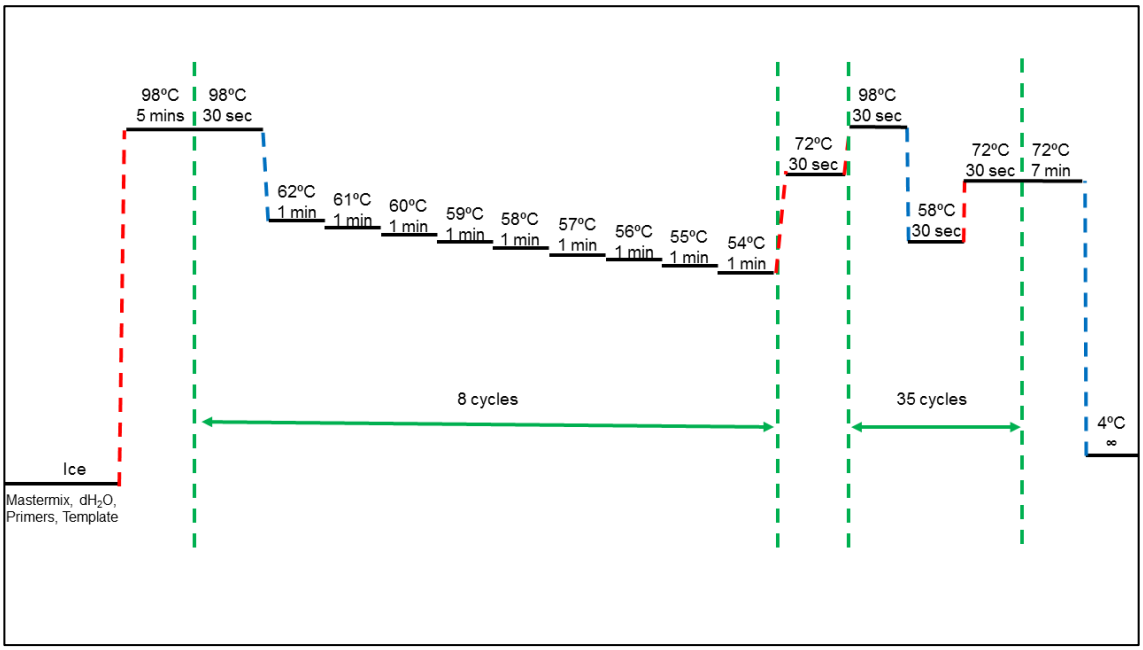

Figure 5.13: PCR conditions for D-Loop primers check. Rather than optimising melting temperature for each primer set, an additional step of 8 cycles with varying annealing temperature (62ºC to 54ºC) was added.

Table 5.8: Reagents for qPCR reaction. Every condition was ran in duplicate.

Reagent	Quantity (µl)
SYBR® Green PCR Master Mix (Thermo Fisher Scientific®, 4309155)	10
dH_2O	6
10 µM Forward Primer (#1-#5)	1
10 µM Reverse Primer (#1-#5)	1
DNA Template (Mouse gDNA/MCEC nDNA/MCEC mtDNA)	2

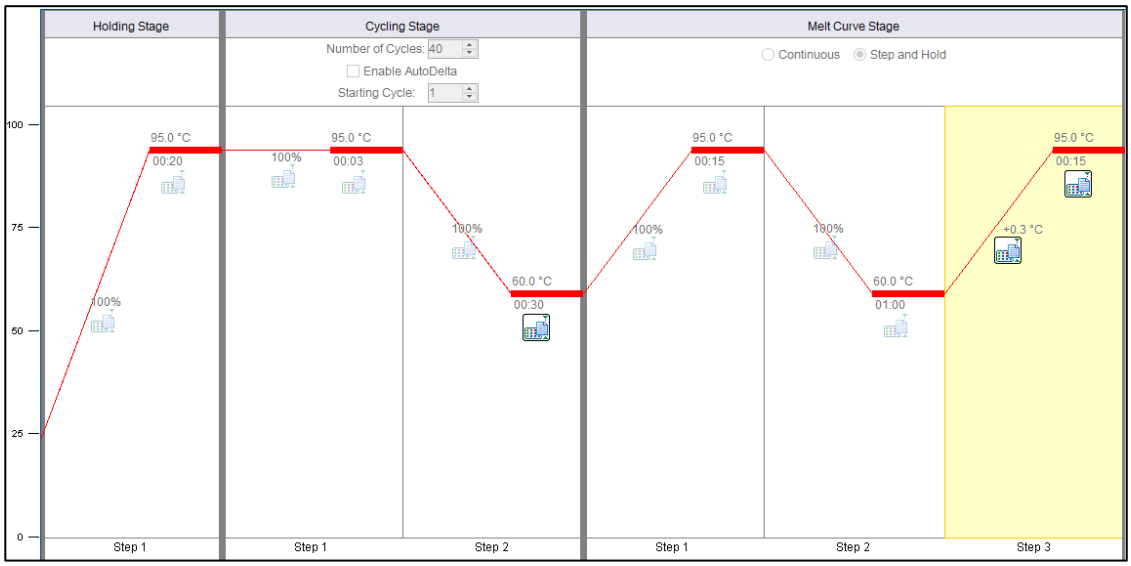

Figure 5.14: Conditions for first qPCR using D-Loop primers. In this experiment, serial dilutions of B6 mouse gDNA were used as template. Melting curve was also performed.

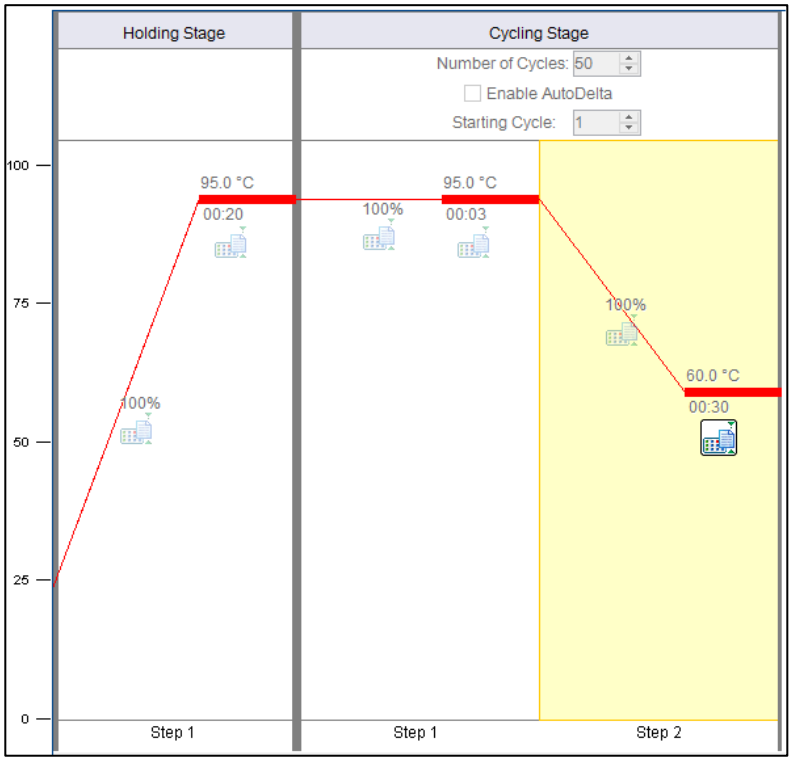

Figure 5.15: Conditions for second qPCR using D-Loop primers. In this experiment, DNA obtained from MCEC nuclear and mitochondrial fractions was used as template.

5.3.6 Methylated-DNA immunoprecipitation (MeDIP) of MCEC mtDNA after infection and fractioning

After validating the D-Loop qPCR primers, a MeDIP experiment was performed. MCEC were seeded on several 15 cm cell-culture dishes (2 for each infection condition) in 20 ml 5% FCS-1% HEPES DMEM culture medium. When the cells reached 80-90% confluence ($18 * 10^7$ cells/dish), infection with the different adenovirus (Adeno-eGFP, Adeno-nuclear DNMT1, Adeno-mitochondrial DNMT1) was performed. Culture medium was removed and MCEC cells were infected with MOI10 adenovirus in serum free DMEM with 1% HEPES.

The next day, the medium containing adenovirus was removed and fresh DMEM with 5% FCS and 1% HEPES was added to the cells. Then, 48 hours after infection, the cells were harvested and fractioning was performed. After obtaining the mitochondrial fraction, its DNA was harvested using a QIAamp DNA Blood Mini Kit (Qiagen®, 51104).

Protocol from Appendix J (Protocol for Crude Cell Lysates and Other Samples) was used. The mtDNA samples were then quantified at the NanoDrop, and 825 ng of each sample were used for MeDIP-qPCR and mtDNA methylation analysis. A Methylamp™ Methylated DNA Capture Kit (Epigentek®, P-1015-48) was used for the MeDIP step.

Briefly, 100 µl of buffer MC1 and 1 µl of anti-5-Methylcytosine (5-mC) antibody (1 mg/ml) was added to each of the wells (1 for each sample), then the wells were covered with parafilm and incubated at room temperature for 60 minutes. During incubation, the 5-mC antibody would bind to the bottom of the wells and will be able to interact with the DNA samples. While waiting for the incubation to finish, the mtDNA samples were processed through sonication. This was performed in order to break the DNA into 100-600 bp and allow for successful

immunoprecipitation and qPCR steps. This sonication step was performed using a 600W Ultrasonic Sonicator (Misonix®, S-4000) connected to a 5.5'' cup horn (QSonica®, 431C2) through a 20 kHz Converter (QSonica®, CL5) (Figure 5.16). The samples were initially resuspended in 110 µl buffer MC2. The cup horn was filled with water and ice and the samples were positioned in a tube rack (QSonica®, 440) and immersed in the cup horn. Then, sonication was performed with the following conditions:

- Amplitude: 40 (Represents % of total power)
- Process time: 10'
- Pulse ON: 20''
- Pulse OFF: 20''

After sonication, the samples were warmed up to 95ºC for 2 minutes and immediately placed on ice until the following step.

At this point, 10 µl were withdrawn from each sample (eGFP, nuclear DNMT1 and mitochondrial DNMT1) to a 1.5 ml tube to be used as input (the part of the sample that would not receive the MeDIP treatment) and put on ice. After 1 hour, the 5-mC antibody solution was removed from the wells which were then washed 3 times with 150 µl MC1 buffer and 1 time with 150 µl MC3 buffer by pipetting in and out. At this point, 100 µl of each the sonicated DNA samples was added to each well, and the wells were covered with parafilm and incubated at room temperature for 120 minutes at 80 rpm on an orbital shaker. Then, the supernatant was removed and the wells were washed 3 times with 150 µl buffer MC3. To release the DNA from the DNA-antibody complex, the wells were treated

with 1 µl proteinase K in 60 µl buffer MC4, capped and incubated for 1 hour at 65ºC.

Afterwards, samples were resuspended in 180 µl 100% ethanol, mixed with 100 µl buffer MC5, applied to spin columns and centrifuged at 13,000 rpm for 30 seconds. Flowthrough was discarded, and 2 additional centrifuge steps were performed adding 200 µl 90% ethanol per column at each step. Finally, the DNA was eluted in 20 µl buffer MC6 through centrifugation at 13,000 rpm for 30 seconds then stored (along with the “input” samples) at -20ºC to be used for qPCR.

Figure 5.16: Setup for the S-4000 sonicator. The sonicator's tip (on the left) was removed and replaced with a 5'5 cuphorn (on the right) and a 20 kHz converter (underneath the cup horn).

5.3.7 Quantitative Real-time PCR after MeDIP

To obtain a percentage of changes in global methylation of the different D-Loop sequences, the MeDIP mtDNA samples were used as a template and tested with the 5 primer sets for D-Loop sequences through quantitative real-time PCR (qRT-PCR). Samples were mixed with qPCR reagents (**Table 5.9**) and qPCR was performed. To calculate the percentage of global methylation compared to the input, the ratio between the cycle threshold (Ct) value of the MeDIP sample and the input was calculated as follows:

- Pull down (MeDIP) Ct value – Input Ct value = ΔCt
- $2^{-\Delta Ct}$ = quantity

This way, it is possible to calculate a percentage of methylated CpG motifs in the MeDIP sample compared to the input (which contains both methylated and unmethylated CpG residues). Then, a comparison between the negative control (eGFP sample) and the treated samples (nuclear DNMT1 and mitochondrial DNMT1 overexpression) can be performed by setting the $2^{-\Delta Ct}$ value of the eGFP sample to 1 and calculating a fold increase.

Table 5.9: Reagents for qPCR reaction. Every sample was ran in triplicates (including input samples).

Reagent	Quantity (µl)
SYBR® Green PCR Master Mix	10
dH_2O	3
10 µM Forward Primer (#1-#5)	1
10 µM Reverse Primer (#1-#5)	1
DNA Template (MeDIP/Input mtDNA)	5

5.3.8 Establishment of MeDIP protocol in London

To establish a reliable MeDIP protocol in London, several conditions were optimized.

5.3.8.1 Sonicator specs

A new 500W Sonicator with a 20 kHz converter (Fisher Scientific®, 12981151) and a cup horn (Fisher Scientific®, 15370372) was obtained. Furthermore, to limit sonication side effects on hearing, a sound enclosure (Fisher Scientific®, 15351211) was used.

5.3.8.2 Sonication conditions

The sonication conditions have been adjusted to reflect changes in the sonicator model and power compared to the one used in Goettingen. Therefore, the sonication conditions used were the following:

- Amplitude: 48
- Process time: 10’
- Pulse ON: 20’’
- Pulse OFF: 20’’

5.3.8.3 DNA sonication and screening of band size

To identify whether the sonication conditions would yield DNA fragments between 150-1000 bp, several DNA samples from different origins were used:

- B6 Mouse genomic DNA
- pCMV-SPORT6-nuclear DNMT1 plasmid (10 kbp length)
- pCMV-SPORT6-mitochondrial DNMT1 plasmid (10 kbp length)

- MCEC genomic DNA (GFP infected)
- MCEC genomic DNA (Adeno-nuclear DNMT1 infected)
- MCEC genomic DNA (Adeno-mitochondrial DNMT1 infected)

About 800 ng of each of the DNA samples were resuspended in either H_2O or MC2 Buffer (from Methylamp™ Methylated DNA Capture Kit) to a final volume of 110 µl. This was done to test whether resuspension in different solution would alter the sonication pattern. A 1.5 ml centrifuge tube was used for each condition and sample. Then, sonication was performed using the conditions described in subchapter 5.3.8.2, and after sonication the samples were loaded onto a 2% agarose gel and ran for 40 minutes at 120V. Finally, the smears caused by sonication were investigated in order to confirm the protocol.

5.3.8.4 MCEC transfection with adenovirus, fractioning and MeDIP-qPCR

For MCEC infection, fractioning and MeDIP-qPCR experiments, the usual protocols (described in subchapters 5.3.2, 2.4 and 5.3.7, respectively) were performed. MCE cells were infected with Adeno-eGFP, Adeno-nuclear DNMT1 and Adeno-mitochondrial DNMT1 vectors using MOI 10, as previously described.

5.3.9 Generation of mtDNMT1 Lentivirus

To establish a stable mtDNMT1 overexpression system in MCE cells while maintaining them in culture medium with FCS, a lentivirus for mtDNMT1 was generated.

5.3.9.1 Cloning strategy for pLenti-puro-mtDNMT1 lentiviral vector

First of all, a pLenti-puro vector (**Figure 5.17**) was obtained from AddGene® (#39481, created by Ie-Ming Shih). The backbone is the same as pLenti4/TO/V5-DEST™ (Thermo Fisher Scientific®, V49810), however the gateway elements between the 2 EcoRV sites are lost and the Zeocin resistance gene is replaced with a puromycin resistance gene for selection in mammalian cells. The vector was supplied in an agar stab and was transformed in DH5α cells. Then, maxiprep was performed and the maxiprep sample was checked through XhoI-KpnI, EcoRV (New England BioLabs®, R0195) and BglII (New England BioLabs®, R0144) digestion.

The original pCMV-SPORT6-mtDNMT1 vector was then modified by inserting a SpeI linker and an XbaI linker at 5' and 3' of mtDNMT1 cDNA, respectively. This was performed in 2 separate reactions. First, the pCMV-SPORT6-mtDNMT1 vector was digested with KpnI enzyme according to the usual protocol with the addition of 2 µl 10X Alkaline phosphatase to promote dephosphorylation, ran on a 1% agarose gel and extracted from the gel. Then, blunting was performed using a DNA blunting Kit (Takara®, 6025). This kit allows the conversion of 3'- and 5'-protruding ends of DNA fragments to blunt ends. Conversion of the two types of protruding ends can be accomplished simultaneously by the 3' → 5' exonuclease and 5' → 3' polymerase activities of T4 DNA polymerase (**Figure 5.18**). The resulting blunt-ended DNA can be ligated efficiently into a blunt-ended vector using the usual DNA ligation protocol. The kit also allows the conversion of protruding ends of vector DNA to blunt ends, and blunt-ended vector is used after dephosphorylation.

So after obtaining the digested vector, the blunting reaction was performed with the reagents supplied with the kit (**Table 5.10**). Briefly, DNA sample was mixed

with 10x DNA blunting buffer and water to obtain 10 µl final volume. The mixture was incubated at 70ºC for 5 minutes and transferred to a 37ºC incubator afterwards. Then, 1 µl of T4 DNA polymerase was added and the mixture was incubated at 37ºC for 5-15 minutes, vortexed vigorously to deactivate T4 DNA polymerase, then placed on ice to ensure deactivation. The sample was then used for overnight ligation with SpeI linker. The ligation mixture was transformed in DH5α, miniprep and restriction checks with SpeI (New England BioLabs®, R0133), SpeI-HindIII and KpnI-HindIII digestion were performed. One of the positive colonies was used for XbaI linker insertion after HindIII digestion, following the same blunting protocol. After DH5α transformation, the clones were checked through SpeI-HindIII and SpeI-XbaI (New England BioLabs®, R0145) digestion and sequencing.

After obtaining the final construct, mtDNMT1 cDNA was inserted into pLenti-puro vector in 2 steps: first the 5' SpeI-XhoI fragment was inserted into pLenti-puro, then the 3' XhoI-XbaI fragment was inserted into pLenti-puro-SpeI-5'mtDNMT1-XhoI. For the subcloning steps, amplification through HST08 Stellar™ Competent Cells (Takara®, 636763) transformation was performed.

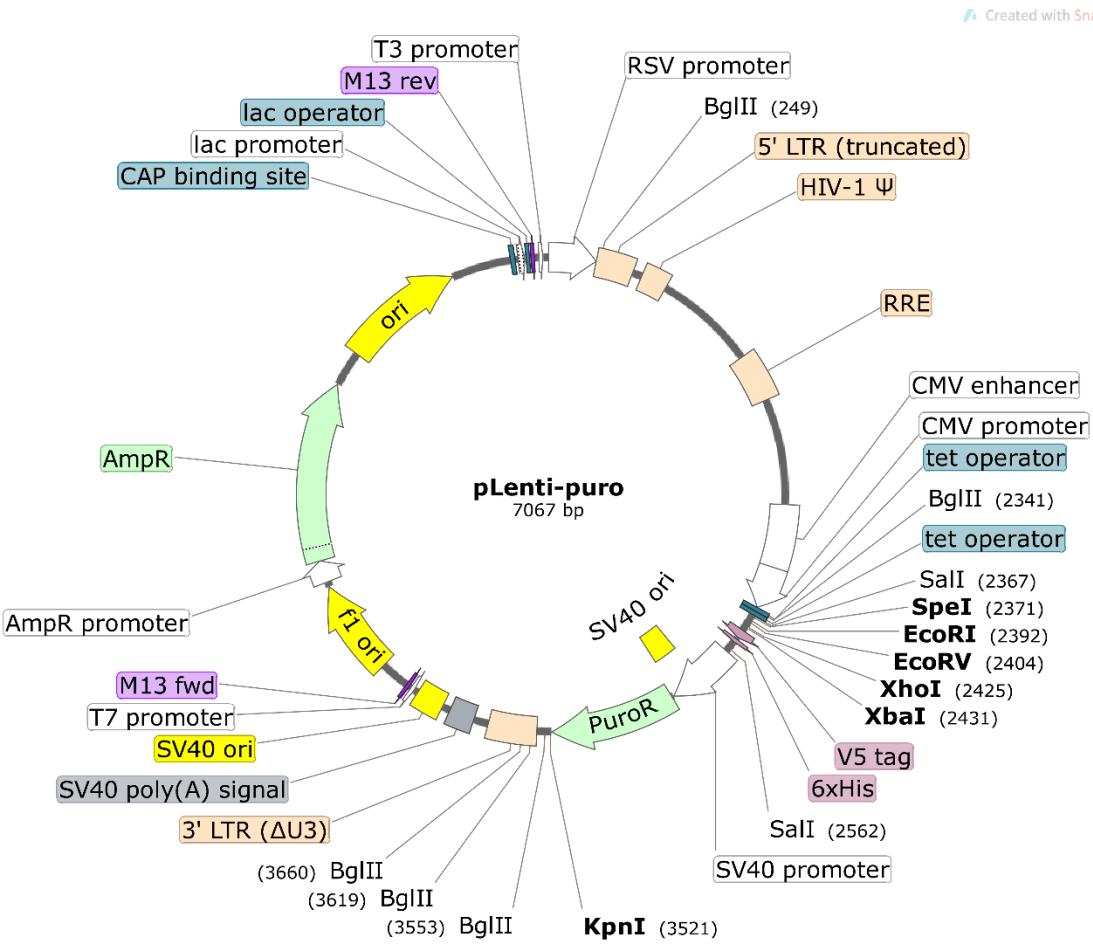

Figure 5.17: pLenti-puro vector map. BglII, EcoRI, KpnI, SpeI, XbaI, XhoI, and restriction sites are shown.

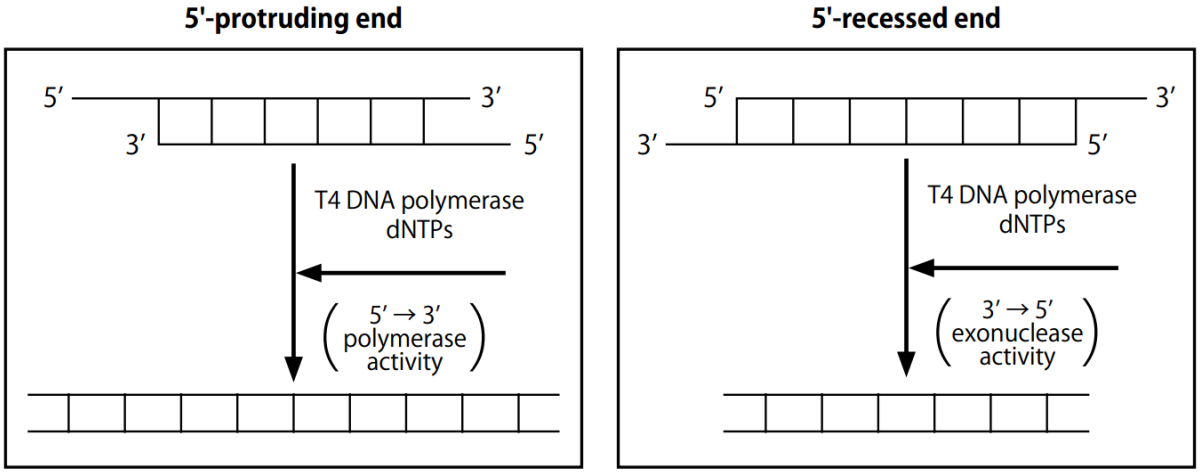

Figure 5.18: Visual protocol for DNA blunting kit.

Table 5.10: Reagents for DNA blunting protocol.

Reagent	Amount
DNA sample (pCMV-SPORT6-mtDNMT1 KpnI digested)	5-10 pmol
10x DNA Blunting Buffer (with dNTP)	1 µl
dH_2O	To 9 µl

5.3.9.2 Packaging and envelope constructs

For the production of lentivirus in HEK293T cells (ATCC®, CRL-3216™), a 2nd generation lentiviral system was used. This system requires a triple transfection of HEK293A cells with 3 separate plasmids:

- Lentiviral transfer plasmid encoding insert of interest (mtDNMT1)
- Packaging plasmid (expressing GAG, POL, TET and REV packaging proteins)
- Envelope plasmid (expressing Vesicular stomatitis virus G protein, VSV-G)

PAX2 (AddGene®, # 35002, created by Malin Parmar) (**Figure 5.19**) and pMD2.G (AddGene®, 12259, created by Didier Trono) (**Figure 5.20**) have been used as packaging and envelope constructs, respectively.

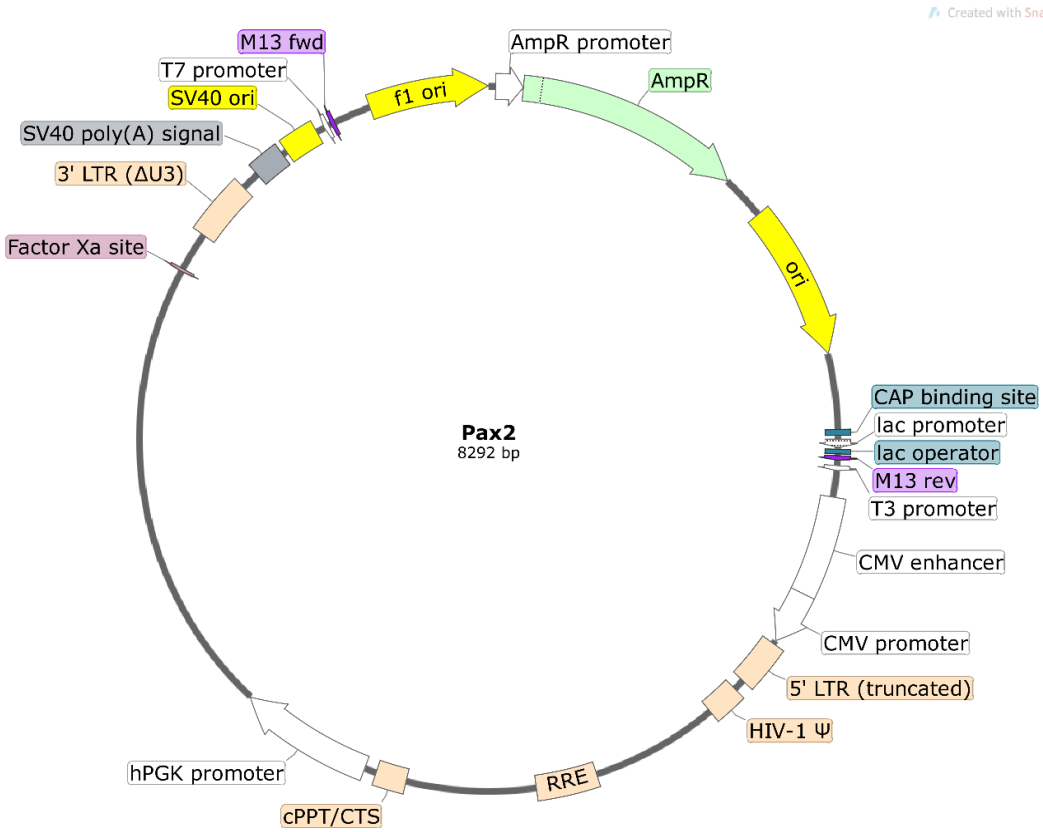

Figure 5.19: Pax2 packaging construct map.

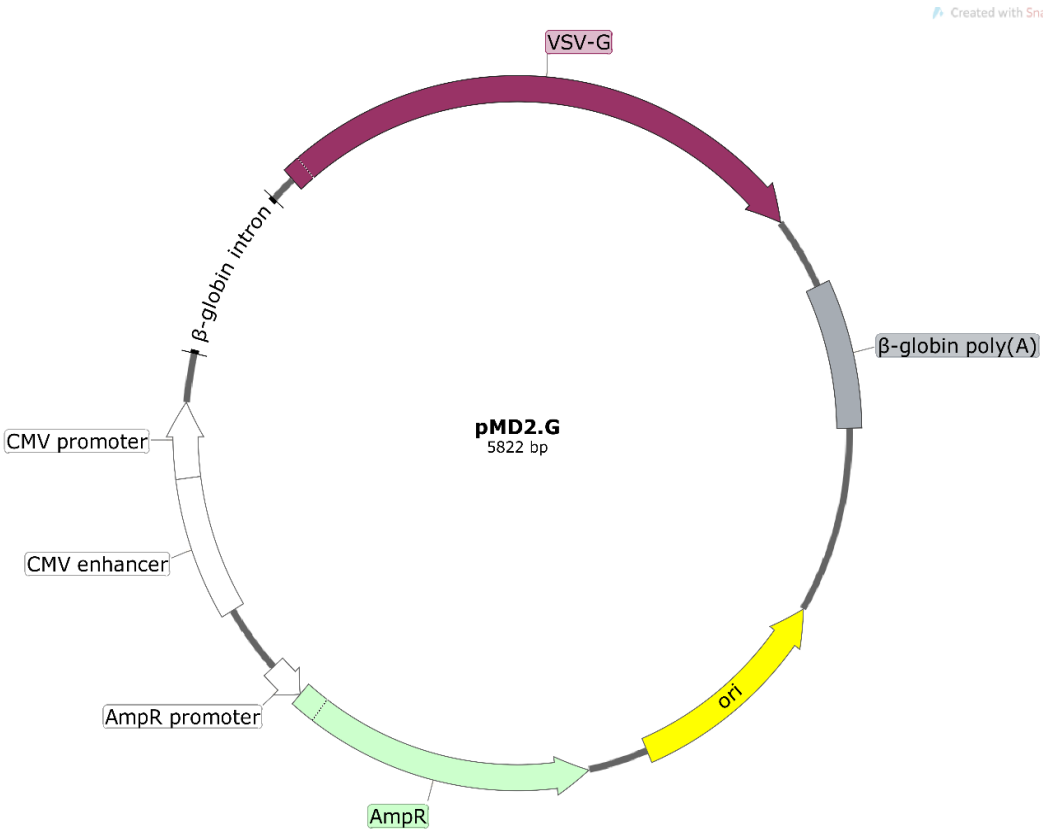

Figure 5.20: pMD2.G envelope constructs.

5.3.9.3 Transfection of HEK293T cells

For the production of lentiviral particles, transfection of HEK293T cells using polyethylenimine hydrochloride (PEI) (764647, Sigma-Aldrich®) was performed. For this purpose, a total of 3 T175 flasks of HEK293T cells were cultured until 70% confluence was reached. The reagents for transfection were mixed in 2 separate 50 ml falcon tubes with 12 ml Opti-Mem for each tube. In one tube only 3 µl of 10 mM PEI were added. In the second tube, the following amounts of plasmids were added:

- 90 µg PAX2
- 120 µg pLenti-puro-mtDNMT1
- 30 µg pMD2.G

After this, the contents of both tubes were mixed together (this will be referred to as transfection media) and left for 20 minutes at room temperature. Finally, 8 ml of transfection media was added to each of the T175 flasks, and incubated for 4 hours at 37ºC. Transfection media were replaced with fresh culture medium after 4 hours.

5.3.9.4 Harvesting of Lentiviral particles from HEK293T cells

Following transfection for 48 hours, the supernatant containing the lentiviral particles was harvested from the T175 flasks, and was placed into clean falcon tubes which were centrifuged at 1200 rpm for 5 minutes. The supernatant was filtered with a 50 ml syringe through a 0.45mm filter, then put into a new tube. The filtered medium containing the virus particles was split into 6 aliquots of 11.5ml each, in ultra-clear tubes for ultra-centrifugation. Tubes were placed into the ultracentrifuge metal vials (previously cleaned with 70% IMS) and finally into the rotor of an Ultracentrifuge with Rotor Log Management Function (Hitachi®, CP100NX). Tubes were ultra-centrifuged at 19900rpm for 2h at 4°C The supernatant was discarded and viruses in each tube were resuspended in 30 µl of DMEM medium, then the tubes were combined together and aliquoted in eppendorf tubes (40 µl per aliquot). Finally, aliquots were stored at -80°C.

For the titration of the lentiviral stock, a Lenti-X™ p24 Rapid Titer Kit (Takara®, 632200) was used. This kit allows you to quickly determine the titer of any HIV-1-based lentiviral supernatant using standard ELISA methods. The wells of the microtiter plate (12 x 8-well strips) are coated with an anti-HIV-1 p24 capture antibody, which quantitatively binds the HIV-1 p24 in the lentiviral samples (p24 is an abundant HIV-1 virus core/capsid protein). Specifically-bound p24 is detected in a typical “sandwich” ELISA format using a biotinylated anti-p24 secondary antibody, a streptavidin-HRP conjugate, and a colour producing substrate (**Figure 5.21**). Colour intensity is measured spectrophotometrically to indicate the level of p24 in the samples, which can then be precisely quantified against a p24 standard curve. p24 values can then be correlated to virus titer of packaging cell supernatants.

To test samples quantitatively, a p24 standard curve (0-200 pg/ml) was prepared. In order to produce a 200 pg/ml stock solution, 20 µl of the p24 positive control stock solution (10 ng/ml) were diluted into 980 µl of fresh complete tissue culture medium (DMEM containing 5% FCS and 1% HEPES) for a 1:50 dilution. Then, a series of four additional standard dilutions of 100, 50, 25 and 12.5 pg/ml were made, and 500 µl of media were dispensed into each of four labelled tubes. Five hundred µl of the 200 pg/ml stock were added to the 100 pg/ml tube and mixed. Then, using a fresh tip, 500 µl of this solution were transferred into the 50 pg/ml tube and mixed. Similar transfers were performed for the 25 and 12.5 pg/ml tubes. After selecting a sufficient number or 8-well strips to accommodate all standards, test specimens, controls and complete culture medium blanks (negative control) in duplicate, 20 µl of lysis buffer were dispensed into each well. Two hundred µl of each standard buffer curve dilution, supernatant samples (1:1000, 1:100,000, 1:500,000 and 1:1,000,000 dilutions) and culture medium were dispensed into duplicate wells, then the plate was incubated at 37ºC for 60 minutes.

After incubation, the content was aspirated from the wells and the plate was washed by filling all wells to the brim with wash buffer, aspirate again, and repeating the whole process 5 times. Then the plate was inverted and tapped firmly on absorbent paper towels. After washing, 100 µl of Anti-p24 antibody were dispensed into each well, then incubation at 37ºC for 60 minutes was performed. Wells were washed once again following the same protocol, then 100 µl of Streptavidin-HRP conjugate were dispensed into each well, and plate was incubated at room temperature for 30 minutes. The plate was washed once again, and 100 µl of Substrate Solution (from the kit) were dispensed into each well. Incubation with light shielding was performed at room temperature for 30 minutes. Finally, the reaction was stopped by adding 100 µl Stop Solution (from the kit)

and the absorbance was measured at 450 nm using a Tecan™ Infinite® 200 PRO NanoQuant spectrophotometer.

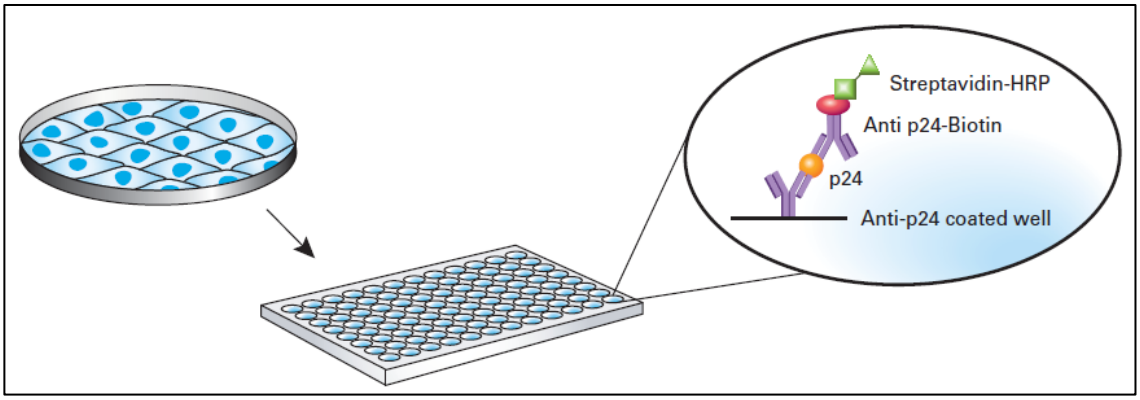

Figure 5.21: General scheme of the Lenti-X p24 Rapid Titer Kit. The presence of bound p24 in the wells is detected using a biotinylated secondary anti-p24 antibody, a streptavidin-horseradish peroxidase conjugate, and a colour-producing substrate. Quantitation is performed by comparing test samples to a p24 standard curve.

5.3.10 Generation of stable mtDNMT1 overexpression MCE cell line

5.3.10.1 Puromycin kill curve

Before proceeding with the infection of MCE cells, a puromycin kill curve experiment was performed. This was done to ensure that the right concentration of puromycin would be used to positively select the cells incorporating mtDNMT1 cDNA and the puromycin resistance gene. MCE cells were seeded onto a 24-well plate, and when they reached 80% confluence were treated with different puromycin concentrations (**Figure 5.22**). After 3 days, cell death was investigated by using a microscope and the lowest dose for 100% cell death was chosen as the optimal concentration to be used for culturing Lenti-mtDNMT1 transfected MCE cells.

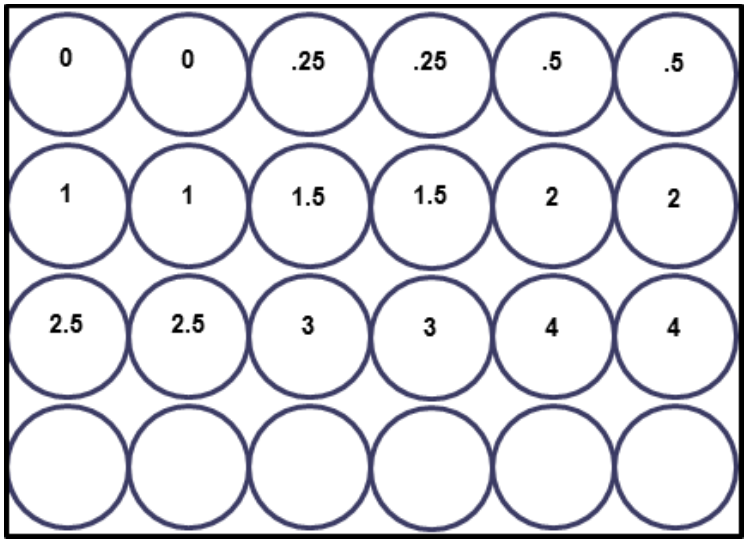

Figure 5.22: Layout of 24 well plate for puromycin kill curve experiment. Numbers within the wells indicate puromycin concentration (µg/ml).

5.3.10.2 Infection of MCE cells

MCE cells were infected with 2 different concentrations of lentiviral particles, MOI5 and MOI10. Cells were seeded in 2 T175 flasks. When cells reached 80% confluence, culture medium was replaced with DMEM containing antibiotic for selection of positive cells (5% FCS, 1% HEPES, 1.5 µg/ml Puromycin). Replacement of medium was performed once every 48 hours, and cells were split every time they reached 80% confluence.

5.3.10.3 Assessment of mtDNMT1 overexpression

To assess mtDNMT1 overexpression, western blotting for DNMT1 was performed. Proteins were harvested and western blotting was performed according to the protocol described in subchapter 2.7.

5.3.11 DNMT1 interaction studies

To investigate and identify potential mtDNMT1 interaction targets, a Co-IP protocol followed by mass spectrometry was performed using MCE cells and both DNMT1 lentivirus.

5.3.11.1 Transfection conditions

MCE cells were seeded on 15 cm culture dishes (2 dishes for each infection condition) with 20 ml DMEM with 5% FCS and 1% HEPES for each dish. When the cells reached 80% confluence, medium was replaced with 20 ml serum-free DMEM and infection with 3 different adenoviruses was performed: Adeno-eGFP (as a negative control), Adeno-nuclear DNMT1 and Adeno-mitochondrial DNMT1.

24 hours after infection, medium was replaced with 20 ml DMEM with 5% FCS and 1% HEPES and the cells were incubated for additional 24 hours. Then, the cells were harvested for Co-immunoprecipitation.

5.3.11.2 Co-immunoprecipitation (Co-IP) protocol

In order to compare nuclear DNMT1 and mitochondrial DNMT1 interaction targets, Co-immunoprecipitation (Co-IP) for the HA-tag was performed using an Immunoprecipitation Kit (Sigma-Aldrich®, 11719386001). Culture medium was removed from the dishes and the cells were washed twice with 5 ml ice-cold PBS per dish to remove any remaining serum proteins from the culture medium. The cells were lysed with 1 ml ice-cold lysis buffer, scraped and collected in a 1.5 ml centrifuge tube (1 for each condition). Then, to reduce background caused by non-specific adsorption of irrelevant cellular proteins, a preclearing step was performed.

Cells were incubated with 50 µl of the homogeneous protein G agarose suspension at room temperature for 3 hours on a rocking platform to form antibody-bead complexes. After this, beads were pelleted through centrifugation at 13,000 rpm for 20 minutes at 4ºC, then the supernatants were moved to fresh 1.5 ml tubes. At this point, 100 µl of supernatant from each sample was taken and stored at -80ºC to be submitted for mass spectrometry as an IgG negative control. The rest of the samples were incubated with 5 µg of the antibody of interest for each sample (GFP or HA-tag) for 1 hour at 4ºC on a rocking platform, then 50 µl of protein G suspension was added to the mixture and incubated overnight at 4ºC on a rocking platform.

The following day, the Protein G-antibody-protein complexes were collected by centrifugation at 13,000 rpm for 30 seconds, the supernatant was discarded and 1 ml of lysis buffer (wash buffer #1, **Table 5.11**) was added in order to resuspend the beads, then the samples were incubated for 20 minutes at 4ºC on a rocking platform. Complexes were collected through centrifugation at 13,000 rpm for 30 seconds, then the wash-incubation-centrifuge steps were performed again. The same procedure was used for further washing steps using wash buffer #2 (**Table 5.12**) and wash buffer #3 (**Table 5.13**).

Table 5.11: Reagents and final concentration for Lysis buffer/Wash buffer #1. The reagents were combined and water to a final volume of 25 ml was added.

Reagent	Final concentration (25 ml)
5 ml Core buffer (CoIP kit)	50 mM Tris-HCl (pH 7.5)
3.75 ml NaCl 1M	150 mM NaCl
2.5 ml Detergent mix (CoIP kit)	1% Nonidet P40 0.5% sodium deoxycholate

1 Complete tablet (CoIP kit)	1 tablet/25 ml

Table 5.12: Reagents and final concentration for Lysis buffer/Wash buffer #2 (high salt concentration). The reagents were combined and water to a final volume of 50 ml was added.

Reagent	Final concentration (50 ml)
10 ml Core buffer (CoIP kit)	50 mM Tris-HCl (pH 7.5)
25 ml NaCl 1M	500 mM NaCl
0.5 ml Detergent mix (CoIP kit)	0.1% Nonidet P40 0.05% sodium deoxycholate

Table 5.13: Reagents and final concentration for Lysis buffer/Wash buffer #3 (low salt concentration). The reagents were combined and water to a final volume of 25 ml was added.

Reagent	Final concentration (25 ml)
1 ml Core buffer (CoIP kit)	50 mM Tris-HCl (pH 7.5)
0.25 ml Detergent mix (CoIP kit)	0.1% Nonidet P40 0.05% sodium deoxycholate

5.3.11.3 Submission of samples and mass spectrometry analysis

The Co-IP samples were submitted for mass spectrometry analysis to the Bioanalytical Mass Spectrometry facility of the Max Planck Institute for Biophysical Chemistry in Goettingen. Samples were ran on an agarose gel, stained with Coomassie Brilliant Blue R-250 Dye (ThermoFisher Scientific®) and submitted for Mass spectrometry. Following submission, the entire procedure was carried on by a member of Dr. Christof Lenz's laboratory.

5.4 Results

5.4.1 Generation of adenoviral vectors for nDNMT1 and mtDNMT1

5.4.1.1 BP Clonase results

Clones of pDONR™221-nuclear DNMT1, pDONR™221-mitchondrial DNMT1 and pDONR™221-DNMT3A were obtained through BP clonase reaction (**Figures 5.23**, **5.24** and **5.25**). These clones were then checked through DNA gel electrophoresis after enzyme digestion, according to the restriction sites included within the sequences (**Figures 5.26**, **5.27** and **5.28**). After confirming the successful recombination for all vectors, these were used for LR Clonase reaction.

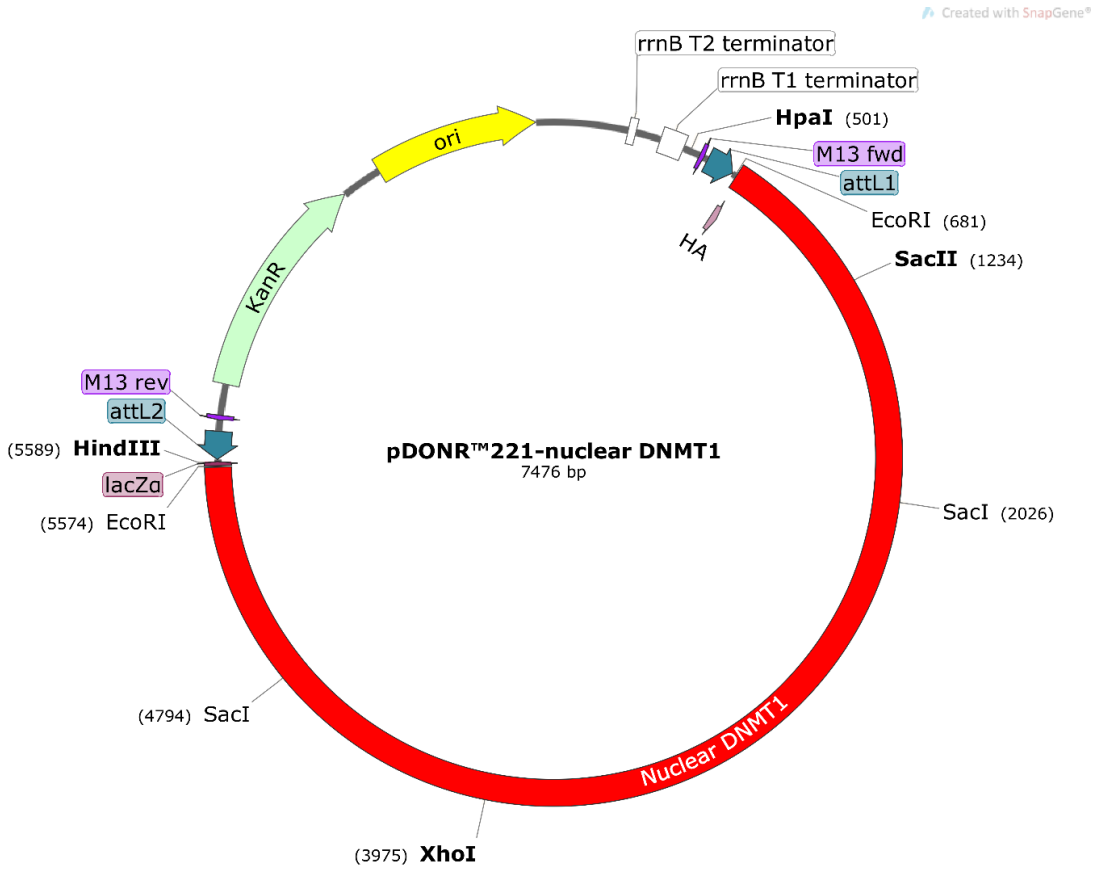

Figure 5.23: pDONR™221-nuclear DNMT1 entry clone after BP reaction. This construct was then used for LR reaction.

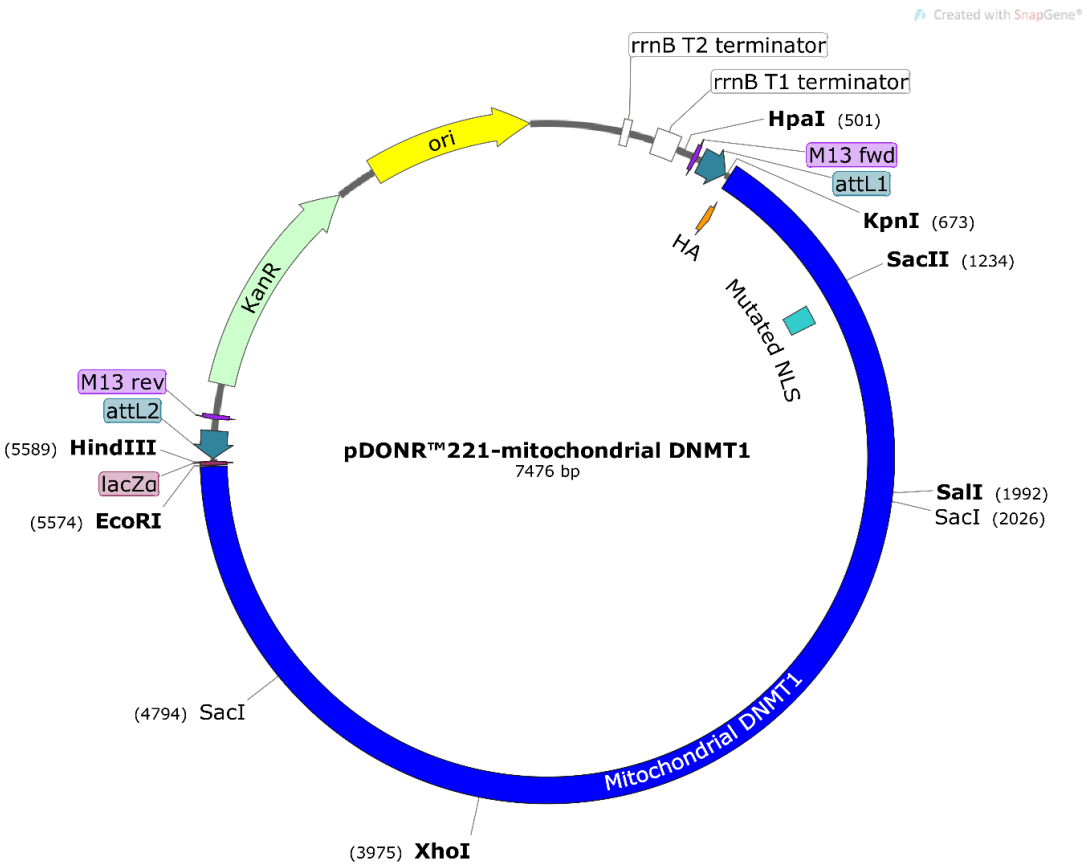

Figure 5.24: pDONR™221-mitochondrial DNMT1 entry clone after BP reaction. This construct was then used for LR reaction.

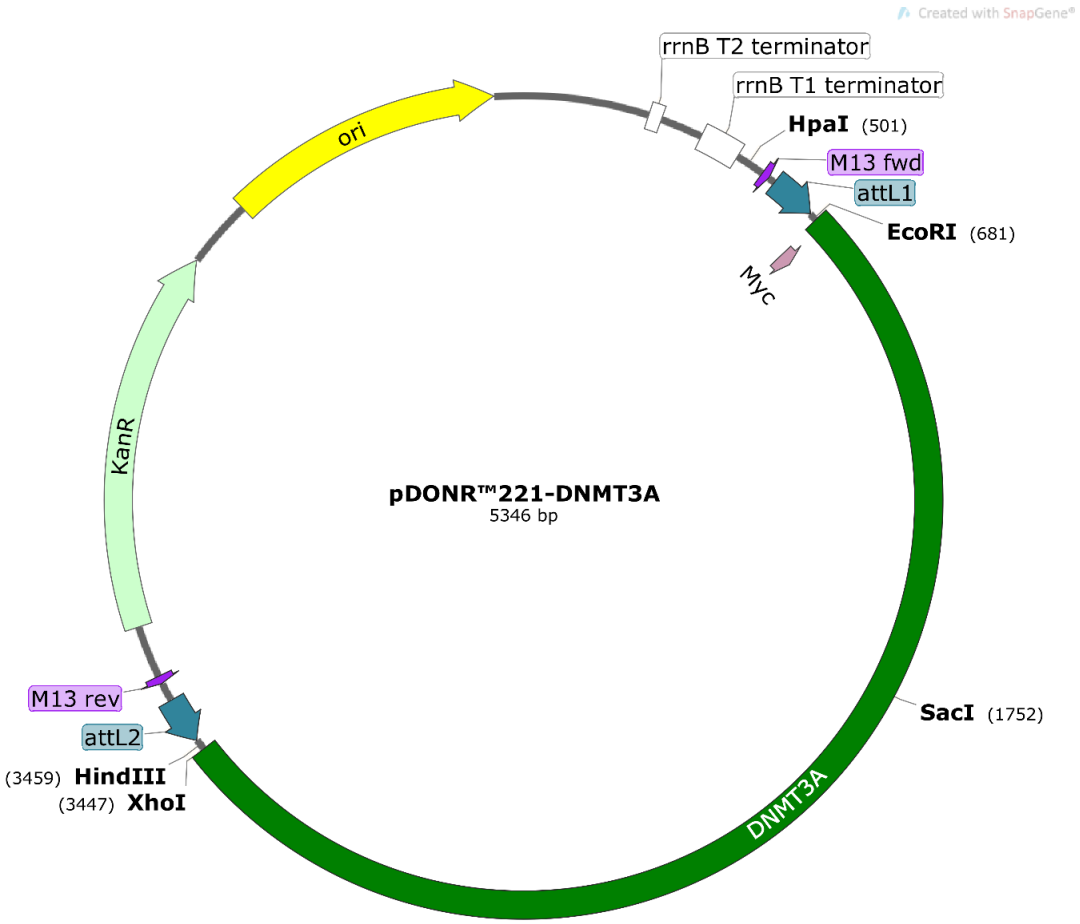

Figure 5.25: pDONR™221-mitochondrial DNMT1 entry clone after BP reaction. This construct was then used for LR reaction.

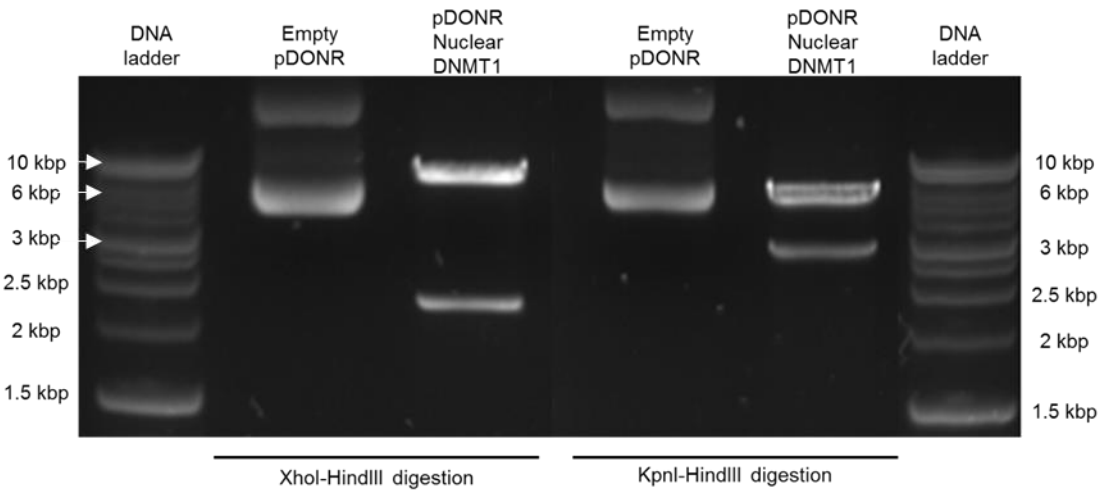

Figure 5.26: DNA gel electrophoresis of empty pDNOR and pDONR-Nuclear DNMT1 after BP reaction. After confirming the restriction pattern, the clone was used for LR clonease reaction.

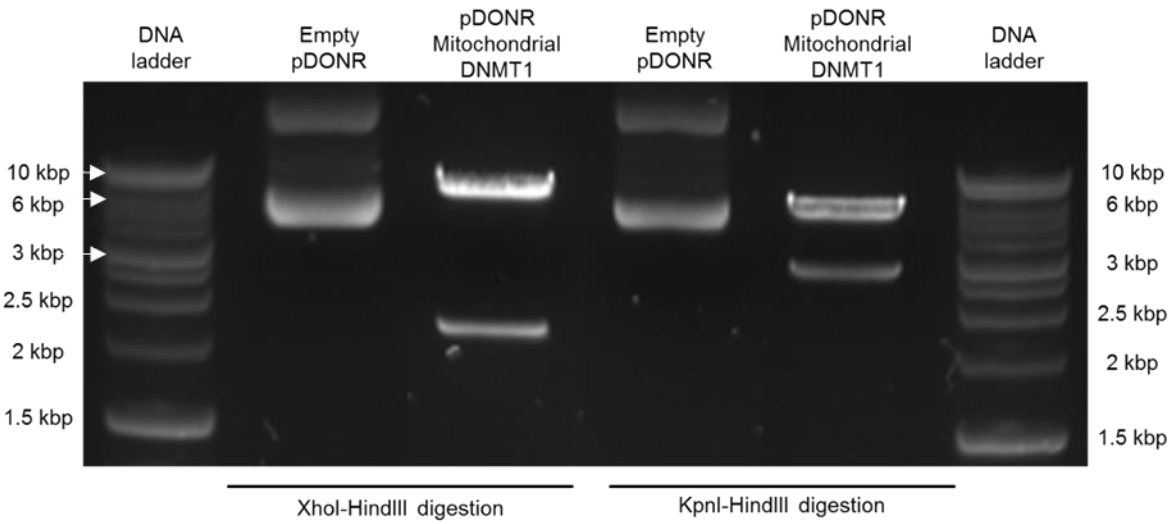

Figure 5.27: DNA gel electrophoresis of empty pDNOR and pDONR-Mitochondrial DNMT1 after BP reaction. After confirming the restriction pattern, the clone was used for LR clonease reaction.

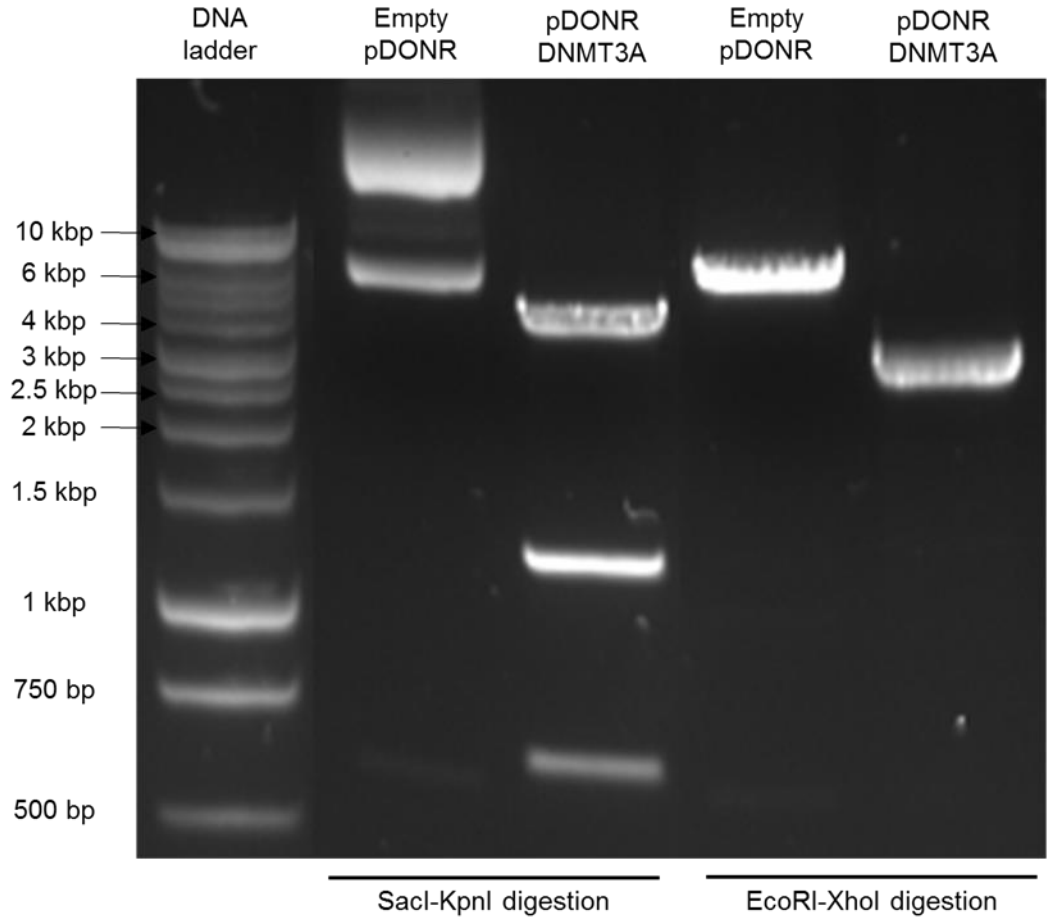

Figure 5.28: DNA gel electrophoresis of empty pDNOR and pDONR-DNMT3A after BP reaction. After confirming the restriction pattern, the clone was used for LR clonease reaction.

5.4.1.2 LR Clonase results

Clones of pAd/CMV/V5 DEST-Nuclear DNMT1, pAd/CMV/V5 DEST-Mitochondrial DNMT1 and pAd/CMV/V5 DEST-DNMT3A were obtained through LR clonase reaction (**Figures 5.29**, **5.30** and **5.31**). These clones were then checked through DNA gel electrophoresis after enzyme digestion, according to the restriction sites included within the sequences (**Figures 5.32**, **5.33** and **5.34**). This confirmed successful recombination of DNMT3 into pAD/CMV/V5 DEST. Since it was not possible to confirm recombination of nuclear DNMT1 and mitochondrial DNMT1 through DNA gel electrophoresis due to several restriction bands, two PCR for 5' and 3' DNMT1 sequences were performed. The PCR product were ran on a DNA gel and the expected bands were obtained (**Figure 5.35**). After confirming the successful recombination for all vectors, these were linearised through PacI digestion and used for HEK293A transfection.

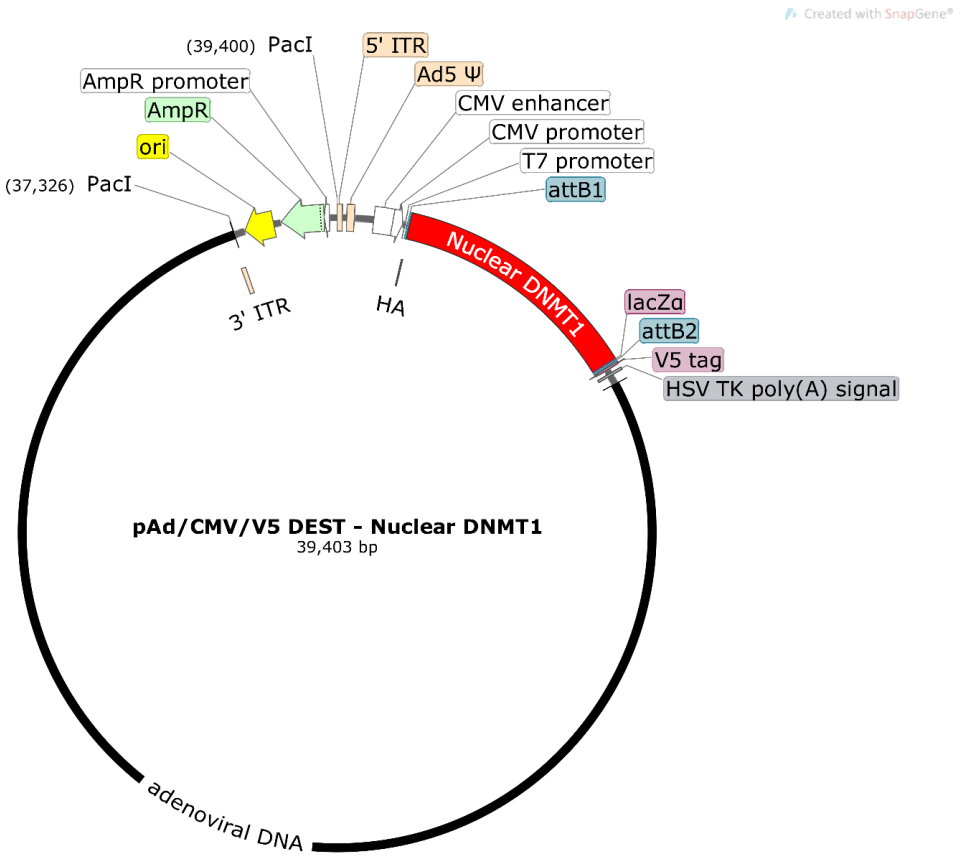

Figure 5.29: pAd/CMV/V5 DEST - Nuclear DNMT1 final clone.

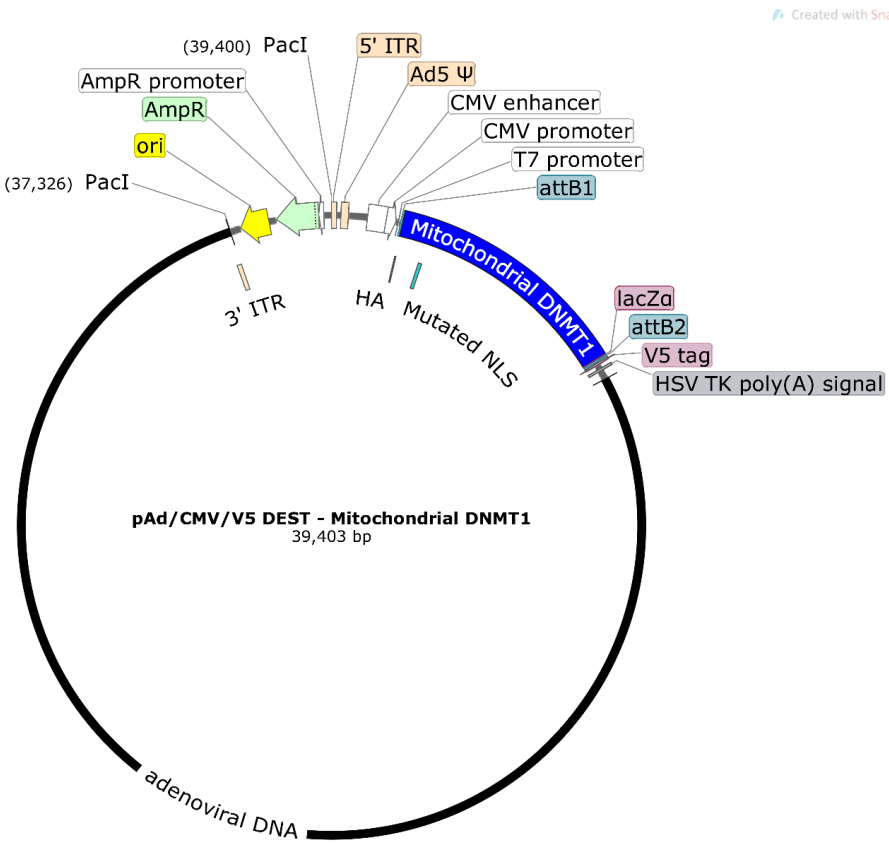

Figure 5.30: pAd/CMV/V5 DEST - Mitochondrial DNMT1 final clone.

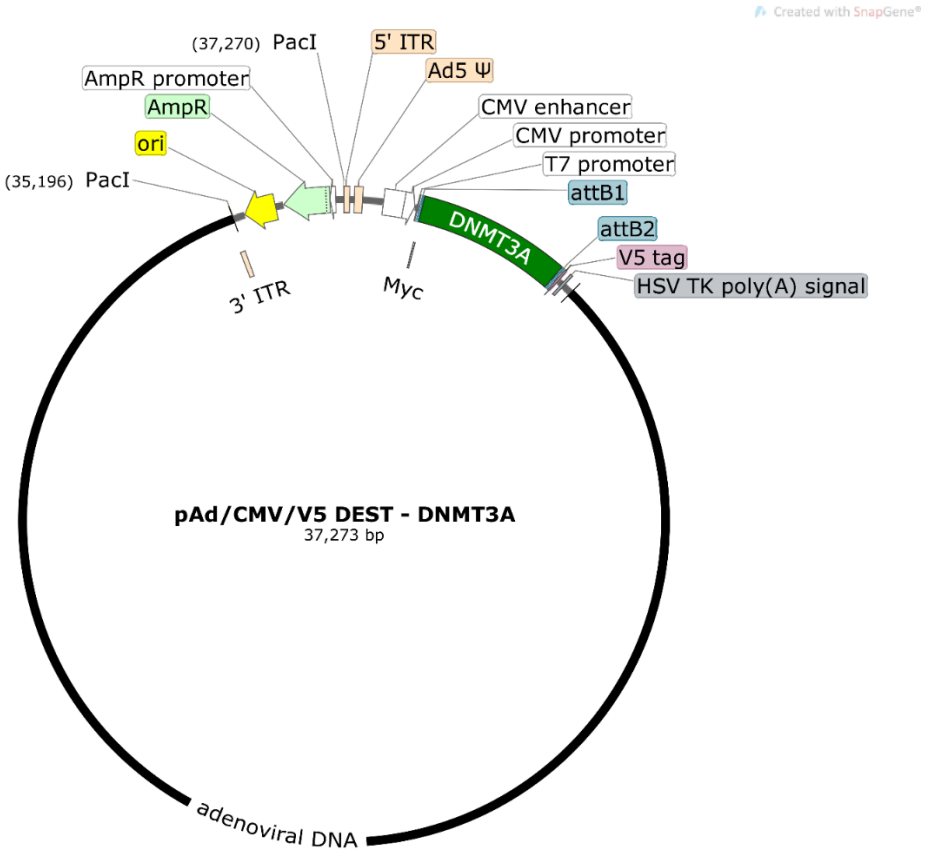

Figure 5.31: pAd/CMV/V5 DEST – DNMT3A final clone.

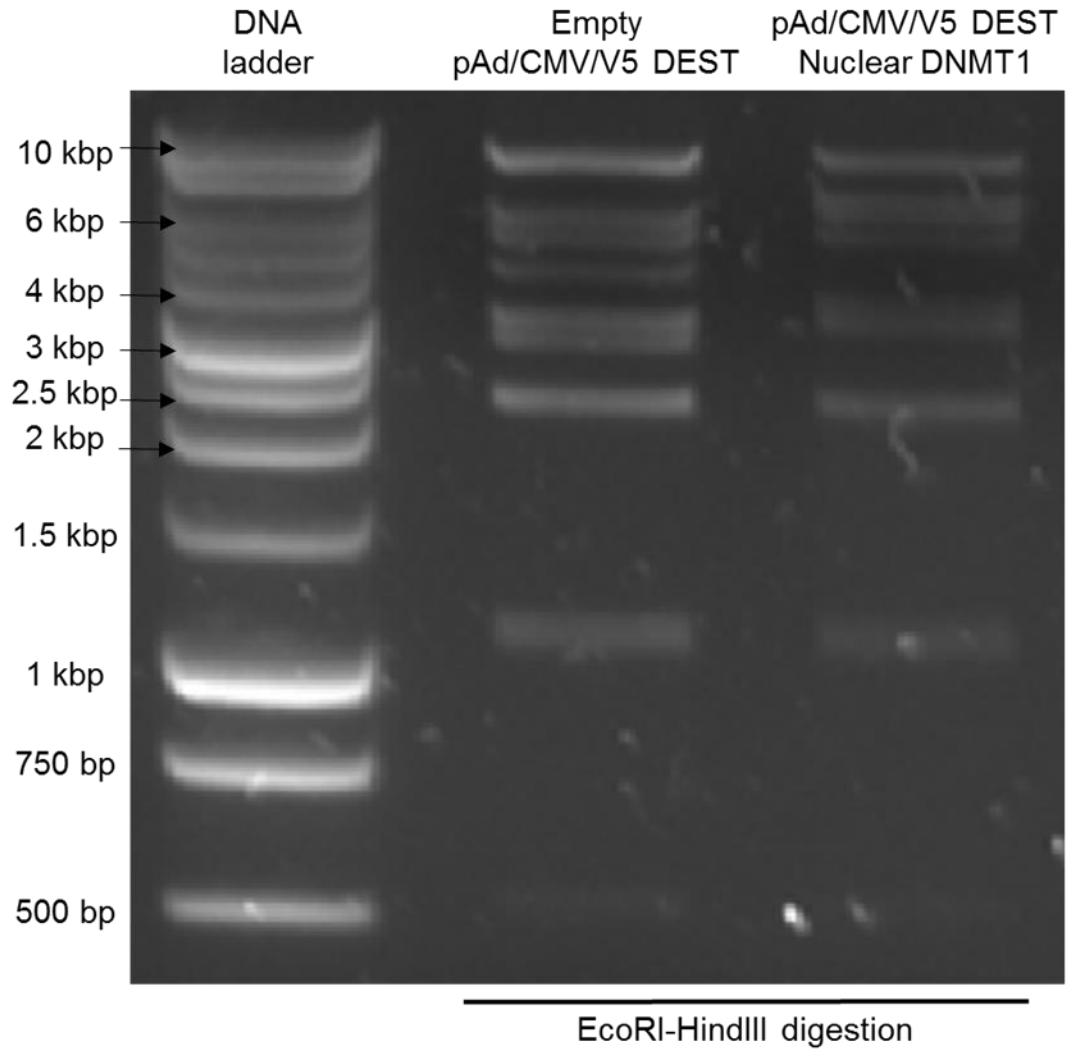

Figure 5.32: DNA gel electrophoresis of empty pAd/CMV/V5 DEST and pAd/CMV/V5 DEST-Nuclear DNMT1 after LR reaction. Since the restriction pattern for pAd/CMV/V5 DEST-Nuclear DNMT1 could not be confirmed properly, PCR for DNMT1 5' and 3' sequences and DNA gel electrophoresis were performed.

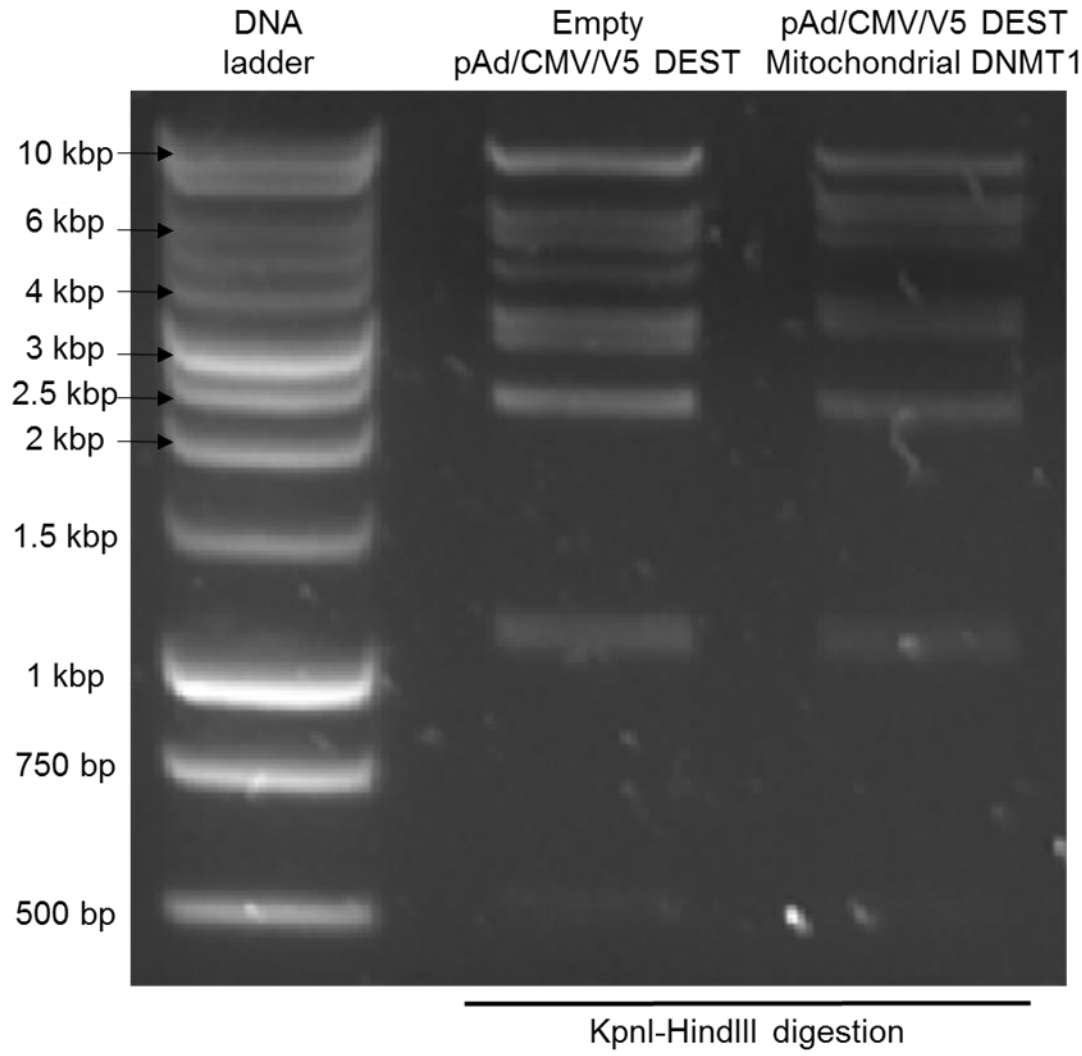

Figure 5.33: DNA gel electrophoresis of empty pAd/CMV/V5 DEST and pAd/CMV/V5 DEST-Mitochondrial DNMT1 after LR reaction. Since the restriction pattern for pAd/CMV/V5 DEST-Mitochondrial DNMT1 could not be confirmed properly, PCR for DNMT1 5' and 3' sequences and DNA gel electrophoresis were performed.

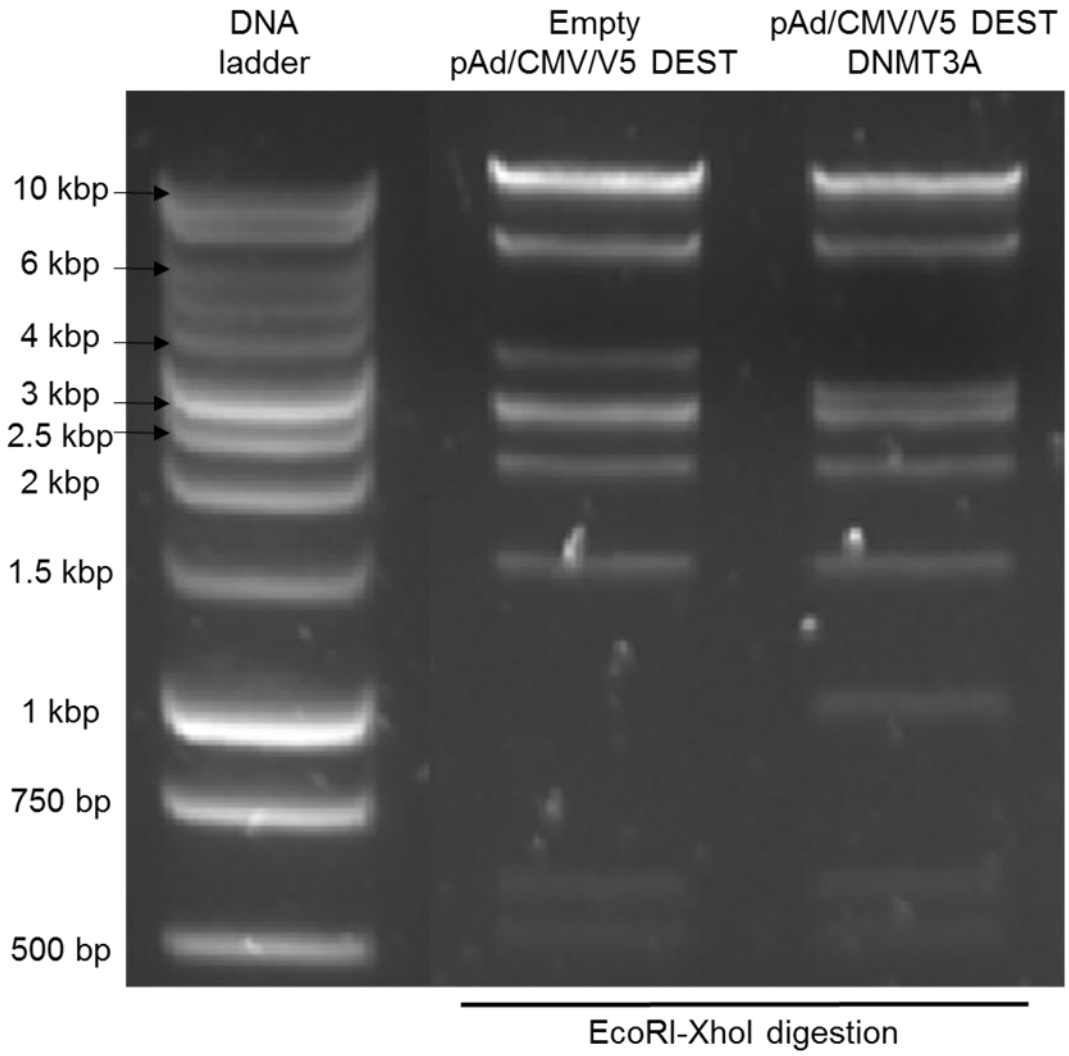

Figure 5.34: DNA gel electrophoresis of empty pAd/CMV/V5 DEST and pAd/CMV/V5 DEST-DNMT3A after LR reaction.

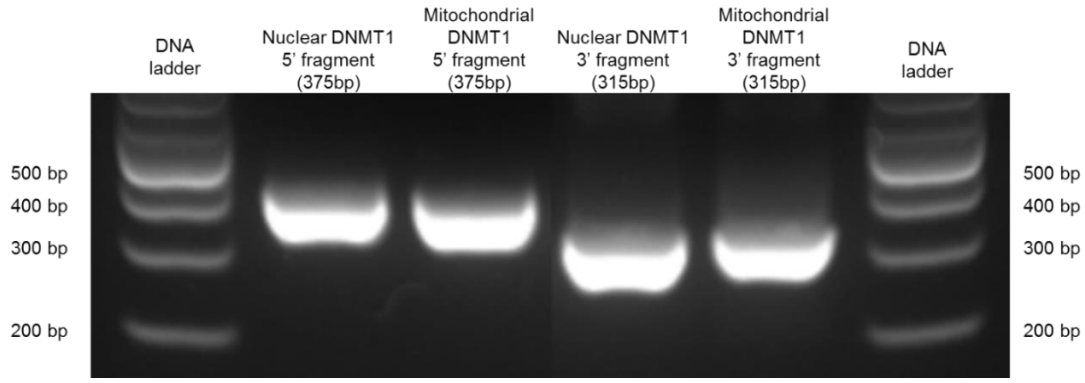

Figure 5.35: DNA gel electrophoresis after PCR for DNMT1 5' and 3' fragments. In order to confirm successful LR clonase recombination, pAd/CMV/V5 DEST-nuclear DNMT1 and pAd/CMV/V5 DEST-mitochondrial DNMT1 clones were used as template.

5.4.1.3 Generation and titration of adenoviral particles

After obtaining adenoviral particles from transfected HEK293A cells, the titer was calculated (**Table 5.14**). From these samples, aliquots were created and stored at -80ºC.

Table 5.14: Titer calculation of adenoviral vectors.

Adenovirus	Titer
Adeno-Nuclear DNMT1	6.322 * 10^9 ifu/ml
Adeno-Mitochondrial DNMT1	4.82 * 10^9 ifu/ml
Adeno-DNMT3A	6.13 * 10^9 ifu/ml

5.4.2 Establishment of DNMT1 overexpression through adenoviral vectors

5.4.2.1 Preliminary overexpression experiments in H9C2 cells

The overexpression features of the adenoviral vectors were investigated through H9C2 cells infection and western blotting (**Figure 5.36** and **Figure 5.37**). No infection, as well as infection with Adeno-LacZ vector, were used as a negative control. Two different multiplicities of infection (MOI) were investigated. After confirming Adeno-Nuclear DNMT1, Adeno-Mitochondrial DNMT1 and Adeno-DNMT3A overexpression features, these vectors were used for infection of MCE cells, a mouse-derived cell line.

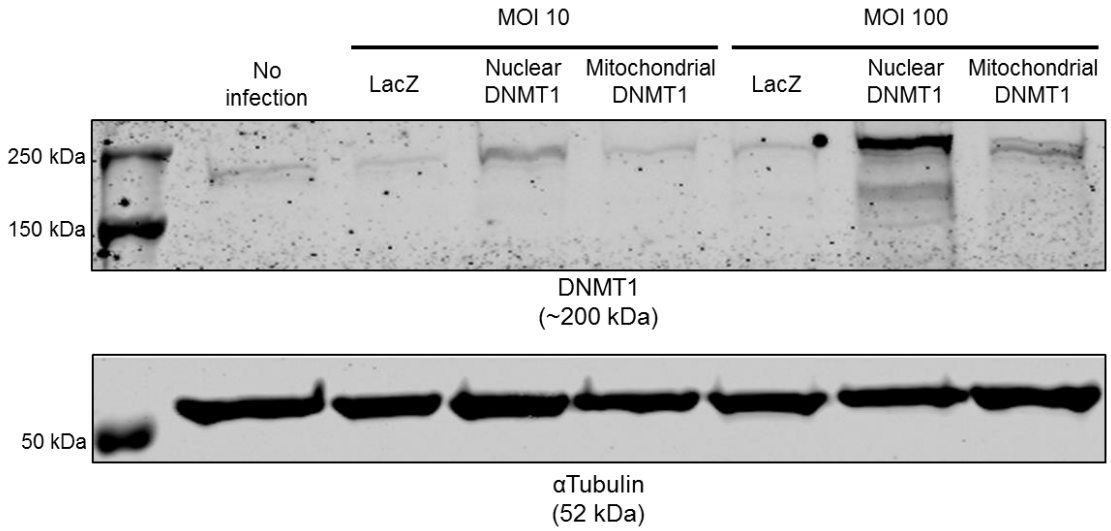

Figure 5.36: Western blotting of H9C2 cells samples infected with Adeno-Nuclear DNMT1 and Adeno-Mitochondrial DNMT1. No infection, as well as infection with Adeno-LacZ, were used as negative control. Two different multiplicities of infections were investigated. After infection, clear nuclear and mitochondrial DNMT1 bands could be observed in all infected sample, especially in MOI 100 samples.

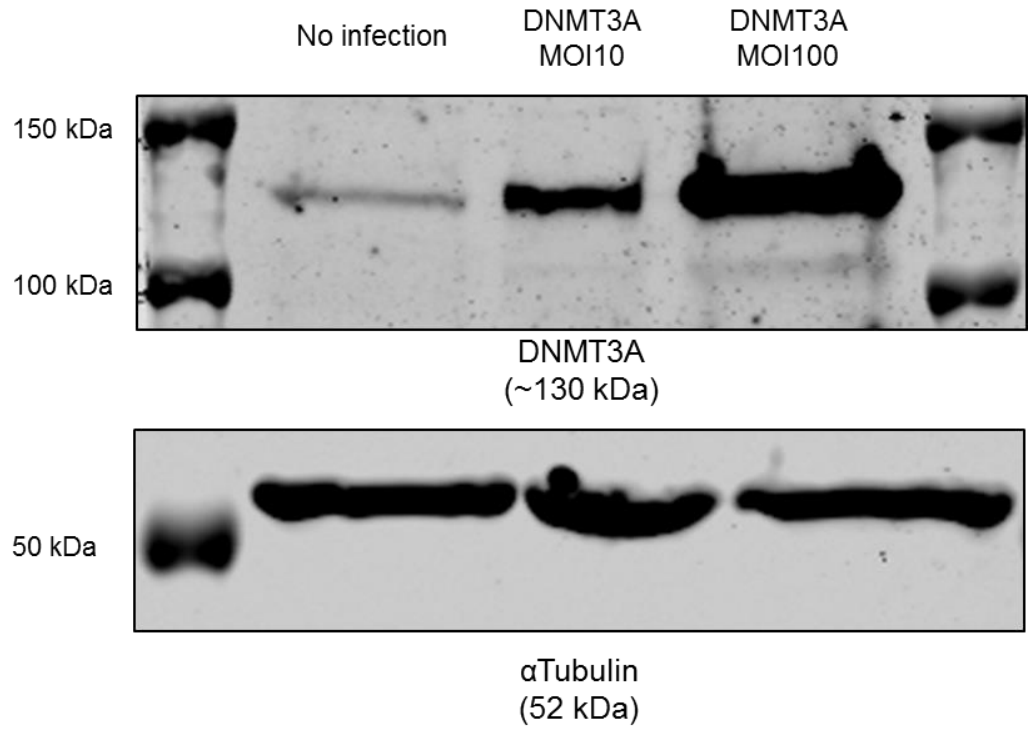

Figure 5.37: Western blotting of H9C2 cells samples infected with Adeno-DNMT3A. Two different multiplicities of infections were investigated. No infection was used as negative control. After infection, strong DNMT3A bands could be observed in all infected sample, especially in MOI 100 samples.

5.4.2.2 Assessment of MOI for MCE cells

To assess the best MOI to use for infection of MCE cells, infection of MCEC with Adeno-GFP was performed. Then, the cells were observed under a brightfield-fluorescence microscope (**Figure 5.38**) and positive cells were counted. After obtaining an infection efficiency of over 95%, MOI 10 was selected for infection of MCE cells.

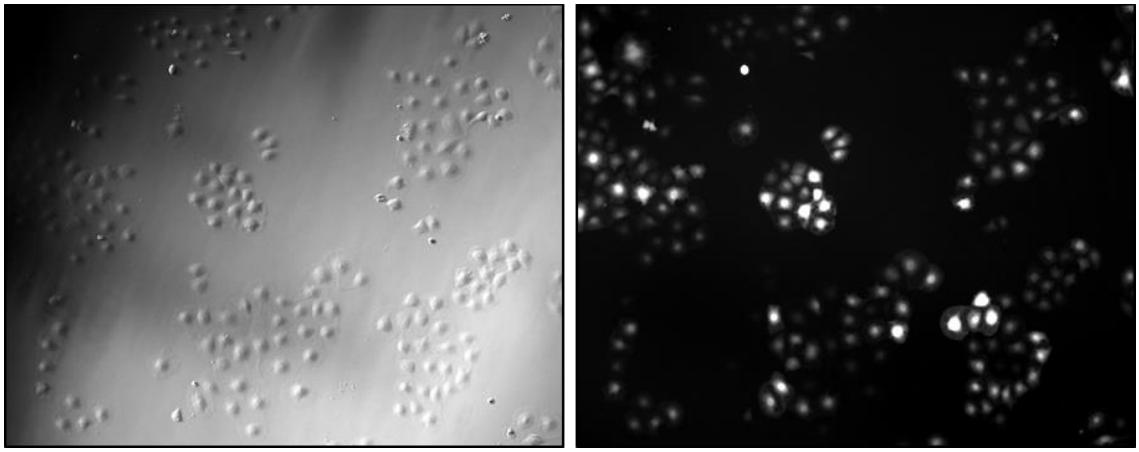

Figure 5.38: Representative images of MCEC cells infected with Adeno-eGFP vector (MOI 10). Total number of cells were imaged through brightfield (on the left), and successfully infected cells were counted through fluorescence microscopy (on the right).

5.4.3 Validation of D-Loop primers for methylation analysis after MeDIP

After designing the D-Loop primer sets through in silico PCR, these were checked through both PCR (using H_2O as negative control) (**Figure 5.39**) and real-time qPCR (**Figure 5.40**) using B6 mouse genomic DNA as a template for both experiments. The PCR experiment yielded the expected band size for all primer sets, whilst no bands were obtained when replacing B6 mouse gDNA template with water. Furthermore, the R^2 (coefficient of correlation) value obtained through real-time qPCR of all primer sets was above 0.99 for all primer sets investigated, allowing to further confirm the efficiency and specificity of all designed primer sets.

Finally, to confirm whether the primers could specifically target mtDNA sequences and not NUMTs, a qPCR experiment using both nuclear DNA and mtDNA from MCE cells was performed.

All primer sets proved to be able to amplify mtDNA sequences more selectively than NUMTs, as expected from in silico PCR predictions (these primer sets

should not amplify for NUMTs) (**Figure 5.41**). After these validation steps, all primers were used for qPCR reactions after MeDIP.

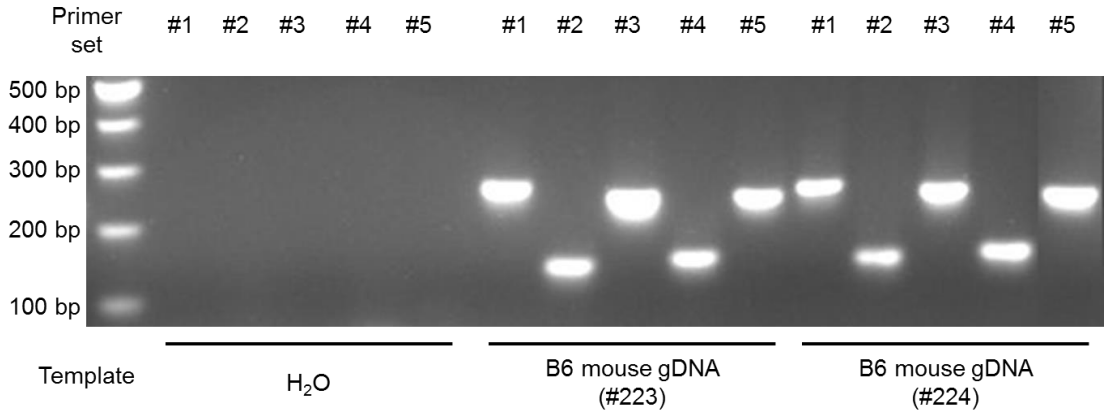

Figure 5.39: DNA gel electrophoresis after PCR using D-Loop primers. B6 mouse gDNA from 2 specimen was used as a template. Water was used as a negative control.

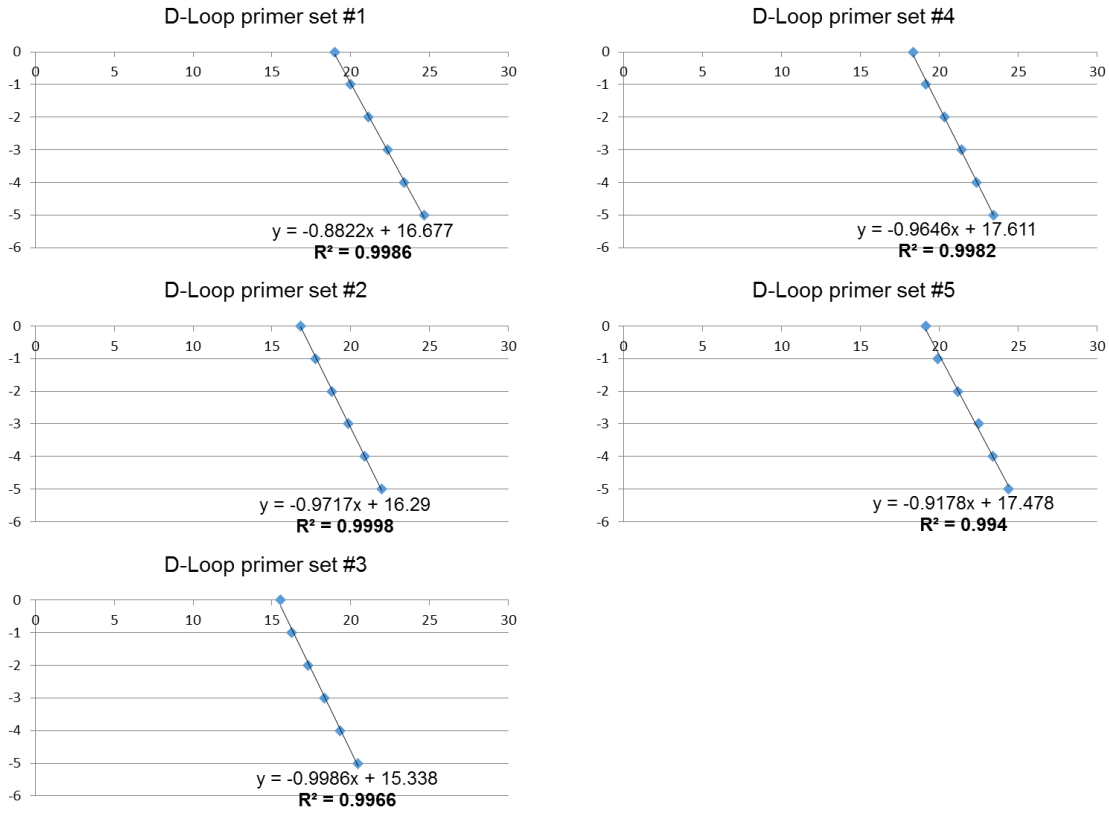

Figure 5.40: Calculation of R^2 value (coefficient of correlation) after real-time qPCR of D-Loop primer sets. The value was above 0.99 for all primer sets investigated.

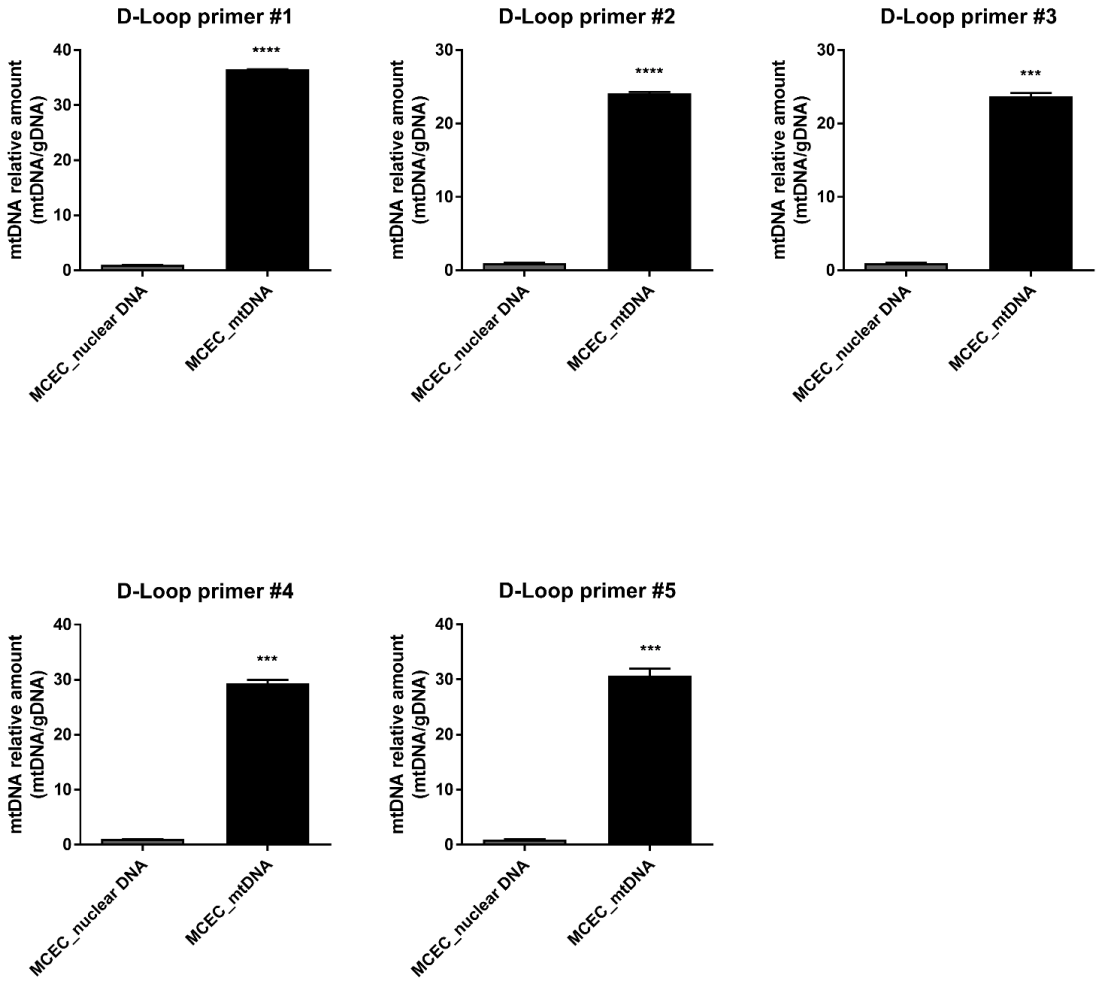

Figure 5.41: Testing the specificity of D-Loop primers using nuclear DNA and mtDNA from MCE cells. Values are expressed as mtDNA relative amount (mtDNA/gDNA). Unpaired two-tailed t-test statistical analysis was performed. Legend: *** = P Value < 0.001, *** = P Value < 0.0001.

5.4.4 MeDIP methylation analysis following nDNMT1 and mtDNMT1 overexpression in MCEC

After overexpressing nuclear DNMT1 and mitochondrial DNMT1 in MCEC through infection with adenoviral vectors, the methylation of mtDNA was investigated through MeDIP-qPCR. Infection with Adeno-eGFP was used as a negative control. Mitochondrial fraction was purified from infected cells and mtDNA was extracted from it. Then, the mtDNA samples were used as a template

for MeDIP, and the final samples were used for real-time qPCR, using the 5 different D-Loop primer sets.

The amount of CpG motifs for each PCR product depends on the sequence targeted by the primer sets (**Figure 5.42**), though the system does not allow for single base resolution. First, the fold increase of global methylation compared to the eGFP was calculated (**Figure 5.43**). No increase was found in any of the D-Loop sequences of samples infected with nuclear DNMT1, suggesting it not playing a key role in affecting D-Loop methylation levels. Conversely, a 3-to-5 fold increase in global methylation was found in D-Loop sequences of samples infected with mitochondrial DNMT1 compared to eGFP control samples. This could mean that mtDNMT1 would not only be able to localise at a mitochondrial level, but also affect its DNA methylation patterns.

Even though the increase in methylation (compared to the input) was higher in D-Loop sequences of mtDNMT1-infected samples compared to eGFP- or nuclear DNMT1-infected samples, the absolute value was still under 1% (**Figure 5.44**). However, these results looked promising, and further efforts were made in order to establish and optimise this protocol in London.

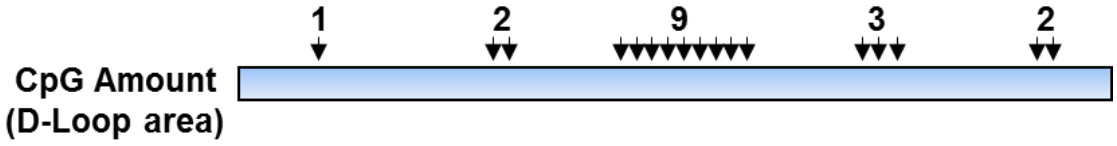

Figure 5.42: CpG amounts for D-Loop areas. Primer set #3 amplifies for the sequence with the highest amount of CpG motifs (9).

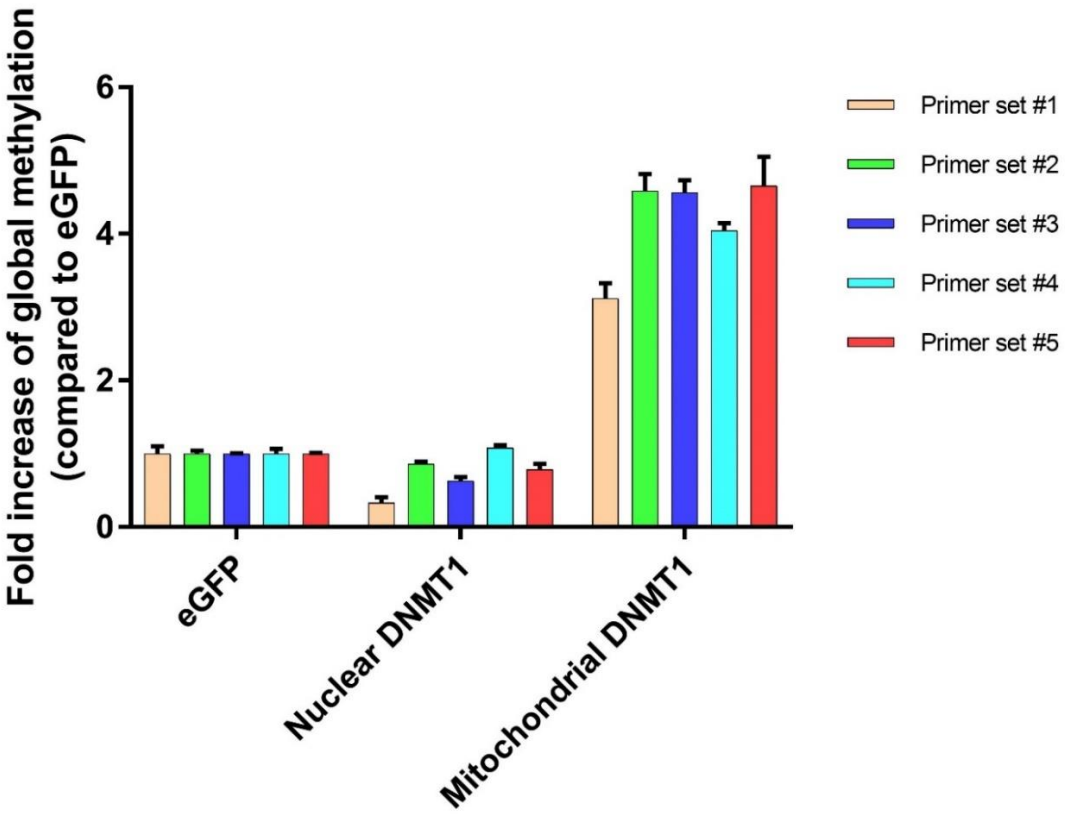

Figure 5.43: Fold increase methylation (compared to eGFP) of mtDNA D-Loop sequences. eGFP, nuclear DNMT1 or mitochondrial DNMT1 overexpression through adenoviral vectors. Values with standard deviation (1 biological replicate, 3 technical replicates).

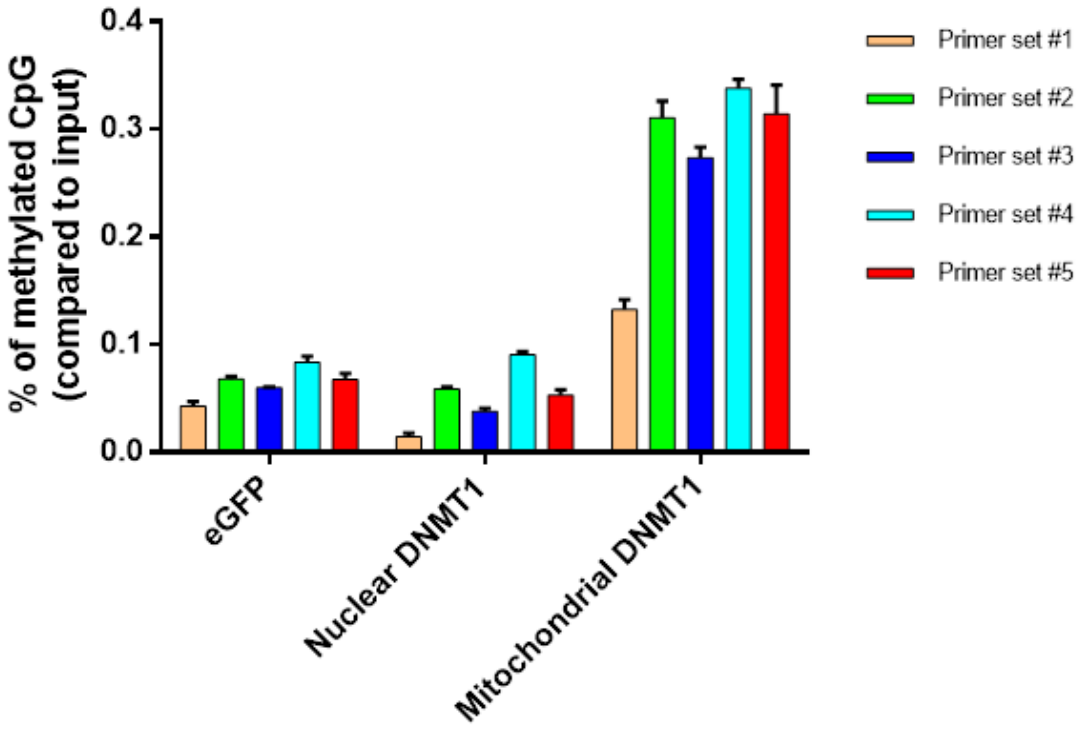

Figure 5.44: Increase in methylation (showed as a percentage increase) of mtDNA D-Loop sequences. eGFP, nuclear DNMT1 or mitochondrial DNMT1 overexpression through adenoviral vectors. Values with standard deviation (1 biological replicate, 3 technical replicates).

5.4.5 Establishment of MeDIP protocol in London

5.4.5.1 Screening of DNA band sizes after sonication

As some of the sonicator's components used in Goettingen could not be obtained when setting up the sonication system in London, efforts were required in order to optimise the sonication step before MeDIP. The sonication conditions used were the same used in Goettingen, and DNA from different sources (B6 mouse gDNA, pCMV-SPORT6 nuclear DNMT1, pCMV-SPORT6 mitochondrial DNMT1, MCEC gDNA from cells infected with adeno-eGFP, adeno-nuclear DNMT1 and adeno-mtDNMT1) was used as a template for sonication. Initially, the DNA samples were resuspended in H_2O, sonicated, and ran on a 2% DNA gel (**Figure 5.45**). Afterwards, the resuspension buffer was changed to MC2 buffer from the

MeDIP kit, in order to better mimic the sonication conditions during the actual pre-MeDIP sonication (**Figure 5.46**).

The samples showed a different sonication pattern depending on both their origin and the sonication buffer. B6 mouse gDNA, pCMV-SPORT6 Nuclear DNMT1 and pCMV-SPORT6 Mitochondrial DNMT1 samples sonicated with water yielded a smear comprised between 400 bp and 100 bp, whereas MCEC gDNA samples' smear was evenly distributed between 1500 bp and 200 bp. When H_2O was replaced with MC2 buffer, the smear of B6 mouse gDNA, pCMV-SPORT6 Nuclear DNMT1 and pCMV-SPORT6 Mitochondrial DNMT1 samples appeared to be mainly localised between 1000 bp and 200 bp.

Since the two pCMV-SPORT6 vectors possess features that resemble mtDNA own features (circular double strand, small size), and the fragments size for these samples fell under the optimal range for MeDIP samples, the sonication conditions as well as the sonication buffer (MC2) were confirmed and adopted for the actual pre-MeDIP sonication step.

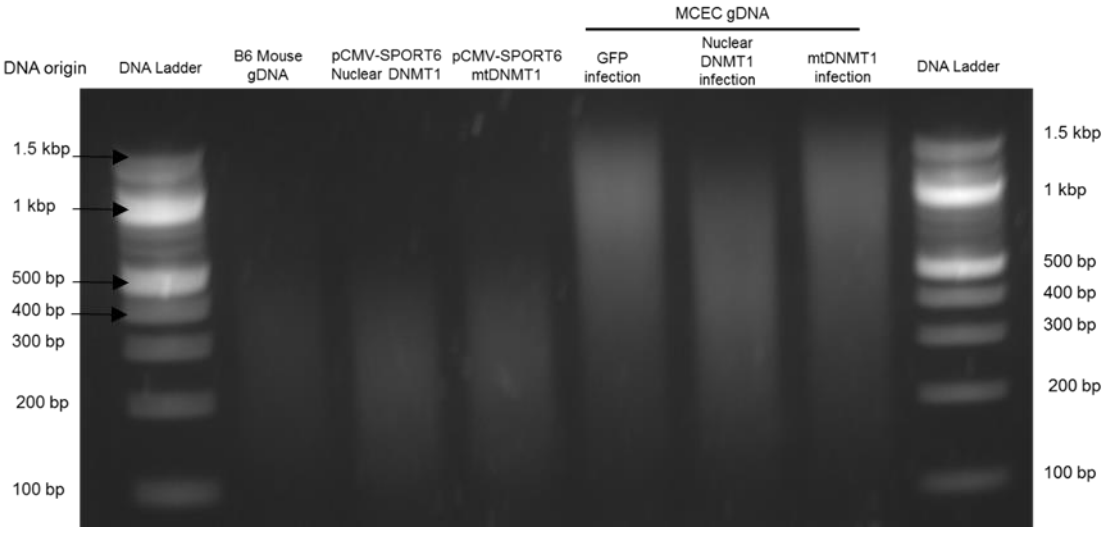

Figure 5.45: DNA gel electrophoresis of DNA samples after sonication (H_2O).

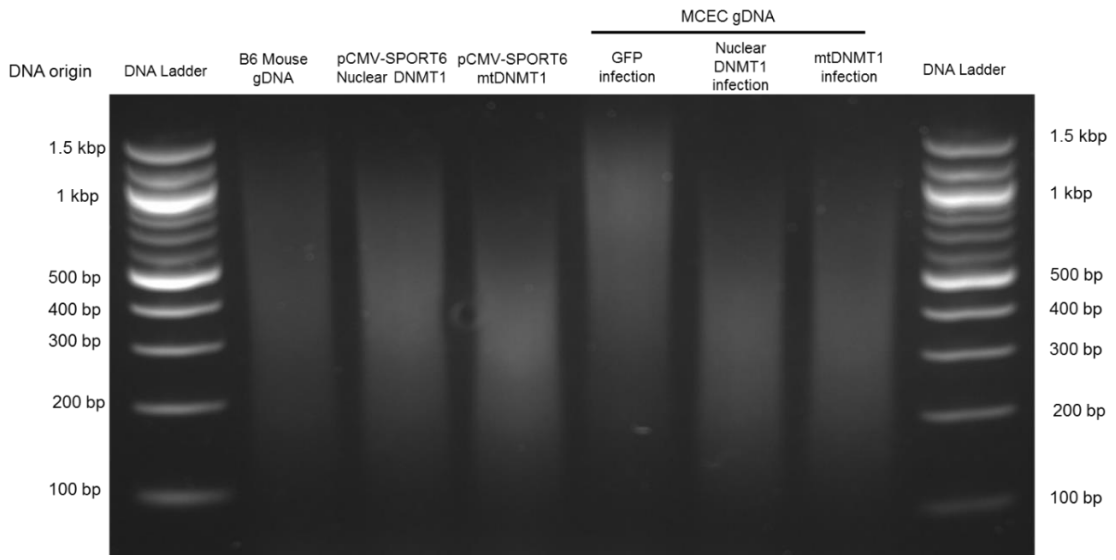

Figure 5.46: DNA gel electrophoresis of DNA samples after sonication (MC2 buffer).

5.4.5.2 D-Loop methylation analysis

Several attempts were performed in order to replicate the data obtained in Goettingen. Each time, the procedure was repeated from the infection step. Following infection, mitochondrial fraction was obtained, then mtDNA was extracted from the fraction and MeDIP-qPCR was performed. The best attempt (**Figure 5.47**) was then combined with the results obtained in Goettingen (**Figure 5.48**). Though statistical analysis was not performed due to sample amount (N=2), there seems to be a tendency of increased methylation of primer sets #1 to #4 sequences after mitochondrial DNMT1 overexpression. However, the results are still immature.

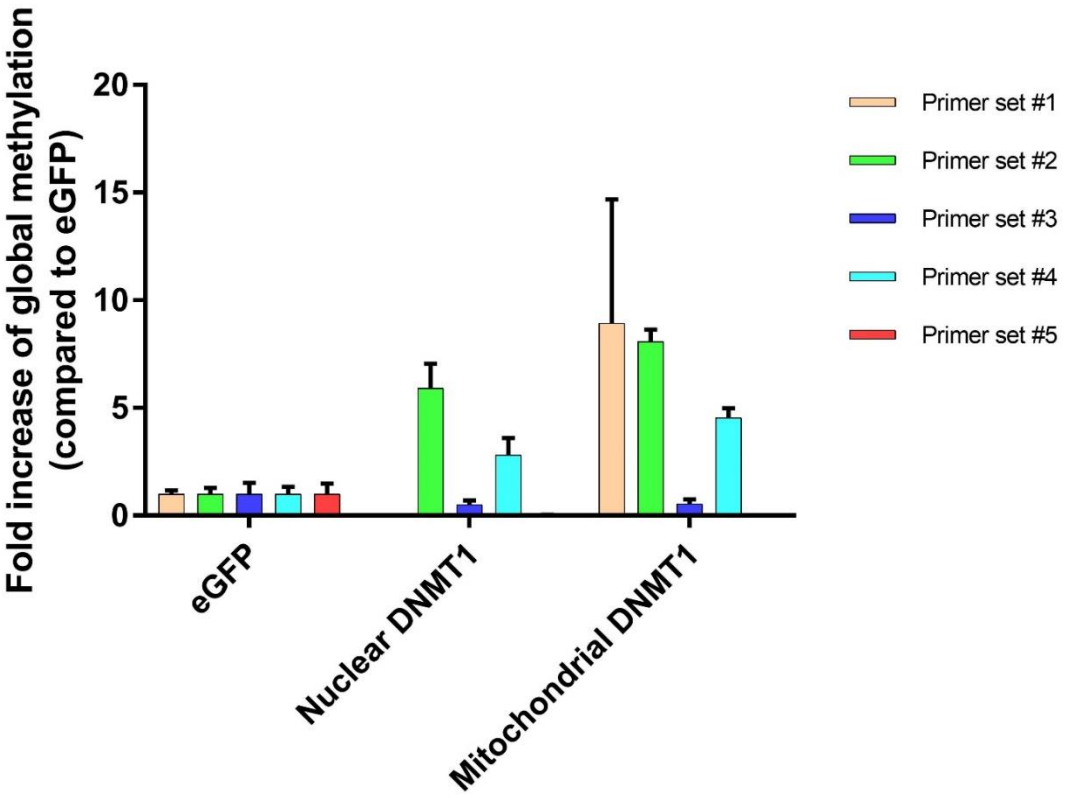

Figure 5.47: Fold increase methylation (compared to eGFP) of mtDNA D-Loop sequences (performed in London). eGFP, nuclear DNMT1 or mitochondrial DNMT1 overexpression through adenoviral vectors. Values with standard deviation (1 biological replicate, 3 technical replicates).

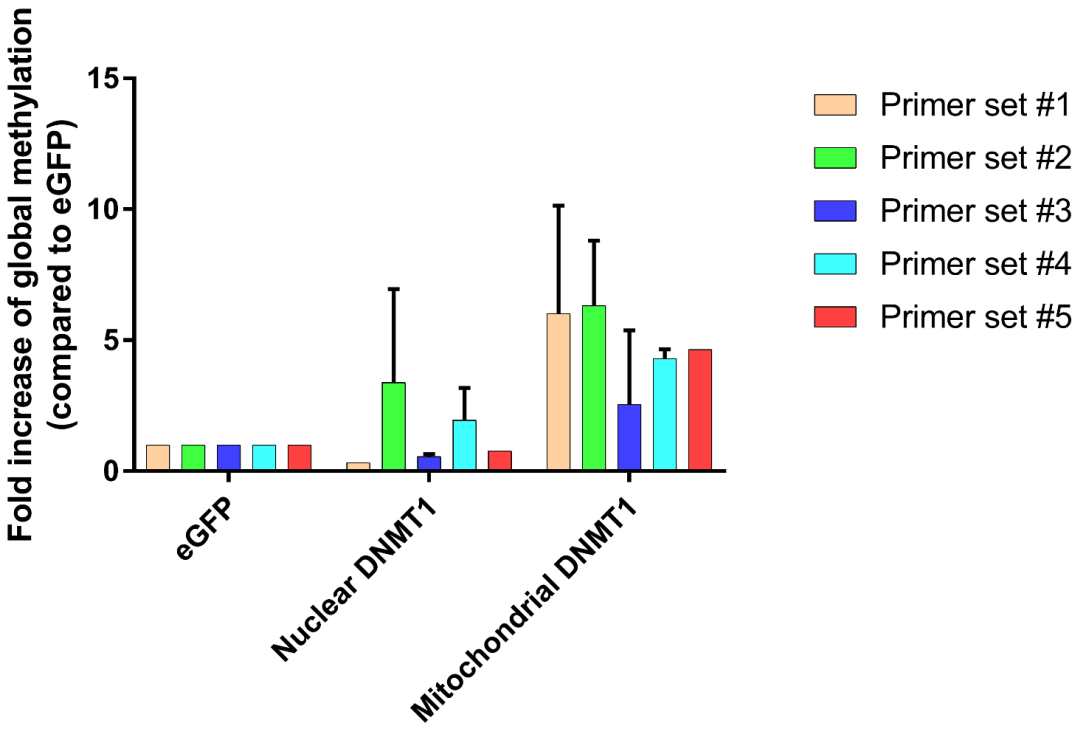

Figure 5.48: Fold increase methylation (compared to eGFP) of mtDNA D-Loop sequences (Combined values). eGFP, nuclear DNMT1 or mitochondrial DNMT1 overexpression through adenoviral vectors. Values with standard deviation, 2 biological replicates (except for primer sets #1 and #5).

5.4.6 Generation of mtDNMT1 lentivirus

5.4.6.1 pLenti-puro-mtDNMT1 cloning results

To test whether a more stable, consistent and strong overexpression of DNMT1 isoforms would be required in order to successfully impact mtDNA methylation patterns, generation of mtDNMT1 lentivirus for stable mtDNMT1 overexpression in MCE cells was performed.

Digestion of the pLenti maxiprep sample confirmed the restriction pattern (**Figure 5.49**). After this, insertion of SpeI and XbaI linkers in the pCMV-SPORT6-mtDNMT1 vector through blunting and ligation was successfully completed (**Figure 5.50**). The insertion of mtDNMT1 into pLenti was performed in two steps. First, the SpeI-XhoI 5' fragment was digested from pCMV-SPORT6-SpeI-mtDNMT1-XbaI and inserted into pLenti-puro (**Figure 5.51**), then the XhoI-XbaI 3' fragment was digested from pCMV-SPORT6-SpeI-mtDNMT1-XbaI and inserted into pLenti-puro-SpeI-XhoI mtDNMT1 5' (**Figure 5.52**).

Digestion of the final pLenti-puro-mtDNMT1 maxiprep sample allowed to confirm proper insertion of mtDNMT1 (**Figure 5.53**), and the vector was used for HEK293 transfection.

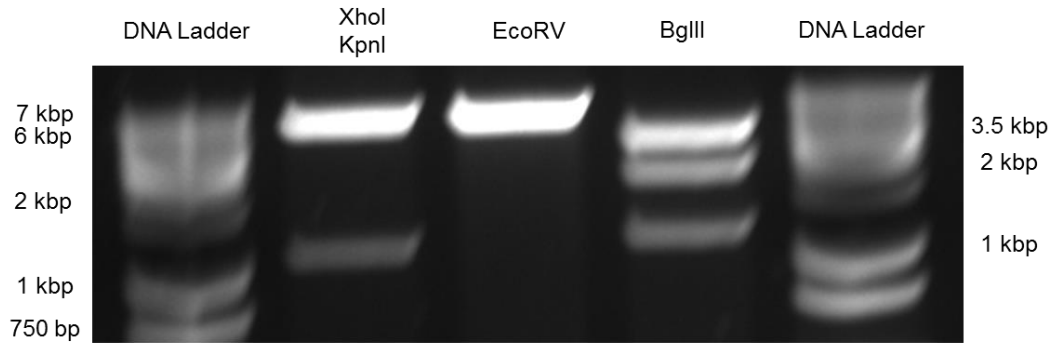

Figure 5.49: DNA gel electrophoresis of pLenti-puro maxiprep sample after restriction digestion.

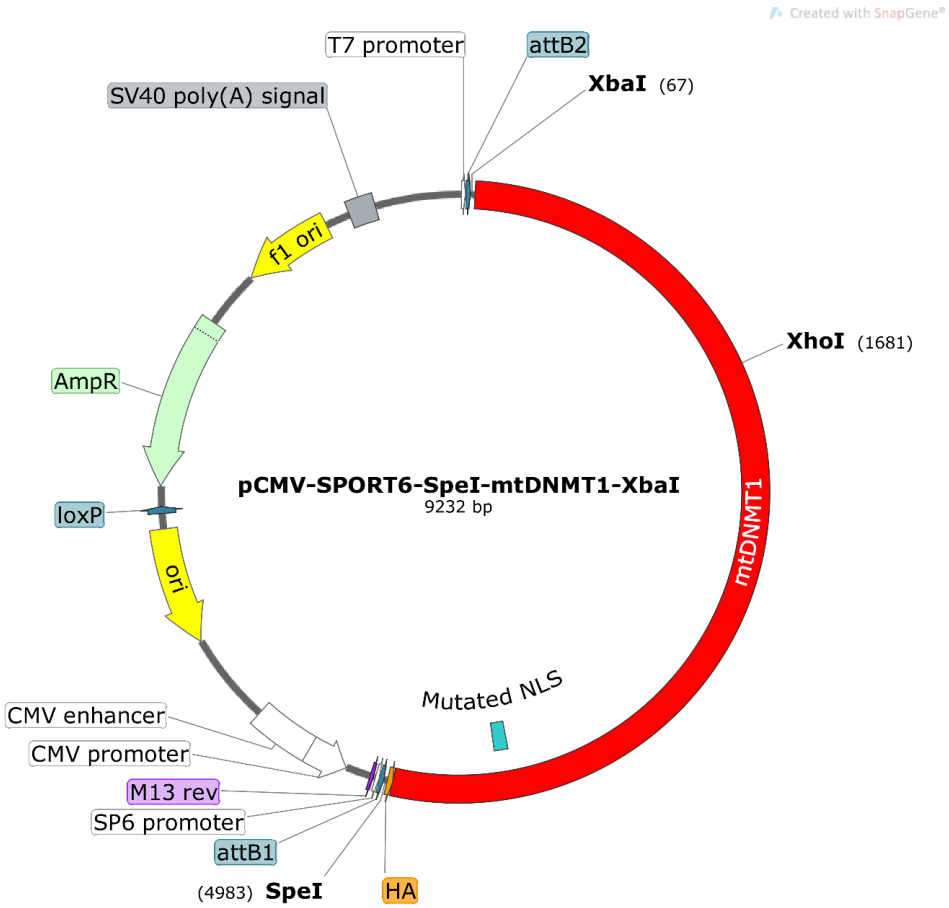

Figure 5.50: pCMV-SPORT6-SpeI-mtDNMT1-XbaI map.

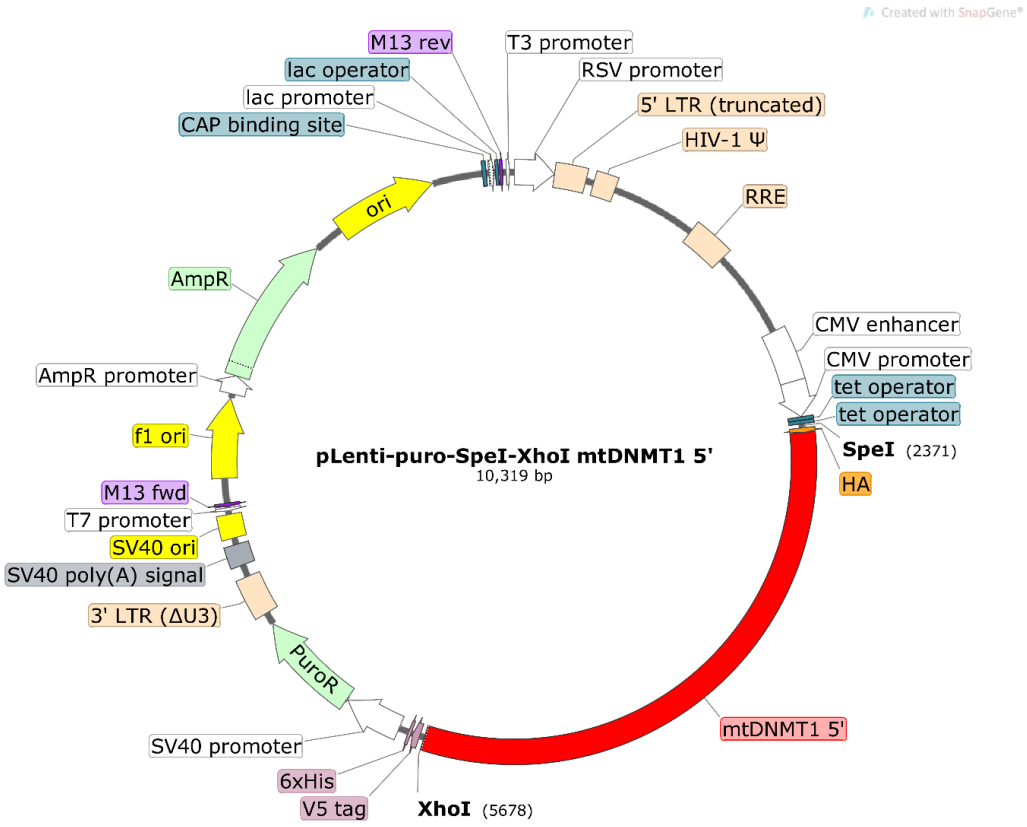

Figure 5.51: pLenti-puro-SpeI-XhoI mtDNMT1 5' map.

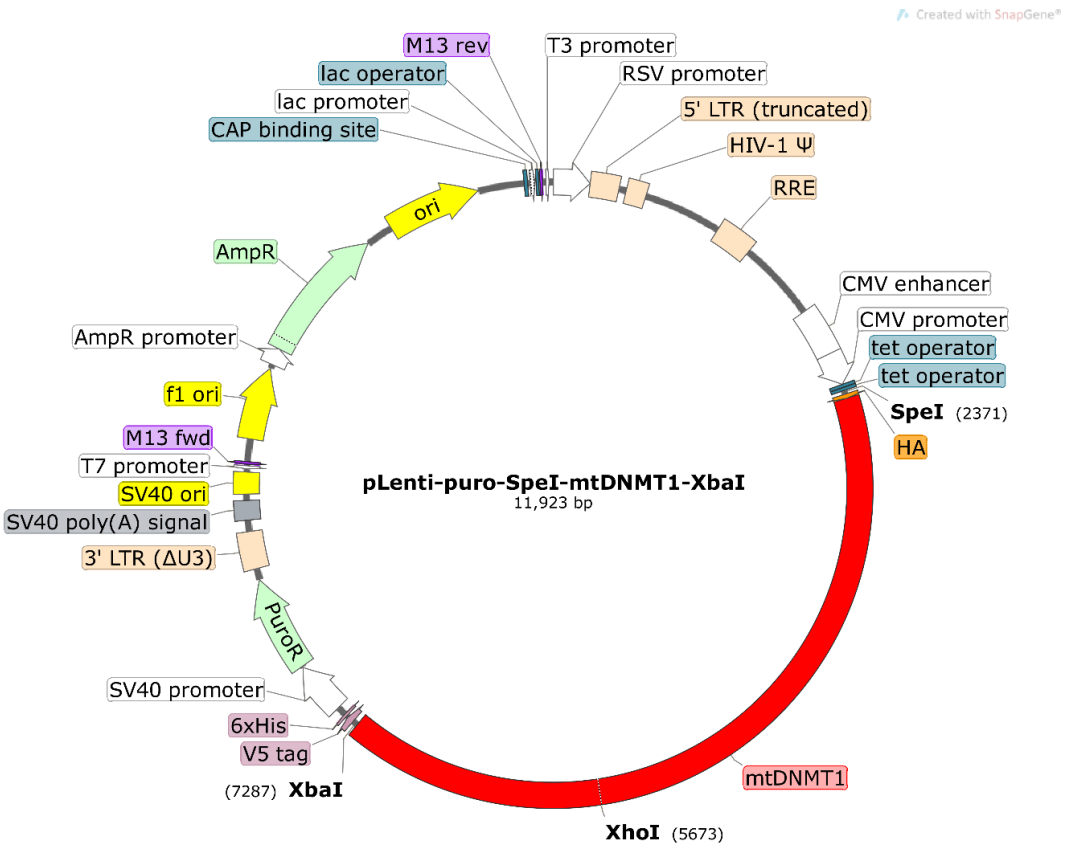

Figure 5.52: Final map for pLenti-puro-SpeI-mtDNMT1-XbaI plasmid.

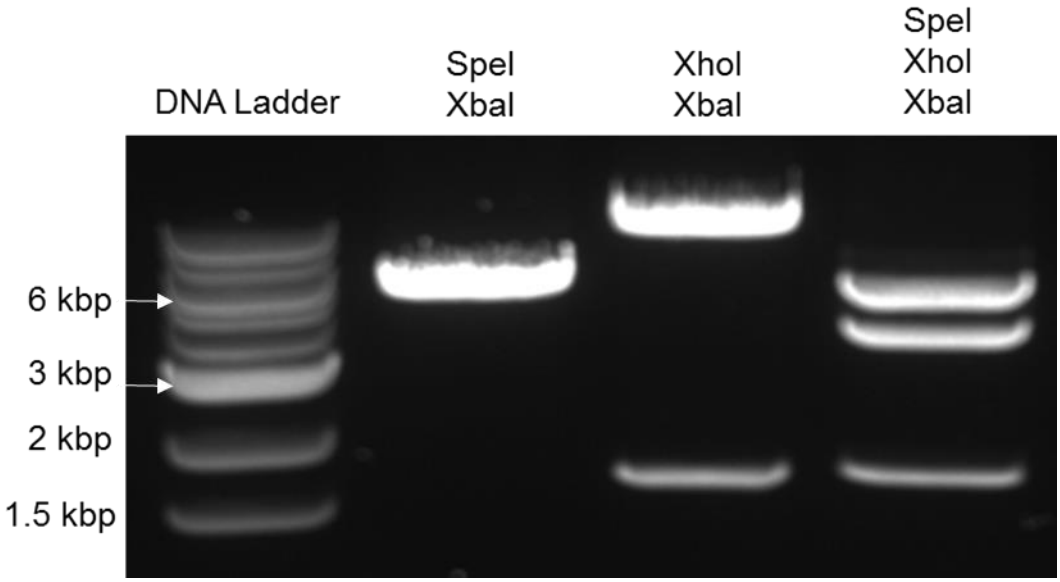

Figure 5.53: DNA gel electrophoresis of pLenti-puro-SpeI-mtDNMT1-XbaI maxiprep sample.

5.4.6.2 Puromycin concentration

After 3 days of treatment, the puromycin concentration that yielded 100% cell death in non puromycin resistant MCE cells is 1.5 µg/ml.

5.4.6.3 Lentivirus titer

After obtaining Lenti-Mitochondrial DNMT1 (Lenti-mtDNMT1) lentiviral particles from transfected HEK293 cells, the titer was calculated (**Table 5.15**). From this samples, aliquots were created and stored at -80ºC.

Table 5.15: Titer calculation of Lenti-Mitochondrial DNMT1 vector.

Lentivirus	Titer
Lenti-Mitochondrial DNMT1	1.85 * 10^9 ifu/ml

5.4.7 Establishment of mtDNMT1 stable overexpression in MCE cells

For establishing stable overexpression of mtDNMT1 in MCE cells, cells were seeded in a T75 flask and infected with Lenti-mtDNMT1 with MOI 5. After 2 days the cells were cultured with 1.5 µg/ml concentration of puromycin in order to select them. Visible cell death was observed after 3 days, and the remaining cells were expanded until the T75 flask was confluent.

The cell line was then expanded, cryotubes were created and stored at -80ºC, and DNMT1 expression analysis was performed through western blotting analysis (**Figure 5.54** and **Figure 5.55**). The establishment of a stable mtDNMT1 overexpression in MCE cells could not be confirmed. This could be due to issues with packaging during production of lentivirus.

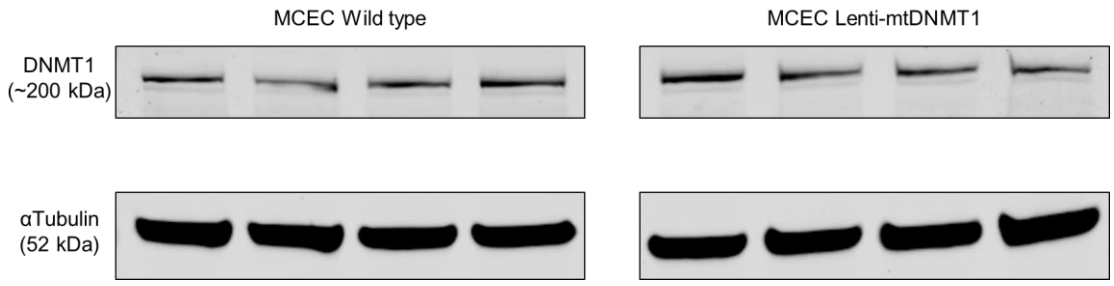

Figure 5.54: Western blotting of MCEC wild type and MCEC Lenti-mtDNMT1 samples for DNMT1 expression analysis. MCEC Lenti-mtDNMT1 cells have been cultured with puromycin.

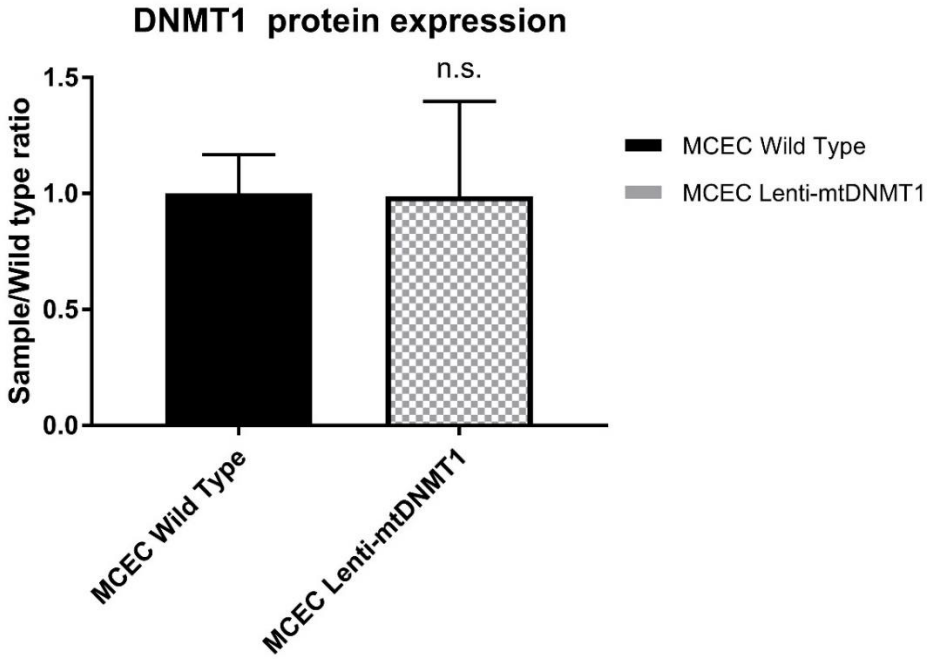

Figure 5.55: Analysis of western blotting signal of MCEC wild type and MCEC Lenti-mtDNMT1 samples. DNMT1 signal was normalised on the housekeeping (αTubulin), then the DNMT1 signal from MCEC Lenti-mtDNMT1 was normalised on the DNMT1 signal from MCEC wild type. Statistical analysis is two-tailed t-test.

5.4.8 DNMT1 interaction studies

5.4.8.1 CoIP preliminary gel and Mass Spectrometry data

Before performing mass spectrometry, the samples obtained through CoIP were ran on a preliminary gel (**Figure 5.56**). A DNMT1 band could not be detected in either of the mitochondrial DNMT1-overexpressed CoIP samples (IgG- and HA-incubated samples), whereas a clear band could be observed in the nuclear DNMT1-overexpressed (HA) sample. Then, mass spectrometry was performed. The signal was expressed as a quantitative value, normalised on total spectra signals.

The signal for the mitochondrial DNMT1-overexpressed CoIP samples (IgG and HA-IP) was equal to the one obtained from the eGFP-overexpressed CoIP

samples (**Table 5.16**). That is, the amount of DNMT1 obtained from this samples after HA immune precipitation was negligible compared to the negative control. Since the point of this study was to investigate the ability of the mitochondrial DNMT1 isoform to bind to a potential co-factor required for mtDNA methylation (and further perform double overexpression experiments after identifying this co-factor), it was concluded that this CoIP-MS experiment was unsuccessful.

There might be different reasons which caused this: first of all, it is possible that something went wrong during one of the CoIP steps. It is also possible that, even though little to no DNMT1 signal could be observed in the mtDNMT1 (HA) pre-MS gel, some mtDNMT1 was immunoprecipitated during the CoIP step, but the software for MS analysis failed to recognize mtDNMT1 sequence as an actual DNMT1 sequence.

Finally, mtDNMT1 overexpression in MCE cells might require a more stable way of overexpression, i.e. developing a MCE-mtDNMT1 stable overexpression cell line through lentivirus infection. Given more time, the hypothesis of a mtDNMT1 co-factor for enhanced mtDNA methylation should be investigated with the aforementioned conditions.

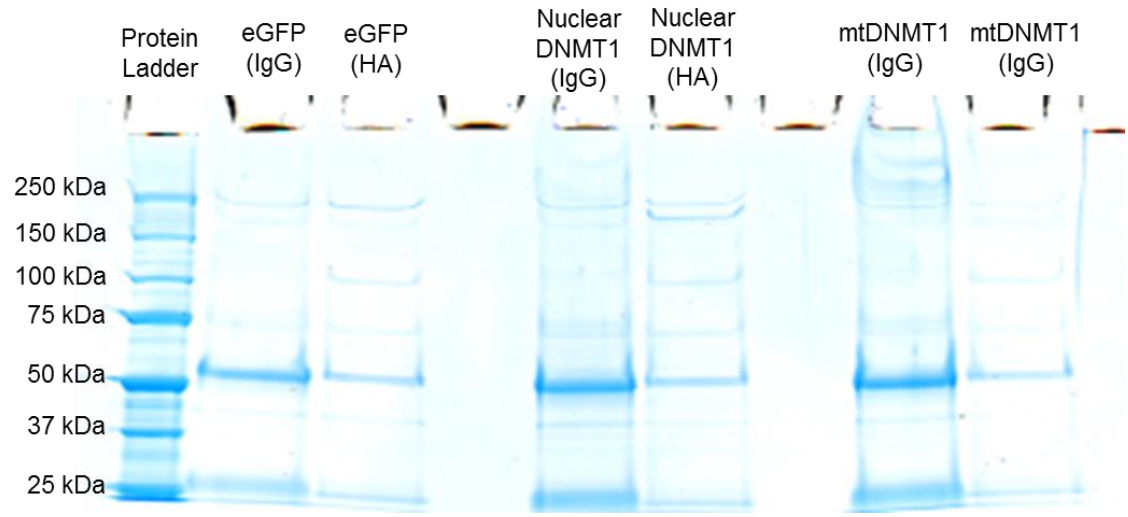

Figure 5.56: Pre-Mass spectrometry agarose gel for CoIP samples.

Table 5.16: Mass spectrometry results after CoIP. Signal is expressed as a quantitative value, normalised on total spectra. Samples mtDNMT1 (IgG) and mtDNMT1 (HA) were loaded twice.

Identified Protein	Accession Number	Molecular Weight	eGFP (IgG) signal	eGFP (HA) signal	Nuclear DNMT1 (IgG) signal	Nuclear DNMT1 (HA) signal	mtDNMT1 (IgG) signal	mtDNMT1 (IgG) signal	mtDNMT1 (HA) signal	mtDNMT1 (HA) signal
DNA (cytosine-5)-methyltransferase 1	sp|P13864| DNMT1_MOUSE	183 kDa	3	3	361.44	362.55	3	3	3	3

5.5 Discussion

In this chapter, in order to achieve higher DNMT1 overexpression and evaluate its effects on mtDNA methylation, adenoviral vectors for nuclear DNMT1, mitochondrial DNMT1 and DNMT3A were generated through BP and LR clonase reactions. After generating adenoviral particles through HEK293A and performing titration, preliminary overexpression experiments were performed on H9C2 cells. Indeed, a certain level of overexpression could be found for every adenoviral vector, with Adeno-DNMT3A showing a really high degree of overexpression.

At this point, the adenoviral vectors were shipped to Prof. Zeisberg's laboratory in Goettingen, where the preliminary MeDIP studies were performed. Once there, optimization of MOI was performed in a Mouse Cardiac Endothelial (MCE) cell line through and Adeno-GFP vector carrying the same backbone of the other adenoviral vectors (serotype V); a MOI of 10 resulted in more than 95% infection efficiency.

After this, primers for qPCR of D-Loop sequences after MeDIP were designed through in silico PCR online tools. The primers were designed to obtain almost 100% coverage of the whole D-Loop, but full coverage could not be obtained due to designing constraints. The primers were then successfully validated through both PCR and qPCR using B6 mice genomic DNA as a template, and their specificity to mitochondrial sequences was further confirmed through qPCR using both genomic and mitochondrial DNA obtained from MCE cells. All of the D-Loop primer sets showed high affinity and specificity for mitochondrial-only sequences, confirming the prediction from the in silico PCR software in regards to their inability to amplify for NUMTs[175,176].

Then, infection of MCE cells using Adeno-GFP, Adeno-nuclear DNMT1 and Adeno-mtDNMT1 was performed, and a first round of MeDIP-qPCR experiments

was performed using the D-Loop primer sets and using mtDNA samples obtained from infected MCE cells as a template. Overall, the infection with Adeno-mitochondrial DNMT1 resulted in a 3-to-5 fold increase in CpG methylation compared to Adeno-GFP. However, the total % of methylation compared to the input samples was still below 1%.

After performing these experiments, I returned to London where I completed the remaining experiments described in this chapter. A sonication system with a new model of sonicator was set up, and the sonication step was optimised again using DNA samples from several origins (B6 mouse genomic DNA, MCEC genomic DNA, pCMV-SPORT6-Nuclear DNMT1, pCMV-SPORT6-Mitochondrial DNMT1). After identifying the best sonication conditions, several rounds of MeDIP-qPCR were performed, but most failed due to no amplification of the samples after qPCR.

In the successfully completed round of MeDIP-qPCR, some of the primer set samples (#1 and #5) failed to show a good amplification pattern, even though their affinity to mitochondrial DNA sequences was validated thoroughly. In these samples, the Ct value did not allow to calculate a fold-increase in methylation.

In the Adeno-mitochondrial DNMT1 infected samples, the primer sets #2 and #4 samples showed a 5-to-15 fold-increase compared to the Adeno-eGFP infected samples, whereas primer set #3 did not show any evident fold-increase. In the Adeno-nuclear DNMT1 infected sample, the primer set #2 and #4 samples showed a 7- and 2-fold increase in CpG methylation compared to the Adeno-eGFP samples, respectively.

The results obtained in London were then combined with the results obtained in Goettingen, but statistical analysis could not be performed due to restricted sample size. In the case of primer sets #1 (for nuclear DNMT1-overexpressed

samples) and #5 (for nuclear DNMT1- and mitochondrial DNMT1-overexpressed samples), the fold-increase could not be calculated after the experiments performed in London due to the absence of signal in the replicates. Overall, the establishment of the MeDIP-qPCR protocol proved to be more complicated than expected, looking promising but still far from being reliable and replicable.

It is possible that this method might not be ideal for investigation of mtDNA sequences as the absence of CpG islands might pose a problem in the reliability and replication of results, as the system might not be sensitive enough to pick up changes that fluctuate below 5%. This might be due to the fact that the MeDIP method relies on the binding specificity and affinity of the monoclonal anti-5-methylcytosine antibody, which has better binding efficiency onto high-density of nearby methylated CpG sites[177]. It is also possible that a higher yield of mtDNA (1-2 µg or more) might be required before MeDIP can be performed in order to avoid loss of amplification and data, however the MeDIP kit is not optimised to handle amounts over 1 µg, and this might also pose a problem in terms of replicability.

In the previous chapter, DNA methylation of mtDNA sequences following plasmid overexpression of DNMT1 isoforms showed a low ratio compared to the control. We wondered whether the reason was the low transfection ratio achieved through plasmid transfection, so adenoviral vectors were obtained. However, even though the infection efficiency of adenoviral vectors is high, the transient infection and overexpression time might still not be enough to exert an effect on the methylation status of mtDNA sequences.

To verify this hypothesis, a lentivirus for mitochondrial DNMT1 stable overexpression in MCEC was generated. After many months of cloning, the final sequence was obtained and lentiviral particles were generated and titrated. After

infecting MCE cells and selecting infected cells through puromycin selection, the overexpression of mtDNMT1 was investigated through Western blotting.

The DNMT1 overexpression was not statistically significant. This might mean either that there might have been problems during the packaging of the lentiviral particles, as the pLenti-puro-mtDNMT1 sequence is over 10 kbp long[178], or that the overexpressed isoform is not stable enough. Furthermore, it is possible that the level of DNMT1 overexpression achieved with this method is not high enough to be detected, or that the overexpressed protein is not stable enough and, as the overexpression is not as potent as the one achieved through plasmid or adenovirus, it gets degraded before it can be detected.

Finally, in an attempt to further elucidate mtDNMT1 role in mitochondria, I started working on the identification of potential DNMT1 co-factors for mtDNA methylation. However, the first CoIP-MS attempt failed to show overexpression bands in mtDNMT1-transfected samples, so the mass spectrometry analysis was not performed.

Chapter 6 : General Discussion

6.1 General overview of findings

This study represents one of the first attempts at elucidating the role of mtDNMT1 on the methylation status of mtDNA. Since it has been reported that mtDNA is involved in heart failure through TLR9 stimulation by unmethylated CpG motifs[34,36,179] and that DNMT1 sequence contains an MLS[90] and might be able to localise at a mitochondrial level, the purpose of this study was to investigate whether it was possible for mtDNMT1 to localise in mitochondria, increase mtDNA methylation and limit TLR9 stimulation.

Overexpression plasmids for DNMT1 isoforms were initially obtained, and allowed to confirm the data from the bibliography as well as to shed more light on the role of the predicted NLS and MLS to effectively allow for DNMT1 nuclear or mitochondrial localisation, respectively. Disruption of NLS resulted in inability of DNMT1 to localise at nuclear level, and most importantly, by adding the MLS to DNMT1 it has been possible to obtain mitochondrial localisation of this protein.

These plasmids are not commercially available and represent a starting point to obtain gold standard DNMT1 overexpression plasmids to study the role of mitochondrial epigenetics in cardiovascular research as well as in other fields[134]. Moreover, these vectors have been used to generate adenoviral and lentiviral vectors for mtDNMT1, which are also not commercially available. These vectors are also important for the field as they might allow for more efficient and stable overexpression of the mtDNMT1 isoform.

This study also allowed to shed some light in regards to the role of methylation in mtDNA. The presence of methylation in mtDNA has always remained controversial over the years[132,133,138,140], and this study identified some of the reasons why this has been the case. As shown in the results chapters, it emerged how important it is to use linearized mtDNA for mtDNA methylation analysis, and

that the basal level of CpG methylation in mtDNA is below 1%. By not digesting the mtDNA prior to bisulphite treatment, the circular form of the DNA can shield it from the base conversion operated by bisulphite, thereby increasing the amount of falsely non-converted C residues in their sequences. It is therefore critical to make sure that mtDNA is fully digested prior to methylation analysis in order to maximise the activity of bisulphite treatment.

Since no comments in regards to the linearization of mtDNA were found in many papers claiming high methylation of mtDNA sequences[52,132,133,180], it is likely that circular mtDNA was used, suggesting that the data shown is an artefact. To further support this hypothesis, a comparison between circular and linear mtDNA was recently reported[150].

The study has also shown how it is possible to investigate the methylation status of mitochondrial sequences through the MeDIP-qPCR protocols. Since it has been shown that almost all of the mitochondrial DNA is duplicated into the genomic DNA in the form of NUMTs[175,176], this study has achieved unbiased MeDIP-qPCR methylation analysis by removing 2 of the main issues undermining the analysis.

First, a two-steps fractioning and DNA extraction of the samples to obtain pure mtDNA samples, and second, performing MeDIP of mtDNA sequences through design of qPCR primers that can specifically target the sequences of interest (i.e. D-Loop) without amplifying genomic DNA sequences. The qPCR primers were tested and their specificity to mtDNA sequences was confirmed thoroughly. Methylation analysis of D-Loop sequences following MeDIP-qPCR experiments highlighted a fold-increase in the methylation ratio of immunoprecipitated D-Loop sequences compared to the Input, however these results proved difficult to replicate and interpret. Since MeDIP is based on the interaction between an

antibody and 5mC, and it has been shown that its affinity and specificity increase the more CpG residues are present on a given sequence[177], it is possible that this protocol might not be specific enough to yield true and consistent data.

Finally, this study took the first steps toward obtaining a cell line with stable mtDNMT1 overexpression through lentivirus infection, as well as trying to elucidate whether a co-factor is required to obtain mtDNMT1-mtDNA binding and increased methylation of mtDNA sequences. Overall, the data obtained suggests that the regulation of mitochondrial epigenetics is more complicated than originally thought, and further efforts will be required to elucidate it.

6.2 Clinical implications of mtDNA methylation

In the UK, more than a quarter of deaths (160,000 each year) result from cardiovascular diseases (CVD) and an estimated 7 million people suffer from CVD (British Heart Foundation statistics, 2016). It is therefore essential to understand the mechanisms that underline CVD in order to identify potential therapeutic targets. The inflammatory response observed in CVD can propagate disease development and ultimately lead to heart failure[34]. Circulating mitochondrial DNA in the form of unmethylated CpG motifs was linked to TLR9 stimulation and the inflammation process which contributes to heart failure[36]. Although the activity of DNMT1 on mtDNA could not be fully elucidated in this study, we can speculate about a protective role during pressure overload and mitophagy. Since there have been reports about how DNMT1 can have other non-catalytic functions[181] and cooperate with DNMT3A in order to achieve de novo methylation[182], the role of DNMT1 in a mitochondrial environment might be to act as a de novo methyltransferase and introduce methyl groups on mtDNA CpG residues, resulting in less TLR9 stimulation. By elucidating the role of DNMT1 at a mitochondrial level, it would be possible to design drugs that increase methylation of mtDNA without impacting the methylation status of gDNA, thereby reducing TLR9 stimulation following pressure overload and release of inflammatogenic mtDNA unmethylated CpG motifs (**Figure 6.1**). Therefore, targeting mtDNA by modifying its methylation status at certain time points could be a potential therapeutic approach to prevent heart failure.

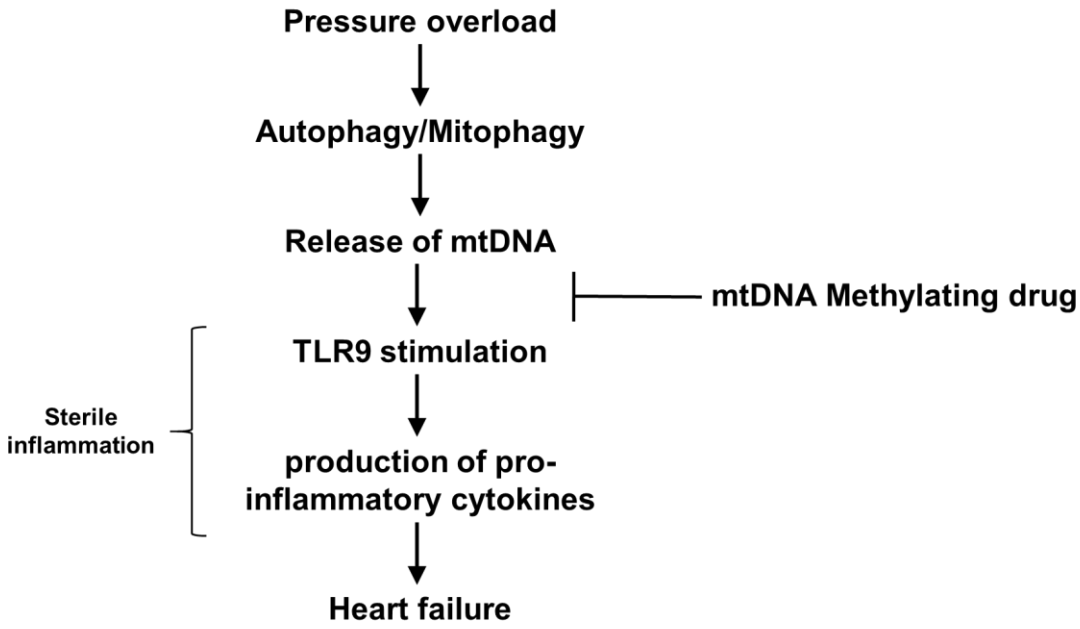

Figure 6.1: Proposed molecular mechanism of action for a methylating agent.

6.3 Study limitations

In this study, plasmid and adenoviral overexpression systems for several DNMT1 isoforms were established, and methylation analysis in the form of sequencing after bisulphite treatment and MeDIP-qPCR was performed. However, no changes in the methylation pattern of mtDNA sequences could be found. The reasons for this are many and involve several steps which might need to be further refined.

First, overexpression of mtDNMT1 does not appear to be very strong (especially after plasmid transfection where the transfection efficiency is about 20-30%), and it is possible that the protein is degraded after overexpression. Moreover, transient overexpression of mtDNMT1 might not be enough to elicit changes in the methylation pattern of mtDNA, and more stable and persistent overexpression might be required instead. Hence, overexpression of mtDNMT1 through plasmid and adenoviral vectors might have to be abandoned in favour of a lentiviral vector system.

Second, the systems used in this study for methylation analysis both have their limits as they are not high-throughput and require several steps. Bisulphite sequencing could not find any methylation after overexpression of nDNMT1, mtDNMT1, DNMT3A or mtDNMT1-DNMT3A in the investigated sequences (COX2 and part of the D-Loop). The protocol is fully optimized to avoid false positives as it includes linearization through HindIII digestion and has single base resolution, however it requires design of specific primers, and the ones used could not be screened for affinity for NUMTs, as they only amplify converted sequences.

The MeDIP-qPCR protocol was used on mtDNA sequences for the first time, but appears to be not fully optimized. The primer sets used have been designed to have unique affinity with mtDNA sequences and none with gDNA sequences (i.e. NUMTs are not amplified) so there are no false positives, however the results obtained were not consistent and replicable. In the future, more concentrated samples might be required as the yield for mtDNA is usually quite low even with a big starting sample (which requires a high amount of adenovirus, hence obtaining a stable overexpression system to eliminate this issue appears to be critical). Furthermore, another issue with this system is that it might not be sensitive enough to detect changes in single CpG residues, as it was initially designed to detect changes in areas with very high CpG content (i.e. CpG islands in gDNA)[177].

6.4 Future work

Another possible limitation of this study is the protective effect that nucleoid proteins[183-185] within mitochondria might have in regards to epigenetic modifications. It is possible that proteins such as TFAM[186] (the main component of nucleoid structures) might shield mtDNA from being methylated by DNMT1.

The first step to further elucidate the role of mtDNMT1 at a mitochondrial level should be to establish a reliable and stable overexpression system for this protein. That is, by obtaining a lentiviral vector that can achieve mtDNMT1 cDNA integration within the host genome and reliably overexpress it, it will be possible to study the long-term effects of mtDNMT1 overexpression on mtDNA methylation.

Once established stable overexpression, methylation analysis through bisulphite sequencing and MeDIP-qPCR should be performed again to test whether the limitations of these systems can be overcome. In this regard, performing TFAM knock-down before methylation analysis might also allow to test the hypothesis of TFAM having a protective role in regards to mtDNA methylation by mtDNMT1.

Furthermore, investigation of mitochondrial co-factors for mtDNMT1 should be performed through Co-IP and mass spectrometry analysis.

Finally, achieving stable overexpression will allow to study whether mtDNMT1 can limit TLR9 stimulation following treatment with compounds that mimic pressure overload and inhibit oxidative phosphorylation, i.e. Angiotensin II and Carbonyl Cyanide m-Chlorophenyl Hydrazone (CCCP).

6.4.1 TFAM silencing in MCE cells

To investigate whether TFAM shielding is the cause of mtDNA protection from methylation, a set of TFAM knock-down experiments in MCE cells was performed as a preliminary study. MCE cells were seeded in a 6 well plates and immediately transfected with 3 different Silencer® Select TFAM siRNAs (ThermoFisher Scientific®, 4390771) as well as a Silencer® Select Negative Control No. 1 scramble siRNA (ThermoFisher Scientific®, 4390843), using Lipofectamine® RNAiMAX (ThermoFisher Scientific®, 13778075) as a transfection reagent. Briefly, the Lipofectamine® RNAiMAX and the siRNAs were diluted in Opti-MEM™ reduced serum medium (Thermo Fisher Scientific™, 31985070) according to the protocol and incubated at room temperature for 10 minutes, then the siRNA-lipid complexes were added to the cells which were then incubated for 2 days at 37ºC. After 1 day, the medium was replaced to culturing medium, and the cells were harvested 48 hours after transfection.

Proteins were extracted from the pellets and quantified, and Western blotting using an Anti-TFAM antibody (Abcam®, ab131607) was performed (**Figure 6.2**). All TFAM siRNAs screened managed to achieve a significant knock-down of TFAM (N=3, $p < 0.001$ or better) (**Figure 6.3**).

Therefore, the transfection conditions used in this preliminary study, as well as all of the screened TFAM siRNAs represent a good starting point for investigation of TFAM protective role in regards to mtDNA methylation by mtDNMT1. Should methylation analysis following TFAM knock-down and mtDNMT1 overexpression show a significant increase in methylation levels of mtDNA sequences, the following steps will involve investigating the expression of mitochondrial proteins, as well as the expression of proinflammatory cytokines following AngII and CCCP treatment.

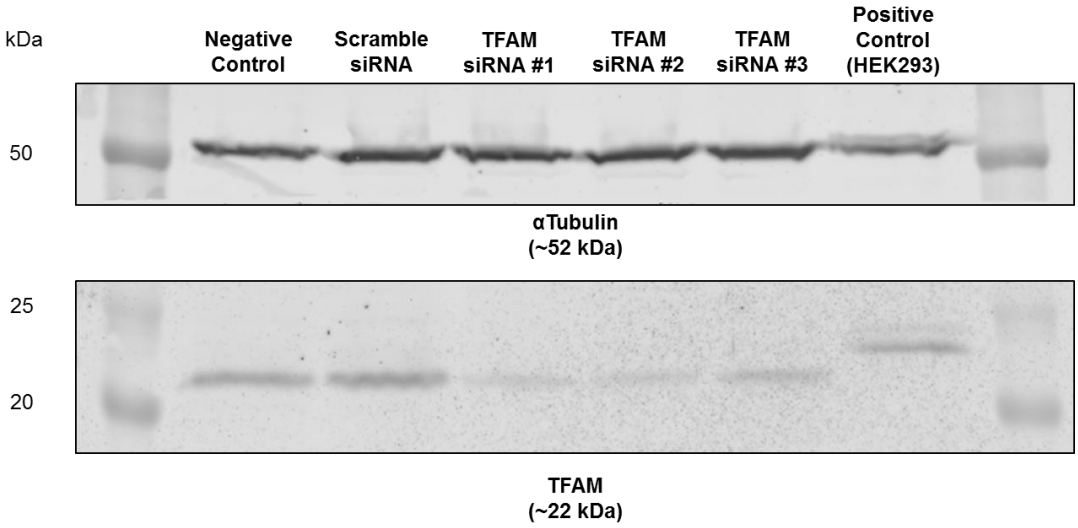

Figure 6.2: Western blot of MCEC samples after 48 hours TFAM knock-down.

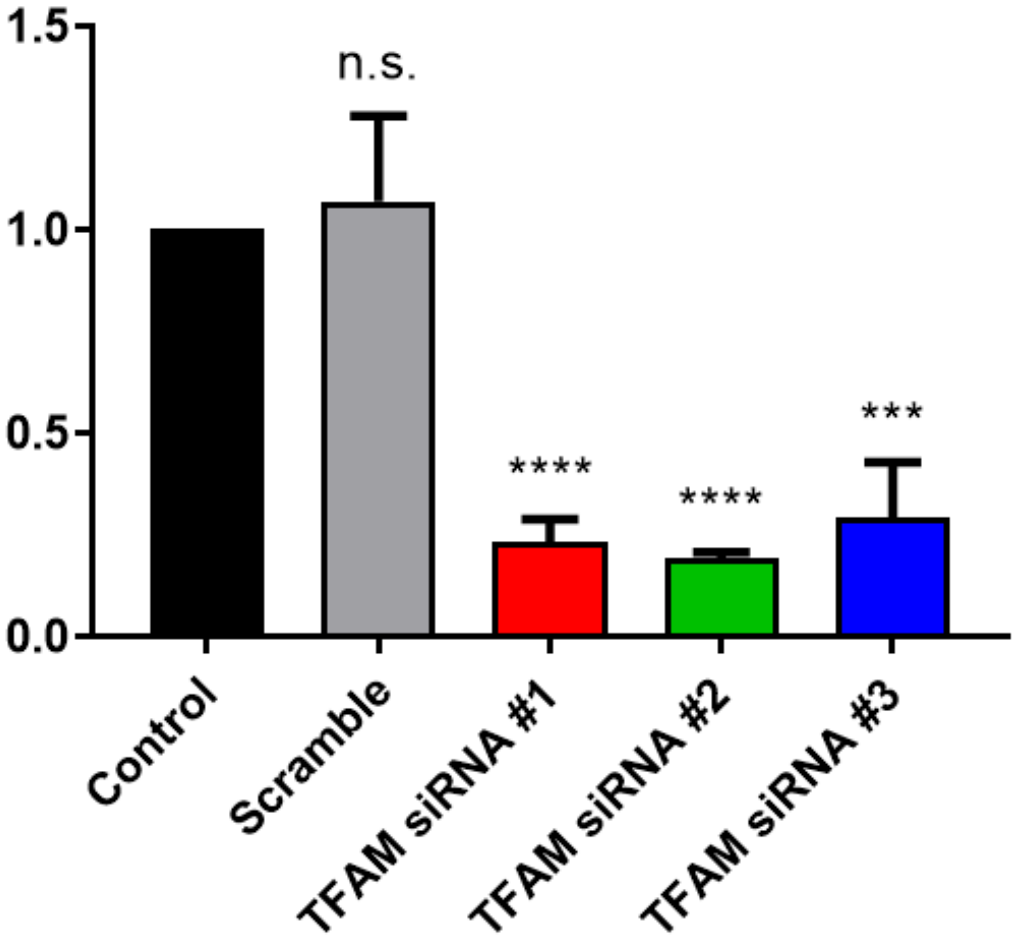

Figure 6.3: Statistical analysis of TFAM knock-down after 48 hours. T-test statistical analysis. N = 3. *** = $p < 0.001$; **** = $p < 0.0001$.

6.5 Conclusions

In conclusion, the work presented in this thesis was an attempt to elucidate the role of mtDNMT1 on mtDNA methylation. Herein, several plasmids, adenoviral and lentiviral constructs were generated and methylation analysis of mtDNA sequences was carried on using both bisulphite sequencing and MeDIP-qPCR analysis. I have demonstrated that the 1st-to-3rd ATG DNMT1 sequence can act as a mitochondrial localisation signal and that a preserved NLS is indeed required for nuclear localisation of this protein. Although many efforts to increase methylation of mtDNA sequences were made, it was not possible to observe any changes in this regard.

Moreover, it is still unclear whether the absence of changes in the methylation pattern is due to insufficient overexpression, whether a co-factor is necessary or whether some of the nucleoid proteins have a protective effect in this regard. It is worth mentioning that all the experiments in this study have been performed under overexpression conditions rather than through pressure overload and inhibition of oxidative phosphorylation conditions via treatment with stimuli (i.e. AngII, CCCP) in an attempt to maximize the efficiency of DNMT1 at a mitochondrial level.

Taken together, the results presented in this thesis provide a necessary experimental starting point to further clarity to the role of mtDNMT1 at a mitochondrial level and its potential role in reducing TLR9 stimulation after pressure overload, with the potential to inspire the design of methylating drugs to reduce inflammation and improve the prognosis of patients with heart failure.

Chapter 7 : Bibliography

1 Coronel, R., de Groot, J. R. & Van Lieshout, J. J. Defining heart failure. *Cardiovascular research* **50**, 419-422 (2001).

2 Medzhitov, R. Origin and physiological roles of inflammation. *Nature* **454**, 428-435, doi:10.1038/nature07201 (2008).

3 Mann, D. L. Inflammatory mediators and the failing heart: past, present, and the foreseeable future. *Circulation research* **91**, 988-998 (2002).

4 Yndestad, A. *et al.* Systemic inflammation in heart failure--the whys and wherefores. *Heart failure reviews* **11**, 83-92, doi:10.1007/s10741-006-9196-2 (2006).

5 Jessup, M. & Brozena, S. Heart failure. *The New England journal of medicine* **348**, 2007-2018, doi:10.1056/NEJMra021498 (2003).

6 Pazos-Lopez, P. *et al.* The causes, consequences, and treatment of left or right heart failure. *Vascular health and risk management* **7**, 237-254, doi:10.2147/VHRM.S10669 (2011).

7 Owan, T. E. *et al.* Trends in prevalence and outcome of heart failure with preserved ejection fraction. *The New England journal of medicine* **355**, 251-259, doi:10.1056/NEJMoa052256 (2006).

8 Borlaug, B. A. & Paulus, W. J. Heart failure with preserved ejection fraction: pathophysiology, diagnosis, and treatment. *European heart journal* **32**, 670-679, doi:10.1093/eurheartj/ehq426 (2011).

9 McMurray, J. J. *et al.* ESC guidelines for the diagnosis and treatment of acute and chronic heart failure 2012: The Task Force for the Diagnosis and Treatment of Acute and Chronic Heart Failure 2012 of the European Society of Cardiology. Developed in collaboration with the Heart Failure Association (HFA) of the ESC. *European journal of heart failure* **14**, 803-869, doi:10.1093/eurjhf/hfs105 (2012).

10 Voelkel, N. F. *et al.* Right ventricular function and failure: report of a National Heart, Lung, and Blood Institute working group on cellular and molecular mechanisms of right heart failure. *Circulation* **114**, 1883-1891, doi:10.1161/CIRCULATIONAHA.106.632208 (2006).

11 Gheorghiade, M. & Bonow, R. O. Chronic heart failure in the United States: a manifestation of coronary artery disease. *Circulation* **97**, 282-289 (1998).

12 McMullen, J. R. J., G. L. Differences between pathological and physiological cardiac hypertrophy: novel therapeutic strategies to treat heart failure. *Clinical and experimental pharmacology & physiology* **34**, 255-262 (2007).

13 Heineke, J. & Molkentin, J. D. Regulation of cardiac hypertrophy by intracellular signalling pathways. *Nature reviews. Molecular cell biology* **7**, 589-600, doi:10.1038/nrm1983 (2006).

14 Komuro, I. & Yazaki, Y. Control of cardiac gene expression by mechanical stress. *Annual review of physiology* **55**, 55-75, doi:10.1146/annurev.ph.55.030193.000415 (1993).

15 Kehat, I. & Molkentin, J. D. Molecular pathways underlying cardiac remodeling during pathophysiological stimulation. *Circulation* **122**, 2727-2735, doi:10.1161/CIRCULATIONAHA.110.942268 (2010).

16 Frey, N., Katus, H. A., Olson, E. N. & Hill, J. A. Hypertrophy of the heart: a new therapeutic target? *Circulation* **109**, 1580-1589, doi:10.1161/01.CIR.0000120390.68287.BB (2004).

17 Haider, A. W., Larson, M. G., Benjamin, E. J. & Levy, D. Increased left ventricular mass and hypertrophy are associated with increased risk for sudden death. *Journal of the American College of Cardiology* **32**, 1454-1459 (1998).
18 Akira, S., Uematsu, S. & Takeuchi, O. Pathogen recognition and innate immunity. *Cell* **124**, 783-801, doi:10.1016/j.cell.2006.02.015 (2006).
19 Mogensen, T. H. Pathogen recognition and inflammatory signaling in innate immune defenses. *Clinical microbiology reviews* **22**, 240-273, Table of Contents, doi:10.1128/CMR.00046-08 (2009).
20 Eisen, A., Benderly, M., Behar, S., Goldbourt, U. & Haim, M. Inflammation and future risk of symptomatic heart failure in patients with stable coronary artery disease. *American heart journal* **167**, 707-714, doi:10.1016/j.ahj.2014.01.008 (2014).
21 Aderem, A. & Ulevitch, R. J. Toll-like receptors in the induction of the innate immune response. *Nature* **406**, 782-787, doi:10.1038/35021228 (2000).
22 Lemaitre, B., Nicolas, E., Michaut, L., Reichhart, J. M. & Hoffmann, J. A. The dorsoventral regulatory gene cassette spatzle/Toll/cactus controls the potent antifungal response in Drosophila adults. *Cell* **86**, 973-983 (1996).
23 Akira, S. & Takeda, K. Toll-like receptor signalling. *Nature reviews immunology* **4**, 499-511, doi:10.1038/nri1391 (2004).
24 Bowie, A. & O'Neill, L. A. The interleukin-1 receptor/Toll-like receptor superfamily: signal generators for pro-inflammatory interleukins and microbial products. *Journal of leukocyte biology* **67**, 508-514 (2000).
25 Kawai, T. & Akira, S. The role of pattern-recognition receptors in innate immunity: update on Toll-like receptors. *Nature immunology* **11**, 373-384, doi:10.1038/ni.1863 (2010).
26 Cuervo, A. M. Autophagy: many paths to the same end. *Molecular and cellular biochemistry* **263**, 55-72 (2004).
27 Kuma, A. *et al.* The role of autophagy during the early neonatal starvation period. *Nature* **432**, 1032-1036, doi:10.1038/nature03029 (2004).
28 Komatsu, M. *et al.* Loss of autophagy in the central nervous system causes neurodegeneration in mice. *Nature* **441**, 880-884, doi:10.1038/nature04723 (2006).
29 Mizushima, N. Autophagy: process and function. *Genes & development* **21**, 2861-2873, doi:10.1101/gad.1599207 (2007).
30 Mizushima, N. The pleiotropic role of autophagy: from protein metabolism to bactericide. *Cell death & differentiation* **12 Suppl 2**, 1535-1541, doi:10.1038/sj.cdd.4401728 (2005).
31 Miyata, S. *et al.* Autophagic cardiomyocyte death in cardiomyopathic hamsters and its prevention by granulocyte colony-stimulating factor. *The American journal of pathology* **168**, 386-397, doi:10.2353/ajpath.2006.050137 (2006).
32 Dammrich, J. & Pfeifer, U. Cardiac hypertrophy in rats after supravalvular aortic constriction. II. Inhibition of cellular autophagy in hypertrophying cardiomyocytes. *Virchows Archiv. B, Cell pathology including molecular pathology* **43**, 287-307 (1983).
33 Nakai, A. *et al.* The role of autophagy in cardiomyocytes in the basal state and in response to hemodynamic stress. *Nature medicine* **13**, 619-624, doi:10.1038/nm1574 (2007).

34 Nakayama, H. & Otsu, K. Translation of hemodynamic stress to sterile inflammation in the heart. *Trends in endocrinology & metabolism* **24**, 546-553, doi:10.1016/j.tem.2013.06.004 (2013).
35 Ahmad-Nejad, P. *et al.* Bacterial CpG-DNA and lipopolysaccharides activate Toll-like receptors at distinct cellular compartments. *European journal of immunology* **32**, 1958-1968, doi:10.1002/1521-4141(200207)32:7<1958::AID-IMMU1958>3.0.CO;2-U (2002).
36 Oka, T. *et al.* Mitochondrial DNA that escapes from autophagy causes inflammation and heart failure. *Nature* **485**, 251-255, doi:10.1038/nature10992 (2012).
37 Gray, M. W. Mitochondrial evolution. *Cold Spring Harbor perspectives in biology* **4**, a011403, doi:10.1101/cshperspect.a011403 (2012).
38 Sickmann, A. *et al.* The proteome of Saccharomyces cerevisiae mitochondria. *Proceedings of the National Academy of Sciences of the United States of America* **100**, 13207-13212, doi:10.1073/pnas.2135385100 (2003).
39 Pagliarini, D. J. *et al.* A mitochondrial protein compendium elucidates complex I disease biology. *Cell* **134**, 112-123, doi:10.1016/j.cell.2008.06.016 (2008).
40 Gray, M. W. & Doolittle, W. F. Has the endosymbiont hypothesis been proven? *Microbiological reviews* **46**, 1-42 (1982).
41 Embley, T. M. & Martin, W. Eukaryotic evolution, changes and challenges. *Nature* **440**, 623-630, doi:10.1038/nature04546 (2006).
42 Anderson, S. *et al.* Sequence and organization of the human mitochondrial genome. *Nature* **290**, 457-465 (1981).
43 Falkenberg, M., Larsson, N. G. & Gustafsson, C. M. DNA replication and transcription in mammalian mitochondria. *Annual review of biochemistry* **76**, 679-699, doi:10.1146/annurev.biochem.76.060305.152028 (2007).
44 Mootha, V. K. *et al.* Integrated analysis of protein composition, tissue diversity, and gene regulation in mouse mitochondria. *Cell* **115**, 629-640 (2003).
45 Andersson, S. G., Karlberg, O., Canback, B. & Kurland, C. G. On the origin of mitochondria: a genomics perspective. *Philosophical transactions of the Royal Society of London. Series B, Biological sciences* **358**, 165-177; discussion 177-169, doi:10.1098/rstb.2002.1193 (2003).
46 Popot, J. L. & de Vitry, C. On the microassembly of integral membrane proteins. *Annual review of biophysics and biophysical chemistry* **19**, 369-403, doi:10.1146/annurev.bb.19.060190.002101 (1990).
47 Sutovsky, P. *et al.* Ubiquitin tag for sperm mitochondria. *Nature* **402**, 371-372, doi:10.1038/46466 (1999).
48 Kaneda, H. *et al.* Elimination of paternal mitochondrial DNA in intraspecific crosses during early mouse embryogenesis. *Proceedings of the National Academy of Sciences of the United States of America* **92**, 4542-4546 (1995).
49 Bogenhagen, D. & Clayton, D. A. Mouse L cell mitochondrial DNA molecules are selected randomly for replication throughout the cell cycle. *Cell* **11**, 719-727 (1977).
50 Scarpulla, R. C. Transcriptional paradigms in mammalian mitochondrial biogenesis and function. *Physiological reviews* **88**, 611-638, doi:10.1152/physrev.00025.2007 (2008).

51 Pollack, Y., Kasir, J., Shemer, R., Metzger, S. & Szyf, M. Methylation pattern of mouse mitochondrial DNA. *Nucleic acids research* **12**, 4811-4824 (1984).
52 Cardon, L. R., Burge, C., Clayton, D. A. & Karlin, S. Pervasive CpG suppression in animal mitochondrial genomes. *Proceedings of the National Academy of Sciences of the United States of America* **91**, 3799-3803 (1994).
53 Collins, L. V., Hajizadeh, S., Holme, E., Jonsson, I. M. & Tarkowski, A. Endogenously oxidized mitochondrial DNA induces in vivo and in vitro inflammatory responses. *Journal of leukocyte biology* **75**, 995-1000, doi:10.1189/jlb.0703328 (2004).
54 Cossarizza, A. *et al.* Increased plasma levels of extracellular mitochondrial DNA during HIV infection: a new role for mitochondrial damage-associated molecular patterns during inflammation. *Mitochondrion* **11**, 750-755, doi:10.1016/j.mito.2011.06.005 (2011).
55 Hajizadeh, S., DeGroot, J., TeKoppele, J. M., Tarkowski, A. & Collins, L. V. Extracellular mitochondrial DNA and oxidatively damaged DNA in synovial fluid of patients with rheumatoid arthritis. *Arthritis research & therapy* **5**, R234-240, doi:10.1186/ar787 (2003).
56 Timmermans, K., Kox, M., Scheffer, G. J. & Pickkers, P. Plasma nuclear and mitochondrial DNA levels, and markers of inflammation, shock, and organ damage in patients with septic shock. *Shock* **45**, 607-612, doi:10.1097/SHK.0000000000000549 (2016).
57 McGill, M. R. *et al.* Serum mitochondrial biomarkers and damage-associated molecular patterns are higher in acetaminophen overdose patients with poor outcome. *Hepatology* **60**, 1336-1345, doi:10.1002/hep.27265 (2014).
58 Tsai, N. W. *et al.* The value of serial plasma nuclear and mitochondrial DNA levels in patients with acute ischemic stroke. *Clinica chimica acta* **412**, 476-479, doi:10.1016/j.cca.2010.11.036 (2011).
59 Wang, H. C. *et al.* The value of serial plasma nuclear and mitochondrial DNA levels in acute spontaneous intra-cerebral haemorrhage. *European journal of neurology* **19**, 1532-1538, doi:10.1111/j.1468-1331.2012.03761.x (2012).
60 Wang, H. C. *et al.* The value of serial plasma and cerebrospinal fluid nuclear and mitochondrial deoxyribonucleic acid levels in aneurysmal subarachnoid hemorrhage. *Journal of neurosurgery* **118**, 13-19, doi:10.3171/2012.8.JNS112093 (2013).
61 Kohler, C. *et al.* Levels of plasma circulating cell free nuclear and mitochondrial DNA as potential biomarkers for breast tumors. *Molecular cancer* **8**, 105, doi:10.1186/1476-4598-8-105 (2009).
62 Ellinger, J., Muller, S. C., Wernert, N., von Ruecker, A. & Bastian, P. J. Mitochondrial DNA in serum of patients with prostate cancer: a predictor of biochemical recurrence after prostatectomy. *BJU international* **102**, 628-632, doi:10.1111/j.1464-410X.2008.07613.x (2008).
63 Hou, Y. L. *et al.* Clinical significance of serum mitochondrial DNA in lung cancer. *Clinical biochemistry* **46**, 1474-1477, doi:10.1016/j.clinbiochem.2013.04.009 (2013).
64 Wang, L. *et al.* Plasma nuclear and mitochondrial DNA levels in acute myocardial infarction patients. *Coronary artery disease* **26**, 296-300, doi:10.1097/MCA.0000000000000231 (2015).

65 Qin, C. *et al.* Release of mitochondrial DNA correlates with peak inflammatory cytokines in patients with acute myocardial infarction. *The anatolian journal of cardiology*, doi:10.14744/AnatolJCardiol.2016.7209 (2016).
66 Liu, J. *et al.* Circulating cell free mitochondrial DNA is a biomarker in the development of coronary heart disease in the patients with type 2 diabetes. *Clinical laboratory* **61**, 661-667 (2015).
67 Liu, J. *et al.* Circulating cell-free mitochondrial deoxyribonucleic acid is increased in coronary heart disease patients with diabetes mellitus. *Journal of diabetes investigation* **7**, 109-114, doi:10.1111/jdi.12366 (2016).
68 Mizushima, N. *et al*. Autophagy fights disease through cellular self-digestion. *Nature* **451**, 1069-1075, doi:10.1038/nature06639 (2008).
69 Waterland, R. A. & Michels, K. B. Epigenetic epidemiology of the developmental origins hypothesis. *Annual review of nutrition* **27**, 363-388, doi:10.1146/annurev.nutr.27.061406.093705 (2007).
70 Maunakea, A. K., Chepelev, I. & Zhao, K. Epigenome mapping in normal and disease states. *Circulation research* **107**, 327-339, doi:10.1161/CIRCRESAHA.110.222463 (2010).
71 Gardner, K. E., Allis, C. D. & Strahl, B. D. Operating on chromatin, a colorful language where context matters. *Journal of molecular biology* **409**, 36-46, doi:10.1016/j.jmb.2011.01.040 (2011).
72 Djebali, S. *et al.* Landscape of transcription in human cells. *Nature* **489**, 101-108, doi:10.1038/nature11233 (2012).
73 Heard, E. & Disteche, C. M. Dosage compensation in mammals: fine-tuning the expression of the X chromosome. *Genes & development* **20**, 1848-1867, doi:10.1101/gad.1422906 (2006).
74 Reik, W. & Walter, J. Genomic imprinting: parental influence on the genome. *Nature reviews genetics* **2**, 21-32, doi:10.1038/35047554 (2001).
75 Otani, J. *et al.* Structural basis for recognition of H3K4 methylation status by the DNA methyltransferase 3A ATRX-DNMT3-DNMT3L domain. *EMBO reports* **10**, 1235-1241, doi:10.1038/embor.2009.218 (2009).
76 Weber, M. *et al.* Distribution, silencing potential and evolutionary impact of promoter DNA methylation in the human genome. *Nature genetics* **39**, 457-466, doi:10.1038/ng1990 (2007).
77 Mathers, J. C. Early nutrition: impact on epigenetics. *Forum of nutrition* **60**, 42-48, doi:10.1159/0000107066 (2007).
78 Heijmans, B. T. *et al.* Persistent epigenetic differences associated with prenatal exposure to famine in humans. *Proceedings of the National Academy of Sciences of the United States of America* **105**, 17046-17049, doi:10.1073/pnas.0806560105 (2008).
79 Yang, J. *et al.* Role of hypoxia-inducible factors in epigenetic regulation via histone demethylases. *Annals of the New York academy of sciences* **1177**, 185-197, doi:10.1111/j.1749-6632.2009.05027.x (2009).
80 Consortium, E. P. The ENCODE (ENCyclopedia Of DNA Elements) project. *Science* **306**, 636-640, doi:10.1126/science.1105136 (2004).
81 Consortium, E. P. An integrated encyclopedia of DNA elements in the human genome. *Nature* **489**, 57-74, doi:10.1038/nature11247 (2012).
82 Inbar-Feigenberg, M., Choufani, S., Butcher, D. T., Roifman, M. & Weksberg, R. Basic concepts of epigenetics. *Fertility and sterility* **99**, 607-615, doi:10.1016/j.fertnstert.2013.01.117 (2013).

83 Lee, T. F., Zhai, J. & Meyers, B. C. Conservation and divergence in eukaryotic DNA methylation. *Proceedings of the National Academy of Sciences of the United States of America* **107**, 9027-9028, doi:10.1073/pnas.1005440107 (2010).
84 Dodge, J. E., Ramsahoye, B. H., Wo, Z. G., Okano, M. & Li, E. De novo methylation of MMLV provirus in embryonic stem cells: CpG versus non-CpG methylation. *Gene* **289**, 41-48 (2002).
85 Tahiliani, M. *et al.* Conversion of 5-methylcytosine to 5-hydroxymethylcytosine in mammalian DNA by MLL partner TET1. *Science* **324**, 930-935, doi:10.1126/science.1170116 (2009).
86 Kumar, S. *et al.* The DNA (cytosine-5) methyltransferases. *Nucleic acids research* **22**, 1-10 (1994).
87 Goll, M. G. *et al.* Methylation of tRNAAsp by the DNA methyltransferase homolog Dnmt2. *Science* **311**, 395-398, doi:10.1126/science.1120976 (2006).
88 Okano, M., Bell, D. W., Haber, D. A. & Li, E. DNA methyltransferases Dnmt3a and Dnmt3b are essential for de novo methylation and mammalian development. *Cell* **99**, 247-257 (1999).
89 Li, E., Bestor, T. H. & Jaenisch, R. Targeted mutation of the DNA methyltransferase gene results in embryonic lethality. *Cell* **69**, 915-926 (1992).
90 Shock, L. S., Thakkar, P. V., Peterson, E. J., Moran, R. G. & Taylor, S. M. DNA methyltransferase 1, cytosine methylation, and cytosine hydroxymethylation in mammalian mitochondria. *Proceedings of the National Academy of Sciences of the United States of America* **108**, 3630-3635, doi:10.1073/pnas.1012311108 (2011).
91 Yoder, J. A., Yen, R. W., Vertino, P. M., Bestor, T. H. & Baylin, S. B. New 5' regions of the murine and human genes for DNA (cytosine-5)-methyltransferase. *The journal of biological chemistry* **271**, 31092-31097 (1996).
92 Corella, D. & Ordovas, J. M. Aging and cardiovascular diseases: the role of gene-diet interactions. *Ageing research reviews* **18**, 53-73, doi:10.1016/j.arr.2014.08.002 (2014).
93 Karcher, J. R. *et al.* Genome-wide epigenetic and proteomic analysis reveals altered Notch signaling in EPC dysfunction. *Physiological reports* **3**, doi:10.14814/phy2.12358 (2015).
94 Manea, S. A., Constantin, A., Manda, G., Sasson, S. & Manea, A. Regulation of Nox enzymes expression in vascular pathophysiology: Focusing on transcription factors and epigenetic mechanisms. *Redox biology* **5**, 358-366, doi:10.1016/j.redox.2015.06.012 (2015).
95 Jiang, F., Zhou, X. & Huang, J. Long non-coding RNA-ROR mediates the reprogramming in cardiac hypertrophy. *PLoS One* **11**, e0152767, doi:10.1371/journal.pone.0152767 (2016).
96 Duygu, B., Poels, E. M. & da Costa Martins, P. A. Genetics and epigenetics of arrhythmia and heart failure. *Frontiers in genetics* **4**, 219, doi:10.3389/fgene.2013.00219 (2013).
97 Mahmoud, S. A. & Poizat, C. Epigenetics and chromatin remodeling in adult cardiomyopathy. *Journal of pathology* **231**, 147-157, doi:10.1002/path.4234 (2013).
98 Manev, H., Dzitoyeva, S. & Chen, H. Mitochondrial DNA: a blind spot in neuroepigenetics. *Biomolecular concepts* **3**, 107-115, doi:10.1515/bmc-2011-0058 (2012).

99 Dzitoyeva, S., Chen, H. & Manev, H. Effect of aging on 5-hydroxymethylcytosine in brain mitochondria. *Neurobiology of aging* **33**, 2881-2891, doi:10.1016/j.neurobiolaging.2012.02.006 (2012).
100 Sun, Z. *et al.* High-resolution enzymatic mapping of genomic 5-hydroxymethylcytosine in mouse embryonic stem cells. *Cell reports* **3**, 567-576, doi:10.1016/j.celrep.2013.01.001 (2013).
101 Chen, H., Dzitoyeva, S. & Manev, H. Effect of valproic acid on mitochondrial epigenetics. *European journal of pharmacology* **690**, 51-59, doi:10.1016/j.ejphar.2012.06.019 (2012).
102 Chestnut, B. A. *et al.* Epigenetic regulation of motor neuron cell death through DNA methylation. *Journal of neuroscience* **31**, 16619-16636, doi:10.1523/JNEUROSCI.1639-11.2011 (2011).
103 Iacobazzi, V., Castegna, A., Infantino, V. & Andria, G. Mitochondrial DNA methylation as a next-generation biomarker and diagnostic tool. *Molecular genetics and metabolism* **110**, 25-34, doi:10.1016/j.ymgme.2013.07.012 (2013).
104 Bestor, T. H. & Ingram, V. M. Two DNA methyltransferases from murine erythroleukemia cells: purification, sequence specificity, and mode of interaction with DNA. *Proceedings of the National Academy of Sciences of the United States of America* **80**, 5559-5563 (1983).
105 Song, J., Rechkoblit, O., Bestor, T. H. & Patel, D. J. Structure of DNMT1-DNA complex reveals a role for autoinhibition in maintenance DNA methylation. *Science* **331**, 1036-1040, doi:10.1126/science.1195380 (2011).
106 Cierpicki, T. *et al.* Structure of the MLL CXXC domain-DNA complex and its functional role in MLL-AF9 leukemia. *Nature structural & molecular biology* **17**, 62-68, doi:10.1038/nsmb.1714 (2010).
107 Allen, M. D. *et al.* Solution structure of the nonmethyl-CpG-binding CXXC domain of the leukaemia-associated MLL histone methyltransferase. *The EMBO journal* **25**, 4503-4512, doi:10.1038/sj.emboj.7601340 (2006).
108 Birke, M. *et al.* The MT domain of the proto-oncoprotein MLL binds to CpG-containing DNA and discriminates against methylation. *Nucleic acids research* **30**, 958-965 (2002).
109 Pradhan, M. *et al.* CXXC domain of human DNMT1 is essential for enzymatic activity. *Biochemistry* **47**, 10000-10009, doi:10.1021/bi8011725 (2008).
110 Leonhardt, H., Page, A. W., Weier, H. U. & Bestor, T. H. A targeting sequence directs DNA methyltransferase to sites of DNA replication in mammalian nuclei. *Cell* **71**, 865-873 (1992).
111 Schmidt, O., Pfanner, N. & Meisinger, C. Mitochondrial protein import: from proteomics to functional mechanisms. *Nature reviews molecular cell biology* **11**, 655-667, doi:10.1038/nrm2959 (2010).
112 Dolezal, P., Likic, V., Tachezy, J. & Lithgow, T. Evolution of the molecular machines for protein import into mitochondria. *Science* **313**, 314-318, doi:10.1126/science.1127895 (2006).
113 Neupert, W. & Herrmann, J. M. Translocation of proteins into mitochondria. *Annual reviews of biochemistry* **76**, 723-749, doi:10.1146/annurev.biochem.76.052705.163409 (2007).
114 Roise, D., Horvath, S. J., Tomich, J. M., Richards, J. H. & Schatz, G. A chemically synthesized pre-sequence of an imported mitochondrial protein can form an amphiphilic helix and perturb natural and artificial phospholipid bilayers. *The EMBO journal* **5**, 1327-1334 (1986).

115 Abe, Y. *et al.* Structural basis of presequence recognition by the mitochondrial protein import receptor Tom20. *Cell* **100**, 551-560 (2000).
116 Vogtle, F. N. *et al.* Global analysis of the mitochondrial N-proteome identifies a processing peptidase critical for protein stability. *Cell* **139**, 428-439, doi:10.1016/j.cell.2009.07.045 (2009).
117 Becker, T. *et al.* Biogenesis of the mitochondrial TOM complex: Mim1 promotes insertion and assembly of signal-anchored receptors. *The journal of biological chemistry* **283**, 120-127, doi:10.1074/jbc.M706997200 (2008).
118 Chacinska, A. *et al.* Mitochondrial presequence translocase: switching between TOM tethering and motor recruitment involves Tim21 and Tim17. *Cell* **120**, 817-829, doi:10.1016/j.cell.2005.01.011 (2005).
119 Mokranjac, D. & Neupert, W. Cell biology: Architecture of a protein entry gate. *Nature* **528**, 201-202, doi:10.1038/nature16318 (2015).
120 Horst, M. *et al.* Sequential action of two hsp70 complexes during protein import into mitochondria. *The EMBO journal* **16**, 1842-1849, doi:10.1093/emboj/16.8.1842 (1997).
121 Hawlitschek, G. *et al.* Mitochondrial protein import: identification of processing peptidase and of PEP, a processing enhancing protein. *Cell* **53**, 795-806 (1988).
122 Sirrenberg, C., Bauer, M. F., Guiard, B., Neupert, W. & Brunner, M. Import of carrier proteins into the mitochondrial inner membrane mediated by Tim22. *Nature* **384**, 582-585, doi:10.1038/384582a0 (1996).
123 Wiedemann, N. *et al.* Machinery for protein sorting and assembly in the mitochondrial outer membrane. *Nature* **424**, 565-571, doi:10.1038/nature01753 (2003).
124 Chacinska, A. *et al.* Essential role of Mia40 in import and assembly of mitochondrial intermembrane space proteins. *The EMBO journal* **23**, 3735-3746, doi:10.1038/sj.emboj.7600389 (2004).
125 Wiedemann, N. & Pfanner, N. Mitochondrial machineries for protein import and assembly. *Annual review of biochemistry*, doi:10.1146/annurev-biochem-060815-014352 (2017).
126 Lange, A. *et al.* Classical nuclear localization signals: definition, function, and interaction with importin alpha. *The journal of biological chemistry* **282**, 5101-5105, doi:10.1074/jbc.R600026200 (2007).
127 Wieckowski, M. R., Giorgi, C., Lebiedzinska, M., Duszynski, J. & Pinton, P. Isolation of mitochondria-associated membranes and mitochondria from animal tissues and cells. *Nature protocols* **4**, 1582-1590, doi:10.1038/nprot.2009.151 (2009).
128 Nass, M. M. Differential methylation of mitochondrial and nuclear DNA in cultured mouse, hamster and virus-transformed hamster cells. In vivo and in vitro methylation. *Journal of molecular biology* **80**, 155-175 (1973).
129 Dawid, I. B. 5-methylcytidylic acid: absence from mitochondrial DNA of frogs and HeLa cells. *Science* **184**, 80-81 (1974).
130 Vanyushin, B. F. & Kirnos, M. D. The nucleotide composition and pyrimidine clusters in DNA from beef heart mitochondria. *FEBS letters* **39**, 195-199 (1974).
131 Shmookler Reis, R. J. & Goldstein, S. Mitochondrial DNA in mortal and immortal human cells. Genome number, integrity, and methylation. *The journal of biological chemistry* **258**, 9078-9085 (1983).

132 Bellizzi, D. *et al.* The control region of mitochondrial DNA shows an unusual CpG and non-CpG methylation pattern. *DNA research* **20**, 537-547, doi:10.1093/dnares/dst029 (2013).
133 Ghosh, S., Sengupta, S. & Scaria, V. Comparative analysis of human mitochondrial methylomes shows distinct patterns of epigenetic regulation in mitochondria. *Mitochondrion* **18**, 58-62, doi:10.1016/j.mito.2014.07.007 (2014).
134 Van der Wijst, M. G. & Rots, M. G. Mitochondrial epigenetics: an overlooked layer of regulation? *Trends in genetics* **31**, 353-356, doi:10.1016/j.tig.2015.03.009 (2015).
135 Agrimi, G. *et al.* Identification of the human mitochondrial S-adenosylmethionine transporter: bacterial expression, reconstitution, functional characterization and tissue distribution. *Biochemical journal* **379**, 183-190, doi:10.1042/BJ20031664 (2004).
136 Chinnery, P. F., Elliott, H. R., Hudson, G., Samuels, D. C. & Relton, C. L. Epigenetics, epidemiology and mitochondrial DNA diseases. *International journal of epidemiology* **41**, 177-187, doi:10.1093/ije/dyr232 (2012).
137 Rebelo, A. P., Williams, S. L. & Moraes, C. T. In vivo methylation of mtDNA reveals the dynamics of protein-mtDNA interactions. *Nucleic acids research* **37**, 6701-6715, doi:10.1093/nar/gkp727 (2009).
138 Hong, E. E., Okitsu, C. Y., Smith, A. D. & Hsieh, C. L. Regionally specific and genome-wide analyses conclusively demonstrate the absence of CpG methylation in human mitochondrial DNA. *Molecular and cellular biology* **33**, 2683-2690, doi:10.1128/MCB.00220-13 (2013).
139 Kelly, R. D., Mahmud, A., McKenzie, M., Trounce, I. A. & St John, J. C. Mitochondrial DNA copy number is regulated in a tissue specific manner by DNA methylation of the nuclear-encoded DNA polymerase gamma A. *Nucleic acids research* **40**, 10124-10138, doi:10.1093/nar/gks770 (2012).
140 Baccarelli, A. A. & Byun, H. M. Platelet mitochondrial DNA methylation: a potential new marker of cardiovascular disease. *Clinical epigenetics* **7**, 44, doi:10.1186/s13148-015-0078-0 (2015).
141 Kim, G. D., Ni, J., Kelesoglu, N., Roberts, R. J. & Pradhan, S. Co-operation and communication between the human maintenance and de novo DNA (cytosine-5) methyltransferases. *The EMBO journal* **21**, 4183-4195 (2002).
142 Rhee, I. *et al.* DNMT1 and DNMT3b cooperate to silence genes in human cancer cells. *Nature* **416**, 552-556, doi:10.1038/416552a (2002).
143 Kato, Y. *et al.* Role of the Dnmt3 family in de novo methylation of imprinted and repetitive sequences during male germ cell development in the mouse. *Human molecular genetics* **16**, 2272-2280, doi:10.1093/hmg/ddm179 (2007).
144 Uysal, F., Akkoyunlu, G. & Ozturk, S. Dynamic expression of DNA methyltransferases (DNMTs) in oocytes and early embryos. *Biochimie* **116**, 103-113, doi:10.1016/j.biochi.2015.06.019 (2015).
145 Chen, T., Tsujimoto, N. & Li, E. The PWWP domain of Dnmt3a and Dnmt3b is required for directing DNA methylation to the major satellite repeats at pericentric heterochromatin. *Molecular and cellular biology* **24**, 9048-9058, doi:10.1128/MCB.24.20.9048-9058.2004 (2004).
146 Frommer, M. *et al.* A genomic sequencing protocol that yields a positive display of 5-methylcytosine residues in individual DNA strands.

Proceedings of the National Academy of Sciences of the United States of America **89**, 1827-1831 (1992).
147 Clark, S. J., Harrison, J., Paul, C. L. & Frommer, M. High sensitivity mapping of methylated cytosines. *Nucleic acids research* **22**, 2990-2997 (1994).
148 Grigg, G. & Clark, S. Sequencing 5-methylcytosine residues in genomic DNA. *Bioessays* **16**, 431-436, doi:10.1002/bies.950160612 (1994).
149 Patterson, K., Molloy, L., Qu, W. & Clark, S. DNA methylation: bisulphite modification and analysis. *Journal of visualized experiments*, doi:10.3791/3170 (2011).
150 Liu, B. *et al.* CpG methylation patterns of human mitochondrial DNA. *Scientific reports* **6**, 23421, doi:10.1038/srep23421 (2016).
151 Rowe, W. P., Huebner, R. J., Gilmore, L. K., Parrott, R. H. & Ward, T. G. Isolation of a cytopathogenic agent from human adenoids undergoing spontaneous degeneration in tissue culture. *Proceedings of the society for experimental biology and medicine* **84**, 570-573 (1953).
152 Wilson, J. M. Adenoviruses as gene-delivery vehicles. *The New England journal of medicine* **334**, 1185-1187, doi:10.1056/NEJM199605023341809 (1996).
153 Wong, C. M., McFall, E. R., Burns, J. K. & Parks, R. J. The role of chromatin in adenoviral vector function. *Viruses* **5**, 1500-1515, doi:10.3390/v5061500 (2013).
154 Hassell, J. A., Lukanidin, E., Fey, G. & Sambrook, J. The structure and expression of two defective adenovirus 2/simian virus 40 hybrids. *Journal of molecular biology* **120**, 209-247 (1978).
155 Tjian, R. The binding site on SV40 DNA for a T antigen-related protein. *Cell* **13**, 165-179 (1978).
156 Graham, F. L., Smiley, J., Russell, W. C. & Nairn, R. Characteristics of a human cell line transformed by DNA from human adenovirus type 5. *Journal of general virology* **36**, 59-74, doi:10.1099/0022-1317-36-1-59 (1977).
157 Bett, A. J., Prevec, L. & Graham, F. L. Packaging capacity and stability of human adenovirus type 5 vectors. *Journal of virology* **67**, 5911-5921 (1993).
158 Freed, E. O. & Martin, M. A. HIV-1 infection of non-dividing cells. *Nature* **369**, 107-108, doi:10.1038/369107b0 (1994).
159 Naldini, L. *et al.* In vivo gene delivery and stable transduction of nondividing cells by a lentiviral vector. *Science* **272**, 263-267 (1996).
160 Zufferey, R. *et al.* Self-inactivating lentivirus vector for safe and efficient in vivo gene delivery. *Journal of virology* **72**, 9873-9880 (1998).
161 Demaison, C. *et al.* High-level transduction and gene expression in hematopoietic repopulating cells using a human immunodeficiency [correction of imunodeficiency] virus type 1-based lentiviral vector containing an internal spleen focus forming virus promoter. *Human gene therapy* **13**, 803-813, doi:10.1089/10430340252898984 (2002).
162 Poeschla, E. M., Wong-Staal, F. & Looney, D. J. Efficient transduction of nondividing human cells by feline immunodeficiency virus lentiviral vectors. *Nature medicine* **4**, 354-357 (1998).
163 Fanales-Belasio, E., Raimondo, M., Suligoi, B. & Butto, S. HIV virology and pathogenetic mechanisms of infection: a brief overview. *Annali dell istituto superiore di sanita'* **46**, 5-14, doi:10.4415/ANN_10_01_02 (2010).

164 Sakuma, T., Barry, M. A. & Ikeda, Y. Lentiviral vectors: basic to translational. *Biochemical journal* **443**, 603-618, doi:10.1042/BJ20120146 (2012).
165 Dull, T. *et al.* A third-generation lentivirus vector with a conditional packaging system. *Journal of virology* **72**, 8463-8471 (1998).
166 Ikeda, Y. *et al.* Continuous high-titer HIV-1 vector production. *Nature biotechnology* **21**, 569-572, doi:10.1038/nbt815 (2003).
167 Anson, D. S. & Fuller, M. Rational development of a HIV-1 gene therapy vector. *Journal of gene medicine* **5**, 829-838, doi:10.1002/jgm.415 (2003).
168 Keshet, I. *et al.* Evidence for an instructive mechanism of de novo methylation in cancer cells. *Nature genetics* **38**, 149-153, doi:10.1038/ng1719 (2006).
169 Rauch, T. *et al.* Homeobox gene methylation in lung cancer studied by genome-wide analysis with a microarray-based methylated CpG island recovery assay. *Proceedings of the National Academy of Sciences of the United States of America* **104**, 5527-5532, doi:10.1073/pnas.0701059104 (2007).
170 Taylor, K. H. *et al.* Ultradeep bisulfite sequencing analysis of DNA methylation patterns in multiple gene promoters by 454 sequencing. *Cancer research* **67**, 8511-8518, doi:10.1158/0008-5472.CAN-07-1016 (2007).
171 Weber, M. *et al.* Chromosome-wide and promoter-specific analyses identify sites of differential DNA methylation in normal and transformed human cells. *Nature genetics* **37**, 853-862, doi:10.1038/ng1598 (2005).
172 Zilberman, D., Gehring, M., Tran, R. K., Ballinger, T. & Henikoff, S. Genome-wide analysis of Arabidopsis thaliana DNA methylation uncovers an interdependence between methylation and transcription. *Nature genetics* **39**, 61-69, doi:10.1038/ng1929 (2007).
173 Straussman, R. *et al.* Developmental programming of CpG island methylation profiles in the human genome. *Nature structural & molecular biology* **16**, 564-571, doi:10.1038/nsmb.1594 (2009).
174 Palmke, N., Santacruz, D. & Walter, J. Comprehensive analysis of DNA-methylation in mammalian tissues using MeDIP-chip. *Methods* **53**, 175-184, doi:10.1016/j.ymeth.2010.07.006 (2011).
175 Ramos, A. *et al.* Nuclear insertions of mitochondrial origin: Database updating and usefulness in cancer studies. *Mitochondrion* **11**, 946-953, doi:10.1016/j.mito.2011.08.009 (2011).
176 Calabrese, F. M., Simone, D. & Attimonelli, M. Primates and mouse NumtS in the UCSC Genome Browser. *BMC Bioinformatics* **13 Suppl 4**, S15, doi:10.1186/1471-2105-13-S4-S15 (2012).
177 Hsu, H. K., Weng, Y. I., Hsu, P. Y., Huang, T. H. & Huang, Y. W. Detection of DNA methylation by MeDIP and MBDCap assays: an overview of techniques. *Methods in molecular biology* **1105**, 61-70, doi:10.1007/978-1-62703-739-6_5 (2014).
178 Kumar, M., Keller, B., Makalou, N. & Sutton, R. E. Systematic determination of the packaging limit of lentiviral vectors. *Human gene therapy* **12**, 1893-1905, doi:10.1089/104303401753153947 (2001).
179 Bhagat, L. *et al.* CpG penta- and hexadeoxyribonucleotides as potent immunomodulatory agents. *Biochemical and biophysical research communications* **300**, 853-861, doi:10.1016/s0006-291x(02)02943-1 (2003).

180 Banerjee, P. *et al.* Application of isolated bacterial consortium in UMBR for detoxification of textile effluent: comparative analysis of resultant oxidative stress and genotoxicity in catfish (Heteropneustes fossilis) exposed to raw and treated effluents. *Ecotoxicology* **23**, 1073-1085, doi:10.1007/s10646-014-1250-6 (2014).
181 Espada, J. Non-catalytic functions of DNMT1. *Epigenetics* **7**, 115-118, doi:10.4161/epi.7.2.18756 (2012).
182 Fatemi, M., Hermann, A., Gowher, H. & Jeltsch, A. Dnmt3a and Dnmt1 functionally cooperate during de novo methylation of DNA. *European journal of biochemistry* **269**, 4981-4984 (2002).
183 Garrido, N. *et al.* Composition and dynamics of human mitochondrial nucleoids. *Molecular biology of the cell* **14**, 1583-1596, doi:10.1091/mbc.E02-07-0399 (2003).
184 Bogenhagen, D. F. Mitochondrial DNA nucleoid structure. *Biochimica et biophysica acta* **1819**, 914-920, doi:10.1016/j.bbagrm.2011.11.005 (2012).
185 Bogenhagen, D. F., Rousseau, D. & Burke, S. The layered structure of human mitochondrial DNA nucleoids. *The journal of biological chemistry* **283**, 3665-3675, doi:10.1074/jbc.M708444200 (2008).
186 Campbell, C. T., Kolesar, J. E. & Kaufman, B. A. Mitochondrial transcription factor A regulates mitochondrial transcription initiation, DNA packaging, and genome copy number. *Biochimica et biophysica acta* **1819**, 921-929, doi:10.1016/j.bbagrm.2012.03.002 (2012).